
Molecular Biomineralization of Octocoral Skeletons: Calcite versus Aragonite

Nicola Conci



München 2020

Molecular Biomineralization of Octocoral Skeletons: Calcite versus Aragonite

Nicola Conci

Dissertation zur Erlangung des Doktorgrades
an der Fakultät für Geowissenschaften
der Ludwig-Maximilians-Universität
München

vorgelegt von
Nicola Conci

München, den 03. März 2020

Erstgutachter: Prof. Dr. Gert Wörheide

Zweitgutachter: PD Dr. Sergio Vargas

Datum der mündlichen Prüfung: 07.05.2020

Index

List of published papers, preprints, manuscripts submitted and in preparation	viii
Authors Contributions	ix
Summary	x
1. Introduction	1
1.1 Biologically Induced vs. Biologically Controlled Biomineralization	2
1.2 Calcium Carbonate Mineralization	3
1.3 Corals: the Engineers of the Reef	4
1.3.1 Octocorallia vs. Scleractinia	4
1.3.2 The Scleractinian Skeleton	5
1.3.3 The Octocoral Skeleton	7
1.3.4 The Mineral Composition of Coral Skeletons	7
1.4 Biological Control over Coral Biomineralization	10
1.4.1 Control over Ion Transport and Availability	10
1.4.2 The Skeleton Organic Matrix	11
1.5 Environmental Control over Coral Biomineralization	12
1.5.21 The <i>mMg:mCa</i> Ratio	13
1.6 Aims of the Study	15
2. New Non-Bilaterian Transcriptomes Provide Novel Insights into the Evolution of Coral Skeletomes.	17
2.1 Abstract	18
2.2 Introduction	19
2.3 Materials and Methods	21
2.3.1 Generation of Octocorals Reference Transcriptomes	21
2.3.2 Database Construction and Homologs Search/Analysis	22
2.3.3 Analysis and <i>in Silico</i> Discovery of Acidic Proteins	22
2.3.4 Homolog Selection for Phylogenetic Analysis	23
2.3.5 Phylogenetic Analysis	23
2.4 Results	23
2.4.1 Distribution Analysis of Skeletogenic Proteins	23
2.4.2 Phylogenetic Analysis of Acidic Proteins	26
2.4.3 Galaxin and <i>Type IV</i> Collagen	28
2.5 Discussion	31

3. Comparative proteomics of octocoral and scleractinian skeletomes and the evolution of coral calcification	34
3.1 Abstract	35
3.2 Introduction	36
3.3 Materials and Methods	37
3.3.1 Extraction of OM proteins	37
3.3.2 SDS-PAGE Analysis	37
3.3.3 Proteomic analysis	38
3.3.4 Bioinformatic analysis of OM proteins	38
3.3.5 Phylogenetic Analysis	38
3.4 Results	39
3.4.1 Shared and species-specific components of the anthozoan skeleton	39
3.4.2 Similarity between scleractinian and octocoral acidic proteins	40
3.4.3 Evolutionary history of octocoral and scleractinian SOMPs	42
3.5 Discussion	45
4. Molecular and mineral responses of calcifying anthozoans grown in artificial Cretaceous seawater	48
4.1 Abstract	49
4.2 Introduction	50
4.3 Materials and Methods	51
4.3.1 Experimental Design.	51
4.3.2 Mineralogical Analyses	53
4.3.3 Transcriptomes Sequencing.	53
4.3.4 Gene Expression Analysis	54
4.4 Results	55
4.4.1 Mineralogical Analyses	55
4.4.2 Gene Expression Analysis	56
4.5 Discussion	58
5. Resilience to climate-change in an octocoral involves the transcriptional decoupling of the calcification and stress response toolkits	61
5.1 Abstract	62
5.2 Results and Discussion	63
.	63
5.3 Materials and Methods	67
5.3.1 Experimental model and subject details	67
5.3.2 Determination of calcification hot-spots along the body axis of <i>P. flava</i>	67
5.3.3 Proteomic analysis of the skeletal organic matrix of <i>P. flavas</i> sclerites	68
5.3.4 <i>In Vivo</i> Experiments	69
5.3.5 RNA Extraction and Library Preparation.	69

6. A 16S rRNA gene sequencing and analysis protocol for the Illumina MiniSeq platform	71
6.1 Abstract	72
6.2 Introduction	73
6.3 Materials and Methods	73
6.3.1 Cultivation and DNA extraction of the 16S mock community	73
6.3.2 16S amplicon library preparation	74
6.3.3 16S sequencing strategy and primer design	76
6.3.4 16S bioinformatics analysis and OTU assignment	77
6.3.5 16S data analysis	77
6.4 Results and Discussion	77
6.4.1 Run performances	78
6.4.2 Terminal G homopolymers	79
6.4.3 Mock community analysis	79
6.4.4 Analysis of environmental samples	81
Concluding Discussion	83
References	87
Appendix A: Supplementary Figures for Chapter 2	114
Appendix B: Supplementary Figures for Chapter 3	124
Appendix C: Supplementary Figures for Chapter 4	130
Appendix D: Supplementary Figures for Chapter 5	138
Appendix E: Supplementary Figures for Chapter 6	140
Declaration	145
Acknowledgements	146

List of published papers, preprints, manuscripts submitted and in preparation.

Nicola Conci, Gert Wörheide, Sergio Vargas (2019). New Non-Bilaterian Transcriptomes Provide Novel Insights into the Evolution of Coral Sceletomes.

Published in: *Genome Biology and Evolution*, Volume 11, Issue 11, November 2019, Pages 30683081, <https://doi.org/10.1093/gbe/evz199> (**Chapter 2**)

Nicola Conci, Martin Lehmann, Sergio Vargas, Gert Wörheide (2019). Comparative proteomics of octocoral and scleractinian skeletomes and the evolution of coral calcification.

In Review in: *Genome Biology and Evolution*

Preprint available at: *Biorxiv*, <https://doi.org/10.1093/gbe/evz199> (**Chapter 3**)

Nicola Conci, Sergio Vargas, Erika Griesshaber, Wolfgang Schmahl, Gert Wörheide. Molecular and mineral responses of calcifying anthozoans grown in artificial Cretaceous seawater.

This manuscript is in preparation for standalone publication (**Chapter 4**)

Sergio Vargas, Thorsten Zimmer, **Nicola Conci**, Martin Lehmann, Gert Wörheide (2020). Resilience to climate-change in an octocoral involves the transcriptional decoupling of the calcification and stress response toolkits.

This manuscript is in preparation for standalone publication (**Chapter 5**)

Monika Pichler, mer Coskun, Ana Sofia Ortega-Arbulu, **Nicola Conci**, Gert Wörheide, Sergio Vargas, William Orsi (2018). A 16S rRNA gene sequencing and analysis protocol for the Illumina MiniSeq platform.

Published in: *Microbiology Open*, Volume 7, Issue 6, November 2018, e00611, <https://doi.org/10.1002/mbo3.611> (**Chapter 6**)

Authors Contributions.

Chapter 2: All authors conceived the study. NC and SV designed the experiments. NC performed the RNA extractions, analysed and interpreted the transcriptome data. NC performed the phylogenetic analyses. NC drafted the manuscript and figures. GW and SV revised the manuscript. GW and SV secured the funding. All authors contributed to the discussion.

Chapter 3: NC, SV and GW designed the study. NC and ML performed the experiments and generated the data. NC performed the phylogenetic analyses. NC analysed and interpreted the data. NC drafted the manuscript and the figures. GW, ML and SV revised the manuscript. GW and SV secured the funding. All authors contributed to the discussion.

Chapter 4: GW, NC, and SV conceived the study. NC and SV designed the experiments. NC performed the RNA extractions. EG and NC carried out the mineralogical analyses. NC analysed and interpreted the data. NC drafted the manuscript and the figures. All authors revised the manuscript and contributed to the discussion. GW and SV secured the funding.

Chapter 5: SV designed the study. NC and TZ performed the protein extractions and analysed the proteomic data. ML carried out the mass spectrometry analysis. TZ did the qPCR analysis and SV generated and analysed the RNA-Seq data. SV drafted the manuscript and figures, and NC contributed writing the discussion. All authors revised the manuscript. GW and SV secured the funding.

Chapter 6: The study was designed by WO. MP, OC, AO and NC performed the DNA extractions. MP produced the library and carried out the DNA sequencing. MP analysed and interpreted the data. NC contributed to the analysis by writing custom scripts for data quality control. MP drafted the manuscript and figures. All authors revised the manuscript and contributed to the discussion. Funding was secured by WO.

Summary

Aragonite and calcite represent the two most common polymorphs of calcium carbonate (CaCO_3) formed biogenically by organisms. The mechanisms that allow animals to selectively deposit aragonite and/or calcite has been extensively studied in molluscs, but information on corals (class Anthozoa, phylum Cnidaria) is lacking. Contrary to scleractinian corals, which exclusively produce aragonite skeletons, members of the coral subclass Octocorallia exhibit both calcitic and aragonitic skeletal structures. They thus represent an interesting target to study biological and environmental control over deposition of CaCO_3 polymorphs in corals.

In this project we selected different octocoral species - characterized by aragonite or calcite skeletons - to investigate the evolution and mechanisms underlying aragonite and calcite biomineralization in corals. Main objectives of this study were 1) the characterization of the molecular machinery employed to deposit the two different CaCO_3 polymorphs, and 2) study the effects of seawater chemistry on skeleton mineralogy and gene expression. In the introductory section (**Chapter 1**) relevant concepts, terminology and background information is provided.

Chapter 2 and **3** aimed at filling the gaps in terms of availability of *-omic* resources for octocorals compared to scleractinians. New resources generated as part of the project include reference transcriptomes and skeletal proteomes for four octocoral species with different biomineralization strategies.

The transcriptomic analysis presented in **Chapter 2** provides a taxonomically comprehensive presence map for homologs of coral calcification genes across early-branching metazoans. By sensibly increasing taxonomic sampling, we expanded the distribution for several genes and reported homologs presence in previously unsurveyed groups. Homologs datasets were used for phylogenetic inferences, which provided insight into the evolution of acidic proteins and allowed to propose an alternative evolutionary scenario for the scleractinian protein galaxin *sensu stricto*.

In **Chapter 3** several new proteins with putative functions in octocoral biomineralization are described. A comparative characterization of skeleton proteomes in Octocorallia and Scleractinia is also provided. This analysis highlighted an extremely low overlap in terms of proteins presence between aragonite and calcite-forming species, while at the same time identifying a small set of proteins that constitute the core proteome of octocoral sclerites. Instances of similarity between scleractinians and octocorals are also listed, and include galaxin-related proteins, carbonic anhydrases and multicopper oxidases. Finally, as in scleractinians, some octocoral skeletogenic proteins appear to have acquired their role in calcification as the result of secondary co-option and following the enrichment - within the sequence - of acidic residues.

Chapter 4 and **5** focused on the interaction between environmental conditions and calcification in octocorals and scleractinians. **Chapter 4** revolves around the effect of the magnesium-calcium molar ratio ($m\text{Mg}:m\text{Ca}$) and its effects on the skeleton polymorph. Exposure to calcite-inducing $m\text{Mg}:m\text{Ca}$ did not cause a polymorph switch in *H. coerulea*, while calcite was incorporated in the skeleton of *M. digitata*. We did not observe changes in expression for skeletogenic proteins, with the exception of one gene coding for the uncharacterized skeleton organic matrix protein 5 (in *M. digitata*) and endothelin converting enzyme 1 (in *H. coerulea*). However, carbonic anhydrases and different calcium transporters and channels were affected, suggesting a potential response to changes in $m\text{Mg}:m\text{Ca}$ centered around ions transport, rather than a direct involvement of the organic matrix. In **Chapter 5**, we exposed

the octocoral *Pinnigrogia flava* to sublethal seawater temperature and lower pH (7.3). We showed how the calcification process in this octocoral is decoupled from the response to stress. Increasing water temperature triggered a stress response but did not affect calcification, while acidification downregulated the expression of several calcification-related genes without causing stress. This represents a mechanistic explanation for the higher tolerance to anthropic stressors exhibited by octocorals.

Finally in **Chapter 6**, an optimized protocol for 16S sequencing in bacteria, using the Illumina MiniSeq available at the Chair for Geobiology & Paleontology of the Department of Earth- and Environmental Sciences at Ludwig-Maximilians-Universität München in Munich (Germany), is presented. This protocol allowed to characterize bacterial communities from different sources, including aquarium seawater, and could thus represent a valuable tool to perform microbiome characterizations from marine organisms in the future.

This dissertation contributes to our understanding of the mechanisms underlying the formation of aragonite and calcite skeletons in corals. It includes the first characterizations of octocoral skeleton proteomes, and led to the identification of several - previously unknown - genes with putative calcification-related functions. These novel targets represent a valuable groundwork for further studies, including functional investigations aiming at elucidating the exact mechanisms behind coral biomineralization. It also shed new light on calcification responses triggered by predicted past and future environmental conditions, providing a better understanding on how corals reacted to changes during their evolutionary history, and their ability to cope with future scenarios.

Chapter 1

Introduction

Chapter 1

Introduction

Biom mineralization refers to the process by which organisms produce minerals. This ability has independently originated several times during Earth's history (Knoll 2003). These include twenty different origins in Metazoa, eight of which within phylum Cnidaria (Romano and Palumbi 1996), and at least four among plants (Knoll 2003). Biom mineralization is taxonomically widespread and skeletons have evolved to serve a diverse array of biological functions. In bacteria, for example, magnetic biom minerals are used for navigation by sensing the Earth's magnetic field (Frankel et al. 1997). In plants, calcium-based and siliceous minerals have been linked to, among other processes, heavy metals detoxification, promoting photosynthesis, regulating ions concentration and avoid predation (see He et al. (2014) for review). Biom minerals are also produced by representatives of several animal phyla and animals have evolved an extraordinary diversity of skeletons in terms of both structure and function (see Murdock and Donoghue (2011) for a general overview). Skeletal structures in animals are composed of either carbonate or phosphate minerals. The former are predominant among invertebrates (e.g. Cnidaria, Mollusca and Echinodermata), while phosphate is characteristic of vertebrates. Exceptions to this are the sponge (phylum Porifera) classes of Demospongiae and Hexactinellida which produce siliceous spicules.

1.1 Biological Induced vs. Biologically Controlled Mineralization

The formation of biom minerals can occur via different processes, and biom mineralization can be broadly defined as biologically induced or biologically controlled based on the degree of control exerted by the organism over the process (Lowenstam 1981; Mann 1983). In the first scenario, mineralization is the (by)product of the interaction between metabolic products resulting from biological/cellular processes, often of single-celled organisms, and their immediately surrounding environment. The absence of biological regulation often entails the presence of impurities in the mineral, and both arbitrary orientation and heterogeneous composition of the crystals (Banfield and Hamers 1997; Frankel and Bazylinski 2003; Weiner and Dove 2003). Biologically induced mineralization is commonly performed by Cyanobacteria (calcareous minerals) (Lowenstam 1986; Power et al. 2007; Obst et al. 2009), prokaryotes inhabiting anaerobic environments (e.g. sulfur-reducing bacteria) (Frankel and Bazylinski 2003) (pyrite and greigite) and plants (Braissant et al. 2004). In contrast, in biologically controlled biom mineralization organisms have evolved sets of macromolecules and specialized cells/structures to control several aspects of the process. Over the years, cell types specialized in skeletogenesis have been identified in several animals including echinoderms (Wilt and H 1988; Ettensohn 1992), molluscs (Kniprath 1981; Marin et al. 2012) and corals (Goldberg and Benayahu 1987; Grillo et al. 1993; Allemand et al. 2004; Allemand et al.

2011). Several of the mechanisms underlying biological control over mineralization remain elusive, but regulatory functions can be classified into two categories. The first is the control over the availability and concentration of required ions at the sites of calcification and it involves proteins such as ion transporters (Sikes and Wheeler 1983; Zoccola et al. 2015; Ramesh et al. 2019) and carbonic anhydrases (Miyamoto et al. 1996; Moya et al. 2008; Feng et al. 2017). Secondly, direct regulation over crystal nucleation and growth is carried out by the skeleton organic matrix (SOM): a complex mixture of macromolecules secreted by skeletogenic cells and eventually occluded within the mineral fraction of the skeleton (Lowenstam 1981; Krampitz et al. 1983; Weiner 1984; Allemand et al. 1998; Clode and Marshall 2003). For corals, both forms of control are discussed in more detail in section 1.4.

1.2 Calcium Carbonate Mineralization

Calcium carbonate (CaCO_3) is among the most commonly minerals deposited by organisms and it is widespread among marine invertebrates. As other minerals, calcium carbonate can naturally form different structures termed polymorphs. Three predominant polymorphic forms exist for CaCO_3 : calcite, aragonite and vaterite (Figure 1.1). Although they share the same chemical composition, polymorphs exhibit differences in terms of physicochemical properties such as stability and solubility. At ambient temperature and atmospheric pressure, calcite represents the most stable form of CaCO_3 , followed by aragonite and vaterite. In controlled set-ups, the formation of different polymorphs can be achieved by modifying experimental variables including temperature, pH or ion concentration (Wray and Daniels 1957; Yagi et al. 1984; Kralj et al. 1990; Tai and Chen 1998). Due to its stability, calcite represents the most common polymorph of biogenic calcium carbonate (Kato et al. 2002; Clfen and Mann 2003). However, despite its metastability, aragonite is also extensively used for skeleton formation. It constitutes the main component of mollusc shells - where it can co-occur with calcite -, and it is the CaCO_3 polymorph formed by different coral (phylum Cnidaria) species, as well as sclerosponges (Demospongiae; Wrheide, 1998; Jackson et al. 2007). Calcite is also found in these phyla and it is additionally present in calcareous sponges (Class Calcarea) and crustaceans (phylum Arthropoda). In seawater, selective precipitation of different polymorph is also influenced by the concentration of certain major ions ((Morse et al. 1997; Balthasar and Cusack 2015), discussed in detail in section 1.5.1). Vaterite is, on the other hand, seldom found in skeletal structures of animals, but significant amounts are found in the otoliths of some fish groups (e.g. sturgeons and salmon) (Carlstrm 1963; Gauldie 1986), and in the spicules of sea squirts (subphylum Tunicata, phylum Chordata) (Radha et al. 2010; Kabalah-Amitai et al. 2013).

to reef formation throughout different periods of Earth's history and represent the main reef-builders today (Veron 1995). Their pivotal role within the reef ecosystem is among the reasons that has made scleractinians one of the main targets for biomineralization research. In contrast, octocorals are commonly referred to as soft corals due to the lower amounts of CaCO_3 produced compared to scleractinian corals.

1.3.1 Octocorallia vs. Scleractinia

About 6000 species forming mineral structures have been to date described in the Anthozoa. Of these, more than 3000 belong to the subclass Octocorallia (Daly et al.), while ca. 2500 species are scleractinian corals (Veron 2013). In addition to shallow tropical reef environments, scleractinian corals inhabit temperate and polar waters (Romano and Cairns 2002). Octocorals are also globally distributed. They are mostly found in tropical reefs or deep sea environments (Prez et al. 2016), up to 6000m (Grasshoff and Others 1981), where they can occur at high density and support biodiverse ecosystems (Krieger and Wing 2002; Mortensen and Buhl-Mortensen 2005). Although the monophyly of Octocorallia and Scleractinia is robust (France et al. 1996; Berntson et al. 2001; Kitahara et al. 2014; Pratlong et al. 2017), phylogenetic relationships within the clades remain elusive and conflicting results between morphologic and genetic-based phylogenies have been reported (Fukami et al. 2008; Kitahara et al. 2010). This is especially true in octocorals where inconsistencies between DNA-sequence markers are observed (McFadden et al. 2006; McFadden et al. 2010). Most soft coral and scleractinian species are colonial, with only one genus (*Taiaroa*) of solitary octocorals reported to date (Bayer and Muzik 1976). Colonies consist of multiple polyps interconnected by tissue (coenenchyma in octocorals and coenosarc in scleractinians). The octocoral polyp bears eight pinnated tentacles - hence the name Octocorallia. This feature represents the diagnostic phenotypic character for the taxon as octocoral groups can exhibit striking morphological differences between each other. Scleractinian polyps are instead characterized by six, or multiple of six, tentacles. An hexamerous arrangement is also observed in other anthozoan groups like sea anemones (order Actiniaria) and black corals (order Antipatharia).

1.3.2 Scleractinian Skeletons

In scleractinian corals, the skeleton, or corallum, is located below soft tissues (Figure 1.2a) and it is anchored to the animal via desmocytes, specialized cells forming protrusions for attachment (Bourne 1899; Muscatine et al. 1997). These cells form part of the aboral ectoderm (or calicoderm), the tissue surrounding the skeleton and responsible for the formation of the skeleton (discussed in section 1.4). It has not yet been determined whether the skeleton and the calicoblastic cells are in direct contact or if a space, termed extracellular calcifying medium (ECM), is present (Allemand et al. 2011). The overall morphology of the skeleton does vary and scleractinian colonies can assume several different forms: branching, encrusting, foliose, massive, tabular and different combinations of these (Figure 1.2c) (Veron and Stafford-Smith 2000). Macroscopically, the skeleton is composed of two distinct elements: corallites and the coenosteum (Figure 1.2a). Corallites are cup-shaped structures of a few millimeters (Ruppert et al. 2004) formed by single polyps. Corallites are interspersed across the skeleton and connected by the coenosteum, the skeletal component secreted by the coenosarc. Corallites consist of a few components: a basal plate, an epitheca and a corallite wall bearing inner (septa) and outer (costae) blade-like structures (Sprung 1999).

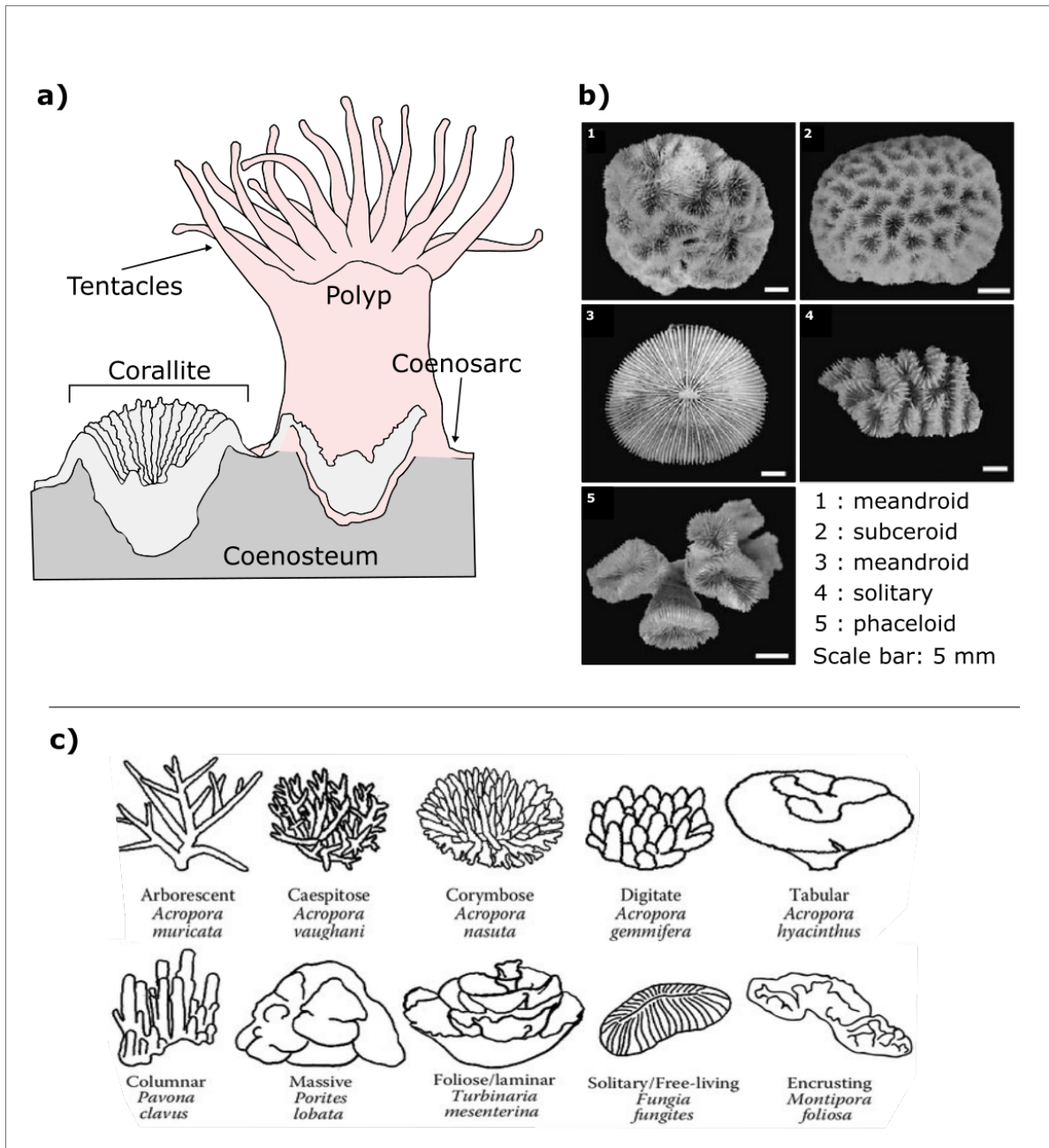


Figure 1.2: Schematic diagram of a scleractinian polyp (pink color) and skeleton (gray color). b) Examples of inter-specific variation in corallite morphology (modified from (Budd and Stolarski, 2009)). c) Different coral colonies growth forms with taxonomic examples (modified from Pratchett et al. (2015)).

Despite this apparent simple construction, the presence-absence of single features, ornaments and different arrangements make the ultimate structure of corallites highly variable between species (Figure 2b) and hence a valuable diagnostic morphological character for taxonomic classification (Wells 1956; Wijsman-Best 1974; Veron and Veron 1986; Veron and Stafford-Smith 2000). Intraspecific morphological differences can, however, also be present within single colonies and can occur within and between different populations (Wijsman-Best 1974; LANG and C 1984). Both genotypic and environmental factors have been proposed as drivers of such diversity (Willis 1985; Zilberberg and Edmunds 1999; Muko et al. 2000; Todd et al. 2004). Species of the genus *Acropora*, for example, exhibit a modified corallite at the apex of each branch where linear growth occurs (Oliver et al. 1983; Oliver 1984; Veron and Stafford-Smith 2000). Instances of environmental control include the correlation between corallite morphology and different feeding strategies (Lewis 1976) or the effects of depth on both the morphology (Klaus et al. 2007) and the distribution (Einbinder et al. 2009) of corallites within the skeleton. Scleractinian skeletons appear in the fossil record from the Middle Triassic (ca. 240 million years ago) with early scleractinians exhibiting surprising diversity (Stanley 2003). Molecular clock analyses do, however, place the origin of Scleractinia in the Paleozoic (ca. 450 Ma) with the two major scleractinian clades of Complexa and Robusta diverging ca. 425 Ma (Romano and Palumbi 1996; Stolarski et al. 2011; Chuang et al. 2017). The presence of ordovician scleractinian-like fossils may be consistent with a Paleozoic origin of the Scleractinia and the subsequent fossil gap possibly due to poor preservation or ephemerality of the coral skeleton (Stolarski et al. 2011).

1.3.3 Octocoral Skeletons

During their evolutionary history, octocorals have evolved different calcification strategies. In the vast majority of soft corals, the skeleton is composed by a multitude of sub-millimetric sclerites, which can exhibit marked diversity between species (Figure 1.3) and have been extensively used as taxonomic characters (Bayer 1981a; Alderslade 2001; Tentori and van Ofwegen 2011; Aharonovich and Benayahu 2012). Mature sclerites are located within the mesoglea, while developing ones are - based on investigations in the precious octocoral *Corallium rubrum* - encapsulated by two scleroblasts, the cells responsible for sclerite formation (Grillo et al. 1993; Goff et al. 2017). Intraspecific differences are also observed and specific morphologies characterize sclerites found in different locations within single colonies (Williams 1986; Williams 1992; Alderslade 2000). Sclerites can be either solitary and dispersed within the coenenchyme or they can aggregate to form axial structures (Fabricius and Alderslade 2001). In some species the axial skeleton consists of a reticulated structure exclusively composed of sclerites that provides the animal with both resistance and flexibility (Cuif 2016). In precious corals (family Coralliidae), the axial skeleton is instead formed via a dual process. The fusion of sclerites - forming the core of the skeleton - is combined with additional CaCO_3 deposition providing a progressive thickening of the axis (i.e. annular growth) (Allemand 1993; Debreuil et al. 2012). The axis can also be predominantly composed of proteinaceous compounds, collectively referred to as gorgonin. (Bayer 1981b). Finally, blue corals belonging to the order Helioporacea produce, unlike other soft corals, a massive skeleton composed of aragonite. The low CaCO_3 production rate of octocorals represents one of the underlying causes of their very intermittent fossil record (Kocurko and Kocurko 1992; Cope 2005; FernandezMartinez et al. 2019) and the classification of several fossils as octocorals remain disputed. Earliest putative octocoral fossil from order Pennatulacea date back to the early Cambrian (Ausich et al. 1998; McMenamin 2000; Wen-Tang et al. 2001; Taylor et

al. 2013), while specimens from order Alcyonacea appeared in the lower Ordovician ((Cope 2005). For blue corals, currently oldest fossils are from the Cretaceous (Eguchi 1948; Colgan 1984).

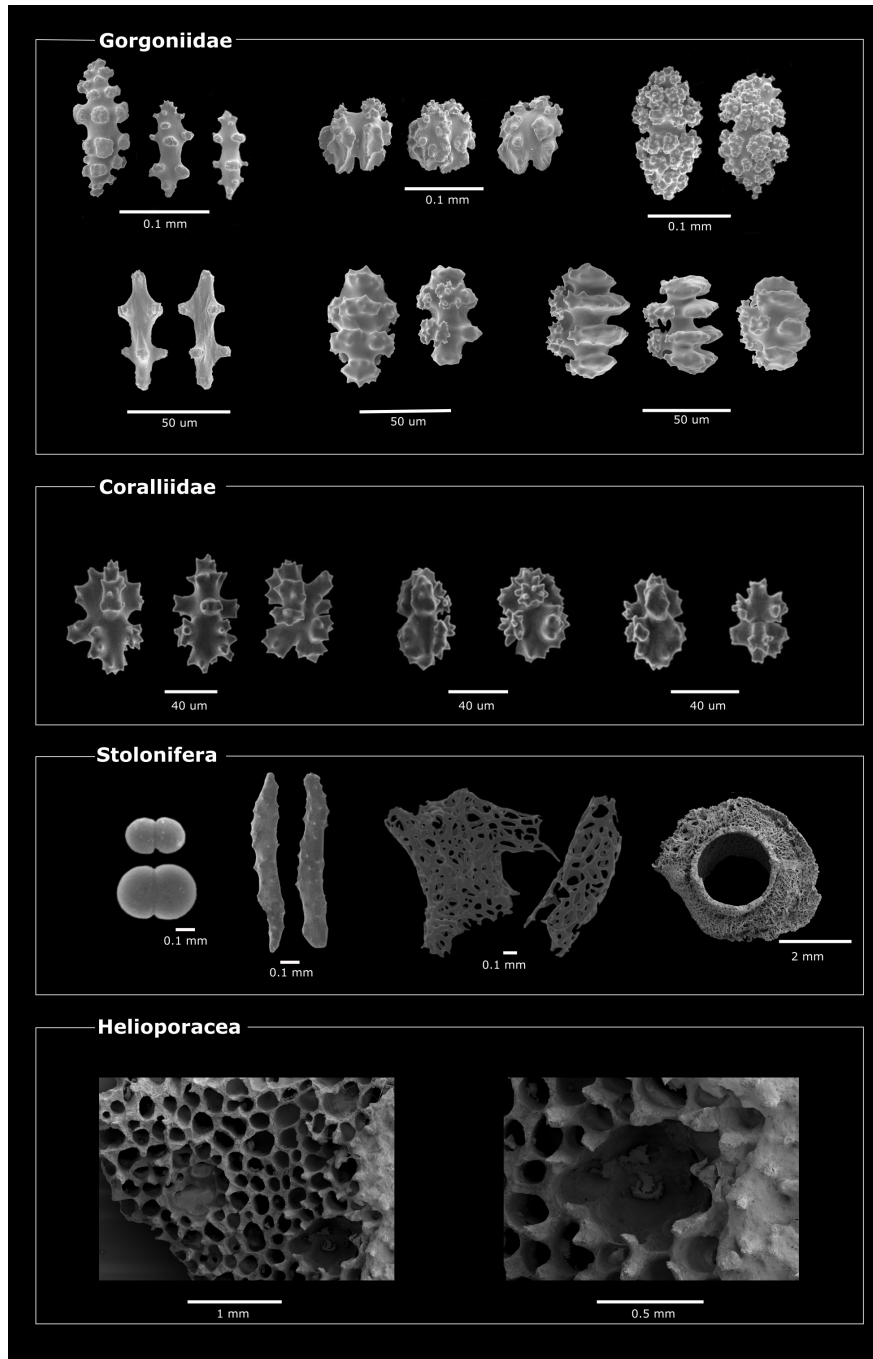


Figure 1.3: Scanning electron microscopy images of sclerites - skeleton in different octocoral groups. In Stolonifera examples of sclerite fusion can be observed. Images sources: Gorgoniidae from Horvath (2019), Coralliidae from (Simpson & Watling, 2011; picture by Les Watling), Stolonifera from Lau et al. (2019) and personal image, Helioporacea (personal images).

1.3.4 Mineral Composition of the Coral Skeleton

Octocorallia and Scleractinia both produce skeletons composed of calcium carbonate, but differ in terms of the CaCO_3 polymorph deposited. With the aforementioned exception of blue corals (Helioporacea), octocoral skeletons are exclusively composed of high-Mg calcite, while modern Scleractinia exclusively form aragonite. Some amounts of calcite can regularly be found in scleractinian corals, but have been linked to diagenesis or filling of boring holes (Houck et al. 1975; Nothdurft et al. 2007; Goffredo et al. 2012). The presence of amorphous calcium carbonate (ACC) has also been reported. The formation of aragonite in larvae and adults of scleractinians appears preceded by the deposition of ACC, which originates within intracellular vesicles in the coral tissues and is subsequently attached to the growing surface of the skeleton (Mass, Giuffre, et al. 2017; Akiva et al. 2018). However, these findings have been disputed and the presence of ACC in coral skeletons remains a matter of debate (DeCarlo 2018). ACC has also been found in octocorals and suggested to act as cementing agent between sclerites (Jeng et al. 2011). In addition to calcium, coral skeletons also contain significant amounts of magnesium (Mg) and strontium (Sr) (Velimirov and Bhm 1976; Weinbauer and Vellmirov 1995). In Octocorals, magnesium content varies between species. Sclerites and skeleton of precious coral contain between ca. 3 mol% (Weinbauer et al. 2000) to ~12 mol% (Floquet and Vielzeuf 2012) - depending on the analytical technique used - while lower values have been reported in *H. coerulea* (Velimirov 1980). In *C. rubrum*, magnesium distribution is not uniform and concentric rings of alternating higher and lower concentration can be observed (Vielzeuf et al. 2008). Magnesium content appears to be unevenly distributed also in scleractinian skeletons. A layered distribution can be observed within aragonite fibers and higher concentration values in correspondence of areas with centers of calcification (COC) (Meibom et al. 2004), areas of the skeleton from which fibrous aragonite - constituting the bulk of the skeleton - appear to originate (Bryan and Hill 1941; Cuif and Dauphin 1998). COC are also enriched in other trace elements including barium, boron, sodium and sulphur (Meibom et al. 2006). Early observations have positively correlated Mg concentration in animal skeletons, including corals, with the temperature of seawater (Chave 1954). This has made skeleton elemental ratios (Mg/Ca and Sr/Ca) proxies to reconstruct past environmental conditions (McCulloch et al. 1994; Mitsuguchi et al. 1996; Gagan et al. 2000; Felis et al. 2004). Such applications have been, however, later questioned (Quinn and Sampson 2002) as other biological, metabolic and environmental factors, such as growth rate or pCO_2 , appear to influence these ratios (Schrage 1999; Fallon et al. 2003; Cole et al. 2016), and conflicting results have been reported depending on the organism studied. Among corals, for example, temperature appears to promote Mg incorporation in the precious octocoral *C. rubrum*, while the Sr/Ca is linked to growth rate (Weinbauer et al. 2000)(Schrage 1999; Fallon et al. 2003)(Weinbauer et al. 2000). Opposite conclusions have been reported for the scleractinian *Porites* spp. with Sr levels driven by temperature and magnesium changing with growth rates (Inoue et al. 2007). Moreover, pre-processing of skeleton samples can also potentially affect elemental ratios (Mitsuguchi et al. 2001).

1.4 Biological Control over Coral Biomineralization

The ability of corals to control the formation of their skeleton has long been debated (Barnes 1970; Mann 1983; Constantz 1986; Cuif and Dauphin 2005; Veis 2005). Today, however, coral biomineralization is widely accepted as being a biologically controlled process. Decades of research have led to the identification of tens of genes/proteins with putative calcification-related functions. During the years, different terminologies have been used to name such protein repertoires: skeletogenic proteins (Jackson et al. 2007), biomineralization toolkit (Drake, Mass, et al. 2013) and skeletome (Ramos-Silva, Kaandorp, et al. 2013). To date, the assignment of calcification-related functions to coral proteins has been based on different experimental approaches including expression studies (Reyes-Bermudez et al. 2009; Le Goff et al. 2016), proteomic (Drake, Mass, et al. 2013; Ramos-Silva, Kaandorp, et al. 2013) and biochemical characterizations (Debreuil et al. 2012; Zoccola et al. 2015). However, functional assays using gene knockdown or gene editing experiments - the gold standard for the study of gene function - in cnidarians have had limited success so far (Lohmann et al. 1999; Smith et al. 2000; Dunn et al. 2007). Recently, a 50% successful transfection rate was reported in scleractinian corals using the CRISPR/Cas9 technique (Cleves et al. 2018). Therefore, although evidence of an involvement in skeletogenesis of certain proteins is strong, individual gene functions and associated phenotypic effects on the skeleton remain unknown until functional studies are carried out.

1.4.1 Control over Ion Transport and Availability

Whether a mineral dissolves or precipitates within a fluid depends on its saturation state (Ω). For CaCO_3 , Ω is defined as the product of $[\text{Ca}^{2+}]$ and $[\text{CO}_3^{2-}]$ in the fluid divided by the concentration of CaCO_3 . If $\Omega > 1$ precipitation occurs, while $\Omega < 1$ causes the mineral to dissolve. Therefore, to increase the concentration of required ions, corals have to continuously supply calcium and carbonate to the sites of calcification in the ECM (Hohn and Merico 2012) (Figure 1.4). The transport of Ca^{2+} to the ECM can occur through both a transcellular and paracellular pathway, depending whether the ions do or don't transit through the cytoplasm of the cells, respectively (Ip et al. 1991; Cohen and McConnaughey 2003; Cuif et al. 2010; Gagnon et al. 2012; Tambutt et al. 2012). Different transporters associated with the transcellular supply of calcium have been identified. The pathway involves at least one calcium channel that allows Ca^{2+} ions to enter calciblastic cells (Zoccola et al. 1999). These are then transferred from the cells to the calcifying medium via a P-type calcium ATPase (Zoccola et al. 2004). Within the cells, calcium acts as a signalling molecule for different cellular processes and its concentration is constantly being tightly regulated. How corals combine cytoplasmic $[\text{Ca}^{2+}]$ regulation and Ca^{2+} transport to the ECM remains uncharacterized, but it appears to involve vesicular transport and one $\text{Na}^+/\text{Ca}^{2+}$ exchanger (Mass, Drake, et al. 2017; Barron et al. 2018). Calcium ATPases in corals could serve a dual function as they couple transport of Ca^{2+} in the ECM with the removal of protons, lowering the pH of the calcifying fluid (McConnaughey 1991; McConnaughey and Whelan 1997; Zoccola et al. 2004). The upregulation of the pH in the ECM compared to seawater promotes calcification by increasing the availability of carbonate ions (Tambutt et al. 2011). In octocorals, the calcifying fluid is pH upregulated compared to surrounding cells (pH 7.89 ± 0.09 and 7.97 ± 0.15 vs 7.44 ± 0.18 respectively), but not with respect to seawater (7.90 ± 0.06 , Goff et al. 2017). Maintaining an alkaline pH is important because it promotes the formation of CO_3^{2-} ions. No transport mechanisms for carbonate have been characterized so far, but a bicarbonate transporter - apparently restricted to cells in the calciblastic layer - is present (Furla et

al. 2000; Zoccola et al. 2015). Carbonic anhydrase (CA) does instead appear to diffuse through the cell membranes (Sultemeyer and Rinast 1996). The availability and concentration of the different carbon species can be regulated by the action of carbonic anhydrases, enzymes that catalyze the interconversion of CO_2 and bicarbonate (Moya et al. 2008; Bertucci et al. 2011; Bertucci et al. 2013).

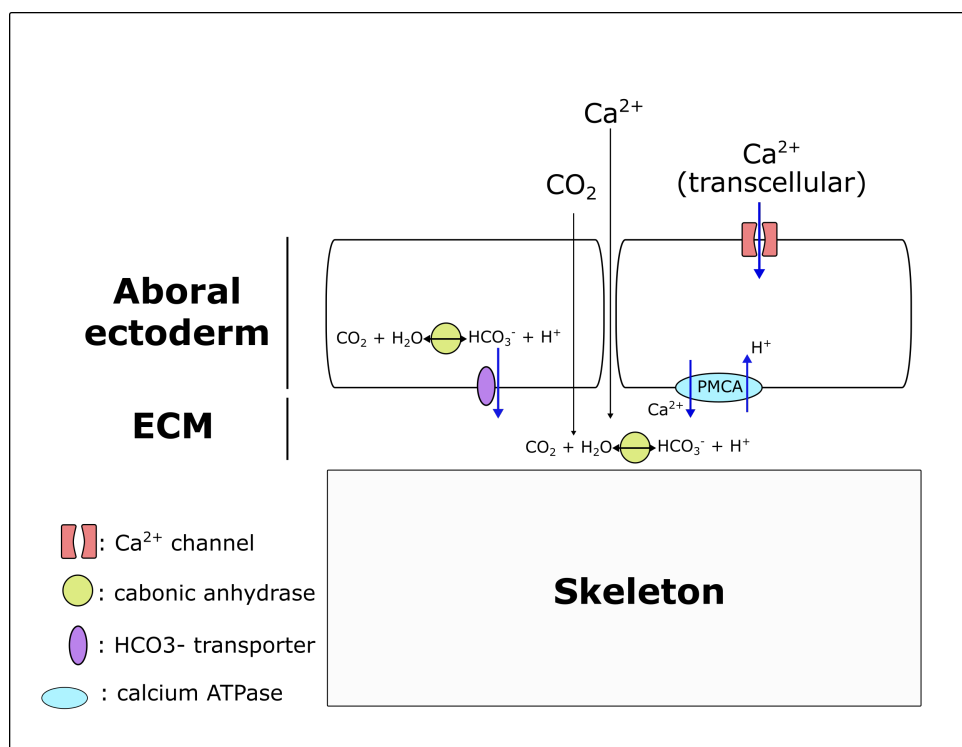


Figure 1.4: Schematic view of ions transport from the calcicoblastic cells to the ECM (extracellular calcifying medium). Vertical blue lines: transcellular pathways. Black vertical line: paracellular transport (Ca^{2+}) and diffusion (CO_2).

1.4.2 The Skeleton Organic Matrix

In addition to the mineral phase - which constituted the vast majority of the skeleton mass - an organic fraction, referred to as the skeleton organic matrix (SOM) is also present. Quantifications of the organic content in coral skeletons are currently hampered by experimental protocols, which involve decalcification and several cleaning and washing steps. These can cause losses of low-molecular weight OM components (Denis Allemand et al., 2011; Puverel et al., 2007) and thus lead to underestimations. Nevertheless, reported estimates have consistently ranged between 0.3 and 2 wt% (percentage of total weight), independently of the species studied and/or extraction method applied (D. Allemand et al., 1994; B. Constantz & Weiner, 1988; J.-P. Cuif et al., 2004; Goffredo et al., 2011; Ramos-Silva, Kaandorp, et al., 2013). Compositionally, the SOM represents a diverse mixture of macromolecules, which include proteins, mono- and polysaccharides (W. M. Goldberg, 2001; Naggi et al., 2018; Takeuchi et al., 2018), lipids (Farre et al., 2010; Reggi et al., 2016) and pigments (Cvejic et al., 2007). Of all SOM components, proteins have to date been the focus of biomineralization research. The first SOM protein was isolated more than a decade ago and named galaxin (Fukuda et al., 2003). The proteins does not contain any known domain, but presents

a characteristic repetition of dicysteine motifs. Its function remains unknown, but the ability to interact with collagen IV was proposed (Mass et al., 2016). Additional observations highlighted a predominance of acidic residues, primarily aspartic acid, and glycine within the skeleton proteome (or skeletome) of scleractinians (Puverel et al., 2005) and octocorals (Rahman & Oomori, 2009). High abundance of aspartate is a feature of different animal skeletons, and has been linked to the negative charges - within the functional group of this amino acid - possibly interacting with Ca^{2+} ions (S. Weiner & Hood, 1975). Highly acidic proteins have been later identified by mass spectrometry-based investigations, which allow the simultaneous characterization of several skeletal proteins, and constitute major components of coral skeletomes. Six acidic proteins with high aspartate content have been detected in *Acropora millepora* (Ramos-Silva, Kaandorp, et al., 2013), while five and two have been characterized in *Acropora digitifera* (Takeuchi et al., 2016) and *Stylophora pistillata* (Drake, Mass, et al., 2013) respectively. These include *A. millepora* secreted aspartic acid-rich proteins (SAARPs) and secreted acidic proteins (SAPs), and the *S. pistillata* coral acid-rich proteins (CARPs) family. Although the exact functions of coral acidic proteins remain elusive, CARPs have been recently observed in Ca^{2+} -transporting vesicles (Mass, Drake, et al., 2017) and found to directly interact in vivo with aragonite and amorphous calcium carbonate (Akiva et al., 2018).

In addition to acidic proteins, scleractinian skeletomes contain several proteins with domains related to cell adhesion and/or extracellular functions, components of the cell cytoskeleton, and sets of uncharacterized proteins with currently no significant hits in public databases (Drake, Mass, et al., 2013; Ramos-Silva, Kaandorp, et al., 2013; Takeuchi et al., 2016). Whether these proteins are 1) the results of insufficient cleaning of the skeleton samples, or 2) random incorporation within the skeleton, or do in fact represent genuine SOM components remains open to discussion (Drake, Massa, et al., 2013; Ramos-Silva, Marin, et al., 2013). To date, two proteins have been isolated and characterized from octocoral skeletal structures. The first (named scleritin) was identified in *C. rubrum*, where it is exclusively expressed by scleroblasts (Debreuil et al., 2012), while the second (ECMP67) was extracted from the sclerites of *Lobophytum crassum* (Rahman et al., 2011). ECMP67 also appeared to drive the formation of calcite in in vitro precipitation experiments. The induction of selective deposition of specific CaCO_3 polymorphs in supersaturated solutions is a common property of coral organic matrix components (Goffredo et al., 2011; Hohn & Reymond, 2019; Laipnik et al., 2019; Reggi et al., 2016). Whether this capacity is retained in vivo however remains to be determined.

1.5 Environmental Control over Coral Biomineralization

Biomineralization in marine invertebrates is intimately linked to environmental conditions, and changes in several physical and chemical properties of the surrounding seawater can significantly affect the process. Linear extension and density of the skeleton in corals for examples have been associated with several environmental parameters including temperature, seawater chemistry and nutrient availability (see Pratchett et al. (2015) for a review). Among environmental variables, seawater pH and surface temperature (SST) have been extensively studied as fluctuations - primarily decreases in pH (also known as ocean acidification, OA) and increases in SST - can have detrimental effects on calcification in several animal groups, including corals (Reynaud et al. 2003; Al-Horani 2005; Cooper et al. 2008; Death et al.

2009; Chan and Connolly 2013; Albright et al. 2016; Behbehani et al. 2019). Tolerance and susceptibility thresholds to abiotic stressors appear however to be species-specific and can differ sensibly between groups (Fabricius et al. 2011; Chan and Connolly 2013). Among corals for example, resistance to OA in octocorals is higher than scleractinians (Lopes et al. 2018), and has been linked to calcification occurring within the animal tissues. The presence of tissue around the mineral structures could act as a protective agent against lower seawater pH (Gabay et al. 2014). This has also been observed among scleractinians, where species with exposed skeleton areas were more affected by acidification than species fully covering their skeleton (Rodolfo-Metalpa et al. 2011). The presence of differential responses to abiotic stress and the existence of winning and losing species in altered scenarios (Fabricius et al. 2011), imply that changes in environmental conditions could also drive changes in future ecosystems composition. This has led the majority of research to examine interactions between calcification and environmental variables and mostly focus on the negative effects of anthropic stressors, and the capacity of corals to calcify in future scenarios. However, studying if and how corals responded when exposed to past conditions can also provide valuable insight into their ability to withstand environmental changes.

1.5.1 The $m\text{Mg}:m\text{Ca}$

One environmental parameter, known to have systematically varied during corals evolutionary history, is the composition of seawater (i.e. concentration of major ions). Among the compositional characteristics of seawater, the ratio of molar concentration between magnesium and calcium ($m\text{Mg}:m\text{Ca}$) is of particular interest for carbonate calcification, as it represents one of the main drivers of inorganic precipitation of different CaCO_3 polymorphs (Morse et al. 1997; Balthasar and Cusack 2015). Throughout the past 600 Mya, concentration of major ions - including calcium and magnesium - in seawater has been governed by emissions of hydrothermal brine occurring along mid-oceanic ridges, and river input (Sandberg 1983; Hardie 1990; Hardie 1996). High rates of oceanic crust production - positively correlated with brine fluxes - have been associated with lower Mg^{2+} concentrations and hence with declines in the $m\text{Mg}:m\text{Ca}$. During the last 500 Mya, variations in crust formation rates (Hays and Pitman 1973; Richards and Engebretson 1992; Cogn and Humler 2004) have caused the $m\text{Mg}:m\text{Ca}$ to oscillate between ca. 1 (calcite-inducing) and 5 (aragonite-inducing). Historically, a $m\text{Mg}:m\text{Ca}$ of 2 has been used as the cutoff value to distinguish aragonite and calcite-favouring environment, respectively referred to as aragonite and calcite seas (Sandberg 1983) (figure 1.5). However, the presence of temperature-dependent gray area in which co-precipitation can occur has been later proposed (Balthasar and Cusack 2015).

The carbonate polymorph of hypercalcifying animals has been linked to the aforementioned oscillations in seawater $m\text{Mg}:m\text{Ca}$, implying a direct control of seawater chemistry on the skeleton mineralogy of major reef builders during different geological times (Stanley and Hardie 1998; Stanley and Hardie 1999). However, although the correlation between $m\text{Mg}:m\text{Ca}$ and the initially adopted mineralogy by organisms is strong, several animal groups have maintained the same polymorph despite subsequent changes in ions concentration (Zhuravlev and Wood 2008). This opens to the possibility of seawater chemistry initially shaping the organism biomineralization strategy and its associated molecular machinery, which can in turn counteract later variations in the $m\text{Mg}:m\text{Ca}$. In the early Triassic for instance, when modern scleractinians appeared in the fossil record and represented the dominating calcifiers, seawater was characterized by a higher $m\text{Mg}:m\text{Ca}$ (ca. 3) (Bruce Railsback and Anderson 1987), which promotes the formation of aragonite and high-Mg calcite. During the Cretaceous period however, oceans experienced

a major decline in magnesium and increase in calcium concentration ($mMg:mC$ reached ca. 1), causing scleractinians to be superseded by bivalves (phylum Mollusca) producing calcitic shells (Kiessling and Baron-Szabo 2004). Despite an overall decrease in calcification output and one recorded instance of a calcitic scleractinian (Stolarski et al. 2007), recent fossil evidence shows that some scleractinian coral groups maintained an aragonite skeleton (Janiszewska et al. 2017). One notable exception to the correlation between seawater conditions and first skeleton mineralogy, are octocorals of the genus *Heliopora*, which produce an aragonite skeleton despite appearing in the fossil record during the early Cretaceous (calcite sea) (Eguchi 1948; Colgan 1984). Although gaps in the fossil record cannot be excluded, warmer seawater surface temperatures - known to promote aragonite formation at low $mMg:mCa$ in controlled settings (Balthasar and Cusack 2015) - during the Cretaceous (Littler et al. 2011), might have mitigated the antagonising effect of lower $mMg:mCa$ ratios.

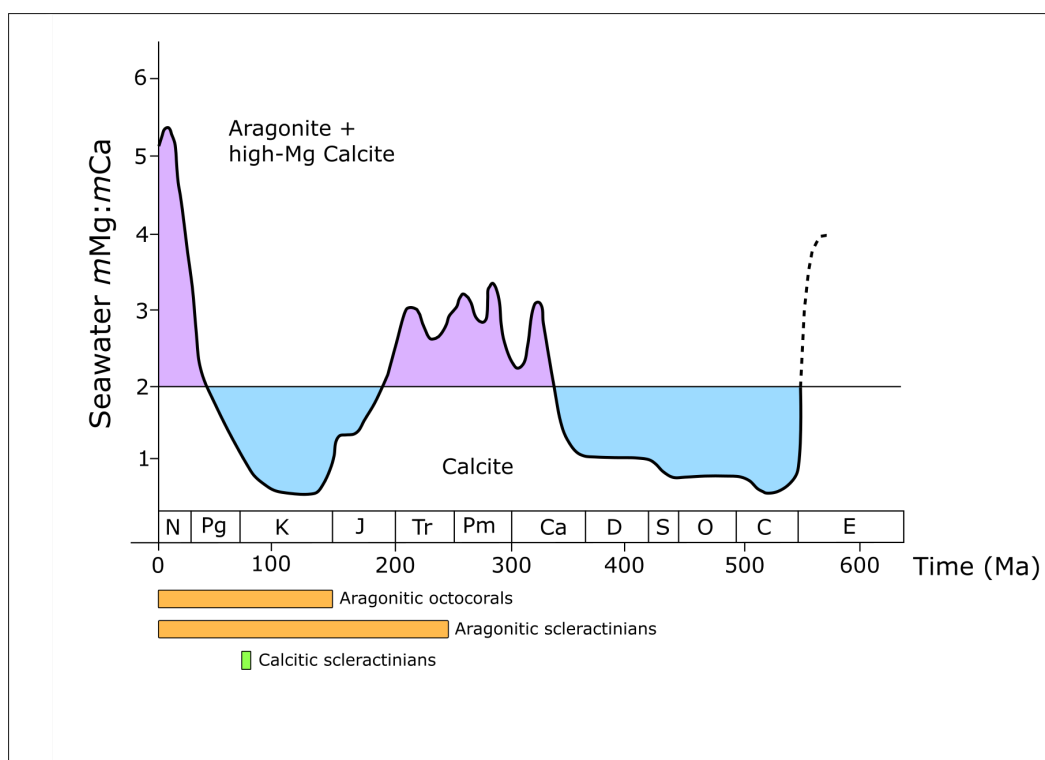


Figure 1.5: Predicted oscillations of seawater $mMg:mCa$ during the last 600 million years. Blue and purple areas indicate calcite and aragonite seas respectively. N: neogene, Pg: Palaeogene, K: Cretaceous, J: Jurassic, Tr: Triassic, Pm: Permian, Ca: Carboniferous, D: Devonian, S: Silurian, O: Ordovician, C: Cambrian, E: Ediacaran. Orange bars represent fossil record for aragonitic anthozoans. Green bars: calcitic scleractinians. Fossil records based on Eguchi (1948), Colgan (1984), Stolarski et al. (2007) and Janiszewska et al. (2017). Curve based on estimates by Hardie (1996) and Demicco et al. (2005). Figure modified from Ries (2010).

The tolerance of corals to switches between aragonite and calcite-favouring conditions has been studied both in vitro and in vivo. Former investigations include the examination of CaCO_3 crystals polymorphs in supersaturated solutions auditioned with total extracts or proteins and lipids from the coral skeleton organic matrix (SOM) (Rahman and Oomori 2009; Goffredo et al. 2011; Reggi et al. 2016; Hohn and Reymond 2019). These experiments highlighted the capacity of SOM components to either promote or inhibit the precipitation of specific CaCO_3 polymorphs. Recently Laipnik et al. (2019) observed that the solution composition (i.e. magnesium content) can influence protein activity and its correct functioning. In vivo studies involved the culture of calcifying species to different $m\text{Mg}:m\text{Ca}$ ratios to determine which polymorph is deposited by the organism. Exposure to calcite-inducing artificial seawater caused significant amounts of low-Mg calcite to be incorporated into mineral structures produced by microbial biofilms (Ries et al. 2008) and algae (Stanley et al. 2002; Stanley et al. 2010). In scleractinian corals, declines in $m\text{Mg}:m\text{Ca}$ ratio led to a decrease in calcification rates and significant calcite presence (up to 30%) in the skeleton (Ries et al. 2006). Notably, calcite amounts appeared correlated with the $m\text{Mg}:m\text{Ca}$ and calcite was observed even at known aragonite-favouring ratios (3.5 and 2.5). These first observations were later corroborated by Higuchi et al (2014), which observed calcite in the skeletal structures of juvenile polyps of the scleractinian *Acropora tenuis*, but only when at ratios < 2 . More recently, Yuyama et al. (2019) reported variations in gene expression in juveniles of the scleractinian *Acropora tenuis* grown in Mg-depleted seawater, leading the authors to postulate the presence of active responses by the coral to contrast the unfavourable conditions to aragonite precipitation. However, information on molecular responses to a simulated cretaceous environment - differing in terms of both $[\text{Ca}^{2+}]$ and $[\text{Mg}^{2+}]$ - remains lacking.

1.6 Aims of the Study

This study aimed at closing existing knowledge gaps concerning biomineralization in Octocorallia compared to Scleractinia, and is composed of two main parts. The first is designed to address the following research question:

- Are there genes specifically involved in the deposition of a single polymorph of calcium carbonate, i.e., aragonite vs. calcite? Or, on the contrary, is the mineralization machinery conserved between groups with aragonite and calcite skeletons?

Related alternative hypotheses include:

- (a) Octocorals producing structures composed of aragonite and calcite use a common set of skeletogenic proteins for the process, and this differs from the toolkit employed by scleractinians.
- (b) Octocorals producing structures composed of aragonite and calcite use a common set of skeletogenic proteins repertoires for the process. This protein set exhibits similarities with Scleractinia.
- (c) Octocorals have evolved polymorph-specific skeletomes to form aragonite and calcite skeletons. Similarities related to CaCO_3 polymorph are also observed between the aragonitic *H. coerulea* and scleractinians.

- (d) Octocorals have evolved polymorph-specific skeletomes to form aragonite and calcite skeletons. Similarities related to CaCO_3 polymorph are not present between the aragonitic *H. coerulea* and scleractinians.

This required the generation of *-omic* (transcriptomic and proteomic) resources for the species of interest. In the light of this, we initially produced a reference transcriptome for the four octocoral target species *Heliopora coerulea* (aragonite), *Pinnigorgia flava* (calcite), *Sinularia* cf. *cruciata* (calcite) and *Tubipora musica* (calcite). These were added to a dataset of early-branching metazoans (phyla Porifera, Ctenophora, Placozoa and Cnidaria), subsequently data mined to produce distribution maps for homologs of calcification-related genes across groups. Secondly, to identify novel research targets and compare octocoral and scleractinian skeletomes, we characterized the skeletal proteome for all aforementioned octocorals and the scleractinian *Montipora digitata*. This firstly involved the establishment of an experimental protocol for the extraction of proteins from different octocorals, followed by protein identification with mass spectrometry and in silico analyses. The obtained information, combined with previously published research on scleractinians, provided the first overview of skeletogenic proteomes across calcifying anthozoans.

The second part of the project did instead revolve around the putative presence of environmental control over biomineralization - with a focus on the seawater $m\text{Mg}:m\text{Ca}$ - that can be summarised by the following alternative scenarios:

- (a) The CaCO_3 polymorph of anthozoan skeletons is primarily controlled by seawater chemistry (i.e. $m\text{Mg}:m\text{Ca}$) and no biological control is exerted by the animal.
- (b) Octocorals and/or scleractinians employ molecular responses to counteract the effects of the $m\text{Mg}:m\text{Ca}$ and their skeleton CaCO_3 polymorph remains unaltered.

This part of the project required the setup of an aquarium experimental system to grow and expose corals to different $m\text{Mg}:m\text{Ca}$. The effects of the $m\text{Mg}:m\text{Ca}$ on the gene expression (RNAseq) and skeleton mineral characteristics (electron microscopy) of the aragonitic blue coral *H. coerulea* and the scleractinian *M. digitata* were then investigated. Additionally, we examined gene expression changes, triggered by seawater temperature and pH, of calcification-related genes in the octocoral *P. flava*.

Aside from the research project on coral biomineralization, my scientific contributions included participating in the development and optimization of pipelines for the analysis of next-generation sequencing data obtained with the Illumina MiniSeq machine available at the Molecular Geo- and Paleobiology Lab, LMU München (Chapter 6).

Chapter 2

New Non-Bilaterian Transcriptomes Provide Novel Insights into the Evolution of Coral Sceletomes.

2.1 Abstract

A general trend observed in animal skeletomes (i.e. the proteomes occluded within the mineral fraction of skeletons) is the copresence of taxonomically widespread and lineage-specific proteins that actively regulate the biomineralization process. Among cnidarians, the skeletomes of scleractinian corals have been shown to follow this trend. However, distributions and phylogenetic analyses of biomineralization-related genes are often based on only a few species, with other anthozoan calcifiers such as octocorals (soft corals), not being fully considered. We de novo assembled the transcriptomes of four soft-coral species characterized by different calcification strategies (aragonite skeleton vs. calcitic sclerites) and data-mined published nonbilaterian transcriptome resources to construct a taxonomically comprehensive sequence database to map the distribution of scleractinian and octocoral skeletome components. Cnidaria shared no skeletome proteins with Placozoa or Ctenophora, but did share some skeletome proteins with Porifera, such as galaxin-related proteins. Within Scleractinia and Octocorallia, we expanded the distribution for several taxonomically restricted genes such as secreted acidic proteins, scleritin, and carbonic anhydrases, and propose an early, single biomineralization-recruitment event for galaxin *sensu stricto*. Additionally, we show that the enrichment of acidic residues within skeletogenic proteins did not occur at the CorallimorphariaScleractinia transition, but appears to be associated with protein secretion into the organic matrix. Finally, the distribution of octocoral calcification-related proteins appears independent of skeleton mineralogy (i.e., aragonite/calcite) with no differences in the proportion of shared skeletogenic proteins between scleractinians and aragonitic or calcitic octocorals. This points to skeletome homogeneity within but not between groups of calcifying cnidarians, although some proteins such as galaxins and SCRiP-3a could represent instances of commonality.

2.2 Introduction

Cnidaria is a monophyletic lineage of marine and freshwater invertebrates currently comprising ca. 9,000 valid species. Their synapomorphy is the cnidocyte, a unique cell type used for locomotion and prey capture (Holstein 1981; Kass-Simon and Scappaticci 2002). Cnidarians have been important reef-building organisms throughout Earth history (Wood 1999) and are the main ecosystem engineers in today's coral reefs (Wild et al. 2011). Several taxa produce a rigid mineral skeleton made of calcium carbonate (CaCO_3) and those are found in the anthozoan order Scleractinia and the subclass Octocorallia, as well as in the hydrozoan families of Milleporidae, Stylasteridae, and Hydractiniidae. Calcification apparently has evolved multiple times independently within Cnidaria (i.e., in scleractinians, Romano and Cairns 2000) and hydractinians (Miglietta et al. 2010), and according to molecular clock estimates the origin of the capacity to calcify arose prior to the appearance of cnidarian skeletons in the fossil record (Cartwright and Collins 2007; Erwin et al. 2011; Van et al. 2016).

A common feature of most calcifying organisms is their ability to biologically control and regulate the formation of their skeletons. Although the degree of such control in cnidarians is still debated and the underlying molecular mechanisms are not entirely understood (Tambutt et al. 2011), two main regulatory mechanisms have been described. The first concerns the transport, availability, and concentration of required ions, and involves proteins such as carbonic anhydrases (Jackson et al. 2007; Moya et al. 2008; Bertucci et al. 2011; Le Goff et al. 2016) and bicarbonate transporters (Zoccola et al. 2015), to establish and maintain a chemical (micro)environment that promotes calcium carbonate precipitation (Sevilgen et al. 2019). The second putatively involves the skeletal organic matrix (SOM), an array of proteins (Puverel, Tambutte, Pereira-Mouris et al. 2005), polysaccharides (Goldberg 2001; Naggi et al. 2018), and lipids (Farre et al. 2010; Reggi et al. 2016) occluded within the mineral fraction of the skeleton (Farre et al. 2010). Skeletal organic matrix proteins (SOMPs) have been suggested to play a role in the promotion or inhibition of crystal growth (Allemand et al. 1998; Clode and Marshall 2003; Puverel et al. 2005), in the regulation of mineral polymorphism (Goffredo et al. 2011) and, more recently, have been shown to regulate the transition from amorphous mineral particles to ordered crystal structures (Von Euw et al. 2017). These proteins are collectively referred to as the skeletogenic proteins (Jackson et al. 2007), biomineralization toolkits (Drake et al. 2013), or skeletomes (Goffredo et al. 2011; Ramos-Silva et al. 2013). The characterization of SOMPs and the study of their evolutionary history is thus essential to unravel the appearance and evolution of biomineralization.

The first protein described and characterized from a coral skeleton was isolated from the organic matrix of the scleractinian coral *Galaxea fascicularis* and thus named galaxin (Fukuda et al. 2003). Galaxins are ubiquitous among scleractinians and putative homologs have been identified in several animal groups, including polychaetes (Sanchez et al. 2007), molluscs (Heath-Heckman et al. 2014), and sea urchins (Sodergren et al. 2006). Although structural similarities with vertebrate usherin (Bhattacharya et al. 2004) led to the proposition of an interaction between galaxin and *type IV* collagen (Bhattacharya et al. 2016), the role of galaxin in cnidarian skeletogenesis remains to be fully resolved (Bhattacharya et al. 2016). Following the first descriptions of single skeletogenic proteins, the advent of tandem mass spectrometry allowed for the simultaneous characterization of several proteins, offering a general overview of coral skeletal proteomes. To date, the proteome of three scleractinian corals: the two acroporids *Acropora digitifera* (Takeuchi et al. 2016) and *Acropora millepora* (Ramos-Silva et al. 2013), and the pocilloporid *Stylophora pistillata* (Drake et al. 2013) have been characterized.

The most abundant fraction of the coral skeletomes so far characterized is represented by acidic proteins (Ramos-Silva et al. 2013; Takeuchi et al. 2016), which supposedly drive crystal nucleation and growth (Wheeler et al. 1981; Addadi et al. 1987). Six acidic proteins have been described from the skeleton of *A. millepora* and two from *S. pistillata*. These include skeletal aspartic acid-rich proteins (SAARPs) (Ramos-Silva et al. 2013) and secreted acidic proteins (SAPs) (Shinzato et al. 2011) both found in *Acropora* species and two *S. pistillata* coral acid-rich proteins (CARP4 and CARP5) (Drake et al. 2013). The CARP family (Mass et al. 2013) is of particular interest as recent research has shown how CARPs interact with both aragonite fibers and amorphous calcium carbonate (ACC) during different ontogenetic stages of coral polyps (Akiva et al. 2018). CARPs also appear to be associated with intracellular vesicles putatively transporting Ca^{2+} ions to the extracellular space (Mass et al. 2017). The nonacidic regions of these acidic proteins match sequences found in other nonbiomineralizing cnidarians and bivalves, making the high occurrence of acidic residues a potential secondary modification linked to biomineralization (Takeuchi et al. 2016).

Surveys of cnidarian transcriptomes and genomes have in fact revealed that only a small proportion of SOMPs in *A. millepora* appears to be taxonomically restricted genes (TRGs) in corals (Ramos-Silva et al. 2013), while the majority of SOMPs (ca. 80% in *A. millepora*) have putative homologs in noncalcifying cnidarians, such as sea anemones and/or *Hydra magnipapillata* (Ramos-Silva et al. 2013). In addition, a recent transcriptome survey of corallimorpharians, skeleton-lacking cnidarians closely related to Scleractinia, has further shown that only six skeletogenic proteins appear to be taxonomically restricted to scleractinian corals (Lin et al. 2017). So far, however, genomic and transcriptomic surveys have mainly focused on comparisons between scleractinian corals and a limited set of noncalcifying cnidarians (e.g., sea anemones, corallimorpharians, and *Hydra*), systematically overlooking octocorals and calcifying hydrozoans (but see Guzman et al. 2018). Thus, very little information is currently available on the distribution of SOMPs across and within different lineages of calcifying cnidarians and consequently the evolutionary history of their biomineralization-related genes remains largely unexplored.

Here, we conducted an analysis of the distribution of putative coral biomineralization toolkit components across Anthozoa. Although functional studies represent the gold standard for the definite identification of genes involved in different biological processes, phylogenetic methods can provide valuable information on the evolution of processes like biomineralization that apparently evolved convergently (Knoll 2003), and help identify candidate proteins for functional studies. Along these lines, our work here allowed us to trace the evolution of skeletogenic protein homologs and investigate observed differences between and within the anthozoan lineages Scleractinia and Octocorallia. In addition, we also compared biomineralization gene repertoires between and within 1) calcifying cnidarians and sponges displaying different calcification strategies (i.e., aragonite vs. calcite deposition, exoskeleton vs. endo-sclerites) such as octocorals and scleractinians or calcareous sponges and the aragonitic demosponge *Vaceletia* sp. and 2) between them and their noncalcifying close relatives. For this, we de novo assembled the transcriptomes of four octocoral species, namely the massive, aragonitic blue coral *Heliopora coerulea*, and calcite producing species *Pinnigorgia flava*, *Sinularia* cf. *cruciata*, and *Tubipora musica*, three sclerites-forming octocorals. These species cover all calcification strategies within Octocorallia. Data-mining of newly generated and publicly available sequence resources was then used to produce fine-scaled phylogenies for selected targets of interest including acidic proteins (e.g., CARPs, SAARPs), galaxin, and carbonic anhydrases. These results contribute to our understanding of the functional diversity and evolutionary history of coral skeletomes.

2.3 Materials and Methods

2.3.1 Generation of Octocorals Reference Transcriptomes

To obtain reference transcriptomes for our target octocoral species, samples of *H. coerulea*, *T. musica*, *Pinnigorgia flava*, and *Sinularia cf. cruciata*, were mechanically collected from colonies cultured in the aquarium facilities of the Chair for Geobiology & Paleontology of the Department of Earth- and Environmental Sciences at Ludwig-Maximilians-Universität München in Munich (Germany) and kept under control conditions (temperature 25.1 ± 0.5 °C, pH 8.2 ± 0.1) for ca. 1 month before fixation in liquid nitrogen and subsequent storage at -80°C . For RNA extraction the samples were homogenized in 1-2 ml TriZol (ThermoFisher) using a Polytron PT Homogenizer (Kinematica), and subsequently centrifuged (20 min at 17,000g at 4°C) to remove remaining skeletal debris. A modified TriZol protocol (Chomczynski and Mackey 1995) was used for RNA purification and the concentration and integrity of the extracted RNA were assessed on a NanoDrop 2100 spectrophotometer and a Bioanalyzer 2100 (Agilent), respectively. For each species, RNA samples with a RIN >8.5 were used to prepare strand-specific libraries that were paired-end sequenced (50 bp reads) on an Illumina HiSeq 2000 sequencer at the EMBL Core Center in Heidelberg (Germany). For *H. coerulea*, additional strand-specific libraries were generated with the SENSE mRNA-Seq Library Prep Kit V2 for Illumina (Lexogen), and sequenced on an Illumina NextSeq 500 at the Kinderklinik und Kinderpoliklinik im Dr von Haunerschen Kinderspital.

Quality control of assembled reads was done with FastQC (www.bioinformatics.babraham.ac.uk) and low-quality reads ($Q < 28$) were removed with the Filter Illumina program from the Agalma-Biolite transcriptome package (Dunn et al. 2013). In addition, reads were mapped against a set of microbial genomes with Bowtie 2 with default parameters (Langmead and Salzberg 2012) and mapping reads were discarded. Transcriptome assembly was performed with Trinity v.2.5.1 (Grabherr et al. 2011). Contigs with a length <300 bp were discarded. Transcriptome completeness was assessed with BUSCO 3.0.2 (Simão et al. 2015). using the Metazoa odb9 data set and protein sequences were predicted with TransDecoder v.3.0.1. Summary statistics for each assembly are provided in Table 1. The bioinformatic workflow used is available at <https://galaxy.palmuc.org>. Reads were deposited at the European Nucleotide Archive (<https://www.ebi.ac.uk/ena>) under Bioproject number PRJEB30452. Assemblies, untrimmed/trimmed alignments, and output tree files from the various analyses are available at https://gitlab.lrz.de/palmuc/concietal_octoskeletomes.

Table 1: Summary Statistics for the Assembled Meta-Transcriptomes

Species	Contigs	N50/Mean Length	BUSCO (C-F-M)
<i>Heliopora coerulea</i>	125,310	1,347/967	90.37.22.5
<i>Pinnigorgia flava</i>	84,267	1,125/874	89.47.63.0
<i>Sinularia cf. cruciata</i>	69,180	857/721	75.5186.5
<i>Tubipora musica</i>	67,632	935/764	86.39.74.0

For BUSCO analysis, percentages of complete (C), fragmented (F), and missing (M) orthologs are provided.

2.3.2 Database Construction and Homologs Search/Analysis

To construct the homolog database of calcification related proteins, newly assembled transcriptomes were added to a sequence database of representatives of the nonbilaterian metazoan phyla Cnidaria, Porifera, Placozoa, and Ctenophora. To construct this, publicly available resources for target organisms (excluding tissue-specific transcriptomes) were uploaded on our local Galaxy server (<https://galaxy.palmuc.org>). When protein sequences were available, these were directly converted to a protein BLAST database (makeblastdb). Nucleotide sequences were first translated with TransDecoder Galaxy Version 3.0.1 (Haas et al. 2013). For cnidarians, BLAST databases were individually searched (BLASTp, e-value cutoff $\leq 1e^{-09}$) to retrieve putative homologs of coral calcification-related sequences. For the Porifera, Ctenophora, and Placozoa, databases provided in Eitel et al. (2018) were searched using the same criteria listed above.

Search queries included scleractinian skeletogenic proteins from *A. millepora* (Ramos-Silva et al. 2013) and *S. pistillata* (Drake et al. 2013), and small cysteine-rich proteins (SCRiPs) from *Orbicella faveolata* (Sunagawa et al. 2009). From *S. pistillata*, two additional SAARP-like acidic proteins that were included in the phylogenetic analysis in Bhattacharya et al. (2016) were additionally used as search queries. Octocoral queries comprised carbonic anhydrases from both *Corallium rubrum* (Debreuil et al. 2012) and *Lobophytum crassum* (Rahman et al. 2006) and scleritin (Debreuil et al. 2012). Features including sequence length and amino acid composition of identified homologs were determined with ProtParam (Gasteiger et al. 2005). To predict the presence of signal peptides, transmembrane regions, and protein domains, SignalP 4.1 (Petersen et al. 2011), TMHMM 2.0 (Sonnhammer et al. 1998), and InteProScan (Jones et al. 2014) were used, respectively.

2.3.3 Analysis and *in Silico* Discovery of Acidic Proteins

Amino-acid composition of skeletal acidic proteins and their nonacidic homologs was estimated with ProtParam ([https:// web.expasy.org/protparam/](https://web.expasy.org/protparam/); last accessed July 20, 2019). The analysis was limited to sequences predicted as complete by TransDecoder (see above). To visually investigate the contribution of changes in acid and basic amino acids to variations in isoelectric point, we performed a principal component analysis (PCA) on sequences grouped according to their phylogeny. Additionally, relative abundance of lysine and aspartic acid for each protein was calculated for the total proteome of seven anthozoan species, for which genomic data are available. Only species with available genomic resources were included in the analysis to avoid potential biases associated with transcriptome assemblies (e.g., missing transcripts due to lack of expression at the time of sampling). The newly sequenced octocoral transcriptomes were datamined to investigate the presence of putative biomineralization-related acidic proteins. Assembled contigs from the meta-assemblies were first assigned to either the host or the symbiont using psytrans (<https://github.com/sylvainforet/psytrans>; last accessed July 17, 2019). Host acidic proteins were identified using a custom script (available in the project repository) using 9% aspartic acid content as the cutoff value and the identified sequences were searched (BLASTp, e-value $1 \leq 1e^{-05}$) against the nonredundant NCBI database. Proteins with no hit or with octocoral-only hits were retained and their distribution mapped across octocoral data sets.

2.3.4 Homolog Selection for Phylogenetic Analysis

For the phylogenetic reconstruction of acidic proteins, all best hit sequences identified through the BLASTp searches described above, were used. Additionally, nonscleractinian sequences retrieved after BLASTp searches were used as query against scleractinian data sets (using BLASTp, e-value $1 \leq 1e^{-09}$). If the corresponding scleractinian best-hit differed from those identified using the previous query, sequences were also considered for phylogenetic analysis. The analyses of galaxin *sensu stricto* (i.e., scleractinian orthologs of *G. fascicularis* galaxin) and galaxin-related proteins (i.e., other putative homologs within and outside scleractinians) are based on all putative homologs (e-value $1 \leq 1e^{-09}$), with the exception of those matching galaxin-like 1 and 2 (ADI50284.1 and ADI50285.1), as these are exclusively expressed during early stages of calcification (Reyes-Bermudez et al. 2009). Predicted, partial sequences of >200 aa long were excluded. In addition to scleractinians, we surveyed taxa in which galaxin-related proteins have been identified, namely Mollusca, Annelida (Class Polychaeta), and Echinodermata. All resulting sequences were searched, using BLASTp, (e-value $1 \leq 1e^{-09}$) against the NCBI nonredundant database to avoid including usherin homologs in the data set. Homologous sponge collagen IV sequences were searched using the *type IV* collagen (Q7JMZ8) identified in the homoscleromorph sponge *Pseudocoriticium jarrei* as query. The analysis was limited to the N-terminal NC1 domain. Sequence of each putative homolog was checked for the presence of conserved cysteines (Aouacheria et al. 2006) and added to the collagen IV-spongins data set in Aouacheria et al. (2006). Finally octocoral homologs for the carbonic anhydrases (CA) CruCA1-6 (Le Goff et al. 2016) were searched in all octocoral data sets considered and added to the CAs data set used in Voigt et al. (2014).

2.3.5 Phylogenetic Analysis

Protein sequences were aligned with MAFFT (Katoh and Standley 2013) and MUSCLE (Edgar 2004) to investigate a possible effect of the aligning algorithm on the final phylogeny. Alignment was followed by a first site selection with Gblocks (Castresana 2002) run within Seaview 4 (Gouy et al. 2010) with the relaxed default parameter, which allows for less stringent site selection. In some instances Gblocks retrieved portions of the signal peptide or did not include well aligned portions of the sequences. Therefore, a final manual curation step was performed. Untrimmed and trimmed alignments can be found in the project repository and in the untrimmed alignments the excluded/included sites can be visualized in SeaView. Best-fit models were determined with Prottest 3 (Darriba et al. 2011). Maximum-likelihood and Bayesian analyses were performed in PhyML 3.1 (Guindon et al. 2010) from Seaview 4 (Gouy et al. 2010) with 500 bootstrap replicates, and MrBayes 3.2 (nrns = 2, samplefreq = 100; Huelsenbeck and Ronquist 2001; Ronquist et al. 2012), respectively. Effective Sample Sizes (EES > 200) and burn-in fractions (0.200.25) were determined with Tracer v.1.6 (<http://tree.bio.ed.ac.uk/software/tracer/>).

2.4 Results

2.4.1 Distribution Analysis of Skeletogenic Proteins

The distribution analysis of SOMP homologs resulted in diverse presence/absent patterns (Figure 2.1). Carbonic anhydrases, peptidases, and extracellular/adhesion proteins display the widest taxonomic distribution, although similarity was often limited to conserved domains within protein sequences.

In Porifera and Cnidaria however, differences could also be observed in terms of domain presence. Among sponges, the zona pellucida (ZP) domain was observed only in Calcarea, while the MAM domain appears to be absent in Demospongiae, as reported in Riesgo et al. (2014). In Cnidaria the cupredoxin domain could not be retrieved in Hydrozoa. In contrast, all SAPs and all small cysteine-rich (SCRiPs) proteins with the sole exception of SCRiP-3a (ACO24832.1), which was detected in Scleractinia and Octocorallia, showed the most taxonomically restricted distribution. Despite the presence of proteins found only among certain scleractinian families (e.g., SAPs, Threonine-rich protein), no protein hitherto isolated from the skeleton of *A. millepora* was found here restricted to acroporids.

No protein was exclusively found in Cnidaria + Placozoa or Cnidaria + Ctenophora, while a small set of coral SOMPs appeared to possess homologs in Cnidaria and Porifera. These include galaxin-related proteins and the uncharacterized *A. millepora* protein USOMP-5 (B8VIU6.1). Although absent in Homoscleromorpha and Hexactinellida, galaxin-related proteins are ubiquitous among calcareous sponges and also found in all three currently described subclasses of Demospongiae. Within Heteroscleromorpha however, differences were observed between groups as no galaxin-related protein was retrieved from the genome of *Amphimedon queenslandica* (Srivastava et al. 2010), while a significant hit was returned from the genome of *Tethya wilhelma* (Francis et al. 2017). The highest occurrence rate for USOMP-5 homologs in sponges was observed in Homoscleromorpha, but matches were detected in all groups. Although no domain was originally reported for B8VIU6.1 in *A. millepora* (Ramos-Silva et al. 2013), analysis of matching sequences from sponges revealed the presence of fibrinogen-related subdomains (IPR014716, IPR036056) within the protein (supplementary figure S2.1). Domain location partly overlaps the conserved region of the protein, and might thus explain the detected local similarity. Cnidaria exclusive proteins showed diverse presence/absence patterns with some SOMPs retrieving putative homologous sequences across the phylums classes while others could be only found restricted to few anthozoan families.

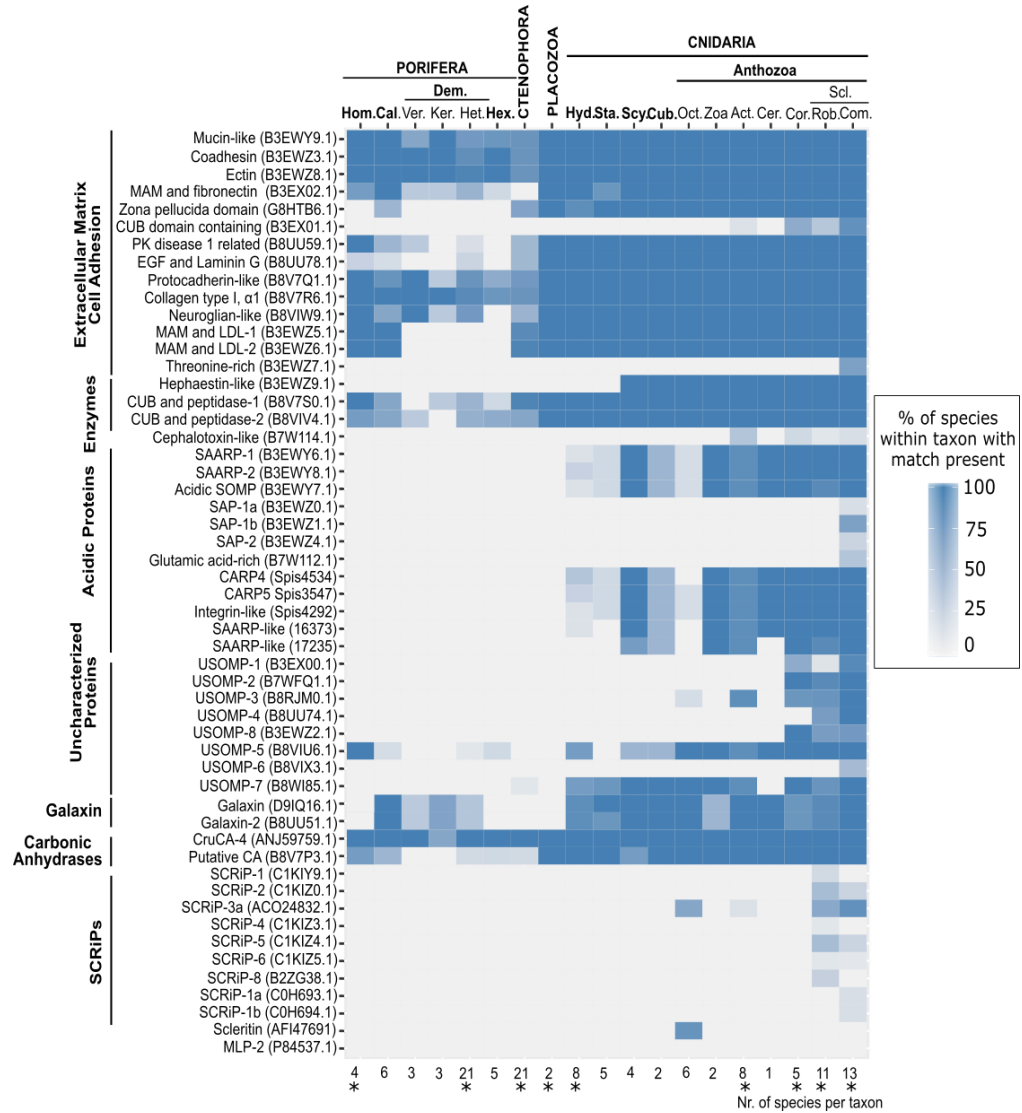


Figure 2.1: Pattern of presence of homologs (BLASTp, e-value $1e^{-09}$) of coral biomineralization-related protein across early branching metazoans. Lower x axis indicates number of species surveyed within a particular group. Asterisk: genomic data available for at least one species within the group. Protein categories Extracellular matrixCell Adhesion, Enzymes, Uncharacterized Proteins, and Galaxins based on Ramos-Silva et al. (2013). Taxa in capital and bold, phyla; taxa in bold, classes; normal text: subclasses or lower taxonomic levels; Hom, Homoscleromorpha; Cal, Calcarea; Ver, Verongimorpha; Ker, Keratosa; Het, Heteroscleromorpha; Dem, Demospongiae; Hex, Hexactinellida; Hyd, Hydrozoa; Sta, Staurozoa; Scy, Scyphozoa; Cub, Cubozoa; Oct, Octocorallia; Zoa, Zoantharia; Act, Actiniaria; Cer, Ceriantharia; Cor, Corallimorpharia; Scl, Scleractinia; Rob, Robusta (Scleractinia); Com, Complexa (Scleractinia).

Acidic proteins SAARPs and CARPs produced significant BLASTp matches among several cnidarian groups, although the presence of acidic regions (i.e., sequences segments enriched in aspartic and glutamic acid) appears to be characteristic of scleractinian corals (see below). Within Octocorallia, homologs of SAARPs and CARPs could be retrieved only in the precious coral *C. rubrum* using BLAST. Nonetheless, in silico analyses of octocoral transcriptomes identified octocoral exclusive, secreted, aspartic-rich proteins in different species. These sequences did not produce significant BLASTp hits against public databases. Members of the SAP acidic family were, on the other hand, detected solely in complex scleractinians, but not only in acroporids as previously suggested (Shinzato et al. 2011; Takeuchi et al. 2016). Homologs of SAP-1b (B3EWZ1.1) are in fact also present within families Dendrophylliidae and Agariciidae. Other uncharacterized proteins (USOMPs) displayed varying presence/absence patterns. USOMP-7 (B8WI85.1) and USOMP-3 (B8RJM0.1) were found across Cnidaria and Anthozoa, respectively. The latter also represents the only difference we detected between aragonitic and calcitic octocorals as this protein was solely found in *H. coerulea*. As reported in Lin et al. (2017), USOMP-1 is present in anemones and scleractinians, while both USOMP-2 and USOMP-8 first appear in corallimorphs. Finally, USOMP4 and USOMP-6 are restricted to scleractinians, although the first is shared by complex and robust corals and the second was only found in the families Acroporidae and Agariciidae. No significant match was detected among octocorals for the acidic carbonic anhydrase MLP-2 (Rahman et al. 2006), while we retrieved homologs across the group for both scleritin and five (CruCA1-5) of the six carbonic anhydrases described for *C. rubrum* (supplementary figures S2.7 and S2.8) (Le Goff et al. 2016), including the putative skeletogenic CruCA-4. No difference has thus been observed here for octocoral calcification-related proteins between aragonite and calcite-depositing species.

2.4.2 Phylogenetic Analysis of Acidic Proteins

Phylogenetic analysis split acidic proteins and their nonacidic homologs into five well-supported clades: two of these (marked as S for skeletogenic clades) are occupied by proteins found occluded in coral skeletons. Only scleractinians are represented within these groups. S1 contains homologs for the acidic SOMP (B3EWY7) and P27 isolated from *A. millepora* (Ramos-Silva et al. 2013) and *S. pistillata* (Drake et al. 2013), respectively. Both of these proteins display shorter acidic regions and a lower aspartic acid content compared with SAARPs and CARPs, which occupy clade S2. Tree topology within this group did however change between phylogenies obtained using different alignment methods (i.e., MUSCLE vs. MAFFT). In the MAFFT-based phylogeny displayed below, (Figure 2.2a) CARPs and SAARPs are split into two distinct subgroups although bootstrap support was low. All other sequences were divided among three nonskeletogenic (NS) clades. Taxonomic diversity for these groups differed and ranged from Cnidaria (NS1) to scleractinians (NS3), while NS2 contained scleractinians and corallimorphs. When aligned with MUSCLE, SAARP-2 grouped with both CARPs, but support was again low (supplementary figure S2.2). The internal topology of clade NS2 was also affected. When aligned with MUSCLE, both *Porites* sequences, together with *Favia* sp. 24967, *Platygyra carnosus* 1685, and *Pseudodiploria strigosa* 22901, were placed as sister group to other scleractinians (supplementary figure S2.2). The split between corallimorphs and scleractinians within NS2 was nevertheless retrieved in both phylogenies.

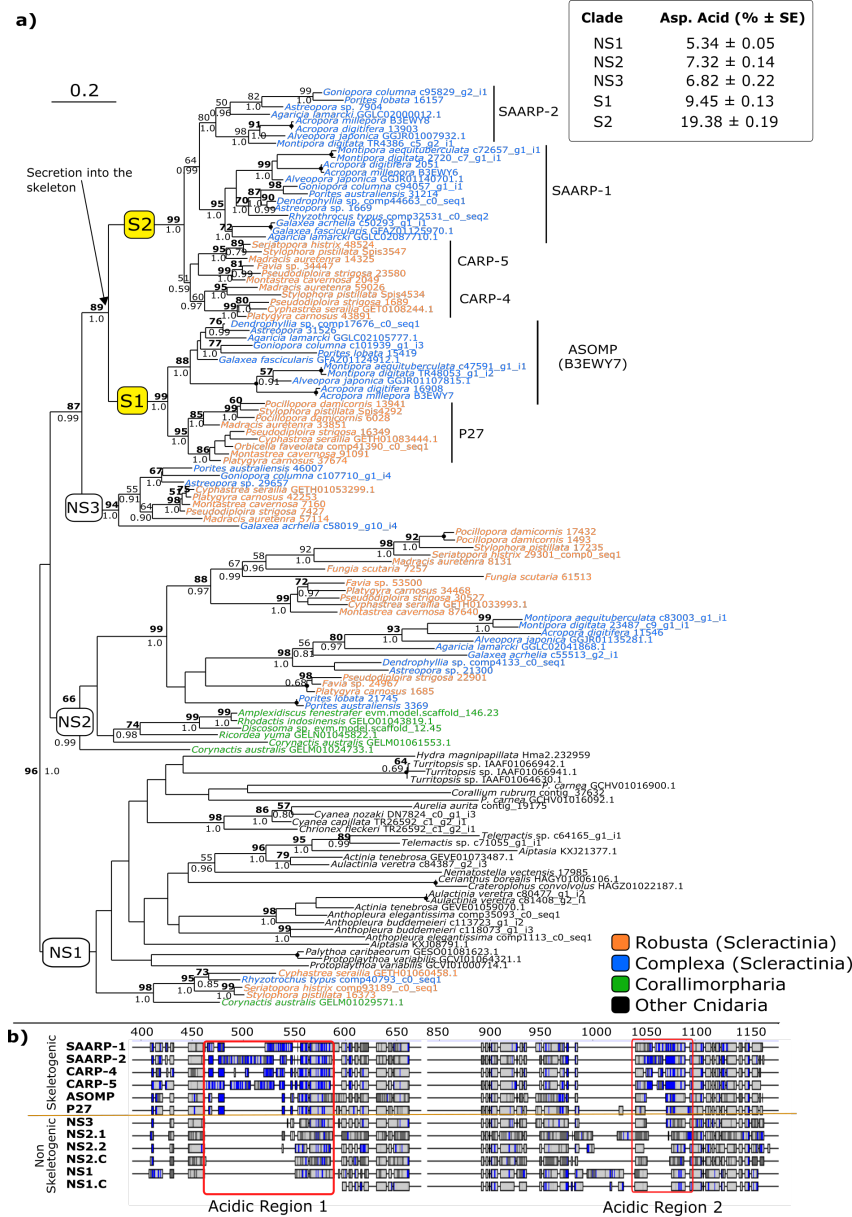


Figure 2.2: (a) Phylogenetic tree (ML, 500 bootstrap replicates) of scleractinian acidic proteins and putative homologs in other cnidarian groups. Best-fit model: WAG+F+G+I. Tree displayed in figure based on protein sequences aligned with MAFFT. MUSCLE-based tree available in supplementary figure S2.2. Bold number: node supported (>50) also in MUSCLE phylogeny. Dot on node indicates 100% bootstrap and 1.0 posterior probability in both phylogenies. Skeletogenic clades (S) (highlighted in yellow) include acidic proteins found in coral skeletons (Drake et al. 2013; Ramos-Silva et al. 2013). NS (nonskeletogenic) clades: acidic proteins not extracted from coral skeletons. (b) Consensus sequences (60%) alignment for each clade. Alignment shows the position and distribution of acidic residues (aspartic and glutamic acid) highlighted in blue. Light gray: other conserved residues. Dark gray: nonconserved residues. Complete alignment available in the project repository. When corallimorph sequences were present in a clade, these were analyzed separately to highlight difference with scleractinian proteins. Corallimorph consensus sequences IDs end in .C. NS2 clade was split into NS2.1 (includes *Porites australiensis* 3369, *Porites lobata* 21745, *Favia* sp. 24967, *Platygyra carnosus* 1685 and *Pseudodiploria strigosa* 22901) and NS2.2 (all other scleractinian sequences) because the position of NS2.1 was not congruent between phylogenies and was also retrieved as sister group to the rest of NS2 scleractinian proteins (supplementary figure S2.2). Top right corner: mean (6 ± SE) content (%) of aspartic acid within acidic proteins.

All other cnidarian sequences grouped with the scleractinian homologs of *S. pistillata* protein 17235 (NS1). As previously reported (Takeuchi et al. 2016), similarity between acidic proteins and their putative homologs is restricted to nonacidic regions. Analysis of clade-consensus sequences shows that the appearance of the aspartic acid-rich regions corresponds with the secretion of the proteins into the skeleton matrix and not with the shift between corallimorphs and scleractinian sequences (Figure 2.2b). Within B3EWY7-P27 the increment in aspartic acid appears restricted to the first acidic region, and it then continues in SAARP1 and CARP4, ultimately escalating in SAARP-2 and CARP-5 which exhibit the longest extension of the first acidic region. The transition from nonskeletogenic to skeletogenic proteins is also marked by a sharp decrease in protein isoelectric point that is mainly driven by the increase in aspartic acid (see above) and a concurrent decline in lysine content (supplementary Figure 2.9). These trends do not apply to the whole scleractinian proteome but are specific to skeletal proteins. Finally, the amount of glutamic acid does appear to remain unaltered between the NC and S clades, although principal components analysis based on sequence composition points to lower contents in clade S2 compared with clade S1.

2.4.3 Galaxin and *Type IV* Collagen

Phylogenetic analysis of metazoan galaxin-related proteins revealed high degrees of polyphyly among lineages both at the phylum and lower levels, with only terminal nodes displaying moderate to high support (Figure 2.3). Taxonomically uniform clades were observed in both MAFFT- and MUSCLE-based phylogenies. These included galaxin-related proteins from calcareous sponges, octocorals and Hydrozoa. However, for the vast majority of these clades, both support and topology were influenced by the alignment algorithm employed. The exception to this general pattern is a scleractinian-only clade comprising both complex and robust corals. The group includes both *A. millepora* skeletogenic (D9IQ16.1 and B8UU51.1) and the original *G. fascicularis* galaxins. The unifying feature of this clade is the RXRR endoprotease target motif described in Fukuda et al. (2003) (supplementary figure S2.4). This RXRR motif is not unique to scleractinians, but it was not detected in any other galaxin-related protein within the group. Its presence thus appears to effectively discriminate a group of galaxins, here dubbed galaxins *sensu stricto*, from galaxin-related proteins. Although the monophyly of galaxins *sensu stricto* was robust to the alignment algorithm, its internal topology was affected, with galaxin-2s and *Rhizotrochus typus* sequences nesting either within Complexa (MAFFT) or Robusta (MUSCLE). When performing the analysis on galaxin *sensu stricto* sequences only, galaxin-2 sequences concordantly grouped together with other complex scleractinians (supplementary figure S2.5), in agreement with the topology derived from the MAFFT alignment and presented in figure 2.3. To investigate putative interactions between galaxin-related proteins and collagen IV, we mapped the distribution of both proteins in Porifera, as both are present but not ubiquitous in the phylum (Figure 2.4). As for galaxin-related proteins, *type IV* collagen is present across calcareous sponges, while Homoscleromorpha are the only sponge class with collagen IV but no galaxin homologs. Collagen IV is also present in both keratose and verongimorph sponges, while within Heteroscleromorpha it appears associated with the freshwater environment. Finally, neither protein is present in glass sponges (Hexactinellida).

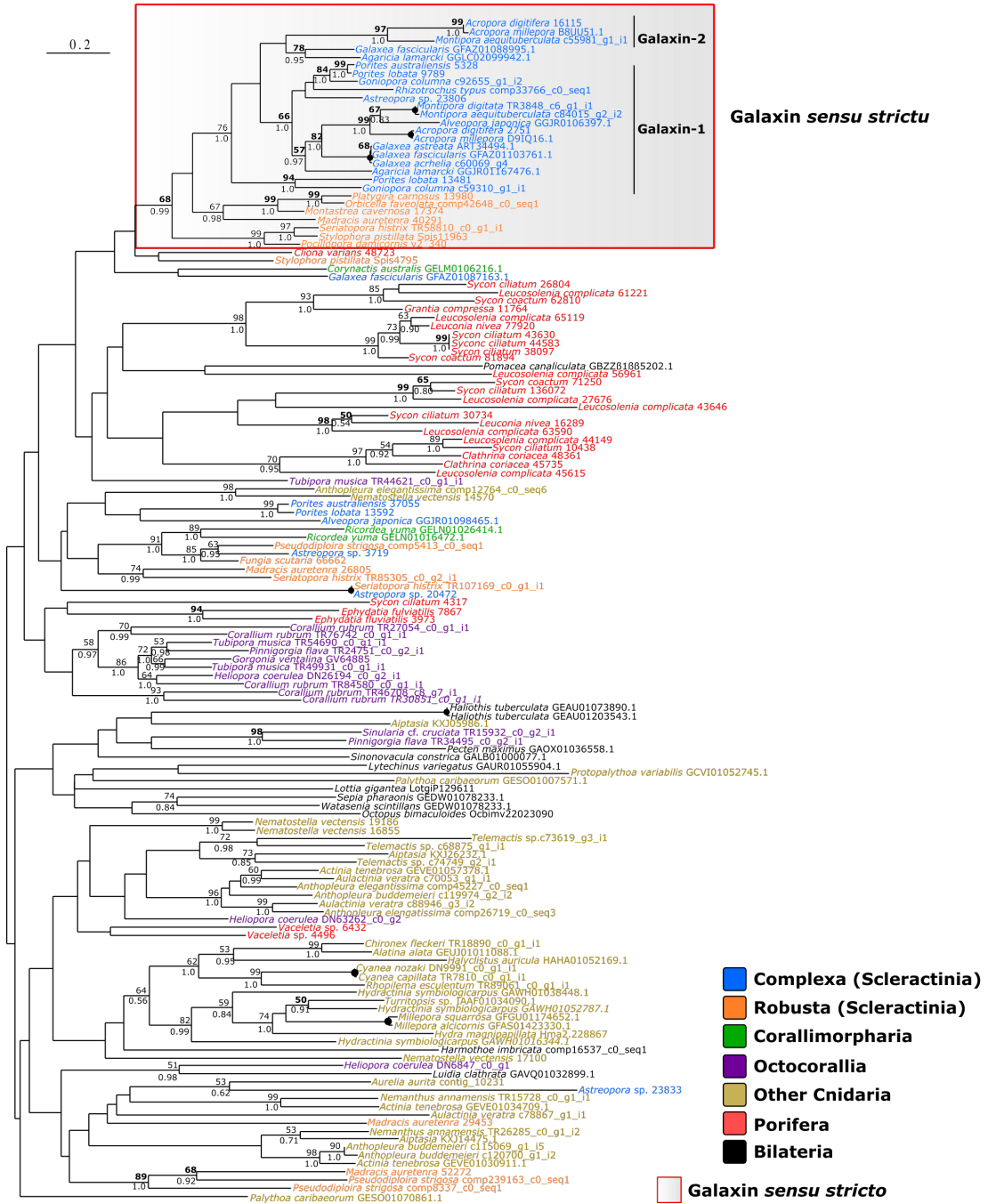


Figure 2.3: Phylogenetic analysis (ML; 500 bootstrap replicates) of metazoan galaxin-related proteins. Tree displayed in figure based on protein sequences aligned with MAFFT. MUSCLE-based phylogeny in supplementary figure S2.3. Bold number: node supported (>50) also in MUSCLE phylogeny. Dot on node indicates full support (100 bootstrap, 1.0 posterior probability) in both phylogenies. Support for nodes with bootstrap <50 not shown regardless of posterior probability value.

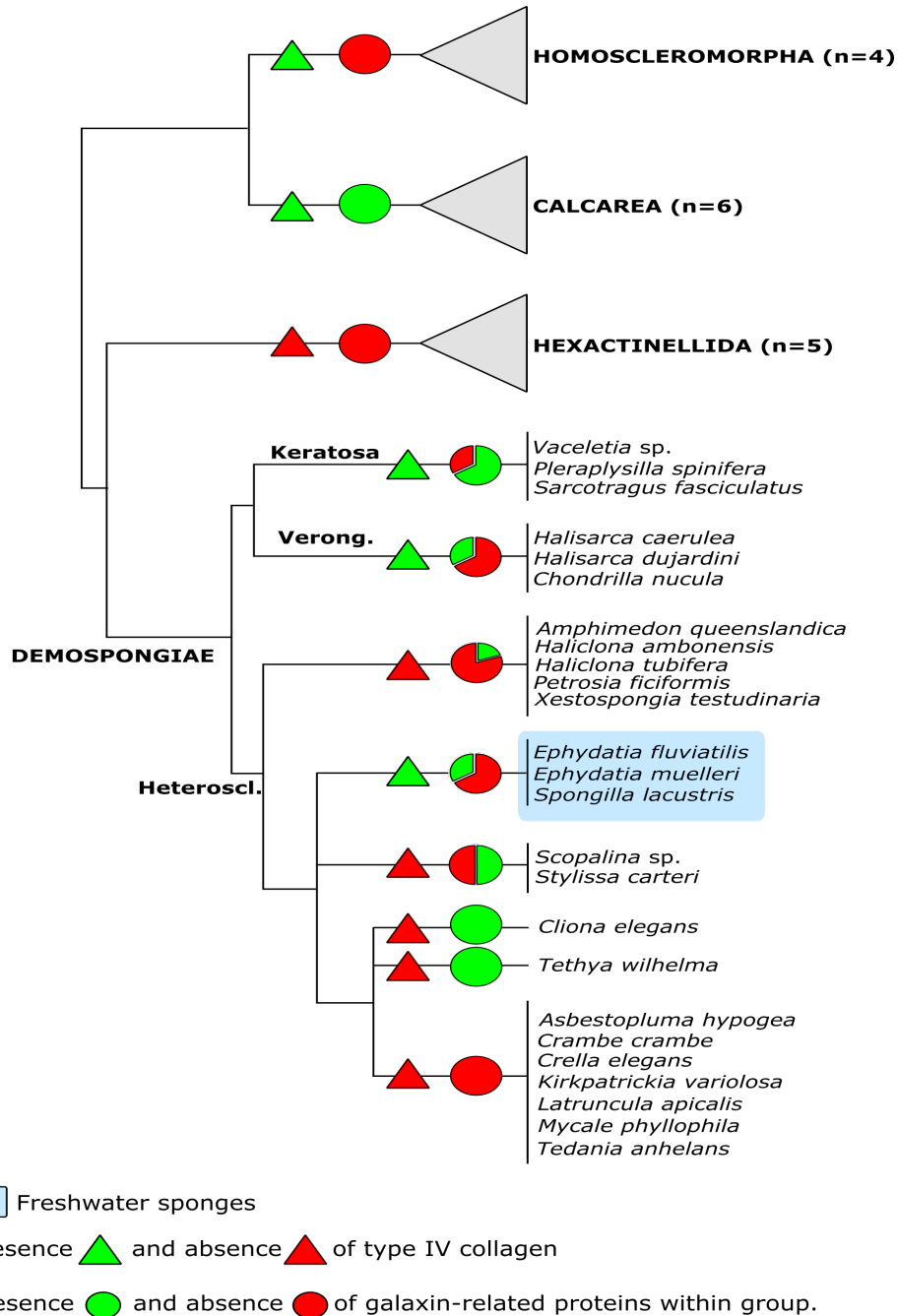


Figure 2.4: Presence-absence analysis of *type IV* collagen and galaxin-related proteins within Porifera. For galaxin-related proteins, data are presented as percentage of species within group in which one significant match (BLASTp, e-value $\leq 1e^{-10}$) was detected. When present, collagen IV was found in all species considered for a particular taxon. Phylogenetic relationships between sponge classes based on Simion et al. (2017). Phylogeny of Demospongiae based on Morrow and Cardenas (2015). Heteroscl., Heteroscleromorpha; Verong, Verongimorpha.

Both phylogenetic analysis resulted in monophyly of collagen IV for all three sponge classes in which the protein is present (supplementary figure S2.6a,S2.6b, Supplementary Material online). In one instance (MAFFT-based phylogeny), support for monophyly of Porifera was also retrieved.

2.5 Discussion

A common feature of skeletal proteomes is the presence of both taxonomically widespread proteins with homologs in other, not necessarily calcifying, organisms and of lineagespecific innovations or TRGs (Ramos-Silva et al. 2013; Kocot et al. 2016). The diversity of evolutionary histories characterizing skeletogenic proteins, make phylogenetic analyses and gene distribution maps a necessary step to examine the evolution of biomineralization. Key to this is the need for extensive taxon sampling. Here, we data-mined available resources across nonbilaterian metazoans to examine the distribution of skeletogenic proteins, allowing comparative investigations of the genetic repertoires of diverse calcifying organisms, and produced detailed phylogenies for key components of coral biomineralization toolkits. As most of the information presented is based on transcriptomic data, the distribution patterns observed for the studied homologs may be underestimated due to transcriptome incompleteness. To mitigate possible sampling biases, and to reduce the impact of different sampling sizes across taxa, gene presence within a taxon was presented and discussed as relative abundance. Secondly, for several SOMP, evidence of indirect involvement in calcification is still lacking and a random incorporation in the skeleton cannot be excluded (Takeuchi et al. 2016). We therefore focus our discussion on proteins that is, acidic SOMP and galaxin for which proteomicindependent evidence for a role in skeleton formation is available (Reyes-Bermudez et al. 2009; Mass et al. 2017; Von Euw et al. 2017).

Distribution analysis reflected evolutionary heterogeneity, with homologs being present across phyla or restricted to selected families. Although a few coral skeletogenic proteins remain largely restricted taxonomically, increased taxon sampling resulted in the expansion of their taxonomic distribution. In these cases, the most common pattern was their presence across phyla, or limited to Cnidaria or Scleractinia, which does not support the involvement of these proteins in biomineralization across groups. SCRiP-3a and galaxin-related proteins are, however, potential targets for future (functional) research, because of their presence pattern (e.g., SCRiP-3a found among calcifying anthozoans only). The distribution of the latter within sponges is of particular interest as we show that these proteins are present in all calcifying species, regardless of their taxonomic position. Moreover, the presence of multiple potential galaxin homologs among calcifying Calcarea and their absence among homoscleromorphs and glass sponges, supports their potential involvement in calcium carbonate biomineralization. As for galaxin-related proteins, collagen IV appears either ubiquitous or absent in different sponge classes, while a patchy distribution can be observed among groups of Demospongiae. Within Heteroscleromorpha presence of *type IV* collagen appears however, as previously hypothesized by Riesgo et al. (2014), associated with the freshwater environment, but among keratose sponges it could be related to the collagenous framework of their organic skeletons (Junqua et al. 1974; Germer et al. 2015). Scleractinian TRGs also exhibited a wider variety of distribution patterns, ranging from being present across both robust and complex corals down to small set of scleractinian families only (e.g., galaxin-2 and SAPs). The former are of particular interest for the evolution of corals. Although different time estimates have been put forward, the accepted consensus places the divergence of Complexa and Robusta in the Palaeozoic, prior to the (ca. 240 Ma) appearance of

fossil modern scleractinians in the early/mid-Triassic (Romano and Palumbi 1996; Stolarski et al. 2011; Chuang et al. 2017). The discovery of palaeozoic scleractinian-like fossils does support a Palaeozoic origin for the group, with consequent fossil gaps likely being caused by poor preservation or abiotic conditions hindering the deposition of skeletons (Stolarski et al. 2011). Whether a particular skeletogenic protein was available to the common ancestor of complex and robust scleractinian corals is thus of particular evolutionary interest as it allows to determine which components of the biomineralization toolkit preceded the Triassic appearance of the skeleton and whether putative palaeozoic scleractinians had access to the same molecular machinery currently employed by modern representatives of the group. In this regard, one biomineralization-related event that might have preceded the Complexa-Robusta divergence appears to be the expansion in the number of acidic residues within acidic proteins. The close phylogenetic relationship between P27 (*S. pistillata*) and B3EWY7 (*A. millepora*) which are best BLAST reciprocal hits supported by the high similarity in the location and structure of their acidic regions. Moreover, such increases in aspartic acid could not be observed within scleractinian total proteomes. This excludes the possibility of higher aspartic content representing a lineage-specific innovation, and supports it being a biomineralization-related event.

A similar scenario could also apply to galaxin *sensu stricto*. These proteins have been proposed to have been independently recruited by and within scleractinians families (e.g., Pocilloporidae, Bhattacharya et al. 2016), implying that the protein acquired its calcification-related role after the Complexa-Robusta split. However, the presence of representatives of both robust and complex corals within the galaxin *sensu stricto* clade described here points to an alternative scenario in which the recruitment of galaxin for biomineralization occurred only once, prior to the divergence of these clades. On the other hand, the relationship between *A. millepora* galaxin 1 and galaxin 2 remains uncertain due to the current lack of support in phylogenetic analyses. Despite this, phylogenetic analysis allows to confidently argue that the protein is present in the family Agariciidae and Acroporidae and it should be considered a true (*sensu stricto*) galaxin. One aspect that remains unsolved concerns the evolutionary history of galaxin *sensu stricto* outside Scleractinia. Extensive divergence between scleractinians and other cnidarians could have eroded the evolutionary signal in these proteins (Foret et al. 2010). Nevertheless, inability to obtain supported phylogenies for galaxin proteins might also be currently exacerbated by the inclusion of several, possibly functionally diverse, galaxin-related proteins in phylogenetic analyses. Similarity between galaxin *sensu stricto* and other galaxin-related proteins is often low and restricted to di-cysteine motifs (personal observations). Combined with the current lack of additional defining features for galaxins, this complicates BLAST-based homolog selection which can lead to the inclusion of unrelated proteins within protein data sets in phylogenetic analyses. Although our analysis is not immune to these limitations, expanding homolog selection beyond best-matches only helped to identify putative erroneous inclusions. An example described here is the *Fungia scutaria* protein 6662. When a galaxin *sensu stricto* sequence is used as a query, this sequence is the only hit in *F. scutaria*. Including multiple galaxin BLAST matches per species did reveal however that the protein is instead a scleractinian galaxin-related protein. The presence of undetected galaxin-related proteins, erroneously considered genuine galaxin *sensu stricto* homologs, could thus explain the previously described galaxin polyphyly (Bhattacharya et al. 2016).

Finally, in contrast to scleractinians, octocoral TRGs were found conserved across soft-coral taxa showing similar distributions. Although the number of calcification-related genes in soft corals is currently extremely limited, intra-Octocorallia analyses are of potential interest, as they might allow for the identification of differences between calcite and aragonite-depositing species, and similarities between

aragonitic animals within Anthozoa (i.e., *H. coerulea* and Scleractinia). The presence of TRGs (such as scleritin) in species belonging to all the three major octocoral clades (McFadden et al. 2006), indicates that TRGs, although restricted to octocorals, were present in the common ancestor of the subclass. On one hand, this points toward a certain degree of commonality in spite of the different biomineralization strategies (calcite vs. aragonite). On the other hand, it could be related to scenarios in which, as galaxin *sensu stricto* (Foret et al. 2010), the protein played a different ancestral function with subsequent lineage specific recruitment events for biomineralization.

Here, we conducted a distribution and phylogenetic analysis of coral biomineralization genes to provide a comprehensive homolog mapping and fine-scaled phylogenies of selected genes. Through a relatively broad taxon sampling, our work allowed us to detect similarities and differences between different taxonomic groups and investigate patterns of protein presence/absence associated with skeleton polymorph. This led to the postulation of a single recruitment for calcification of galaxin *sensu stricto* and provided a detailed phylogeny of coral acidic proteins that revealed the increase of acidic residues during cnidarian evolution. We also provide insights into the evolution of proteins likely involved in biomineralization, such as sponge collagen IV. With the inclusion of four new octocoral transcriptomes, we have closed the existing taxon bias toward certain cnidarian taxa, specifically scleractinian corals, however gaps still exist. For instance, groups like calcifying hydrozoans remain unexplored and their inclusion in future studies on biomineralization will certainly contribute to our understanding of this process in Cnidaria. Proteomic investigations of the SOM of calcifying cnidarians other than scleractinian corals and of sponges might reveal the presence of shared skeleton components adding support to the transcriptomic presence patterns described here, and will help discover lineage-specific innovations linked to calcification in these groups.

Chapter 3

Comparative proteomics of octocoral and scleractinian skeletons and the evolution of coral calcification.

3.1 Abstract

Corals are ecosystem engineers of the coral reefs, one of the most biodiverse but severely threatened marine ecosystems. The ability of corals to form the three dimensional structure of reefs depends on the precipitation of calcium carbonate under biological control. However, the exact mechanisms underlying this biologically controlled biomineralization remain to be fully unelucidated, for example whether corals employ a different molecular machinery for the deposition of different calcium carbonate (CaCO_3) polymorphs (i.e., aragonite or calcite). Here we used tandem mass spectrometry (MS/MS) to compare skeletogenic proteins, i.e., the proteins occluded in the skeleton of three octocoral and one scleractinian species: *Tubipora musica* and *Sinularia cf. cruciata*, both forming calcite sclerites, the blue coral *Helipora coerulea* with an aragonitic rigid skeleton, and the scleractinian aragonitic *Montipora digitata*. We observed extremely low overlap between aragonitic and calcitic species, while a core set of proteins is shared between octocorals producing calcite sclerites. However, the same carbonic anhydrase (CruCA4) is employed for the formation of skeletons of both polymorphs. Similarities could also be observed between octocorals and scleractinians, including the presence of a galaxin-like protein. Additionally, as in scleractinians, some octocoral skeletogenic proteins, such as acidic proteins and scleritin, appear to have been secondarily co-opted for calcification and likely derive from proteins playing different extracellular functions. In *H. coerulea*, co-option was characterized by aspartic acid-enrichment of proteins. This work represents the first attempt to identify the molecular basis underlying coral skeleton polymorph diversity, providing several new research targets and enabling both future functional and evolutionary studies aimed at elucidating the origin and evolution of biomineralization in corals.

3.2 Introduction

The capacity of animals to actively control the deposition of mineral skeletons has been a long debated topic, with different models of calcification being proposed over the years. In the *organic matrix mediated* (Lowenstam 1981) or *'biologically controlled'* (Mann 1983) scenario, an animal employs sets of macromolecules to guide the deposition of its mineral skeletal structures. In line with this, several biomineralization-related processes including crystal nucleation and growth (Liu et al. 2012; Wheeler et al. 1981; Mitterer 1978; Von Euw et al. 2017), or the induction of a given calcium carbonate (CaCO_3) polymorph (i.e. aragonite and calcite) (Amos et al. 2010; Falini et al. 1996; Goffredo et al. 2011; Rahman et al. 2011) appear to be regulated by proteins included in the skeleton organic matrix (OM): a diverse array of proteins, polysaccharides (Goldberg 2001; Naggi et al. 2018), and lipids (Farre & Dauphin 2009; Farre et al. 2010) occluded within the mineral fraction of the skeleton. Over the last few years, advances in proteomic research have enabled the simultaneous characterizations of several OM proteins in different groups of marine calcifying invertebrates, including molluscs (Marie et al. 2010, 2013; Mann & Jackson 2014), corals (Drake et al. 2013; Ramos-Silva et al. 2013; Takeuchi et al. 2016), brachiopods (Jackson et al. 2015) and echinoderms (Mann et al. 2008; Flores & Livingston 2017; Flores et al. 2016). These studies showed that invertebrate skeletal proteomes include varying fractions of novel proteins - producing no significant matches against DNA sequence databases - and do exhibit contrasting rates of conservation between and within lineages. For instance, about 40% of the skeletal proteome is shared among echinoderms (Flores & Livingston 2017), while in molluscs the fraction of shared proteins is only about 10% (Kocot et al. 2016). Although a core set of proteins appears to be conserved across molluscs, irrespective of the morphological features of the shell (Arivalagan et al. 2017), the occurrence of both aragonite and calcite layers within the shell allowed Marie et al. (2012) to compare skeleton organic matrix proteins (SOMPs) associated with different CaCO_3 polymorphs. The different proteins specifically associated with the aragonitic or calcitic shell layers suggest that molluscs may use different molecular mechanisms for the deposition of these structures (Marie et al. 2012). In corals (class Anthozoa, phylum Cnidaria), putative relationships between structural characteristics of the skeleton, like its CaCO_3 polymorph, and the molecular machinery employed for its formation, have hitherto only been marginally addressed, although some skeletogenic coral proteins have been suggested to drive the in vitro crystallization of specific calcium carbonate polymorphs (Goffredo et al. 2011; Rahman et al. 2011). However, no study to date has leveraged mass spectrometry-based protein discovery methods to characterize and compare skeletal proteomes across corals that exhibit different biomineralization strategies, i.e., those that produce aragonite vs. those that produce calcite. CaCO_3 skeleton-producing anthozoan corals belong in two different clades, namely the order Scleractinia (stony corals; subclass Hexacorallia) and in the subclass Octocorallia (soft corals). As major contributors to CaCO_3 deposition, scleractinians have been the focus of extensive biomineralization-related research, and skeletogenic proteomes have been characterized for different scleractinian species (Drake et al. 2013; Ramos-Silva et al. 2013; Takeuchi et al. 2016). However, the uniformity in biomineralization strategies (i.e., aragonitic exoskeleton) present among scleractinians makes this group inappropriate to investigate the biological regulation of skeletal polymorph deposition and its evolution. On the contrary, the occurrence within Octocorallia of both calcite and aragonite skeletons offers a unique opportunity to compare the skeletogenic repertoires associated with different skeletal structures and CaCO_3 polymorphs. Despite this, information on octocoral biomineralization-related proteins is extremely limited (but see Debreuil et al. (2012; 2011) and Rahman

et al. (2011)), and transcriptomic-proteomic coupled data is hitherto not available for this group. Here, we used tandem mass spectrometry (MS/MS) to characterize the skeletogenic proteome of three soft coral species exhibiting different skeleton morphologies and mineralogies: the leather coral *Sinularia* cf. *cruciata* and the pipe organ coral *Tubipora musica*, both characterized by the production of calcite sclerites, and the massive, aragonitic blue coral *Heliopora coerulea*. To compare skeletogenic repertoires between scleractinians and aragonitic octocorals, we additionally examined the proteome of the stony coral *Montipora digitata*. Our work represents the first study of skeleton diversity across and within anthozoan corals providing 1) the identification of several new coral biomineralization-related proteins, and 2) a comparative analysis examining putative relations between polymorph and type of skeletal structure, and the molecular machinery employed by corals for its formation.

2.3 Materials and Methods

3.3.1 Extraction of OM proteins

Samples of *T. musica*, *H. coerulea*, *Sinularia* cf. *cruciata* and *M. digitata*, cultured in research aquaria (closed artificial seawater systems) were bleached in 5% NaOCl (Sigma-Aldrich) for 72 hours to remove the tissue and other potential contaminants. They were subsequently rinsed several times with ultrapure water and oven-dried at 37°C. Clean skeletons were ground to powder with a mortar and pestle, and again bleached (5% NaClO solution for 5 hours), washed with ultrapure water and oven-dried at 37°C. The skeleton powder was decalcified with 10% acetic acid for 24 hours at room temperature on an orbital shaker. The decalcification solution was centrifuged (14,000 g, 30 min, 25°C) to separate the acid soluble (ASM) and insoluble (AIM) fractions. The obtained insoluble pellets were washed several times with ultrapure water, dried and stored at -80°C until further analysis. The supernatants (ASM) were desalted and concentrated using Amicon Ultrafiltration devices (15 ml, 3 kDa cut-off), and the ASM proteins were precipitated following the method described in Wessel and Flügge (1984). Briefly, four volumes of methanol, one of chloroform and three volumes of water were added to one volume of sample and the solution was centrifuged at 14,000 g for 20 min at 25°C. After centrifugation, the supernatant was discarded. Three volumes of methanol were added and the solution was centrifuged again. The resulting protein pellets were air-dried and stored at -80°C. For each species, two skeleton samples from the same colony were independently processed.

3.3.2 SDS-PAGE Analysis

ASM and AIM proteins were dissolved in 2X Laemmli buffer (95% buffer - 5% beta-mercaptoethanol) (BioRad). As observed by Ramos-Silva et al. (2013), AIM pellets were only partly dissolved. Samples were denatured for 2 minutes at 95°C and loaded on 12.5% polyacrylamide gels. SDS-PAGE was run on a BioRad MiniProtean Tetra Cell at constant voltage for ca. 70 minutes. Proteins were visualized after staining with ProteoSilver Silver Stain Kit (Sigma-Aldrich) (Supplementary Figure B1) with the Precision Plus Protein Dual Color Standards (BioRad) as a size marker.

3.3.3 Proteomic analysis

For mass spectrometry analysis, sample aliquots were loaded on a 12.5% acrylamide gel and run as described above. In an effort to reduce potential variability due to technical factors, we included replicates within the experimental design. These include triplicates for each OM fraction (soluble and insoluble) for each of the two per-species extractions. However, the presence of technical causes underlying the non-detection of SOMPs cannot be completely excluded. Three replicates per fraction per sample (n=6 per sample, n=12 per species) were excised from the gel and digested with trypsin prior to analysis on a Bruker Impact II Q-ToF mass spectrometer (Bruker Corp. Billerica, Massachusetts, USA) coupled with an Ultimate 3000 RSLC nano liquid chromatography (Thermo Fisher, Waltham, Massachusetts, USA). Peptide separation was performed using an Acclaim PepMap RSLC column with 75 μm diameter, 25 cm length, C18 particles of 2 μm diameter and 100 \AA pore size (Thermo Fisher, Waltham, Massachusetts, USA). Data were analyzed using MaxQuant 1.5.2.8 (Cox & Mann 2008). Common contaminants, potential symbiont and bacterial sequences were filtered and peptides were mapped against sequence datasets for the target species. Sample processing and mass spectrometry were performed by the MSBioLMU Unit at the Biology Department I of the Ludwig-Maximilians University in Munich (Germany). Sequences with at least two unique matching peptides were considered for downstream analysis.

3.3.4 Bioinformatic analysis of OM proteins

Identified OM proteins were annotated by Blastp (cut off e-value: $1e^{-10}$) against the NCBI non-redundant database. Distribution of homologs (S.Mat 1) of octocoral and *M. digitata* SOMPs was subsequently assessed within a set of cnidarian genomes and transcriptomes (Voolstra et al. 2015; Shinzato et al. 2011; Voolstra et al. 2017; Pralong et al. 2015; Jeon et al.; Liew et al. 2016) with Blastp applying the same search criteria described above. Presence of signal peptide, transmembrane regions, GPI-anchor was predicted with SignalP 4.0 (Petersen et al. 2011), TMHMM 2.0 (Krogh et al. 2001) and PredGPI (Pierleoni et al. 2008) respectively. Protein isoelectric point was determined with ProtParam (Gasteiger et al. 2005). The amino acid composition of the acidic proteins detected was computed with a custom script available at https://gitlab.lrz.de/palmuc/Concietal_proteomics_skeletomes. Relative amino acid frequencies and distribution of aspartate residues within acidic proteins were determined on sequences predicted as complete after removal of the signal peptide sequence. For the distribution of aspartate residues, a frequency table of the distance between aspartate residues within a protein was first computed. Median distance values and amino acid frequencies were then used to perform principal component analysis (PCA) of acidic proteins.

3.3.5 Phylogenetic Analyses

For phylogenetic inference, protein queries were blasted against a database of cnidarian sequences. The following e-value cutoffs were used: $1e^{-05}$ (scleritin), $1e^{-20}$ (carbonic anhydrase) and $1e^{-50}$ (hephaestin-like). Sequences predicted as 'internal' (i.e. lacking both 3' and 5' ends) by TransDecoder were discarded and a minimum length filter of 250 and 600 residues was applied to significant hits for carbonic anhydrase (CA) and hephaestin-like, respectively. For the former, sponge and human sequences used in Voigt et al. (2014) were added to the dataset. Carbonic anhydrases from the green algae *Chlamydomonas reinhardtii* (P20507) and *Desmodesmus* sp. (AOL92959.1) were used as outgroup. Sequences were aligned with both MUSCLE (Edgar 2004) and MAFFT (Katoh & Standley 2013), and best-fit models

were estimated with Prottest 3.4 (Darriba et al. 2011). Maximum-Likelihood Analysis was performed in Seaview 4 (Gouy et al. 2010) using PhyML 3.1 (Guindon & Gascuel 2003), while MrBayes 3.2 was used for bayesian inferences. Trees were sampled every 100th generation (nrns=2) and burn-in fraction for each analysis was determined after visual inspection of the trace files using Trace v1.6 (available at <http://tree.bio.ed.ac.uk/software/tracer>). All alignments, trees, and protein sequences used for phylogenetic analyses are available at https://gitlab.lrz.de/palmuc/Concietal_proteomics_skeletons.

3.4 Results

3.4.1 Shared and species-specific components of the anthozoan skeleton

The discovery and subsequent annotation of anthozoan skeleton organic matrix proteins (SOMPs) retrieved between 12 and 54 proteins, with low protein numbers shared between octocoral species. However, simultaneously small sets of skeletogenic proteins shared between organisms at different taxonomic levels were identified (Figure B1). These included instances of proteins being secreted in the skeleton of both scleractinians and octocorals. The aragonitic octocoral *H. coerulea* did not exhibit higher similarity to aragonitic scleractinians compared to calcitic soft corals, suggesting that the CaCO_3 polymorph had no noticeable effect on skeleton conservation between groups.

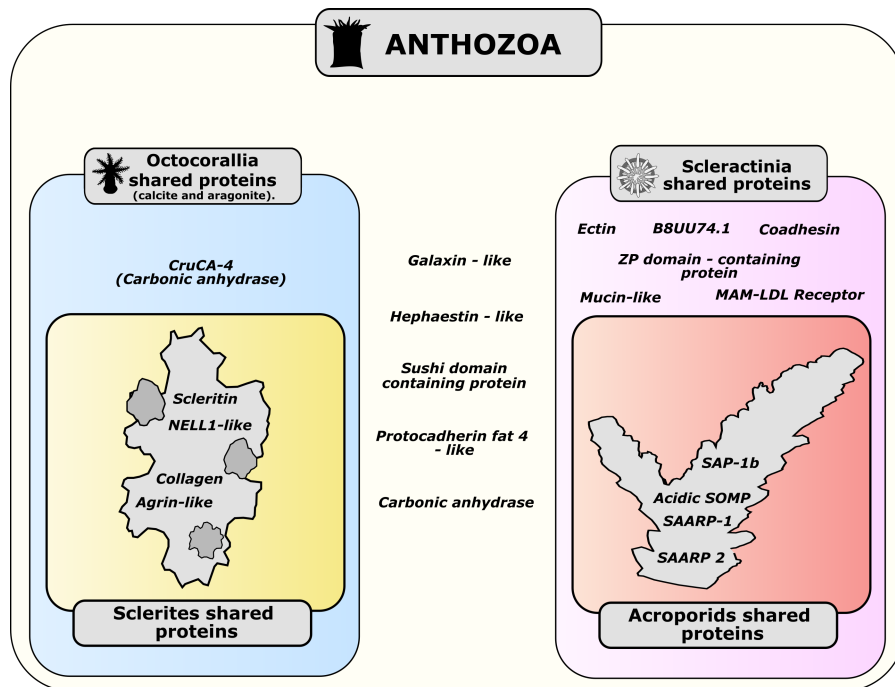


Figure 3.1: Overview of shared skeleton proteins across Anthozoa. Alcyonacea includes the proteomes of *T. musica* (this study) and *S. cf. cruciata* (this study). Calcitic octocorals: Alcyonacea + involvement of scleritin in *C. rubrum* (Debreuil et al. (2012)). Octocorallia: Alcyonacea + *H. coerulea* (this study) + involvement of CruCA4 in *C. rubrum* (Le Goff et al. (2016)). Acroporiidae: proteomes of *M. digitata* (this study) + *A. digitifera* (Takeuchi et al. (2016) + *A. millepora* (Ramos-Silva et al. (2013)). Scleractinia: Acroporidae + proteome of *S. pistillata* (Drake et al. 2013)..

Common to all four species analyzed is a Sushi-domain containing-like protein also containing NIDO (IPR003886), AMOP (IPR005533) and Von Willebrand factor D (IPR001846) domains. This same arrangement is present in the mucin-like B3EWY9 found in the *A. millepora* SOMP, and the proteins identified in this study also share local similarity with protein P13 from the skeleton of *S. pistillata*. Other proteins secreted in both scleractinian and octocoral skeletons include a putative homolog of galaxin, a hephaestin-like multicopper oxidase (MCO), one cell adhesion protocadherin Fat 4-like protein, and carbonic anhydrases. The first one, galaxin, was detected in the sclerites of *T. musica* (TR44621—c0.g1.i1) and we named it octogalaxin-1. In addition to the characteristic presence of multiple di-cysteine motifs, this protein is - as in scleractinians - predicted to be secreted and the signal peptide is followed by a R-X-R-R endoprotease target motif (Fukuda et al. 2003). The multicopper oxidase was found in *S. cf. cruciata* (TR42435—c0.g1.i1) and the protocadherin-like proteins were identified in the skeleton of *H. coerulea* (DN66065.c0.g1.i4). Although our comparative analysis of octocoral skeletal proteomes did not find evidence of a conserved octocoral biomineralization toolkit, we found homologs of *Corallium rubrum*'s carbonic anhydrase CruCA-4 (Le Goff et al. 2016) in both aragonitic and calcitic species. One CruCA4 homolog was found in *S. cf. cruciata*, while in the aragonitic blue coral two homologs of CruCA4 were detected. As reported for *C. rubrum* (Le Goff et al. 2016; Del Prete et al. 2017), the histidine residue involved in the proton transfer is not conserved in all other homologs of the protein (Supplementary Figure SB2). Mutation of the His64 residues have been linked to decreases in efficiency (Vullo et al. 2008). Additionally, one of the two *H. coerulea* carbonic anhydrases (DN64689.c5.g1.i4) is predicted to be an acatalytic carbonic anhydrase-related protein (Supplementary Figure SB2). Four additional proteins are present in the sclerites of both calcitic octocorals analyzed and they represent best reciprocal hits between the two species. This sclerite toolkit includes 1) scleritin, 2) an agrin-like protein consisting of repeated Kazal domains (IPR036058) and one C-terminal WAP (IPR008197) domain, 3) a kinase C-binding, NELL1-like protein and 4) one collagen alpha-chain like protein. Two scleritin-like sequences (TR40200—c16.g1.i1 and TR42410—c0.g2.i1) were detected in *T. musica*, while only one match was produced in *Sinularia*. Agrin is a glycoprotein which in humans participates in cell-matrix interactions (Groffen et al. 1998), and agrin-like protease inhibitors have been recently found in the skeleton of the seastar *Patiria miniata* (Flores & Livingston 2017). NELL-1 is, on the other hand, involved in bone formation in vertebrates (Aghaloo et al. 2007; Zou et al. 2011). The NELL1-like protein identified here also exhibit local similarity to P32 (kielin-like), a secreted protein found in the skeleton of *S. pistillata* (Drake et al. 2013).

In the scleractinian *M. digitata*, with the exception of the secreted acidic protein SAP-1a, we retrieved the entire acidic protein repertoire previously isolated from the skeletons of *A. millepora* and *A. digitifera* (Ramos-Silva et al. 2013; Takeuchi et al. 2016). This includes both secreted aspartic acid-rich proteins SAARP-1 and SAARP-2, the acidic secreted organic matrix protein B3EWY7 and the secreted acidic protein SAP-1b. In addition, putative orthologs for *A. millepora* mucin-like (B3EWY9), coadhesin-like (B3EWZ3.1) and carbonic anhydrase (B8V7P3.1) were also present. Of note is the presence in *M. digitata* of a lithostatine-like protein containing a c-type lectin domain. The presence of this domain is a common feature for skeletogenic proteins in several marine invertebrates, such as mollusks (Mann et al. 2000; Matsubara et al. 2008; Weiss et al. 2000), see Sarashima et al. (2006) for a review), and birds (Mann & Siedler 2004, 2006). SOMPs with sequence similarity to lithostatin and c-type lectin-like proteins have been characterized from the skeletons of echinoderms (Wilt 2002) but have to our knowledge not been reported in corals to date.

3.4.2 Similarity between scleractinian and octocoral acidic proteins.

Two acidic proteins (DN60904_c0.g1.i1 and DN65627_c8.g3.i2) were detected in the organic matrix of *H. coerulea* and one in *T. musica* (TR43768—c0.g2.i1). Both do not currently match any published sequence available in public databases (Blastp e-value cut-off: $1e^{-05}$) outside of Octocorallia. As for scleractinians acidic SOMPs, homologs of *H. coerulea* acidic protein 1 exhibit higher isoelectric points which are related to lower aspartic acid contents. In an effort to investigate sequence similarities between octocoral and scleractinian acidic SOMPs and their non-acidic homologs in a phylogenetic independent way, we conducted a PCA analysis based on sequence amino acid composition and the distribution (i.e. median distance) of aspartate residues along the sequence (Figure B2).

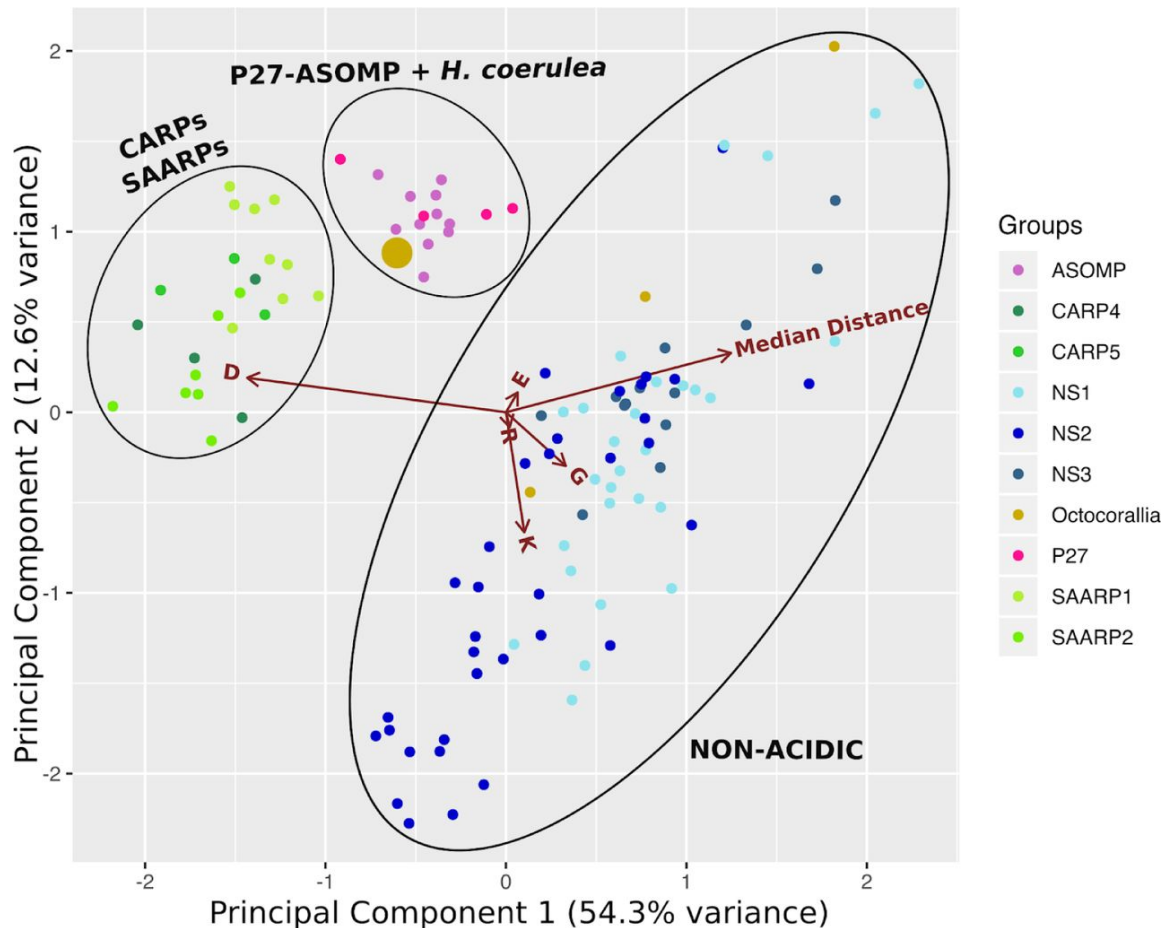


Figure 3.2: Principal component analysis (PCA) of anthozoan acidic SOMPs and their non-acidic homologs. PCA based on protein amino-acid composition and distribution - as median distance between residues - of aspartic acid along each sequence. Numbering of non-skeletogenic (NS) groups based on Conci et al. (2019). Only the 5 most contributing variables are displayed. Large golden circle: *H. coerulea* acidic protein-1 (DN60904_c0.g1.i1). Small golden circles: putative non-acidic homologs of *H. coerulea* acidic protein-1.

Despite not displaying significant similarity to scleractinian sequences, *H. coerulea* acidic protein-1 grouped together with the scleractinian acidic protein ASOMP-P27 (Ramos-Silva et al. 2013; Drake et al. 2013; Conci et al. 2019). Main sequence features contributing to the clustering patterns observed are similarities in aspartic acid content and distribution within the protein sequence. Non-acidic homologs of *H. coerulea* acidic protein-1 clustered with other non-acidic proteins. Apart from exhibiting lower aspartate contents, proteins within this group appear characterized by a higher lysine and glycine content compared to their acidic putative homologs.

3.4.3 Evolutionary history of octocoral and scleractinian SOMPs.

To further explore the evolutionary history of octocoral and scleractinian SOMPs we conducted phylogenetic analyses of protein sequences derived from the skeletome for scleritin, multicopper oxidases and carbonic anhydrases. Information on scleritin secretion into octocoral skeletons was integrated with previously estimated scleritin presence-absence data (Figure B3a). Phylogenetic analysis split scleritin homologs into two distinct and well supported clades (Figure B3b). The three sequences identified in *T. musica* and *S. cf. cruciata* grouped together with the scleritin originally described in *C. rubrum* by Debreuil et al. (2012), alongside all other scleritin homologs found in octocoral species characterized by the presence of calcitic sclerites (Figure B3a).

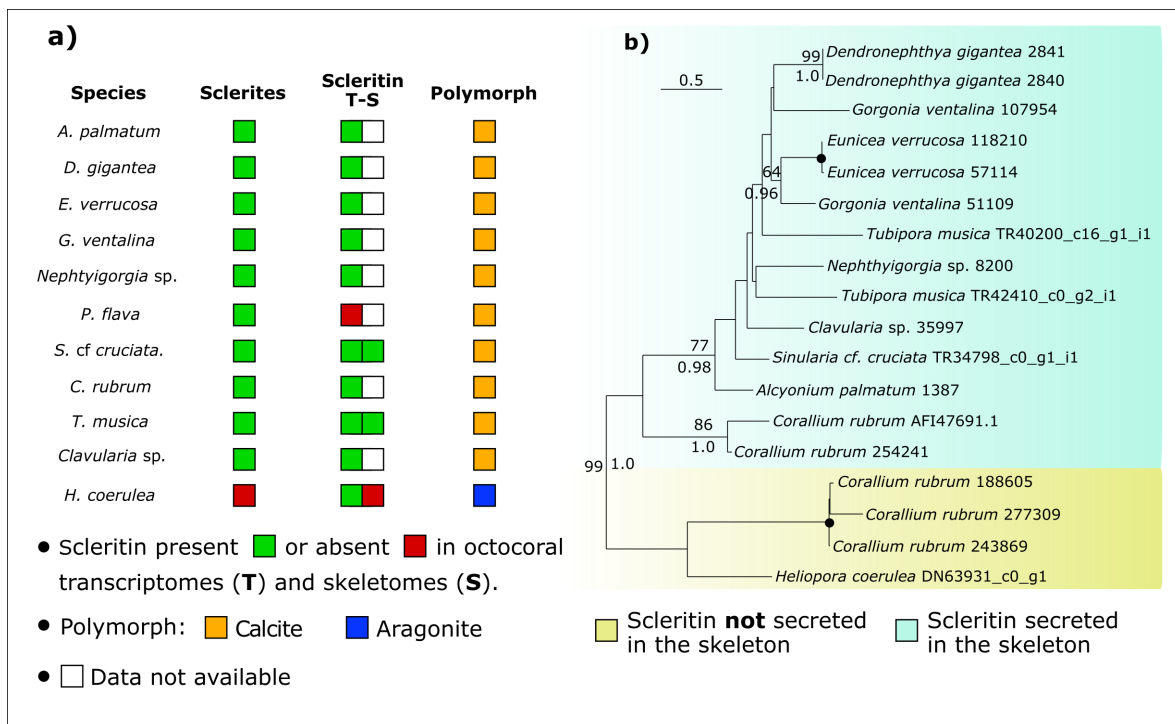


Figure 3.3: a) Presence-absence of scleritin in octocoral skeletomes in relation to skeletal structures. b) Phylogenetic analysis of scleritin. Protein sequences were aligned with MUSCLE and Maximum-Likelihood analysis (400 replicated) was done with Seaview 4. Bayesian analysis was performed with MrBayes 3.2. Black dot on node indicates full support (100% bootstrap value and 1.0 posterior probability). Involvement of scleritin in *C. rubrum* biomineralization based on (Debreuil et al. 2012). Phylogeny based on MAFFT aligning algorithm in Supplementary Figure SB3.

We, therefore, referred to this clade as skeletogenic since all the scleritin sequences implicated to date in octocoral biomineralization are comprised within it. A second group, termed 'non-skeletogenic' includes the scleritin-like protein expressed in the tissues but not found occluded in the skeleton of *H. coerulea*, and three other putative scleritin homologs found in *C. rubrum*.

To infer a phylogenetic tree for hephaestin-like proteins, putative homologs were searched across Cnidaria using the three multicopper oxidases described in Takeuchi et al (2016) as query. Each query protein formed a different clade populated by scleractinian and corallimorph sequences (Figure B4, Supplementary Figure SB4). Proteins present in scleractinian skeletons all grouped within clade 1.

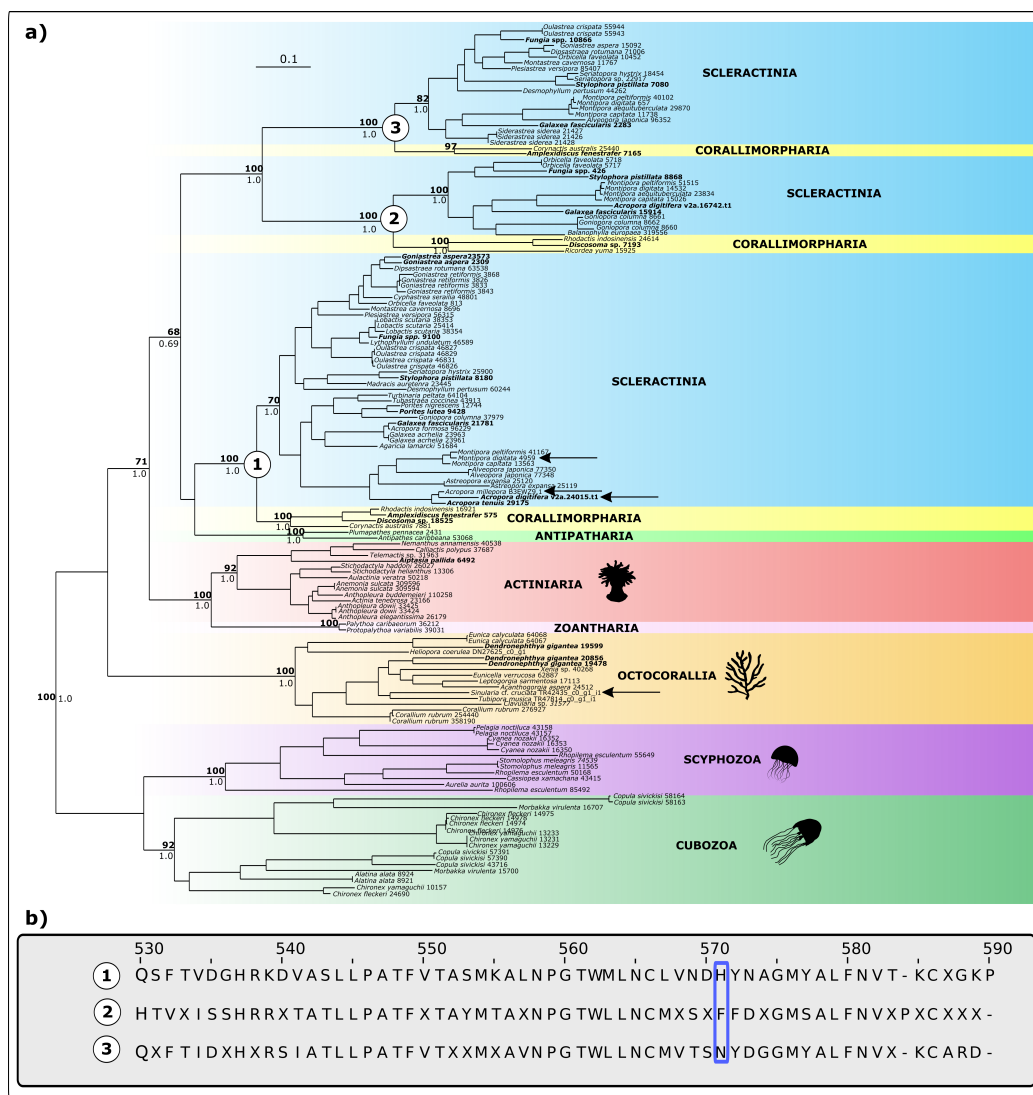


Figure 3.4: a) Phylogenetic analysis (400 bootstrap replicates) of cnidarian multicopper oxidases (MCOs). Aligning algorithm: MAFFT. Best-fit model: WAG+G+I. Number on nodes: bootstrap support and posterior probability values. Support values in bold: node supported (> 50) in MUSCLE-based phylogeny (Supplementary Figure SB4). b) Section of multiple consensus (60%) sequences alignment for the three corallimorph + scleractinian clades. Blue box highlights the absence of the type-I copper binding histidine in clades 2 and 3. Histidine classification based on Takeuchi et al. (2016).

All other cnidarian taxa formed well-supported monophyletic groups. Homologs identified in black corals (Antipatharia) grouped within clade 1 but with low support. Analysis of the consensus sequence alignment shows that one of the histidines involved in copper binding is not present in hephaestin-like proteins from clade 2 and 3, while all copper-binding residues listed in Takeuchi et al. (2016) are conserved across clade 1 and all other cnidarian groups, including octocorals and the protein secreted in the sclerites of *S. cf. cruciata*.

Finally, all homologs of the carbonic anhydrase CruCA4 occupied the same clade (Figure B5, Supplementary Figure SB5). This group also included the *H. coerulea* CA-related protein we found in the skeleton of this species. Scleractinian biomineralization related CAs did, on the other hand, split into three distinct groups.

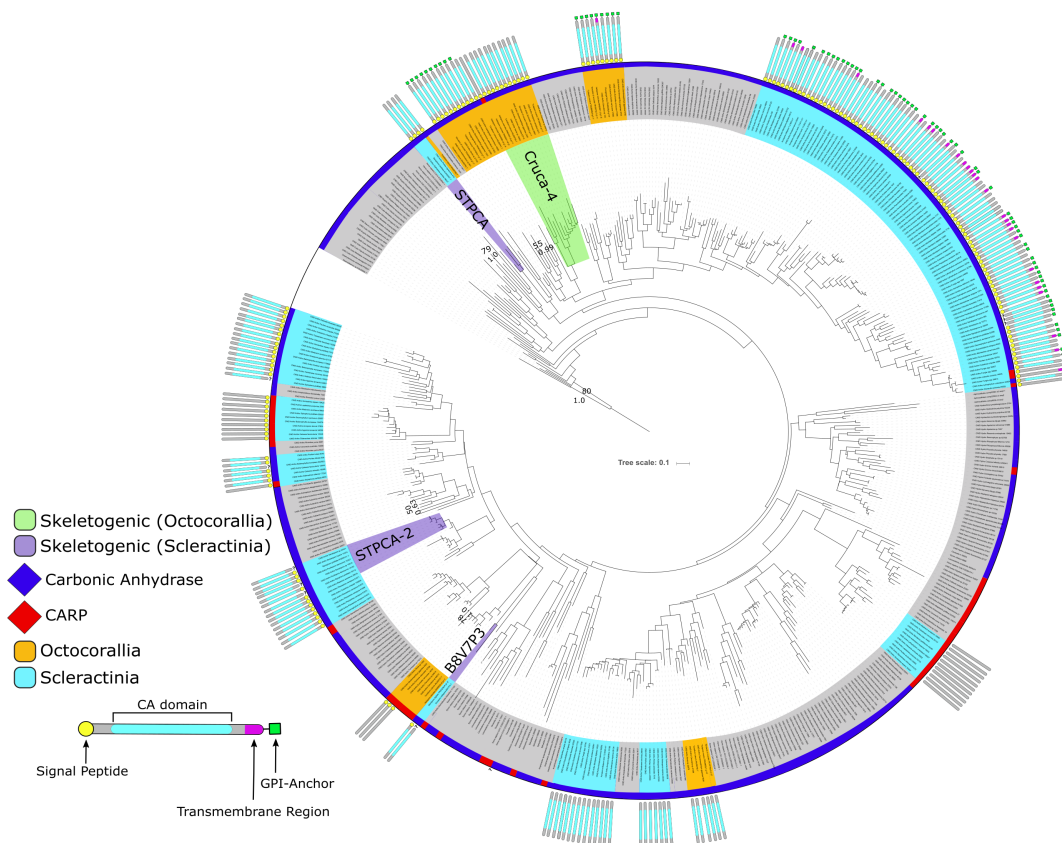


Figure 3.5: Maximum-likelihood analysis (400 bootstrap replicates) of cnidarian carbonic anhydrases and carbonic anhydrases related proteins (CARPs). Sequences aligned with MAFFT. MUSCLE-based phylogeny in Supplementary Figure B5. Best-fit model: WAG+G+I. Involvement of CruCA4, STPCA, STPCA-2 and B8V7P3 based on Le Goff et al. (2016), Moya et al. (2008), Bertucci et al. (2011) and Ramos-Silva et al. (2013) respectively. Other taxa include: *Homo sapiens*, Porifera, Cubozoa, Hydrozoa, Staurozoa, Scyphozoa, Ceriantharia, Actiniaria, Corallimorpharia. Outgroup: *Chlamydomonas reinhardtii* (P20507) and *Desmodemus* sp. (AOL92959.1)

3.5 Discussion

Determining which morpho-mineralogical features of coral skeletons are biologically controlled, and which result from environmental effects, remains a key unresolved aspect of coral biomineralization. Here we exploited the co-presence of aragonite and calcite-forming species within Octocorallia, a unique feature among Anthozoa. We provide a first insight into the diversity of proteins occluded within the coral's CaCO₃ skeleton, i.e., the skeleton, of species employing different calcification strategies. The identification of several octocoral skeleton organic matrix proteins (SOMPs), in addition to providing new targets for follow up research, also allowed to perform comparative analyses with previously published and the newly characterized *M. digitata* proteome. Our work represents the first examination of the diversity of skeletogenic toolkits across Anthozoa and its relation to the variety of biomineralization strategies displayed by this group.

We have reported low overall proteome overlap, while simultaneously highlighting instances of skeletogenic proteins shared both between and within scleractinians and octocorals. Among these, some proteins are associated with skeleton organic matrices occluded in both aragonitic and calcitic skeletons. Protein presence in the skeleton does not automatically constitute evidence for involvement in biomineralization, as random incorporation within the mineral fraction cannot be excluded. Nevertheless, for different SOMPs present in different groups, proteomic-independent information is available, including, among others, galaxins (Reyes-Bermudez et al. 2009) and carbonic anhydrases (Tambut et al. 2006; Le Goff et al. 2016). This also applies to aspartic acid-rich proteins, on which extensive research has been conducted (Mass et al. 2013, 2016; Von Euw et al. 2017). Thus the acidic proteins found in *H. coerulea* and *T. musica* could be potential key players in the formation of octocoral skeletons and represent interesting targets for future functional investigations. For other proteins, its presence in the skeleton may not be directly linked to mineral deposition, while still be necessary for the calcification process. For instance, protease inhibitors such as the agrin-like proteins found here in octocoral sclerites are common components of skeleton matrices where they likely prevent matrix degradation caused by different proteases (Marie et al. 2010). Also, the hephaestin-like proteins found here in octocoral sclerites could serve as deposits for toxic metals, as proposed for scleractinian skeletons (Ramos-Silva et al. 2013). Alternatively, this could also be linked to ultraviolet radiation absorbance of Fe³⁺ and the capacity of the skeleton to serve as an anti-UV defense structure (Reef et al. 2009). Therefore, although not related to biomineralization, the presence of the same protein in sclerites suggests that octocoral skeletal structures might be employed for functions similar to those found among scleractinians. On the other hand, caution has to be exercised when discussing differences between species due to protein absences as the interpretation of protein absences in proteomic data is affected by multiple factors linked to both sample characteristics and sample processing (Chandramouli & Qian 2009; Michalski et al. 2011; Feist & Hummon 2015) that can reduce the detectability of peptides during mass spectrometry. In light of the above, we focused our results and their interpretation on the presence of coral SOMPs for which proteomic-independent information is available.

Of particular interest, is the secretion of octo-galaxin 1 in the sclerites of octocorals. This represents, to our knowledge, the first report of a galaxin-related protein in anthozoan calcitic skeletons. Phylogenetic analyses of galaxin-related proteins (Bhattacharya et al. 2016) suggest that these proteins are polyphyletic in anthozoans, which in turn suggests that octocoral and scleractinian galaxins represent an instance of convergent evolution. Nevertheless, the fact that only *T. musica*'s octo-galaxin 1 possess

the endoprotease target motif, characteristic of scleractinian skeletogenic galaxins (Fukuda et al. 2003), and that the observed polyphyly within galaxin phylogenies are likely affected by the inclusion of false homologs, sensitivity to analytical parameters, and aligning algorithms (Conci et al. 2019) makes it difficult to rule out the hypothesis of an ancient, biomineralization-related recruitment of (octo)galaxins prior to the divergence of octocorals from the remaining Anthozoa. Similarity in protein features between galaxins *sensu stricto* (see Conci et al. 2019) and galaxin-like proteins, combined with the current lack of support for the deep phylogenetic relationships among these proteins, make understanding the evolution of galaxins difficult and future studies should attempt to provide robust phylogenies for these proteins in order to assess whether their recruitment for biomineralization in Anthozoa is ancient or convergent.

In addition to the presence of homologous skeletogenic components in the skeleton of scleractinians and octocorals, biomineralization in the latter appears to be characterized by evolutionary processes previously proposed for scleractinians, like the enrichment of aspartic acid residues within non-acidic proteins (Takeuchi et al. 2016; Bhattacharya et al. 2016) and the recruitment for calcification of proteins with diverse ancestral biological functions. As for scleractinian galaxin (Fort et al. 2010), the ubiquitous expression of scleritin homologs across Octocorallia, and its restricted presence in the skeleton of sclerite-forming species suggests a different ancestral function for this protein and a subsequent recruitment for calcification, consistent with the hypothesis of a biomineralization-related recruitment of galaxins for biomineralization in octocorals. Although genomic data remains essential to assess and compare scleritin repertoires in soft corals, the presence of multiple scleritin homologs in *C. rubrum* and *T. musica* reported here points to a gene expansion of scleritins in species forming sclerites. The extent and taxonomic distribution of these expansions, as well as their evolutionary dynamics, remain to be determined once a better sampling of octocoral genomes is available.

While CaCO₃ polymorph and biomineralization strategy do appear to be correlated with presence/absence patterns of some octocoral skeletogenic proteins, the involvement of CruCA4 in octocoral calcification appears independent of these factors. The current lack of support for deep divergence events during the evolutionary history of Octocorallia does not allow us to provide time estimates for the involvement of CruCA4 in mineralization in octocorals. Efforts to resolve deep divergences in Octocorallia are currently hampered by several factors including rapid radiation (McFadden et al. 2006), slow mitochondrial evolution and inconsistent results between nuclear and mitochondrial markers (see McFadden et al. (2010) for review). The last comprehensive phylogenetic analysis of the subclass split the group into three major clades (McFadden et al. 2006). Species from the genera *Sinularia* and *Tubipora* grouped within the same group, while *Corallium* and *Heliopora* species were included in the other two clades indicating that CruCA4 function as a skeletogenic protein in species belonging to all major octocoral clades and that its involvement in calcification occurred very early on in the evolutionary history of the group.

Finally, within scleractinians, proteomic characterization of the *M. digitata* OM found several putative orthologs of *A. millepora* skeletogenic proteins being secreted into the skeleton. These include acidic proteins from both the SAARP and SAP families and the acidic SOMP B3EWY7. Although the number of shared proteins represent less than a quarter of the overall *A. millepora* skeleton proteome - a sensibly lower percentage than the one between *A. millepora* and *A. digitifera* - these proteins account for nearly 90% of the peptides detected by mass spectrometry in *A. millepora*. This suggests that all major components of the acroporid toolkit have been successfully retrieved in *M. digitata*, highlighting a high degree of conservation of the skeleton of Acroporidae despite a low fraction of proteins being shared. The discovery and description of skeletogenic proteins represents one of the first essential steps to

study biological control in animal biomineralization. Here we have applied a proteomics-based approach to identify and characterize the skeletal proteome of different coral species, covering the diversity of calcification strategies displayed across Anthozoa. In addition to contributing new evolutionary insights on coral biomineralization, this work provides several new targets for future functional investigations. The new data availability for both calcite and aragonite-forming octocoral species is of particular interest, as it opens up the possibility for *in vivo* investigations on biological control over CaCO_3 polymorph in corals.

Chapter 4

Molecular and mineral responses of calcifying anthozoans grown in an artificial Calcite Sea.

4.1 Abstract

The formation of skeletal structures composed of different calcium carbonate polymorphs (aragonite and calcite) is regulated both biologically and environmentally. By promoting the formation of aragonite or calcite, changes in environmental conditions - primarily in the molar ratio of magnesium and calcium ($m\text{Mg}:m\text{Ca}$) during so-called Calcite (below 2) or Aragonite (above 2) seas - have had profound impacts on the distribution and performance of marine calcifiers throughout the Earth's history. Nonetheless, the fossil record shows that some species appear to have counteracted such changes and kept their skeleton polymorph unaltered. Here we exposed the aragonitic octocoral *Heliopora coerulea* and the scleractinian *Montipora digitata* to Calcite Sea-like $m\text{Mg}:m\text{Ca}$ with various levels of changes in magnesium and calcium concentration and monitored both mineralogical (i.e., CaCO_3 polymorph) and gene expression changes. The two species exhibited different responses: *H. coerulea* maintained its skeleton polymorph unaltered, while *M. digitata* presented considerable amounts of calcite under $m\text{Mg}:m\text{Ca}$ of 1.5. Expression of skeleton organic fraction (organic matrix) components, such as acidic proteins and galaxins, remained substantially unaltered. In *H. coerulea*, overexpression of calcium channels highlighted the presence of a coping response to changes in seawater calcium concentration. Although several differentially expressed genes remain uncharacterized. Our results suggest that control over skeleton polymorph is potentially related to the regulation of ion supply and concentration rather than direct interaction between skeletogenic proteins and the mineral phase.

4.2 Introduction

The ability to biologically control the biomineralization process is a common feature of many organisms forming mineral structures. In corals (class Anthozoa, phylum Cnidaria) biological control is exerted by both regulating the availability and concentration of required ionic components (Moya et al. 2008; Bertucci et al. 2011; Zoccola et al. 2015; Le Goff et al. 2016) and the production of a variety of macromolecules, collectively referred to as the skeleton organic matrix (SOM). These are secreted into the calcification space and are eventually occluded within the skeleton mineral. Several regulatory functions have been attributed to the SOM both in corals and other marine calcifiers (*e.g.* molluscs and echinoderms). These include crystal nucleation, formation and inhibition (Wheeler et al. 1981; Allemand et al. 1998; Peled-Kamar et al. 2002; Clode and Marshall 2003; Puvarel et al. 2005; Von Euw et al. 2017), and controlling the calcium carbonate (CaCO_3) polymorph of the skeleton (Thompson et al. 2000; Goffredo et al. 2011).

The effects that different organic compounds have on CaCO_3 polymorphs (aragonite, calcite) have been investigated mostly through *in vitro* precipitation experiments. Addition of total SOM extracts (Hohn and Reymond 2019), proteins (Rahman and Oomori 2009; Goffredo et al. 2011) and lipids (Reggi et al. 2016) isolated from coral skeletons have been shown to either promote or inhibit the formation of specific CaCO_3 polymorphs and affect crystal shape. Recently Laipnik et al. (2019) observed that protein-driven *in vitro* precipitation of different CaCO_3 polymorphs is also related to the magnesium concentration ($[\text{Mg}^{2+}]$) in the solution used. The absence of aragonite formation - the naturally occurring polymorph in scleractinian skeletons - at low magnesium values led the authors to argue that seawater $[\text{Mg}^{2+}]$ could represent a key factor for the functioning of skeletogenic proteins.

Seawater chemistry - with the molar ratio of magnesium and calcium ($m\text{Mg}:m\text{Ca}$) representing one of the key factors - has in fact been long included among the main drivers of selective inorganic precipitation of different CaCO_3 polymorphs (Morse and Mackenzie 1990; Morse et al. 1997; Balthasar and Cusack 2015). The $m\text{Mg}:m\text{Ca}$, in particular, holds special evolutionary interest. Its estimated fluctuations in the last 600 million years caused alternating periods of calcite- and aragonite-favouring environments (Sandberg 1983) that robustly correlate with the preferred skeleton polymorph of the dominant reef builders during those geological periods (Stanley and Hardie 1998; Stanley and Hardie 1999). During the Cretaceous, for example, when the $m\text{Mg}:m\text{Ca}$ dropped to ca. 1 (compared to the modern value of 5.2), scleractinian corals were replaced by calcitic bivalves (rudists, Phylum Mollusca) and instances of cretaceous calcitic scleractinians appear to be present in the cretaceous fossil record (Stolarski et al. 2007). Recently, however, the finding of aragonitic coral fossils from cretaceous sediments showed that, although potentially impaired in their capacity to build their skeleton, coral species were able to deposit aragonite under chemically adverse conditions. Cretaceous aragonitic fossils have also been reported for blue corals (order Helioporidae, subclass Octocorallia) (Eguchi 1948; Colgan 1984), the only soft corals known to produce massive aragonite skeletons. The effects of $m\text{Mg}:m\text{Ca}$ on the skeleton polymorph of corals might therefore differ among species, with some corals enacting countermeasures to compensate for unfavourable environments.

The ability of corals to counteract the putative decisive influence of seawater chemistry on polymorph formation has been tested *in vivo*, by exposing animals to different $m\text{Mg}:m\text{Ca}$ ratios. In an early work, Ries (2006) observed an increase in the presence of calcite in the skeleton of three scleractinian corals, with the amount of calcite correlating inversely to the seawater $m\text{Mg}:m\text{Ca}$ ratio. These observations

were later corroborated by Higuchi et al (2014) which reported changes in CaCO_3 polymorph in the skeleton of *Acropora tenuis* juveniles, albeit at lower $m\text{Mg}:m\text{Ca}$ ratios compared to Ries (2006). More recently, Yuyama et al. (2019) reported variations in gene expression in the scleractinian coral *A. tenuis* grown in Mg-depleted seawater. Changes included the up-regulation of several putatively skeletogenic genes, leading the authors to suggest that corals actively respond to unfavourable chemical conditions for aragonite precipitation. Despite these studies, where only the Mg-content was manipulated and calcium levels kept constant, the molecular responses of corals $m\text{Mg}:m\text{Ca}$ ratios differing in both the concentration of calcium and magnesium that are comparable to calcite sea conditions remain unknown. Understanding if and how modern coral species respond to past seawater conditions could therefore further our understanding of their evolutionary history, and their future ability to cope with changes in seawater chemistry.

Here, we combined molecular and mineralogical analyses to investigate the effects of $m\text{Mg}:m\text{Ca}$ ratios resembling those observed during calcite sea condition on aragonitic corals. We exposed *Montipora digitata* (Scleractinia) and the blue coral *Heliopora coerulea* (Octocorallia) to both calcite and aragonite-inducing seawater. To match modern (control settings; ratio of 5.2) and past values (treatment settings; ratios of 2.5 and 1.5) (Hardie 1996), both calcium and magnesium concentrations were manipulated. The two target species were selected for their potential different responses. *Montipora digitata* was susceptible to calcite-inducing seawater in previous experiments (Ries et al. 2006), while the fossil record for *H. coerulea* indicated that this species was resilient to past calcite-inducing oceanic conditions. We used gene expression analysis (RNA-seq) to characterize the molecular response of these corals and used electron backscatter diffractometry (EBSD) and energy dispersive spectroscopy (EDS) to investigate crystallographic and compositional changes induced by the seawater chemistry. Our results indicate a higher tolerance to changes in $m\text{Mg}:m\text{Ca}$ of octocorals compared to scleractinians. Although several expression changes involve currently uncharacterized genes, the molecular response of the corals appears to be related to ion transport and ion availability rather than regulation via organic matrix proteins.

4.3 Materials and Methods

Fragments of *H. coerulea* and *M. digitata* were mechanically obtained from coral colonies cultured in the aquarium facilities of the Chair for Geobiology & Paleontology of the Department of Earth- and Environmental Sciences at Ludwig-Maximilians-Universität München in Munich (Germany). Following fragmentation, corals were allowed to recover for ca. one month prior to the start of each experiment. Two days before the start of each experiment, coral samples were incubated for ca. 36 hours in a 10% alizarin red solution to later distinguish skeleton deposited before and after the experiment.

4.3.1 Experimental Design

Two time-shifted replicates were performed for each target species and each experiment lasted ca. six weeks (22.07-10.09 and 01.11-12.12 2018 for *M. digitata* and 04.01-28.02 and 01.03-15.04 2019 for *H. coerulea*). The experimental setup (illustrated in Figure 4.1) consisted of three 8 L aquarium tanks: one (control tank) characterized by $m\text{Mg}:m\text{Ca}$ of 5.2 (10mM Ca^{2+} - 52 mM Mg^{2+}) and two treatment

tanks with ratios 2.5 (17mM Ca^{2+} + 47 mM Mg^{2+}) and 1.5 (25mM Ca^{2+} - 37 mM Mg^{2+}). In all three tanks the sum of $[\text{Ca}^{2+}]$ and $[\text{Mg}^{2+}]$ was equal and set at 62 mmol. A single source of Mg^{2+} and Ca^{2+} -free seawater was used for all three tanks. The $m\text{Mg}:m\text{Ca}$ was adjusted by dissolving $\text{CaCl}_2 \cdot \text{H}_2\text{O}$ and $\text{MgCl}_2 \cdot 6\text{H}_2\text{O}$ in ultrapure MilliQ water and adding it to each tank. Water was replaced in each tank every 48 hours. Recipes for the different artificial seawater used are available as supplementary material (available online at https://gitlab.lrz.de/ra34lem/corals_calcite_sea). Prior to the experiment, the composition of each solution was independently confirmed using inductively coupled plasma optical emission spectrometry (ICP-OES). Analyses were conducted at the Chemistry and Pharmacy Department of the Ludwig-Maximilians-Universität München. Throughout each experiment, the concentration of magnesium and calcium in the tanks was measured after each water exchange with an EDTA-based titration method, using the Total Hardness Titration Kit (Hach).

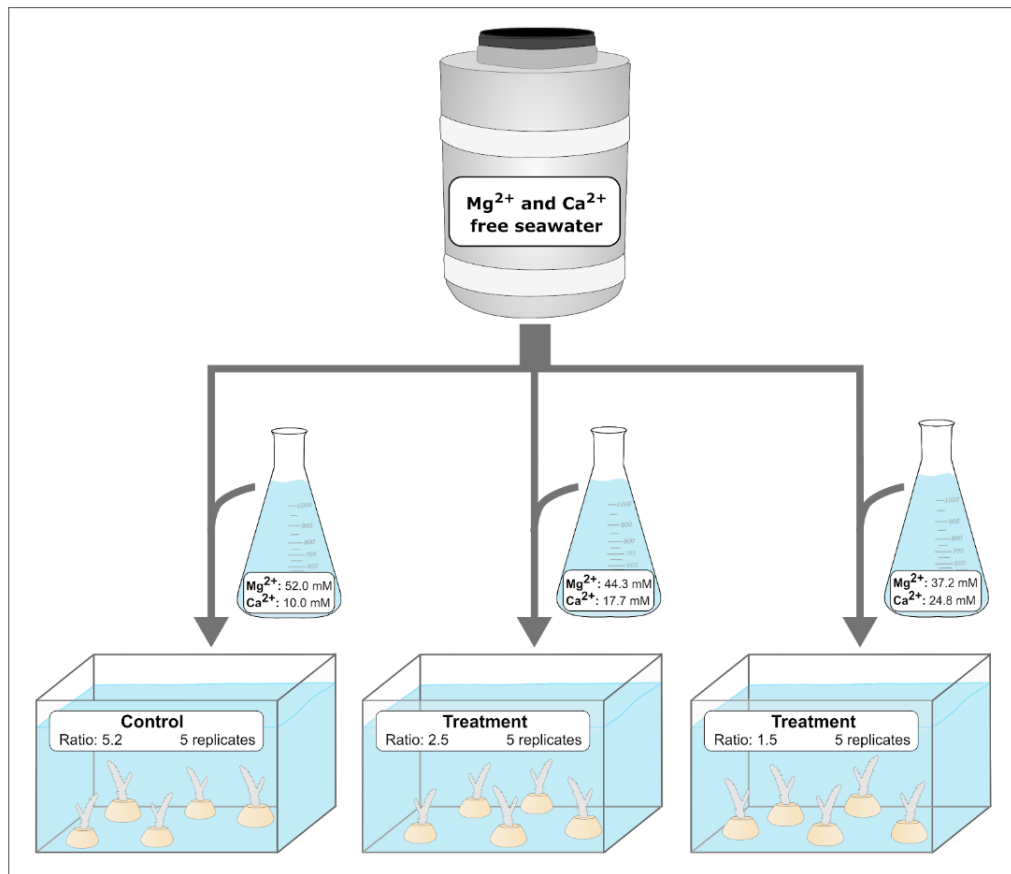


Figure 4.1: Schematic diagram of the experimental design. For each species the experiment was repeated twice (22.07-10.09 and 01.11-12.12 2018 for *M. digitata* and 04.01-28.02 and 01.03-15.04 2019 for *H. coerulea*).

To allow acclimatization, corals in treatment tanks were initially exposed for two days to $m\text{Mg}:m\text{Ca}$ ratios of 5.2, 4.0 and 3.0. At the end of each experiment two coral fragments from each tank (for

mineralogical analysis) were bleached for 24 hrs in 5% NaOCl, washed several times in ultrapure water and air dried. Three corals from each tank were flash frozen in liquid nitrogen and stored at -80°C until RNA extraction.

4.3.2 Mineralogical Analysis

To prepare coral samples for mineralogical analysis, skeletons were first thoroughly washed with deionized water and then air dried. Samples were embedded in polypropylene molds using ca. 30 ml of Epofix Resin (Struers) and 4 ml of Resin Hardener. Samples were placed in a vacuum desiccator to degas and polymerize for 24 hours. Embedded skeletons were grinded using P320, P600 and P1200 silicon carbide paper (Buehler), and flushed with deionized water to remove resin and silicon residues. First round of polishing was carried out with 3 μ m polycrystalline diamond suspension for ca. 10-15 minutes. Samples were then attached to cylinder weights with Thermoplastic Cement at 100-150°C. After reaching room temperature, samples were finally polished (for ca. three hours) with MicroFloc in a Vibromet using a 50 nm Alumina suspension, and washed. Prior to EBSD and EDS analysis, polished samples were coated with 4-8 nm of carbon and mounted on a sample holder with 70°C orientation. For each sample, an 'inner' and 'outer' area were analyzed to obtain information for skeleton sections deposited before and after the start of the experiment. EBSD and EDS measurements were performed with a Hitachi SU5000 field emission SEM operated at 20kV. The microscope is equipped with an electron backscatter diffraction (EBSD) and energy dispersive spectroscopy (EDS) detectors (Oxford Instruments). Measurements were conducted using the AZtech Suite (Oxford Instruments), while phase and orientation maps were produced with the CHANNEL 5 HKL software (Schmidt and Olesen 1989; Randle and Engler 2000).

4.3.3 Transcriptome Sequencing]

Coral samples were homogenized in 1-2 ml of Trizol (ThermoFisher) using a Polytron PT Homogenizer (Kinematica) and centrifuged at 15,000 g for 10 minutes to remove residual skeleton powder. RNA was extracted according to a modified TriZol protocol (Chomczynski and Mackey 1995). Modifications included the substitution of 50% of the isopropanol with a high-salt solution (1.2 M sodium chloride and 0.8 M sodium citrate) in order to avoid the coprecipitation of polysaccharides and other potential contaminants. RNA purity and integrity were assessed on a NanoDrop 2100 spectrophotometer and a Bioanalyzer 2100 (Agilent), respectively. For sequencing, samples with a RIN value > 8.0 were considered. Strand-specific libraries were prepared with the SENSE mRNA-Seq Library Prep Kit V2 for Illumina (Lexogen) and paired-end sequenced (50 bp) on an Illumina HiSeq1500 at the Gene Center of Ludwig-Maximilians-Universität München.

Sequences were quality controlled with FastQC (www.bioinformatics.babraham.ac.uk) and low quality reads removed with the Filter Illumina program from the Agalma-Biolite transcriptome package (Q value cut off: 28) (Dunn, Howison, and Zapata 2013). Sequenced reads from *M. digitata* and *H. coerulea* have been deposited at the European Nucleotide Archive (<https://www.ebi.ac.uk/ena>) under Bioproject Number PRJEB36989 and PRJEB36990 respectively. For the assembly of *H. coerulea* previously sequenced reads (PRJEB30452) were also used.

Transcriptome assembly was performed with a custom pipeline (Rivera et al., unpublished) combining the output of multiple assemblers to produce a consensus assembly. Software included in the

workflow are rnaSPAdes (Bushmanova et al. 2019), SOAP (Li et al. 2008), Trans-ABYSS (Robertson et al. 2010), Trinity 2.8.5 (Grabherr et al. 2011) and Velvet (Zerbino 2010). Different outputs were compared and a consensus assembly built using EvidentialGene (Gilbert 2019). Contigs of length < 300 bp were discarded. Host and symbiont contigs were separated with psytrans (available at <https://github.com/sylvainforet/psytrans>) using the *Dendronephthya gigantea* (Jeon et al., n.d.) and *Acropora digitifera* (Shinzato et al. 2011) genomes for assigning host contigs of *H. coerulea* and *M. digitifera* sequences respectively. Transcriptome completeness was assessed against the BUSCO 3.0.2 odb9 metazoan database (Simao et al. 2015). Summary statistics of the transcriptomes are provided in Table 2.

Table 2: Summary Statistics for the Assembled Meta-Transcriptomes

Species	Contigs	N50 - Mean Length	BUSCO (C-F-M)
<i>H. coerulea</i>	117,440	1083 - 844	94.6 - 2.6 - 2.8
<i>M. digitata</i>	71,676	819 - 705	90.4 - 4.3 - 5.3

For BUSCO analysis, percentages of complete (C), fragmented (F), and missing (M) orthologs are provided.

4.3.4 Gene Expression Analysis

For gene expression analysis, reads files of each species were mapped against their metatranscriptome (host and symbiont contigs) using Salmon 0.11.2 (Patro et al. 2017) available on our local Galaxy server (galaxy.palmuc.org/). A count matrix was obtained with the `abundance_estimates_to_matrix.pl` script provided with Trinity (Grabherr et al. 2011). To perform coral and symbiont analysis separately, host and symbiont transcript IDs were used to extract the corresponding information from the count matrix. Differential expression analysis was performed using DESeq2 (Love et al. 2014). Presence of technical batch effects (supplementary Figures S4.1 and S4.2) was included in the model for DESeq2 analysis design (experiment + condition + experiment:condition). Differentially expressed genes with p-value < 0.01 and log-fold changes $- 2 >$ and > 2 were considered for further analyses. For the gene ontology analysis, enriched GO terms associated with different treatments in both species were determined with topGO (Alexa and Rahnenfuhrer 2010), using Fishers exact test. The complete DESeq2 and topGO analysis workflows and outputs are available online as supplementary materials at https://gitlab.lrz.de/ra34lem/corals_calcite_sea/.

4.4 Results

4.4.1 Mineralogical Analysis

Mineralogical analysis on the skeletons of the octocoral *Heliopora coerulea* and the scleractinian *Montipora digitata* revealed species-specific responses to variations in the magnesium/calcium ratio of seawater (Figure 4.2a). No change in polymorph could be observed in either species under control condition ($m\text{Mg}:m\text{Ca} = 5.2$) and under $m\text{Mg}:m\text{Ca}$ of 2.5 (Figures S4.1a, S4.2a, S4.3 and S4.4a).

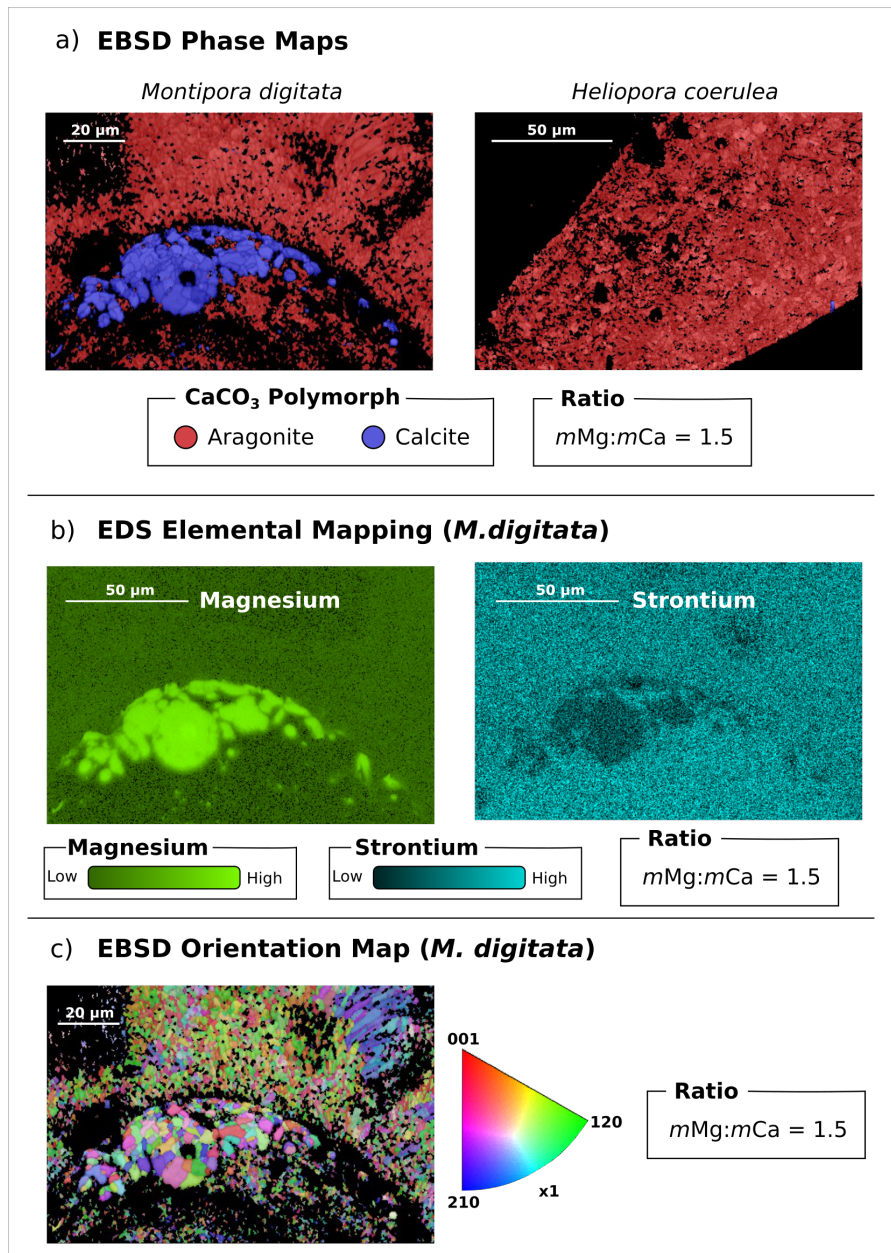


Figure 4.2: **a)** Phase map for *M. digitata* and *H. coerulea* grown under ($m\text{Mg}:m\text{Ca} = 1.5$). **b)** EDS elemental mapping of magnesium and strontium in calcite of aragonite of *M. digitata*. **c)** Inverse pole figure (IPF, x-axis) of *M. digitata*.

Under calcite-inducing conditions ($m\text{Mg}:m\text{Ca}$ of 1.5), we did not detect changes in the polymorph of CaCO_3 in *H. coerulea*, while both aragonite and calcite were present in the skeleton of *M. digitata* (Fig. 4.2a).

The newly formed calcite did not exhibit a uniform distribution within the imaged sample, but was clustered within a single area (Figure 4.2a). To further characterize the newly formed calcite we combined EDS with EBSD analysis to obtain compositional and orientation information. EDS mapping showed higher magnesium and lower strontium contents in the calcitic portion of the skeleton (Figure 4.2b), while EBSD highlighted the different crystal shape between aragonite and calcite (Figure 4.2c). Uneven strontium distributions were also detected in both newly formed and older skeleton sections of *H. coerulea*, i.e., in the skeleton deposited prior to the start of the experiment (Figure S4.4b). The differences in strontium distribution in different parts of the *H. coerulea* skeleton may therefore be uncorrelated to different $m\text{Mg}:m\text{Ca}$ values.

4.4.2 Gene Expression Analysis

Strong differences between species were observed for changes in gene expression, with *H. coerulea* showing markedly higher numbers of differentially expressed genes (DEGs) (p-value < 0.001; $-2 > \log$ fold change > 2) under both treatment conditions (Figure 4.3a). Principal component analysis (PCA), based on log-transformed expression values relative to control, highlighted high variance within control and treatment samples of *M. digitata*, and between experimental replicates (supplementary Figure S4.5 and S4.6), and might explain the low number of DEGs detected in *M. digitata*. In both species, some gene expression changes were common to both treatments, although the majority of differentially expressed genes appears specific to single treatment conditions ($m\text{Mg}:m\text{Ca}$ 2.5 or 1.5). In *H. coerulea*, the vast majority of differentially expressed genes was observed under $m\text{Mg}:m\text{Ca}$ of 2.5.

To investigate the effect of changes in calcium and magnesium concentration on the corals, we examined DEGs associated with calcium binding and transport (based on Gene Ontology, supplementary material 6). Different calcium-interacting proteins were up and down-regulated under $m\text{Mg}:m\text{Ca}$ of 2.5, while no change for genes related to magnesium was detected. A smaller group of genes also increased in expression with $m\text{Mg}:m\text{Ca} = 1.5$. Among calcium transporters, four voltage-dependant calcium channels alpha subunits (matching L, N and T type channels), two transient receptor potential channel-like proteins, and one mitochondrial proton/calcium exchanger-like gene increased in expression when corals were exposed to $m\text{Mg}:m\text{Ca}$ of 2.5 (Figure 4.3b).

Other up-regulated genes included different calcium-sensing proteins like synaptotagmins, neurocalcin-like and several protein kinases. Among calcium-interacting proteins some also represented known components of the extracellular matrix. Of these, mucins exhibited a mixed response, with different transcripts being up and downregulated (Fig. 4.3b), while one matrix metalloproteinase and one cartilage-associated matrix protein were upregulated under $m\text{Mg}:m\text{Ca} = 2.5$ and both treatment conditions respectively. As for skeletogenic proteins, no known component of the *H. coerulea* or *M. digitata* skeleton organic matrix was detected among differentially expressed genes. Expression of one agrin-like protein - found in the sclerites of different octocorals (Conci et al. 2019) - was nevertheless downregulated in *H. coerulea* under $m\text{Mg}:m\text{Ca} = 1.5$. Finally, exposure of *H. coerulea* to $m\text{Mg}:m\text{Ca}$ of 1.5, caused an increase in expression for genes involved in proteolysis (supplementary material 5), which in corals has been found correlated with stress responses (Aguilar et al. 2019).

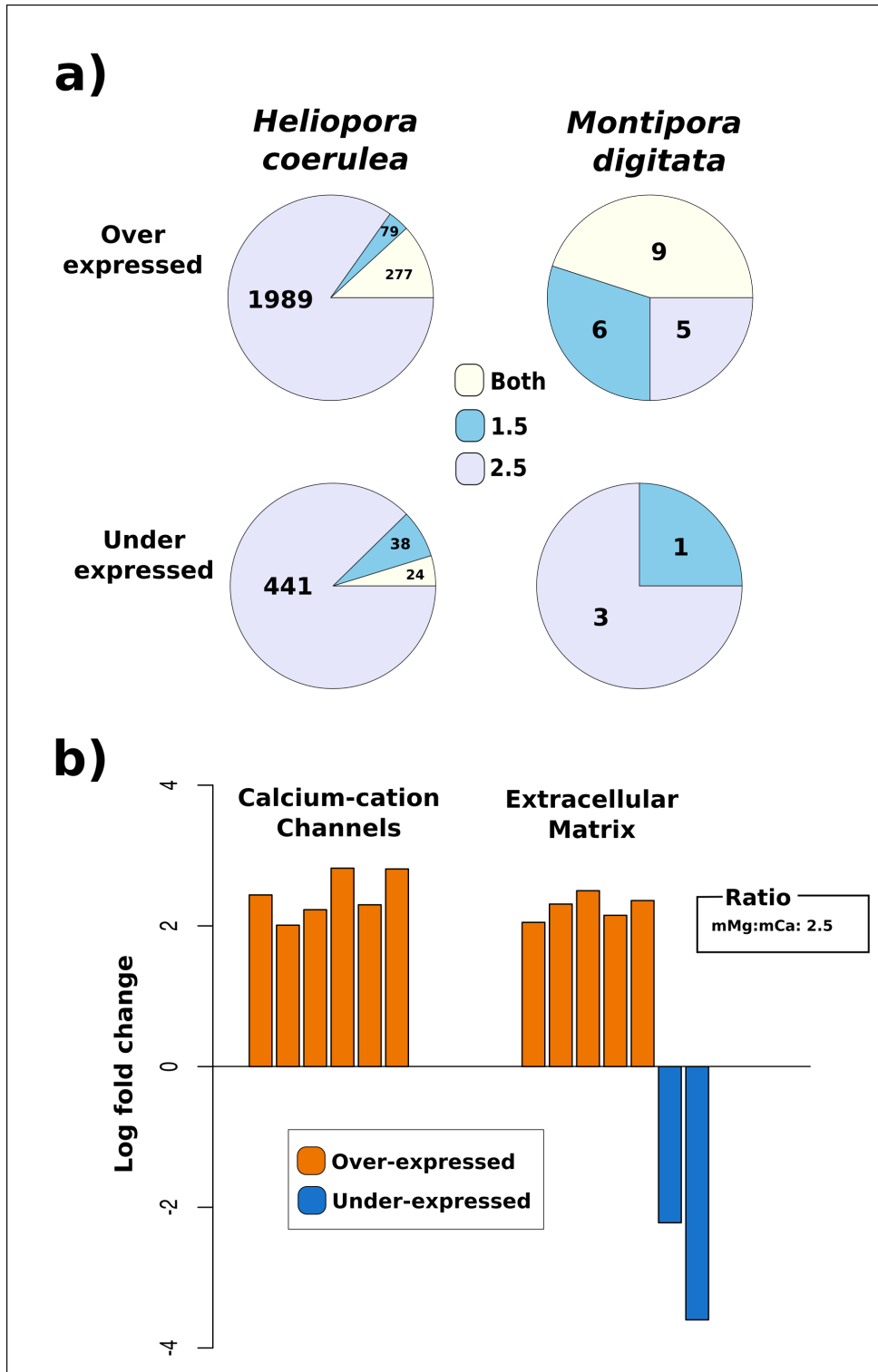


Figure 4.3: Phase and EBSD orientation map for *M. digitata* and *H. coerulea* grown under control conditions ($mMg:mCa = 2.5$)

4.5 Discussion

Formation of coral skeletons is intimately linked to cellular/molecular processes, and the surrounding environmental conditions. Among the latter, the magnesium/calcium molar ratio of seawater ($mMg:mCa$) has significantly influenced the polymorph of calcium carbonate ($CaCO_3$) in marine cements, and the polymorph initially adopted by marine calcifiers during the last 500 myr (Zhuravlev and Wood 2008). However, organisms also appeared to be less affected by subsequent changes in seawater chemistry promoting the precipitation of a different polymorph. For example, the fossil record of scleractinian corals and octocorals of the genus *Heliopora* shows the presence of species producing aragonitic skeletons during the Cretaceous (Eguchi 1948; Colgan 1984; Janiszewska et al. 2017), a geological period in which the deposition of low-magnesium calcite was favoured. Manipulation experiments conducted in artificial cretaceous-like water, have, however, highlighted the inability of modern scleractinian corals to fully counteract the effects of $mMg:mCa$ changes, leading to significant amounts of calcite being deposited within their skeletons (Ries et al. 2006; Higuchi et al. 2014). In this light, we exposed the aragonitic octocoral *Heliopora coerulea* and the scleractinian coral *Montipora digitata* to different $mMg:mCa$ to examine and compare their responses. To recreate Calcite Sea-like conditions experienced by corals, $mMg:mCa$ were manipulated by changing both calcium and magnesium concentration. We examined variations in skeleton mineralogy and changes in the expression of genes assumed to be involved in calcification.

The analysis of the $CaCO_3$ polymorphs of the corals skeletons showed a species-specific response to $mMg:mCa$. Aragonite formation appeared unaltered in *H. coerulea*, while significant amounts of calcite were observed in the skeleton of *M. digitata*. Nevertheless, the majority of the skeleton consisted of aragonite in all samples for both species. This study provides the first insight on $mMg:mCa$ effects on octocoral skeletons, and while previous data on these specific effects is not available, our results suggest that octocorals may have higher tolerances to changes in ocean chemistry with respect to their ability to maintain their skeleton polymorph. This hypothesis is in line with previous studies on other calcification stressors (e.g., ocean acidification OA) (Gabay et al. 2014; Lopes et al. 2018). Higher tolerance to OA in octocorals has been linked to skeletal structures being internal and thus surrounded by the animal tissues (Gabay et al. 2014). However, this does not likely apply to *H. coerulea*, as its skeleton is external. Resilience to $mMg:mCa$ changes appear therefore directly linked to the calcification process and not to location of the skeleton. On the other hand, what observed in *M. digitata* is in partial accordance with previous investigations. The previously reported correlation between $mMg:mCa$ and skeleton calcite percentage was not observed. As in Ries et al. (2006) the calcite portion of the skeleton exhibited higher magnesium content. Here we have additionally shown higher magnesium contents are paired with lower strontium level and observed differences in grain size between the calcite and aragonite portion of the skeleton.

Although comparisons between studies have to take technical and analytical variability into account, they can provide valuable insights. During the last 600 myr for instance, shifts between Aragonite and Calcite Seas have been characterized by changes in both calcium and magnesium concentration (Hardie 2003). When recreating past environmental conditions in controlled experimental setups, artificial seawater formulation (i.e. calcium and magnesium concentration) is thus of primary importance, especially if results are discussed in evolutionary context. In fact, when calcium concentration was kept at modern values (ca. 10mM) as in Higuchi et al. (2014), calcite could only be observed at magnesium levels lower than what experienced by corals during the Calcite Sea in the late Mesozoic. Contrarily, when both

[Ca²⁺] and [Mg²⁺] are manipulated, calcite formation occurs (Ries et al. 2006). Increasing calcium concentration, and consequently the solution saturation state (Ω), is known to promote the precipitation of calcite at higher *mMg:mCa* ratios (De Choudens-Sanchez and Gonzalez 2009), despite the inhibitory effect exerted on calcite formation by Mg²⁺ ions (Fyfe and Bischoff 1965; Bischoff 1968; De Boer 1977). In corals, calcium is exchanged between seawater and calcification fluids via both paracellular (Gagnon et al. 2012) and active transcellular transport (Tanbutt et al. 1996; Hohn and Merico 2015). Due to calcium's role in many metabolic processes (for review see Clapham (2007)), concentration inside the cells has to remain tightly controlled. The simultaneous transport of calcium and the maintenance of calcium homeostasis in the cytosol appears to be achieved through calcium accumulation within vesicles (Mass et al. 2017). Different transporters have been associated with calcium transcellular transport including calcium channels, Ca²⁺-ATPases and proton exchangers (Zoccola et al. 1999; Zoccola et al. 2004; Barott et al. 2015; Barron et al. 2018). The regulation of calcium transport allows corals to maintain higher calcium concentration in calcifying fluids ([Ca²⁺]_{cf}) in respect to seawater (Sevilgen et al. 2019). Up-regulation of [Ca²⁺]_{cf} can also be enhanced in response to changes in environmental conditions. In some coral species for example calcium increases counteract decreases in saturation state of calcifying medium caused by decreases in seawater pH (DeCarlo et al. 2018). Different studies have in fact examined the effects of ocean acidification on carbonate and calcium chemistry at calcification sites (Allison et al. 2018; Mollica et al. 2018). In this light, corals could thus theoretically maintain aragonite deposition under low *mMg:mCa* ratios by regulating the saturation state of their calcifying fluid by decreasing [Ca²⁺].

The expression changes for different voltage-dependant Ca²⁺-channels and calcium transporters, observed in *H. coerulea*, indicate the presence of a response by the octocoral to increased seawater [Ca²⁺], possibly including calcifying fluids and the maintenance of the aragonite polymorph. Information on single calcium transporters involvement in octocoral biomineralization is to date extremely scarce. It is thus not possible to determine if and which of the up-regulated channels/transporters is participating in the process. Further characterizations of calcium transport machinery in octocorals could provide further insight on the localization and role of single calcium channels, and possibly corroborating the hypothesis of *H. coerulea* controlling aragonite precipitation through the regulation of calcium transport. As for the partial inability of *M. digitata* to counteract the effects of low *mMg:mCa*, seawater pH manipulations have shown the reduced capacity of *Acropora* species - taxonomically closely related to *Montipora* (Kitahara et al. 2010) - to regulate [Ca²⁺]_{cf} in response of environmental changes, compared to other species (DeCarlo et al. 2018). Moreover, presence of a stress response in *H. coerulea* - when exposed to *mMg:mCa* = 1.5 - suggests that corals species might differ in resilience to suboptimal Ca²⁺ and Mg²⁺ ranges. Very little is known about corals' overall tolerance to changes in [Ca²⁺] and [Mg²⁺], as most investigations have so far focused on responses to changes in total salt content (Kerswell and Jones 2003; Berkelmans et al. 2012). Recently, Yuyama et al. (2019) reported down-regulation of several stress-related genes under low magnesium concentrations, but information on stress caused by higher calcium contents is to our knowledge not available.

Finally, we did not detect changes in expression of genes coding for skeleton organic matrix (SOM) proteins of *H. coerulea* and *M. digitata* (Conci et al. 2019). Some extracellular matrix proteins were however found over-expressed at lower *mMg:mCa* ratios, but none are known to directly interact with calcium or crystal formation. These included one putative coral homolog of cartilage-related matrix protein, matrix metalloproteinases involved in the proteolytic processing of other extracellular matrix

proteins (Mann et al. 2010), and proteins with mucin and coadhesin-like features, common components of extracellular matrices and involved in cell-substrate or cell-cell adhesion (Engel 1991; Marin et al. 2000; Mosher and Adams 2012). In a recent work however, Yuyama et al. (2019) reported overexpression for several coral skeletogenic proteins, such as acidic proteins and galaxins. The high variability observed between and within experiments - especially for *M. digitata* - might have prevented us from detecting expression changes linked to SOM proteins. Therefore, a *mMg:mCa*-driven response by the organic matrix cannot be excluded.

Here we have exposed the aragonitic octocoral *H. coerulea* and the scleractinian *M. digitata* to calcite-inducing *mMg:mCa* and assessed the presence of changes in skeleton polymorph and expression of calcification-related genes. This work provides the first comparative study of octocoral and scleractinian responses to changes in *mMg:mCa*. The two species were found to respond differently with calcite being absent and present in the skeleton of *H. coerulea* and *M. digitata*, respectively. Gene expression analysis for *H. coerulea* highlighted changes for different genes associated with calcium transport, pointing to biological control over CaCO_3 polymorph involving the homeostasis of calcifying fluids rather than direct interaction of matrix proteins with the mineral.

Chapter 5

Resilience to climate-change in an octocoral involves the transcriptional decoupling of the calcification and stress response toolkits

5.1 Abstract

Up to one-third of all described marine species occur in coral reefs (Knowlton et al. 2010) threatened by local (e.g., overfishing and eutrophication (Hughes 1994; Jackson et al. 2001; Pandolfi et al. 2003)) and global (e.g., ocean acidification and global seawater warming (Hoegh-Guldberg et al. 2007; Hughes et al. 2018; Hughes et al. 2019)) anthropogenic action. Although these threads are expected to have a net detrimental effect on reefs, experiments in mesocosm systems and volcanic CO₂ seeps have shown that some organisms can remain unaffected or benefit from the anthropogenically induced environmental change (Rodolfo-Metalpa et al. 2011; Comeau et al. 2013). Soft corals are generally more resilient to climate change-induced stress (Gabay et al. 2013; Ruzicka et al. 2013; Gabay et al. 2014; Gmez et al. 2015) than stony corals and could replace them in future reefs (Inoue et al. 2013; Ruzicka et al. 2013). However, the molecular mechanisms leading to the resilience to anthropogenic-induced stress observed in these animals remain unknown. Here, we use manipulative experiments, proteomics, and transcriptomics to show that the molecular toolkit used by *Pinnigorgia flava*, a common indo-pacific gorgonian, to deposit its calcium-carbonate skeleton is not affected by climate change. Sublethal, simulated global warming triggered a stress response in *P. flava* but did not affect the expression of the 28 transcripts encoding Skeletal Organic Matrix (SOM) proteins present in this species' skeleton. Exposure to simulated ocean acidification did not cause a stress response but triggered the downregulation of many transcripts, including an osteonidogen homolog present in the SOM. The observed transcriptional decoupling of the skeletogenic and stress-response toolkits provides a mechanistic explanation for the resilience to anthropogenically-driven environmental change observed in soft corals.

5.2 Results and Discussion

Octocorals (., soft-corals and gorgonians) are common inhabitants of coral reefs, where they provide refuge to numerous invertebrate species and increase the spatial complexity of these ecosystems. After extreme climatic events, such as anomalously strong El Niño events (Ruzicka et al. 2013), or under extreme environmental conditions, like those prevailing in volcanic-seep acidified waters (Inoue et al. 2013), octocorals can outgrow stony corals and become dominant, causing compositional shifts with ecosystem-wide effects. Since growth in octocorals requires the deposition of new calcium-carbonate skeletal elements (calcite sclerites) to support the colony structurally (Lewis and Vonwallis 1991), the capacity of these organisms to outcompete stony corals under environmentally stressful conditions must be somehow linked to their ability to calcify in extreme environments. Indeed, octocorals are capable of sustaining their calcification rates under adverse environmental conditions (Gabay et al. 2013; Inoue et al. 2013; Gabay et al. 2014; Gmez et al. 2015).

To understand the molecular basis for the resilience to climate change of the octocoral calcification machinery, we first investigated the spatial dynamics of new sclerite production in colonies of *P. flava* using calcein staining and fluorescence microscopy. This species produces new sclerites along the entire colony axis, usually at the polyps (Figure 5.1), with no identifiable calcification hotspots. *Leptogorgia virgulata*, one of the few other octocoral species where data on calcification dynamics exist, also deposits new sclerites along its body axis but with an increase in sclerite production at the colony tips (Kingsley and Watabe 1989). Sclerite growth in octocorals involves the synthesis by sclerocytes of skeletal organic matrix (SOM) proteins and its transport to a sclerite-forming vacuole where primordia mostly made of irregularly shaped CaCO₃ crystals form (Kingsley 1984). Sclerite primordia continue growing by the deposition of more regular crystals in an extracellular space created by multiple sclerocytes (Goldberg and Benayahu 1987). The lack of a marked zonation in the production of new sclerites in *P. flava* indicates that active sclerocytes intersperse along the colony axis and that no spatial differences in the expression of SOM encoding transcripts should be expected in this species under normal conditions. Hence, the exposure of colonies of *P. flava* to simulated, anthropogenically-driven environmental stress factors capable of inducing changes in the expression level of SOM encoding transcripts should impair the deposition of new sclerites at the colony level, affecting the ability of octocorals to sustain growth under these conditions and outcompete other reef organisms such as stony corals.

To evaluate the effect of different climate-change scenarios on the expression of SOM encoding transcripts in *P. flava*, we used nano liquid chromatography coupled mass spectrometry to characterize the acid-soluble (ASM) and acid-insoluble (AIM) fractions of the SOM proteome extracted from sclerites of *P. flava*. After filtering potential contaminants (e.g., keratins, trypsin), we identified a total of 28 transcripts as the SOM proteome of *P. flava*. Label-free quantification (LFQ) using the MaxLFQ algorithm (Cox et al. 2014) revealed 14 proteins with a higher abundance in the AIM, seven proteins exclusive to the ASM, and five proteins that appeared in both fractions (Figure 5.1). Biochemically, seven of the detected SOM proteins are membrane-bound, containing either transmembrane domains (N=3), GPI anchors (N=3), or both (N=1). About 46% (N=13) of the SOM proteins detected contain signal peptide motifs, indicating that these proteins are secretion targets (Figure 5.1).

Similarity-based searches against the UniProt knowledgebase (i.e., UniProtKB) revealed that the *P. flava* skeletal proteome is composed of proteins similar to those previously isolated from the skeletons of both soft and stony corals (Drake et al. 2013; Ramos-Silva et al. 2013; Conci, Lehmann, et al. 2019).

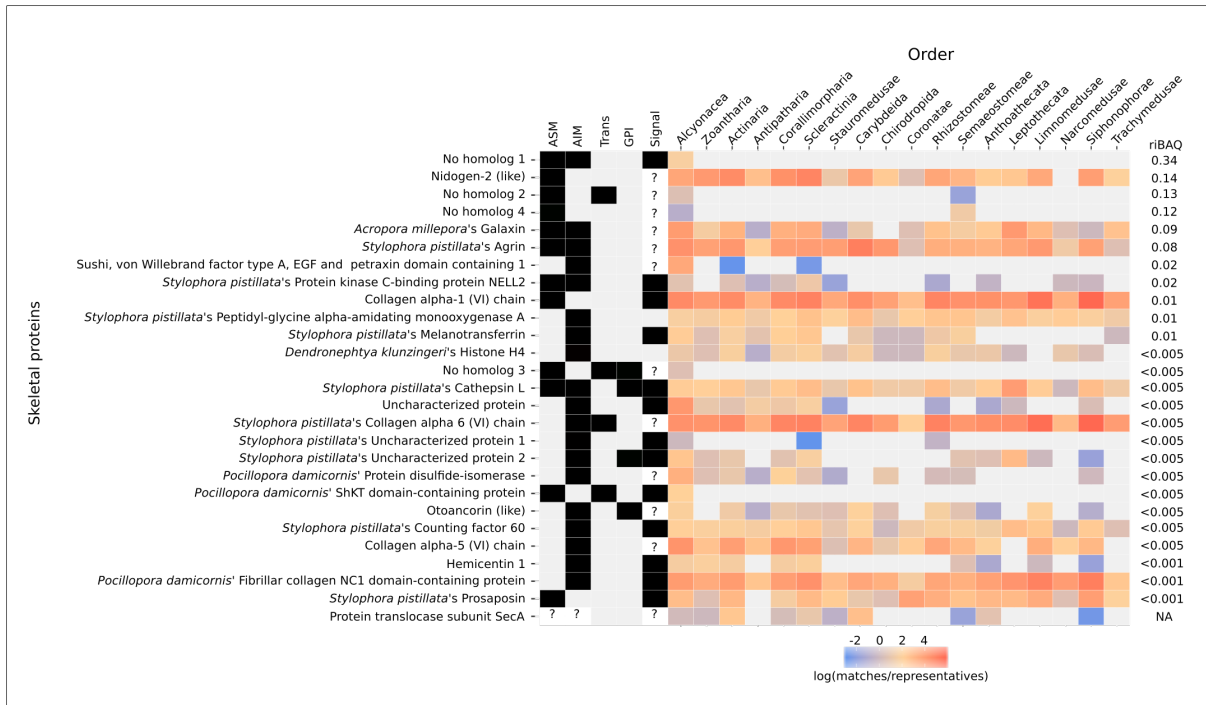


Figure 5.1: Skeletal proteome of *Pinnigorgia flava*. Upper: isolated and in situ calcein stained sclerites, note the distribution of newly deposited CaCO_3 around the polyp. Lower: presence/absence in the acid soluble (ASM) and insoluble (AIM) matrix, biochemical properties, distribution among cnidarians and abundance in the skeletal proteome of 27 proteins present in the skeleton of *P. flava*.

For instance, we found several components of the extracellular matrix, like collagens and laminin, glycoproteins with calcium-binding domains, like nidogen 2 (osteonidogen) and agrin, and proteins likely involved in cell adhesion, like otoancorin, hemicentin and several proteins containing von Willebrand factor type A (VWA) domains. Finally, we also found a protein similar to galaxin, two proteins enriched in aspartic-acid residues (acidic, pI ca. 3.4) with no significant UniProt blast hits, and several other proteins with diverse functionalities (e.g., disulfide isomerase or protease activity). To further gain information on the relative importance of these proteins, we estimated relative protein abundances using iBAQ (Schwanhuser et al. 2011). According to this metric, six proteins had abundances $>5\%$ in the skeletal proteome of *P. flava*. The two acidic proteins ranked first and third, osteonidogen and collagen were the second and fourth most abundant proteins, and galaxin and agrin ranked fifth and sixth in abundance. These six proteins account for 90% of the total iBAQ-derived skeletal protein abundance (Figure 5.1). On average, the remaining proteins account for only 0.5% ($pm0.6\%$) of the total iBAQ-derived abundance.

Octocoral skeletal proteomes contain a mixture of taxonomically restricted and widespread elements (Conci, Lehmann, et al. 2019). To assess the distribution of the detected *P. flava* SOM proteins among cnidarians, we screened a database composed of 120 transcriptomes from representatives of this phylum (Figure 5.1). In agreement with previous analyses, the skeletal proteome of *P. flava* includes proteins with a widespread distribution among cnidarians, such as all detected collagens, agrin, osteonidogen, galaxin, and several enzymes, among others. These proteins are typical components of animal basement membranes (Erickson and Couchman 2000) and are thus likely to have a broad distribution within Cnidaria and generally within Metazoa. Other proteins, like hemicentin or the protein kinase Nell 1,

displayed a more patchy occupancy and were found mostly in other anthozoans. Finally, only a few SOM components, namely the two acidic proteins found, a serine protein-kinase receptor and a protein similar to laminin, had a restricted taxon occupancy with significantly similar proteins found almost exclusively in other octocorals (i.e., Order Alcyonacea).

In contrast to stony corals, octocorals are resilient and tolerant of climate change-induced stress (Inoue et al. 2013; Gmez et al. 2015). A possible mechanism explaining this is the hypothesized protective role of the octocoral tissues that effectively isolate sclerocytes from the surrounding seawater, allowing them to deposit new sclerites to support growth under stressful conditions (Gabay et al. 2014). Under this "calcification as usual" scenario, stressful environmental conditions should not lead to a significant change in the expression of transcripts involved in calcification, like those encoding SOM proteins. To test this prediction, we exposed colonies of *P. flava* to conditions simulating global warming and ocean acidification and used RNA-Seq to assess how these climate change-driven stress factors affect colony-level transcription. Exposure to sublethal, high seawater temperatures (ca. 31 °C) resulted in the modulation of 751 transcripts (Benjamini-Hochberg corrected $p < 0.05$), with 221 and 108 transcripts down (\log_2 fold change ≤ -1) or upregulated (\log_2 fold change ≥ 1) in heat-treated colonies. GO-term enrichment analyses revealed that heat-stressed colonies actively modulated transcripts involved in redox homeostasis and protein folding, including two representatives of the heat-shock protein 70 family, and processes like cell death and immune response (Figure 5.2). This response is in line with observations in stony corals exposed to similar environmental conditions (Barshis et al. 2013) and indicates that the sublethal heat treatment was successful in triggering a stress response in the exposed colonies. Heat stress did not, however, result in a significant change in the expression of any of the 28 transcripts encoding SOM proteins in *P. flava*, and only caused the significant downregulation of two proteins -one carbonic anhydrase and one galaxin- out of 27 calcification-related proteins previously identified in octocorals (Conci, Wrheide, et al. 2019). In contrast, heat stress resulted in a generalized down-regulation of calcification related transcripts (four of five tested) in the stony coral *Acropora hyacinthus* (Barshis et al. 2013).

In agreement with previous observations in highly resilient corals species, such as *Montipora digitata* (Gonzlez-Pech et al. 2017), ocean acidification did not trigger a stark stress response in *P. flava*. Colonies of this species exposed to simulated ocean acidification significantly ($p < 0.05$) downregulated a set of 70 transcripts enriched in transcripts involved in vacuolar transport and transmembrane signaling, among others, and including skeletogenesis-related GO-terms such as the "Regulation of bone mineralization" or "Bone trabecula formation". Downregulated transcripts included one calcification-related, uncharacterized skeletal matrix protein, and two SOM-encoding transcripts, namely osteonidogen - the second more abundant SOM protein - and a prosaposin-homolog. Although the precise role of these proteins in sclerite deposition remains unknown, mammalian osteocytes and osteoclasts overexpress osteonidogen (Bechtel et al. 2012), and mutations in human prosaposin cause Guacher's disease, a disorder characterized by the deterioration of the skeleton (Vaccaro et al. 2010). Thus, a direct involvement of these proteins in calcification in octocorals seems also plausible. The modest effect of ocean acidification on calcification-related transcripts in *P. flava* contrasts with the reported up and downregulation of four and 26 SOM-encoding transcripts in primary polyps of *Acropora millepora* (Ramos-Silva et al. 2013) and with the generalized upregulation observed in adult *Siderastrea siderea* colonies (Davies et al. 2016) exposed to these same conditions, and point to fundamental differences in the regulation of the calcification molecular toolkit between soft and stony corals exposed to climate change-driven environmental stress.

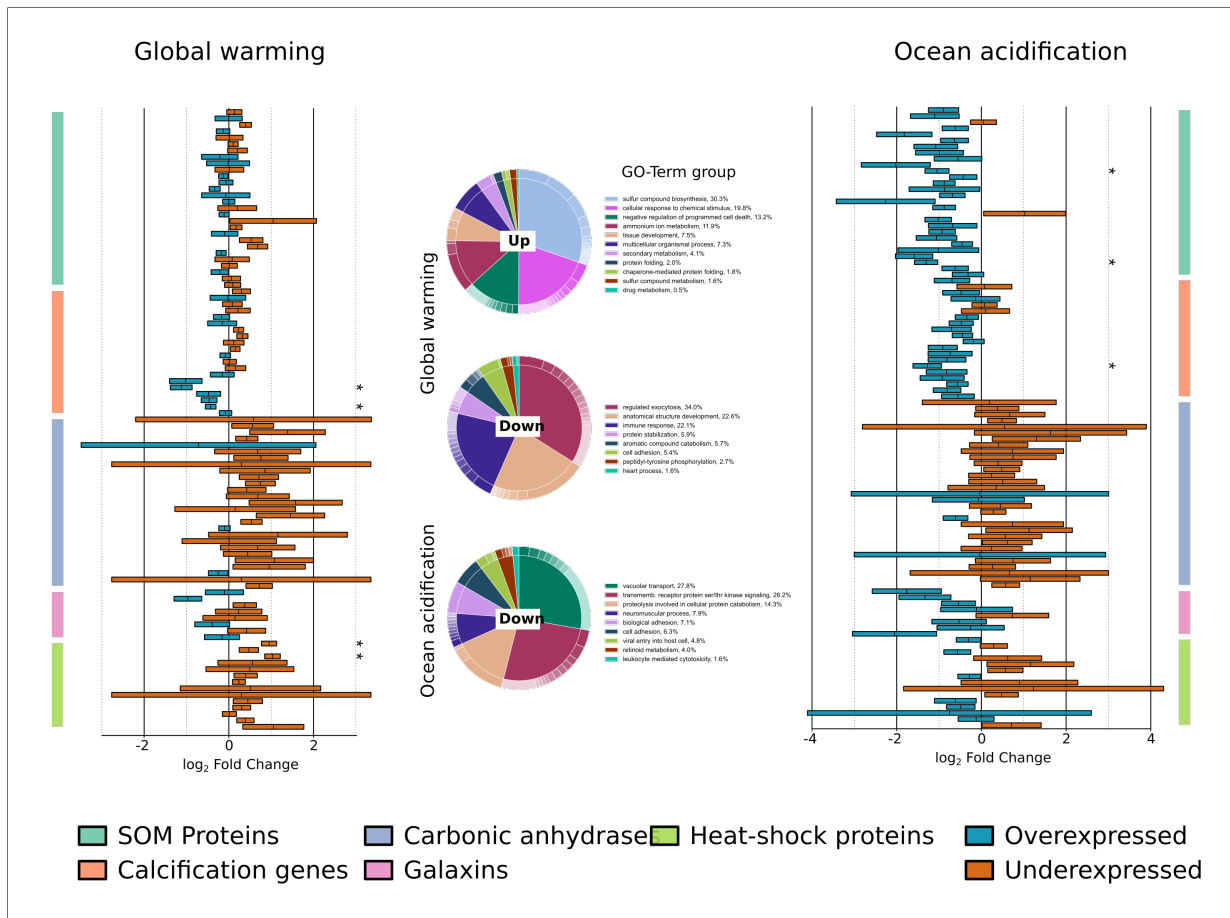


Figure 5.2: Changes in gene expression of 27 SOM proteins, calcification related proteins sensu Conci et al. (2019), carbonic anhydrases, galaxins and heat-shock proteins in *P. flava* colonies exposed to simulate sea surface warming and ocean acidification. Enriched GO-terms in the set of over or underexpressed genes under each treatment is provided in the middle panel.

To respond more rapidly to and survive episodes of environmental stress, resilient stony corals constitutively upregulate components of the coral cell death and immune pathways, and genes involved in response to stress, like heat-shock proteins (Barshis et al. 2013). The concomitant downregulation of genes involved in calcification observed during environmental stress in these organisms (Barshis et al. 2013; Ramos-Silva et al. 2013) suggests that the transcriptional frontloading of the stress response toolkit comes at the expense of the coral calcification machinery and could lead to its collapse. Accordingly, colonies of *S. siderea* exposed to ocean acidification and warming show a parabolic response of calcification, mostly driven by the abrupt drop in calcification rates under more extreme environmental regimes (Castillo et al. 2014). In contrast, our results indicate that octocorals mechanistically decouple the transcriptional regulation of the calcification and stress-response toolkits and sustain the production of all the molecules necessary for the formation of new sclerites during events of climate change-driven environmental stress. The linear response of octocoral calcification rates under conditions of ocean acidification (Gmez et al. 2015) supports this idea as it indicates that the observed drop in calcification is mostly driven by the environmental setting, not by the response of the octocorals, as expected from a "calcification as usual" strategy. Under long-term adverse conditions, this strategy gives octocorals a

competitive advantage over other species adapted to respond better to episodic stress and can lead to the community shifts observed in many reef locations (Inoue et al. 2013; Ruzicka et al. 2013).

In summary, our results provide mechanistic insights into octocoral resilience to climate change. They indicate that the fundamental differences in the way in which the calcification and stress-response toolkits of soft and stony corals interplay lie at the base of the different responses to climate change observed in these groups. Extreme climatic events, like the heat waves affecting the Great Barrier Reef in 2016 and 2017 (Hughes et al. 2019), are likely to increase in frequency as a consequence of anthropogenic-induced global climate change and will undoubtedly impact marine communities in unprecedented ways. Processes such as acclimation and adaptation (Palumbi et al. 2014), acting at organismal- and population-levels, and phenomena affecting the community, like ecological memory (Hughes et al. 2019), shape the response of coral reefs to these environmental pressures. We show that, compared to stony corals, octocorals use different gene regulation strategies to face climate change. Thus, understanding the diversity of molecular mechanisms involved in resilience, as well as their regulation in different reef organisms, is pivotal to predicting the future of the world coral reefs.

5.3 Materials and Methods

5.3.1 Experimental model and subject details

Experiments were done using clonal pieces of a colony of *Pinnigorgia flava* (Nutting, 1910) kept at 25°C and an 12:12 hour light cycle in a 642 L marine aquarium system at the Department of Geo- and Environmental Sciences, Section Paleontology and Geobiology, Ludwig-Maximilians-Universität Munich. *P. flava* is a colonial zooxanthellate soft coral (Octocorallia) endemic to the Great Barrier Reef and sporadically found in the coral triangle in SE Asia. It is characterized by non-anastomosing, pinnated light purple branches with brownish polyps. Sclerites are white to yellow in color. Among the sclerites, c-shaped spindles, which can bend and appear v- or s-shaped, spindles and capstans can be observed. Polyp sclerites are rod-like. Currently *P. flava* is classified in the family Gorgoniidae.

5.3.2 Determination of calcification hot-spots along the body axis of *P. flava*

We used calcein, a calcium-binding fluorescent dye which is permanently incorporated into the skeletal tissue, to investigate the distribution of calcification sites along *P. flava*'s body axis (Holcomb, Cohen, and McCorkle 2013/2). We incubated three colonies of *P. flava* for 72 hours in a glass container with 500ml of a 50g/ml calcein disodium salt (Sigma-Aldrich) in 0.2 μ m filtered artificial seawater (supplementary figure S5.1). We exchanged the seawater with fresh seawater+calcein every 24 hours. After staining, we fixed the colonies in 80% EtOH and stored them at ca. 5°C until further processing. To assess whether calcification preferentially occurs on the tip of the colonies or, on the contrary, the calcification hot-spots are distributed along the colony body axis, we cut the colonies from top to bottom every 5 mm using a sterile scalpel, and placed each piece in 1.5 ml microcentrifuge tubes containing 1 ml of sodium hypochlorite (NaOCl 10%; Fluka). After three hours of incubation in bleach, we rinsed the sedimented sclerites six times with distilled water and stored them in 80% ethanol. To determine the number of stained sclerites per colony region, we placed a sample of sclerites onto glass slides, let the ethanol evaporate, embedded them in Eukitt quick-hardening mounting medium (Fluka Analytical) and

covered the sample with a glass coverslip to dry for at least 24 hours. We then observed the sclerites under epifluorescence (excitation filter band pass 420-490 nm, barrier filter 515 nm long pass) on a Leica DMLB microscope coupled to a Leica DFC 480 camera and an I3 filter set. We exposed the stained sclerites for 10 seconds and acquired pictures using Leica Application Software LAS V4.5. For each tip, middle and bottom sclerite sample of every colony, we sampled along one horizontal transect crossing the slide from left to right and counted stained and total sclerites at a 100X magnification.

5.3.3 Proteomic analysis of the skeletal organic matrix of *P. flavas* sclerites

To determine the skeletal proteome of *P. flava*, we sampled four colonies of about 4 cm in length from the aquarium and incubated them in sodium hypochlorite (5%, Fluka) for 72 hours under moderate shaking (30 rpm; IKA Rocker 3D digital) to isolate the sclerites. We then rinsed the sedimented sclerites six times with Milli-Q water and dried them at 37°C for 24 hours. This procedure yielded approximately 0.75 g of dry sclerites, which we ground with a mortar and pestle before incubating again in sodium hypochlorite (2%) for four hours under moderate mixing (30 rpm). After bleaching, we rinsed the powder six times with Milli-Q water and dried it overnight at 37°C. To dissolve the calcitic mineral, we incubated the dry powder at room temperature in 10% acetic acid overnight, under moderate mixing (20 rpm). We centrifuged the resulting solution at 13,500 rpm for 30 minutes to separate the acetic insoluble matrix (AIM), which sediments to form a pellet, from the acetic soluble matrix (ASM), which remains dissolved in the supernatant. In the case of the ASM, we centrifuged (4600 rpm for 70 minutes at 16°C) the supernatant through 15 mL Amicon ultrafiltration devices with a 3 kDa cutoff membrane. Proteins were precipitated from the desalted solution following the method described by Wessel and Flügge (1984). Briefly, four volumes of methanol, one volume of chloroform and three volumes of MilliQ water were added to one volume of sample. Solution was centrifuged at 5,500 rpm for 15 minutes. The upper phase was discarded and three volumes of methanol added, followed by centrifugation at 5,500 rpm for 15 min.

We air-dried the resulting ASM pellet and resuspended both the ASM and AIM fractions in 95% Laemmli buffer + 5% β -mercaptoethanol. We used a 1-dimensional sodium dodecyl sulfate-polyacrylamide (SDS-PAGE) minigel (Mini-PROTEAN Tetra System, Bio-Rad, USA) to electrophoretically separate the skeletal organic matrix proteins prior to mass spectrometry. To visualize the extracted SOM protein fractions, we ran an SDS-PAGE for 90 minutes at 80V increasing the voltage to 100V after the gel front passed the boundary between the stacking and the resolving gel. We used the Precision Plus Protein Dual Xtra Standard (Bio Rad, 12 band, 2kD-250kD) as a size standard and stained the gel after fixing for 20 minutes in a fixation solution (50% ethanol, 4% MilliQ and 10% acetic acid), washing in 30% ethanol for ten minutes, and in Milli-Q water for ten minutes, with silver nitrate using the Proteo Silver Plus Silver Stain Kit (Sigma-Aldrich, USA). For this, we incubated the gel in sensitizer solution for 10 minutes, washed it as described above and equilibrated it for 10 minutes in silver solution. Before developing, we washed the stained gel again for one minute with Milli-Q water and submerged it in developing solution for 5 minutes. After stopping the development reaction we washed the gel for 15 minutes in Milli-Q water. We used an orbital shaker at 60 rpm for all steps described above. For mass spectrometry, we ran the SDS-PAGE with the extracted SOM protein fractions for 40 minutes at 80V until the protein extracts passed the boundary between the stacking and the resolving gel, stopped the run at this point and manually excised the bands with a sterile scalpel. We then subjected the isolated proteins to alkylation, reduction and tryptic digestion (0.1 $\mu\text{g}/\mu\text{l}$ trypsin at 37°C, overnight). We used an LTQ

Orbitrap mass spectrometer (Thermo Fisher Scientific, Waltham, Massachusetts, USA) coupled with a Rheos Allegro liquid chromatograph (Flux Instruments GmbH, Basel, Switzerland) to analyze three μ l of the digested sample after separation using a self-made column of 75 μ m diameter, 15 cm length, C18 particles of 2 μ m diameter and 100 \AA pore size (Dr. Maisch GmbH, Ammerbruch-Entringen, Germany). We prepared the MS grade mobile phases as follows A) water containing 10% acetonitrile (ACN), B) ACN containing 10% water, each combined with 0.1% formic acid. We used the following gradient: 40 min (0-23% B), 40 min (23-85% B), 5 min (85-100% B), 25 min (100% B), 3 min (100-0% B) and 20 min (0 % B) for re-equilibration, and a constant 40 μ l/min flow at RT (22°C). We used the programs Xcalibur 2.0 (Thermo Fisher Scientific Inc., 30 Waltham, USA) and MaxQuant Version 1.5.2.8 (Cox and Mann 2008) to acquire and analyze the MS/MS data, respectively. The LC-MS/MS results were filtered to remove hits from known standard contamination sources using the common Repository Adventitious Proteins (cRAP) database before mapping the peptides against a transcriptome reference for *P. flava* (Conci, Wrheide, and Vargas 2019). A total of six technical replicates were analysed to evaluate the consistency with which a protein was detected in the SOM fractions. We translated the transcripts found to be present in the SOM fractions and annotated them against the UniProtKB database using blastp. In addition, we used SignalP 4.0 (Petersen et al. 2011) to respectively predict the presence of signal peptides, transmembrane regions and GPI anchors within the protein sequences.

5.3.4 *In vivo* experiments

To assess the effect of global warming on *P. flava*, we randomly assigned nubbins (n=18) to six 10L aquaria filled with ca. 6 L artificial seawater. Water evaporation was compensated every day with water filtered by reverse osmosis. We partially immersed these tanks in a 360L water tank with a constant temperature of ca. 25.4°C (supplementary figure S5.1) and kept the octocorals at ambient atmospheric pCO₂ in a 12:12 light/dark regime using GHL Mitras LX 6200-HV LED lights that yielded 10 kLux at the water surface. To provide an adequate water mixing in each tank, we used a submersible water pump (300 L/h; Eheim, Germany). After an acclimation period of four days, we randomly selected three tanks and gradually increased the water temperature to 30-31°C during five days (ca. 1°C per day) using a 50W water heater (Eheim, Germany). We then kept the *P. flava* colonies at 30-31°C for 3 days. Afterwards, we cut octocorals in two lower and upper sections using sterile scissors and flash frozen them in liquid nitrogen before storing them at -80°C until further processing. During the course of the experiment, we monitored the water temperature every minute using PCE-PHD 1 dataloggers (PCE, Germany) and, additionally, we manually measured the temperature of all aquaria twice a day (in the morning and the evening) using a regular thermometer (TFA, accuracy \pm 0.5°C). We also measured water conductivity, pH, density, redox potential on a daily basis, and several nutrients and minerals every other day. Finally, we measured the total alkalinity of the water at the beginning and the end of the experiment using the Orion total alkalinity test kit (Thermo Scientific, USA) and used the program CO2SYS (Pierrot, Lewis, and Wallace 2006) with a dissociation constants for boric acid and K1 and K2 from Mehrbach et al. (1973) refit by Dickson and Millero (1987), KSO₄ from Dickson (1990) and pH on the total scale.

We assessed the effect of ocean acidification on twelve colonies of *P. flava* distributed in two 30 L tanks (control and treatment) connected to a 320L salt-water mother tank. To lower (0.1 drop per day) the seawater pH, we pumped CO₂ into the treatment tank to achieve a pH of 7.8 (from a starting value of 8.2). We kept the pH stable during a period of three days, and lowered it again to 7.6 over three days.

After reaching pH=7.6, we allowed the octocorals to acclimate during three days before decreasing the pH to its final value of 7.3. This pH was maintained for a period of ca. 2 months. The pH was monitored throughout the whole experiment using a PCE-PHD 1 datalogger (Hersteller). The pH of the mother and control tank was 8.2 throughout the experiment. As in the temperature experiment above, we kept the octocorals on a 12:12 h light/dark regime, at ca. 25°C water temperature. At the end of the experiment, we cut the octocorals at the base using sterile scalpels, flash frozen them in liquid nitrogen before storing them at -80°C until further processing.

5.3.5 RNA extraction and library preparation

We extracted total RNA from the upper section of the octocorals using the Direct-zol RNA MiniPrep kit (Zymo Research) following the manufacturers protocol. We assessed the purity and integrity of the RNA extracts using a Nanodrop ND-1000 spectrophotometer (Thermo Fisher Scientific, USA) and a Bioanalyzer 2100 (Agilent Inc., USA), and used Lexogens SENSE Total RNA-Seq Library Prep kit according to the manufacturers instructions to generate Illumina-ready transcriptomic libraries for all samples. We sequenced the libraries (50 PE) in a HiSeq2000, quality controlled the program filter-illumina from the bioclite suite and mapped them to the *P. flava* reference transcriptome (Conci, Wrheide, and Vargas 2019) using Salmon (Patro et al. 2017). We analysed the resulting count matrix using DESeq2 (Love, Huber, and Anders 2014) and used the resulting list of differentially expressed genes for GO-term enrichment analyses using TopGO (Alexa and Rahnenfuhrer 2016).

Chapter 6

A 16S rRNA gene sequencing and analysis protocol for the Illumina MiniSeq platform.

6.1 Abstract

Highthroughput sequencing of the 16S rRNA gene on the Illumina platform is commonly used to assess microbial diversity in environmental samples. The MiniSeq, Illumina's latest benchtop sequencer, enables more costefficient DNA sequencing relative to larger Illumina sequencing platforms (*e.g.*, MiSeq). Here we used a modified custom primer sequencing approach to test the fidelity of the MiniSeq for highthroughput sequencing of the V4 hypervariable region of 16S rRNA genes from complex communities in environmental samples. To this end, we designed additional sequencing primers that enabled application of a dualindex barcoding method on the MiniSeq. A mock community was sequenced alongside the environmental samples in four different sequencing runs as a quality control benchmark. We were able to recapture a realistic richness of the mock community in all sequencing runs, and identify meaningful differences in alpha and beta diversity in the environmental samples. Furthermore, rarefaction analysis indicated diversity in many environmental samples was close to saturation. These results show that the MiniSeq can produce similar quantities of highquality V4 reads compared to the MiSeq, yet is a costeffective option for any laboratory interested in performing highthroughput 16S rRNA gene sequencing.

6.2 Introduction

Continued improvements in DNA sequencing technologies have greatly helped in the democratization of sequencing (Tringe & Hugenholtz, 2008) and highthroughput sequencing of the 16S rRNA marker gene is widely used to assess diversity and composition of microbial communities (e.g., Bartram, Lynch, Stearns, MorenoHagelsieb, & Neufeld, 2011; Caporaso et al., 2012; Huber et al., 2007; Sogin et al., 2006). However, the startup and maintenance costs associated with highthroughput sequencing still hamper access to these technologies by smaller laboratories.

Illumina's MiniSeq benchtop platform enables costefficient highthroughput DNA sequencing relative to larger sequencing platforms (e.g., MiSeq). Thus, the goal of this study was to assess the quality of the MiniSeq generated 16S rRNA gene sequence data and to evaluate if this platform is a feasible option for performing 16S rRNA gene highthroughput sequencing. This would open the possibility for smaller labs to perform their own highthroughput 16S rRNA gene sequencing, because the MiniSeq is a benchtop sequencer available for ca. 30% of the cost compared to the MiSeq. Furthermore, the reagent kits for the MiniSeq are also ca. 30% the cost of the MiSeq, yet are capable of generating up to 8 million pairs of reads, and the High Output version of this kit produces a volume of sequence data up to 25 million reads (Illumina 2016a).

The dualindexed custom primer 16S rRNA gene sequencing protocol for the V4 hypervariable region is widely applied in microbial diversity studies (Kozich, Westcott, Baxter, Highlander, & Schloss, 2013), but was originally developed for sequencing on the MiSeq platform. Thus, our aim was to optimize this dualindexed custom primer 16S sequencing protocol for the MiniSeq platform, in order to test the fidelity of the MiniSeq for 16S rRNA gene sequencing. Our modifications to the existing highthroughput 16S rRNA sequencing protocol (Kozich et al., 2013) use new sequencing primers to adapt this method for the MiniSeq. We performed multiple highthroughput sequencing runs targeting the V4 hypervariable region of the 16S rRNA gene derived from complex environmental samples, alongside a mock community with a known number of different species. Platform fidelity was assessed by alpha diversity analyses of a mock community of known species composition, which shows that with the proper quality controls the MiniSeq is capable of producing quality 16S rRNA gene sequence data that can be used to rapidly and reliably assess microbial diversity in complex environmental samples.

6.3 Materials and Methods

6.3.1 Cultivation and DNA extraction of the 16S mock community

To create a mock community (>3 dissimilarity threshold), pure cultures were isolated from soil, human skin, cell phone swabs, freshwater and saltwater, and grown on agar plates for 37 days at room temperature. For genomic DNA extraction, a small amount of each bacterial strain was transferred into a 2 ml sterile lysing Matrix E tube and 800 μ l of preheated (60°C) sterile filtered C1 extraction buffer (38 ml saturated NaPO₄ [1 mol/L] buffer, 7.5 ml 100% ethanol, 4 ml MoBio's lysis buffer solution C1 [MoBio, Carlsbad, CA], 0.5 ml 10% SDS) was added. The samples were homogenized for 40 s at a speed of 6 m/s using a QuickPrep24 5G homogenizer (MP Biomedicals, Santa Ana, CA) and heated for 2 min at 99°C in an Eppendorf ThermoMixer C (Thermo Fisher Scientific, Waltham, MA), followed by two freezethaw (−80°C / room temperature) cycles to lyse bacterial cells. After repetition of the homogenizing step, the

samples were centrifuged for 10 min at 10,000 g in a Heraeus Pico 21 centrifuge (Thermo Fisher Scientific, Waltham, MA). Microbial DNA was purified using the MoBio PowerClean Pro DNA CleanUp Kit (Qiagen, Hilden, Germany) following the manufacturer's instructions using 100 μ l of the supernatant. DNA was quantified fluorometrically on the Qubit version 3.0 (Life Technologies, Grand Island, NY) using the Qubit dsDNA high sensitivity assay kit (Life Technologies).

To confirm the number of species in the mock community, the full length 16S rRNA gene of each isolate was amplified and sequenced by Sanger sequencing. Two conserved primers (27f, 1492r) were used to amplify the entire gene during PCR with the following conditions: initial denaturation at 95°C for 3 min; 30 cycles of denaturation at 95°C for 30 s; annealing at 56°C for 30 s; elongation at 72°C for 1 min and a final 5 min extension at 72°C. Individual reactions consisted of 1 μ l template DNA, 5 μ l 5x Green GoTaq Flexi Buffer (Promega), 3 μ l MgCl₂ (25 mmol/L), 1 μ l fw primer (10 μ mol/L), 1 μ l rv primer (10 μ mol/L), 12.9 μ l nucleasefree water, dNTP Mix (10 mmol/L), and 0.1 μ l GoTaq Green DNA Polymerase (Promega). The amplicons were subjected to Sanger sequencing using the facilities of the Biocenter of the LudwigMaximilian University (LMU), Martinsried. To confirm dissimilarity thresholds of $\geq 3\%$ for all 18 species, we aligned the sequences using BLAST version 2.2.26+ (Altschul, Gish, Miller, Myers, & Lipman, 1990). We pooled the isolates at equimolar concentration and created technical replicates of the mock community to assess the reproducibility of the method.

Environmental samples included salt marsh sediments, freshwater pond sediments, marine sponges, salt water aquaria, and carbonate biofilms (Figure 6.3). Samples to assess levels of contamination (which were also sequenced, and OTUs removed from the environmental samples) were collected from dust in three different labs in the building where the sequencing and PCR amplifications were performed. Genomic DNA of environmental samples (Run A, n = 45; Run B, n = 88; Run C, n = 84; Run D, n = 90) was extracted according to the protocol of Orsi et al. (2017). In brief, samples were transferred to either 50ml or 2ml Lysing Matrix E tubes containing 1.4 mm ceramic spheres, 0.1 mm silica spheres, and one 4 mm glass sphere (MP Biomedicals, OH) following each incubation. 15 ml (for 50 ml tubes) or 1 ml (for 2 ml tubes) of the extraction buffer (C1 lysing buffer (MoBio, Carlsbad California), 10% SDS, 100% ethanol, and 1 mol/L Na₂HPO₄) was added and homogenized for 40 s in a FastPrep 5G homogenizer at a speed of 6 m/s. Then, the supernatant containing the DNA was purified with the DNeasy PowerClean Pro Cleanup Kit (Qiagen, Germany). Extracted DNA was quantified by using the Qubit doublestranded DNA (dsDNA) high sensitivity assay kit and a Qubit 3.0 fluorometer (Invitrogen, Eugene, OR).

6.3.2 16S amplicon library preparation

For Runs A and B, the V4 region of the 16S rRNA gene was amplified with unique barcoded PCR primers 515F (5' AATGATACGGCGACCACCGAGATCTACAC NNNNNNNN **TATGGTAATT** GT *GT-GCCAGCMGCCGCGGTAA* 3') and 806R (5' CAAGCAGAAGACGGCATAACGAGAT NNNNNNNN **AGTCAGTCAG** CC *GGACTACHVGGGTWTCTAAT* 3') (see Table S3 in the supplemental material for barcodes). For Runs C and D, we used modified 515FY/806RB primer constructs (515FY: 5'GTGYCAGCMGCCGCGGTAA; 806RB: GGACTACNVGGGTWTCTAAT), which include the latest changes that increase coverage of Thaumarchaeota (Parada, Needham, & Fuhrman, 2016) and further enable capturing of a greater diversity of the marine SAR11 clade (Apprill, McNally, Parsons, & Weber, 2015) (Table S3). The primer sequences all consist of the appropriate Illumina adapter (P5 or P7; underlined) complementary to the oligonucleotides on the flow cell, an 8nt index sequence representing the unique barcode for every sample (N region), a 10nt pad sequence (bold), a 2nt linker (GT, CC), and

the specific primer for the V4 region (*italic*) (Figure 6.1). All samples were amplified on the Biometra TProfessional Thermocycler (Biometra, Gttingen, Germany) in a total reaction volume of 24 μ l including 2 μ l template DNA, 5 μ l 5x Green GoTaq Flexi Buffer (Promega), 1 μ l forward primer (10 μ mol/L), 1 μ l reverse primer (10 μ mol/L), 1 μ l dNTP Mix (10 mmol/L), 3 μ l MgCl₂ (25 mmol/L), 0.2 μ l GoTaq Green DNA Polymerase (Promega), and 12.8 μ l nucleasefree water. PCR program was run as follows: initial denaturation at 95°C for 3 min, followed by 30 cycles of denaturation at 95°C for 30 s, annealing at 56°C for 30 s, elongation at 72°C for 1 min and a final elongation step at 72°C for 5 min.



Figure 6.1: Schematic description of the dualindex sequencing strategy on the MiniSeq. Reading the figure from top to bottom shows the sequential order of pairedend sequencing steps (four total). Turn around indicates the step of pairedend turn around on the flow cell surface. The sequencing proceeds in the direction of the flow cell surface, which in this figure is located on the right side (arrows point in direction of sequencing reaction). Sequencing starts by using Read 1 primer to sequence Read 1, followed by Index 1 primer to generate Index 1. The MiniSeq only uses the oligonucleotides on the flow cell for bridging and both the second index and the paired read are sequenced after the clusters are turned around. Hence an Index 2 primer is needed to sequence Index 2. Read 2 is then sequenced by using the Read 2 primer (after Kozich et al., 2013). Sequencing primers for only the forward primer 515FY (Parada et al., 2016) are shown, for sequencing primers needed for the 515F primer (Caporaso et al., 2012) please see Table 1 for all sequencing primers

The barcoded DNA amplicons were analyzed on a 1.5% (w/v) agarose gel, and excised and purified for sequencing using the Zymoclean Gel DNA Recovery Kit (Zymo Research, Irvine, CA), adding 15 μ l of buffer EB to elute DNA. After gel extraction, DNA concentrations were measured using Qubit and diluted first to 10 nmol/L and then to a final 1 nmol/L in a serial dilution before the samples were pooled (adding 5 μ l of every sample).

6.3.3 16S sequencing strategy and primer design

We had to design additional Index 2 sequencing primers (see Table 1) to enable the dualindex barcoding method on the MiniSeq. Without these additional index sequencing primers on the MiniSeq, it is impossible to demultiplex the samples after the run because the Index 2 sequences will not be sequenced. An additional Index 2 sequencing primer is needed because, as opposed to the MiSeq, the MiniSeq only reads Index 2 after the clusters have been turned around to sequence the pair reads (see Figure 6.1). Sequencing proceeds in the direction of the flow cell and starts by generating Read 1 (150 bp) using Read 1 sequencing primer, followed by obtaining Index 1 (8 bp) using Index 1 sequencing primer. Clusters are turned around using the oligonucleotides provided on the flow cell. After bridging, Index 2 sequencing primer generates Index 2 (8 bp) and Read 2 sequencing primer finally obtains Read 2 (150 bp).

Table 3: Custom sequencing primers used in this study to sequence the 16S rRNA gene (V4 region) amplicons

V4 sequencing Primer	Sequence (5'3')	Cartridge position	Total volume (μ l)	Final concentration (μ mol/L)
a)				
Read1.515F	TATGGTAATTGTGTGCCAGCMGCCGCGGTAA	24	16.5	10
Read2.806R	AGTCAGTCAGCCGACTACHVGGGTWTCTAAT	25	18.3	10
Index1.806R	ATTAGAWACCCBDGTAGTCCGGCTGACTGACT	28	24.6	10
Index2.515F	TTACCGCGGCKGCTGGCACACAATTACCATA	28	25.3	10
b)				
Read1.515FY	TATGGTAATTGTGTGYCAGCMGCCGCGGTAA	24	16.5	10
Read2.806RB	AGTCAGTCAGCCGACTACNVGGGTWTCTAAT	25	18.3	10
Index1.806RB	ATTAGAWACCCBNGTAGTCCGGCTGACTGACT	28	24.6	10
Index2.515FY	TTACCGCGGCKGCTGRCACACAATTACCATA	28	25.3	10

The primers were diluted and loaded into the specified positions on the Illumina reagent cartridge. We used primers shown in (a) for sequencing Runs A and B, where primers shown in (b) were used for sequencing Runs C and D. We used the additional Index 2 sequencing primers to perform four pairedend 16S rRNA sequencing runs on the MiniSeq (Runs AD). For all runs, we used the MiniSeq Mid Output Reagent Kit (300 cycles) including a reagent cartridge, a singleuse flow cell and hybridization buffer HT1. To prepare our normalized amplicon libraries for sequencing, we followed the MiniSeq Denature and Dilute Libraries Guide (Protocol A) (Illumina 2016d) with some customizations. For run A, we combined 500 μ l of the denatured and diluted 16S library (1.8 pM) with 20 μ l of denatured and diluted Illumina generated PhiX control library (1.8 pM). The method used to align sequences to PhiX to determine the error profiles is made possible by the software provided by Illumina that is preinstalled on the sequencer. This is calculated automatically by the software after each run, as long as the PhiX has been added to the library loaded into the reagent cartridge. For Run B, C, and D, we combined 350 μ l of the 16S library (1.8 pM) with 150 μ l of a denatured and diluted genomic sponge library (*Ephydatia fluviatilis*, 1.8 pM) and additionally added 15 μ l of PhiX (1.8 pM). The final 1.8 pM libraries were loaded into the Load samples well of the reagent cartridge. For each run, we used four custom sequencing primers Read 1, Index 1, Index 2, and Read 2, which were diluted and loaded into the correct position of the reagent cartridge (see Table 1). The results of the MiniSeq sequencing runs and the 16S rRNA gene sequences from the mock community are publicly available in the ENA Project PRJEB24504.

6.3.4 16S bioinformatics analysis and OTU assignment

Demultiplexing and base calling were both performed using bcl2fastq Conversion Software v2.18 (Illumina, Inc.). All bioinformatics analysis were conducted in USEARCH version 9.2.64 (Edgar, 2010) and QIIME version 1.9.1 (Caporaso et al., 2010). The initial step was to assemble pairedend reads using the fastq_merge_pairs command with default parameters allowing for a maximum of five mismatches in the overlapping region. Stringent quality filtering was carried out using the fastq_filter command. We discarded lowquality reads by setting the maximum expected error threshold (E_max), which is the sum of the error probability provided by the Q score for each base, to 1. Reads were dereplicated and singletons discarded. Reads were clustered into OTUs sharing 97% sequence identity using the heuristic clustering algorithm UPARSE (Edgar, 2013), which is implemented in the cluster_otus command. The algorithm performs de novo chimera filtering and OTU clustering simultaneously (Edgar, 2013). The usearch_global command assigned the reads to OTUs and created an OTU table for further downstream analysis. Taxonomy was assigned in QIIME (Caporaso et al., 2010) through BLASTn searches 2.2.26+ (Altschul et al., 1990) with an identity threshold of 90% (hits below 90% identity were not considered) against the SILVA ribosomal RNA gene database (Quast et al., 2013) release for QIIME SILVA123. As a quality control step, we removed all OTUs containing <10 sequences and which had no BLASTn hit. Spurious OTUs were identified in the mock community as those OTUs with a closest BLASTn hit to organisms that were not in the original mock community. The OTU tables were rarefied to the sample containing the lowest number of sequences, with a threshold of >10,000 sequences (all samples having less than 10,000 sequences were removed from analyses prior to the rarefaction step).

6.3.5 16S Data Analysis

In order to investigate beta diversity structures of our samples, we performed downstream analysis in R version 3.3.0 (R Development Core Team 2011). Nonmetric multivariate (NMDS) analyses of the microbial communities were calculated using a BrayCurtis distance in the Vegan package (Oksanen et al., 2017). Analysis of Similarity (ANOSIM) was performed using 999 permutations with a BrayCurtis distance. Rarefaction analyses on environmental samples were performed in QIIME version 1.9.1 using both observed species and chao1 metrics.

6.4 Results and Discussion

The main modification of our MiniSeq protocol from the dualindex sequencing method of Kozich et al. (2013) is the use of an additional index sequencing primer. This additional index sequencing primer is necessary because the MiniSeq does not sequence the second index using adapters present on the flow cell surface as the MiSeq does. Rather, the MiniSeq reads Index 2 only after the clusters have been turned around to sequence the pairedend reads (figure 6.1). Thus, in addition to the three sequencing primers described by Kozich et al. (2013), we designed and used new Index 2 sequencing primers, Index2.515FY (5'TTACCGCGGCKGCTGRCACACAATTACCATA3') and Index2.515F (5'TTACCGCGGCKGCTG-GCACACAATTACCATA3') to enable the dualindex barcoding method on the MiniSeq (see Table 1 for all sequencing primers). We tested this modified approach on four different 16S rRNA sequencing runs including diverse environmental samples as well as a mock community composed of 18 different bacterial species. The mock community was created from pure cultures, whose 16S rRNA genes were determined

Table 4: Custom sequencing primers used in this study to sequence the 16S rRNA gene (V4 region) amplicons. Runs A and B were performed with primers 515F/806R (Caporaso et al., 2012), and Runs C and D were performed with primers 515FY (Parada et al., 2016) and 806RB (Apprill et al., 2015) PF: passing filter.

	Cycles	Yield	% \geq Q30	Aligned (%)	Error rate (%)	Cluster PF (%)	Reads (in Mio.)	Reads PF (in Mio.)
Cluster density 76 ± 9 K/mm ²	Run A							
Read 1	151	589.25 Mbp	95.18	8.06	1.49	73.28 ± 13.91	5.4	3.9
Index 1	8	27.50 Mbp	94.86	0.00	0.00	73.28 ± 13.91	5.4	3.9
Index 2	8	27.48 Mbp	90.50	0.00	0.00	73.28 ± 13.91	5.4	3.9
Read 2	151	589.04 Mbp	88.96	1.24	1.37	73.28 ± 13.91	5.4	3.9
Totals	318	1.23 Gbp	92.10	8.02	1.37			
Cluster density 170 ± 3 K/mm ²	Run B							
Read 1	151	1.58 Gbp	89.12	24.85	0.93	85.65 ± 1.28	12.2	10.5
Index 1	8	73.73 Mbp	86.14	0.00	0.00	85.65 ± 1.28	12.2	10.5
Index 2	8	73.74 Mbp	80.91	0.00	0.00	85.65 ± 1.28	12.2	10.5
Read 2	151	1.58 Gbp	88.58	24.43	0.65	85.65 ± 1.28	12.2	10.5
Totals	318	3.31 Gbp	88.61	24.64				
Cluster Density 124 ± 1 K/mm ²	Run C							
Read 1	151	1.28 Gbp	95.48	12.19	0.40	95.52 ± 0.54	8.9	8.5
Index 1	8	59.56 Mbp	93.75	0.00	0.00	95.52 ± 0.54	8.9	8.5
Index 2	8	59.57 Mbp	93.39	0.00	0.00	95.52 ± 0.54	8.9	8.5
Read 2	151	1.28 Gbp	94.21	11.98	0.45	95.52 ± 0.54	8.9	8.5
Totals	318	2.67 Gbp	94.79	12.09	0.43			
Cluster Density 120 ± 5 k/mm ²	Run D							
Read 1	151	1.23 Gbp	94.35	8.79	0.93	94.95 ± 1.15	8.6	8.2
Index 1	8	57.34 Mbp	95.23	0.00	0.00	94.95 ± 1.15	8.6	8.2
Index 2	8	57.35 Mbp	93.20	0.00	0.00	94.95 ± 1.15	8.6	8.2
Read 2	151	1.21 Gbp	91.17	8.64	0.65	94.95 ± 1.15	8.6	8.2
Totals	318	2.56 Gbp	91.87	8.71				

through Sanger sequencing to be $>3\%$ different (Table S6.1). Environmental samples were collected from salt marsh sediments, freshwater pond sediments, marine sponge, beach sediments, salt water aquaria, and microbial biofilms recovered on carbonate sediments.

6.4.1 Run Performances

Run A yielded a total of 1.23 Gbp with cluster density of 76 ± 9 K/mm² and $>73\%$ of the clusters passing filter (PF) (Table 2). For Run A, $>92\%$ of all bases from both reads were assigned a quality score of $Q \geq 30$ with an estimated error rate of 1.37% (Table 2). This first attempt appeared to be underclustered considering the low cluster density. According to Illumina's specifications (Illumina 2016b), the recommended cluster density for the midoutput kit (300 cycles) on the MiniSeq is 170220 K/mm². Hence, we optimized cluster density by increasing the genetic diversity of the samples for sequencing runs B, C and D, by spiking in an additional Illumina library of genomic DNA from a marine sponge at a ratio of 1:3 (see Methods). Spiking in the genomic DNA resulted in clusters PF $> 80\%$ for Runs BD, which is expected for optimized cluster density on the platform. For Runs C and D, clustering efficiency of PF $> 95\%$ was achieved. For example, sequencing Run B generated 3.31 Gbp with a cluster density of 170 ± 3 K/mm² and $>84\%$ of clusters PF (Table 2). Run B had 88% of all bases from both reads assigned a quality score of $Q \geq 30$ with an estimated error rate of 0.8%. Run C yielded 2.67 Gbp with a cluster density of 124 ± 1 K/mm² and $>95\%$ of the clusters PF (Table 2).

For Run C, a $Q \geq 30$ was achieved by 94% of all bases, with an estimated error rate of 0.43%. Sequencing Run D generated 2.56 Gbp with a cluster density of 120 ± 51 K/mm² and $>94\%$ of the clusters PF (Table

2). In Run D, 93% of bases had a quality score of $Q \geq 30$ with an estimated error rate of 0.47%. We note that it is difficult to distinguish sequencing errors from PCR errors, and thus refer to the error rates predicted for the amplicons from the PhiX data as estimated error rates as these do not account for PCR errors.

6.4.2 Terminal G homopolymers

The MiniSeq uses a 2channel sequencing by synthesis (SBS) method compared to the 4channel SBS technology used on the MiSeq and HiSeq instruments. Clusters appearing in red and green are cytosine (C) and thymine (T) nucleotides, respectively, whereas adenine (A) bases are detected in both channels and appear yellow. Guanine (G) nucleotides are unlabelled clusters and are seen in neither channel hence they appear black (Illumina 2016c). In our first 16S rRNA sequencing run (Run A) that had relatively poor quality (cluster density 76 ± 9 K/mm², PF < 80%), 7% of forward reads and 8% of reverse reads had long (>10) terminal polyG strings (see Figure S6.1). As G indicates lack of sequencing signal with the Illumina 2dye chemistry (e.g., black), this may be due to underclustering on the flow cell, low diversity in the 16S libraries, or partially amplified V4 PCR fragments carried over during the gel extraction. For this first lowquality run, we removed all sequences with G homopolymers >10 nucleotides prior to data analysis as the polyG homopolymers could apply to all OTUs. Long polyG strings were also not detected in the data from the other 16S sequencing runs (Runs BD), which had genomic DNA spiked in to increase the nucleotide diversity. Thus, the phenomenon of terminal polyG homopolymers appears to be due to the low diversity inherent in 16S sequencing datasets, as this was also not observed in any of our prior genome or transcriptome sequencing libraries on the MiniSeq (data not shown). Thus, we recommend that researchers mix separately indexed genomic libraries together with their 16S rRNA gene libraries when sequencing on the MiniSeq to reduce the number of terminal G homopolymers. Under these conditions, our results show that a cluster density >120 K/mm² and percent of clusters passing filter $\geq 90\%$ provide for a highquality run. We urge caution when analyzing rare taxa (Sogin et al., 2006) with 16S data generated on the MiniSeq, as the lowsequencing depth may not be sufficient. Moreover, sequences with terminal polyG homopolymers need to be carefully accounted for as they could lead to spurious OTUs. Other modern methods of analysis such as DADA2 (Callahan et al., 2016) could assist with polyG containing reads and other erroneous reads in MiniSeq 16S rRNA gene amplicon data.

6.4.3 Mock community analysis

Because the V4 hypervariable region is ca. 250 bp in length the 150 bp pair of reads produced by the MiniSeq overlap 50 bp on average, this may impact diversity estimates (because mismatches in the overlapping contigs are used to assess errors and platform fidelity). We used OTU clustering to see whether the true richness could be recovered in the mock community. For Run A, we had 6 replicates, whereas for Run C and D, 3 replicates were sequenced. After data processing (see Methods), the UPARSE algorithm (Edgar, 2013) recovered 17 of the 18 species in our mock community and 4 spurious OTUs in Run A, 15 species plus 2 spurious OTUs in Run C and 16 species plus 1 spurious one in Run D (Figure 6.2). The mock community was not sequenced alongside the environmental samples in Run B, but mock community sequences from the other three sequencing runs were clustered together with the environmental samples in Run B to assess the diversity in the generated data set. In this case, the number of species found in the mock community was also close to its true composition (16 out of 18 species, 3 spurious OTUs). Six different bacterial species were found among the spurious OTUs derived from the

replicated sequencing runs, of which two were similar (order and family level, respectively) to taxa from the mock community that were not detected. These two spurious OTUs might have been misclassifications due to sequencing errors. The remaining four are presumed to be either contaminants, or derived from sample cross talk. Thus, the UPARSE method could accurately recover the microbial richness from our MiniSeq 16S rRNA gene data. Other studies using UPARSE also showed that the number of OTUs generated with this method is in close concordance with the number of species in mock communities (e.g., Edgar, 2013; Flynn, Brown, Chain, MacIsaac, & Cristescu, 2015). While the exact number of OTUs in the mock community was not obtained (Figure 6.2), mock communities are rarely recovered at the exact richness after 16S highthroughput sequencing with variability reaching >30% of the richness in the original mock community even under stringent criteria (Edgar, 2013). This is typically attributed to additional undetected contaminants, potential multiple rRNA gene copies harbored by some of the genomes, and single sequencing errors that can occur in low abundance in the sample index barcodes (Edgar, 2016). Furthermore, analysis of a mock community sequenced in parallel with environmental samples is challenging due to sample cross talk that can occur partly due to errors in the barcodes themselves (Edgar, 2016). This can occur either during PCR or sequencing, but is difficult to assess if the environmental samples contain similar strains as the mock community. In our case, several of the strains (*Pseudomonas fluorescens*, *Vibrio natriegens*, *Pseudoalteromonas flavipulchra*) in our mock community are closely related to organisms in the environmental samples from marine sediments and corals that were sequenced (Table S1). Thus, it is difficult to speculate on the exact degree of sample cross talk in our sequencing runs.

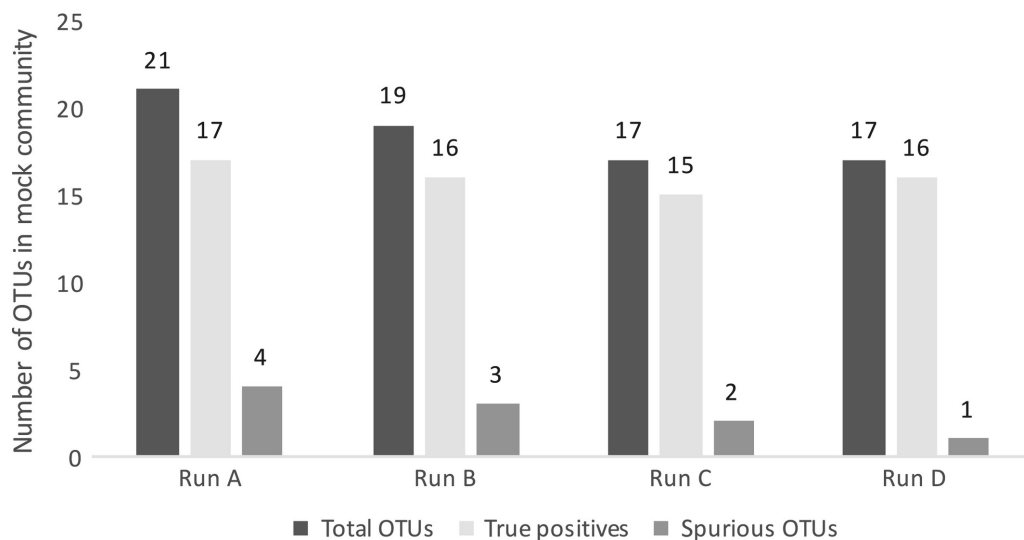


Figure 6.2: OTU assessment for the mock community composed of 18 defined species. UPARSE generated an accurate estimate of the microbial community in all performed 16S rRNA sequencing runs, given the low number of spurious OTUs

6.4.4 Analysis of environmental samples

Our quality control procedures for the MiniSeq 16S rRNA gene data appears to be reasonably prudent, because the richness of our recovered mock community OTUs relative to the starting richness falls within the variability of stringently controlled mock community sequence analyses (Edgar, 2013). To control for contamination, we also sequenced lab dust samples and extraction blanks and removed OTUs shared with the environmental samples. After removal of contaminant OTUs, a significantly different (ANOSIM: $p = .001$, $R: .9$) microbiome for each sample was observed (Figure 6.3). Given that the richness of the mock community is close to the true value, these beta diversity analyses show that the MiniSeq is a viable platform for highthroughput 16S rRNA gene sequencing studies of microbiomes.

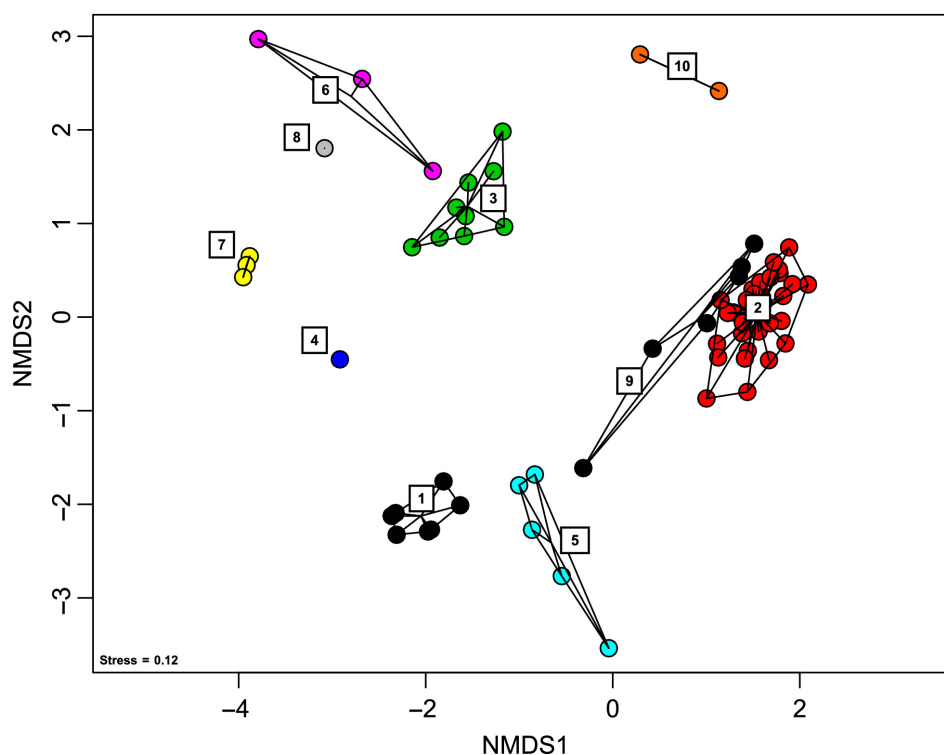


Figure 6.3: Nonmetric multidimensional scaling analysis showing microbial beta diversity of the 16S data sets. (1) mock community replicates, (2) pond sediments (Niederlibbach, Germany), (3) saltmarsh sediments (Cape Cod, MA), (4) salt water aquaria, (5) marine sponge, (6) sandy beach sediments (Obidos lagoon), (7) microbial mats (Obidos lagoon, Portugal), (8) salt marsh sediments (Pt Judith, RI), (9) pond sediments (Niederlibbach, Germany), and (10) carbonate biofilms (Liguria Springs, Italy)

Furthermore, samples included in the rarefaction analysis reached saturation, indicating the MiniSeq can sample diversity adequately from environmental samples (Figure S6.2). For each run, there was variability (0.54%–13.91%) in the number of reads (clusters PF) obtained per sample, with Runs C and D having the least variability in sequencing depth between samples (Table 2). Runs C and D were also the highest quality in terms of % clusters passing filter. These data show that even for a sequencing run with 90 samples, after pooling the samples at equimolar concentrations a highquality run (>90% of clusters PF) on the MiniSeq can provide upwards of ca. 50,000 reads per sample (Table S2).

For future testing of the fidelity of the MiniSeq for 16S rRNA gene sequencing we encourage other researchers to use mock communities constructed from named isolates with highquality genome sequences (e.g., from the DSMZ culture collection: www.dsmz.de), that are not present in the environmental samples. This would reduce potential bias due to sample cross talk with the mock communities, as well as the possibility of multiple 16S rRNA gene copies or paralogs in mock communities constructed de novo that lack complete genome sequences.

Comparing sequencing fidelity across platforms is a feasible way of validating highthroughput sequencing approaches (Caporaso et al., 2012). However, mock communities can also be used as a way to test the fidelity of highthroughput sequencing platforms (BentezPez, Portune, & Sanz, 2016; Caporaso et al., 2011). Thus, while we do not compare our results to those obtained from larger sequencing platforms, for example, a MiSeq (as described by Caporaso et al., 2012), the analyses of the mock community show that the MiniSeq is able to capture a realistic picture of its microbial diversity. For continued testing of the fidelity of the MiniSeq platform for 16S rRNA gene sequencing, future test would benefit from a direct comparison between the same libraries sequenced on both the MiSeq and MiniSeq. For MiniSeq Run D we successfully sequenced 90 samples while yielding ca. 50,000 reads (both forward and reverse) on average per sample. Thus, while the MiniSeq does not provide a sequencing depth equivalent to that of the HiSeq needed for larger scale projects, it represents a new platform for smaller scale sequencing projects (e.g., up to 96 samples, with ca. 50,000 reads per sample) at a reduced per base cost compared to the MiSeq. Our protocol thus increases feasibility for small laboratories to perform their own highthroughput sequencing of the 16S rRNA marker gene.

Concluding Discussion

Coral biomineralization refers to the ability of corals (phylum Cnidaria, class Anthozoa) to construct their skeleton. Although several mechanisms, underlying coral calcification, remain to be elucidated, the combined presence of biological (exerted by the animal) and environmental (linked to abiotic parameter) control, over the process, is widely accepted (Allemand et al. 2004). The calcium carbonate (CaCO_3) polymorph (aragonite or calcite) of the skeleton is among the properties influenced by molecular and environmental factors (Ries 2010; Goffredo et al. 2011). Research on coral calcification has however so far focused on the exclusively aragonitic scleractinian corals (class Anthozoa, order Scleractinia), because of their pivotal ecological role as main reef builders. Contrary, the subclass Octocorallia (class Anthozoa) comprises both aragonite and calcite-forming species (Perez et al. 2016). This provides the unique opportunity to study how coral skeletal structures - characterized by different mineralogies - have evolved, and how organisms and the environment exert control over the deposition of calcite and aragonite. In light of the above, this work aimed at characterizing and comparing the *biomineralization toolkit* (Drake et al. 2012), or *skeletome* (Ramos-Silva et al. 2013) (i.e., the protein sets employed by corals to regulate the process), in different octocorals. The objective was to determine whether aragonite and calcite-forming species share the same molecular machinery, or if they have rather evolved different protein repertoires for calcification. Secondly, the effects of seawater chemistry (i.e., magnesium-calcium molar ratio, $m\text{Mg}:m\text{Ca}$) on the expression of biomineralization-related genes and on the CaCO_3 polymorph of octocoral and scleractinian skeletons were examined.

In terms of skeletome similarities, proteomic analyses revealed polymorph-specific biomineralization toolkits in the skeleton of *Heliopora coerulea* (aragonite) and calcite-forming octocorals. At the same time, a core set of skeletogenic proteins is shared by species forming calcite sclerites, pointing to a common origin for sclerites in octocoral groups. Similarities were also observed between octocorals and scleractinian proteomes (Drake et al. 2013; Ramos-Silva et al. 2013; Conci et al. 2019). Instances of commonality included proteins identified in both calcitic and aragonitic octocorals. A higher degree of similarity between scleractinians and aragonitic octocorals could not be observed. At the transcriptome level, both taxonomically restricted and conserved skeletogenic proteins are shared across Octocorallia. Ratios between novel and conserved skeletogenic proteins have been found to vary across groups. In molluscs for instance, distribution of several shell-forming protein families is restricted to single classes (e.g., Gastropoda and Bivalvia) with instances of protein presence in single species only (Jackson et al. 2010; McDougall et al. 2013), while in scleractinian corals - as described here for octocorals - the fraction of taxonomically restricted (i.e., possessing homologs in scleractinians only) proteins is limited (Lin et al. 2017). The presence of low overlap between proteomes, and the concurrent taxonomically broad distribution of octocoral skeletogenic genes, suggest that homologs of genes with calcification-related functions in one octocoral species are also actively transcribed in other species, despite not constituting part of the skeleton proteome. This aspect is of evolutionary interest as it does suggest that the evolution of octocoral skeletomes might have included a number of co-options events.

Co-option is the use of existing traits for new functions by organisms. Gene co-option is a common evolutionary event, often based on gene duplication followed by the acquisition by paralogs (i.e., genes that arise via duplication) of novel specialized functions, and can apply to both structural and developmental,

or regulatory genes (True and Carroll 2002). Co-option has been observed in different biological processes, including biomineralization. In sea urchins (phylum Echinodermata) for example, the vascular endothelial growth factor (VEGF) pathway - regulating vascularization in Bilateria - appears to have been co-opted for spiculogenesis (Morgulis et al. 2019). Co-option of calcification-related proteins has also been proposed for molluscs (Aguilera et al. 2017), brachiopods (Shimizu et al. 2017) and scleractinian corals (Ramos-Silva et al. 2013), while information on octocorals was not available prior to this work. Although the absence of genome-level comparisons did not allow conclusive identification of gene duplication or gene family expansion, a list of candidate co-option events could be provided here based on distribution analyses and phylogenetic inferences, with two instances being observed in both octocorals and scleractinian skeletons. The first involves galaxin-related proteins, previously isolated from scleractinian skeletons (Fukuda et al. 2003; Ramos-Silva et al. 2013), and here first identified in the skeleton organic matrix of octocorals. Although the phylogeny of scleractinian galaxin could be reconstructed confidently here, showing it included a single early recruitment event, the evolutionary history within Octocorallia and the phylogenetic relationships between octocoral and scleractinian galaxins still remain elusive. The extensive polyphyly - within Cnidaria - characterizing galaxin-related proteins appears nevertheless to point to multiple independent recruitment among coral groups. Secondly, as in scleractinians (Takeuchi et al. 2016), recruitment of acidic skeletogenic proteins in *H. coerulea* appear to have been the result of co-option, and involving the addition within the proteins sequence of aspartic acid-rich regions.

In conclusion, in terms of octocoral skeleton evolution, this work showed different protein sets being employed by aragonite and calcite-forming octocorals. These results are consistent with the hypothesis of a different origin and different mechanisms of formation for aragonitic and calcitic skeletons structures. In both calcitic and aragonitic species, the evolution of skeletogenic protein repertoires involved both the addition of novel organic matrix components and possible co-option of proteins with ancestral biological functions. In of the above, in addition to functionally characterizing the role played by single proteins during biomineralization, future research should also focus on such protein homologs to determine the ancestral functions of skeletogenic proteins prior to their recruitment for calcification. Despite analytical/technical limitations, and possible incorporation of random proteins into the skeleton, potentially contributing to the observed differences, inclusion of both technical and biological replicated, within the proteomic studies, increased the study robustness. Finally, although similarities between scleractinians and octocorals were detected, the hypothesis of polymorph-driven similarities between the aragonitic *H. coerulea* and scleractinians could not be corroborated.

The second part of the project investigated the effects of the molar magnesium-calcium ratios ($m\text{Mg}:m\text{Ca}$) on skeleton polymorphism and gene expression in the aragonitic octocoral *H. coerulea* and the scleractinian *Montipora digitata*. The $m\text{Mg}:m\text{Ca}$ represents one of the main drivers of aragonite and calcite selective precipitation in seawater and has influenced skeleton CaCO_3 polymorphism of major calcifiers during the last 500 myr (Stanley and Hardie 1998). Although impaired in their calcification rates (Ries et al. 2006; Ries 2010), some coral groups maintained the ability to deposit aragonite during calcite-favouring geological periods (Calcite Seas) (Colgan 1984; Janiszewska et al. 2017). The mechanisms allowing corals to counter the effects of $m\text{Mg}:m\text{Ca}$ remain largely unexplored, including potential regulation via calcification-related proteins. Main research objective was to determine, characterize and compare potential responses to calcite-inducing $m\text{Mg}:m\text{Ca}$. For the mineralogical analyses, electron backscatter analysis (EBSD) and energy dispersive spectroscopy (EDS) were used. This allowed us to

determine the CaCO₃ polymorph secreted, obtain information on the distribution of Ca²⁺ and Mg²⁺ in the skeleton of both species, and present the first EBSD mapping on aragonite crystal orientation for *H. coerulea*. The non-destructive nature of these analytical techniques also allows potential future follow up analyses to be conducted on the same samples and areas investigated in this study.

The results presented in Chapter 4 highlighted different responses to artificially induced Calcite Sea conditions between Octocorallia and Scleractinia. The hypothesis of biological control over skeleton CaCO₃ polymorphism was supported by calcite absence in *H. coerulea*, while co-presence of aragonite and calcite in *M. digitata* suggest an (at least) partial environmental effect in scleractinians. The response of *H. coerulea* provides first insight on the effects of Calcite Sea-like conditions on octocoral skeletons, and represents - to the best of knowledge - the first instance of a coral withstanding the effects of low *mMg:mCa* on its skeleton polymorph. This is nevertheless in agreement with the fossil record of the genus *Heliopora*, which includes aragonite-forming species during the Cretaceous (Calcite Sea) period (Eguchi 1948; Colgan 1984). By comparing results and experimental setups of this study with previous research (Ries et al. 2006; Higuchi et al. 2014), it could be shown how calcium, and not magnesium, might have primarily driven CaCO₃ polymorph deposition in corals during Calcite Sea times (e.g., during the Cretaceous). The ability to maintain aragonitic skeletons under low *mMg:mCa* might thus be related to regulation of calcium levels in calcifying fluids. The consistent overexpression of calcium channels and transporters in *H. coerulea* is consistent with this hypothesis. These proteins have previously been linked to scleractinian biomineralization (Zoccola et al. 1999), while information on octocorals has not been available to date. Voltage-dependent calcium channels are bound to the membrane of different cell types and implicated in several biological processes (Catterall et al. 2005; Clapham 2007;). Further research, focusing on spatial expression and biological function, is thus required to confirm an involvement in biomineralization, and corroborate the hypothesis of calcification-related calcium channels intervening in maintenance of CaCO₃ polymorph through the regulation of calcium concentration.

Although no known component of the skeleton organic matrix (SOM) of both species (Conci et al. 2019) was detected among differentially expressed genes, an involvement of coral SOM in polymorph regulation could not be confidently excluded. Principal component analysis (PCA) showed presence of batch effects, related with the different experimental replicates, and high within-sample variance. These primarily characterized *M. digitata* analyses, explaining the sensibly lower number of differentially expressed genes compared to *H. coerulea*. The presence of batch effects is a common feature of high-throughput studies and can reduce statistical power (Leek et al. 2010). Presence of false negatives might have thus prevented the statistically significant detection of differentially expressed genes associated with the organic matrix. Gene expression changes for skeletogenic proteins, as observed by Yuyama and Higuchi (2019), might thus have occurred, but not consistently between experiments. In addition, several differentially expressed genes code for currently uncharacterized proteins, potentially representing true skeleton organic matrix components not detected by mass spectrometry. Removing batch effects, by analysing single experimental replicates separately, could potentially increase numbers of differentially expressed genes and allow more comprehensive comparisons, although reducing biological significance of the results. Alternatively, follow up experiments should increase the number of biological replicates, which has been shown to enhance the detection of differentially expressed genes increasing (Schurch et al. 2016). In conclusion, these experiments highlighted the capacity of aragonitic octocorals, contrary to scleractinians, to maintain their skeleton polymorph unaltered in artificial calcite-inducing seawater.

Thus explaining their presence during the cretaceous Calcite Sea. Despite providing only a partial view of the molecular responses induced by Calcite Sea-like conditions, based on the gene expression analysis, the hypothesis of a regulation framework centered around calcium transport and availability at calcification, was proposed.

This study has expanded our understanding of skeleton formation in octocorals, obtaining in turn a more complete picture of anthozoan biomineralization. It provides insight into the molecular machineries associated with different biomineralization strategies, with a focus on the deposition of different polymorphs of calcium carbonate.

References

- Addadi L, Moradian J, Shay E, Maroudas NG, Weiner S. 1987. A chemical model for the cooperation of sulfates and carboxylates in calcite crystal nucleation: Relevance to biomineralization. *Proc. Natl. Acad. Sci. USA.* 84:2732-2736.
- Aghaloo T, Jiang X, Soo C, Zhang Z, Zhang X, Hu J, Pan H, Hsu T, Wu B, Ting K, et al. 2007. A study of the role of nll-1 gene modified goat bone marrow stromal cells in promoting new bone formation. *Mol. Ther.* 15:1872-1880.
- Aguilar C, Raina J-B, Foret S, Hayward DC, Lapeyre B, Bourne DG, Miller DJ. 2019. Transcriptomic analysis reveals protein homeostasis breakdown in the coral *Acropora millepora* during hypo-saline stress. *BMC Genomics* 20:148.
- Aguilera F, McDougall C, Degnan BM. 2017. Co-option and de novo gene evolution underlie molluscan shell diversity. *Mol. Biol. Evol.* 34:779-792.
- Aharonovich D, Benayahu Y. 2012. Microstructure of octocoral sclerites for diagnosis of taxonomic features. *Mar. Biodivers.* 42:173-177.
- Akiva A, Neder M, Kahil K, Gavriel R, Pinkas I, Goobes G, Mass T. 2018. Minerals in the pre-settled coral *Stylophora pistillata* crystallize via protein and ion changes. *Nat. Commun.* 9:1880.
- Albright R, Caldeira L, Hosfelt J, Kwiatkowski L, Maclaren JK, Mason BM, Nebuchina Y, Ninokawa A, Pongratz J, Ricke KL, et al. 2016. Reversal of ocean acidification enhances net coral reef calcification. *Nature* 531:362-365.
- Alderslade P. 2000. Four new genera of soft corals (Coelenterata: Octocorallia), with notes on the classification of some established taxa. *Zool. Meded.* 74:237-249.
- Alderslade P. 2001. Six new genera and six new species of soft coral, and some proposed familial and subfamilial changes within the Alcyonacea (Coelenterata: Octocorallia). *Bull. Biol. Soc. Wash.* 10:15-65.
- Alexa A, Rahnenfuhrer J. 2016. topGO: Enrichment Analysis for Gene Ontology. R package version 2.40.0. Available at: bioconductor.org/packages/topGO (accessed 08.05.2020)
- Algeo TJ, Luo GM, Song HY, Lyons TW, Canfield DE. 2015. Reconstruction of secular variation in seawater sulfate concentrations. *Biogeosciences* 12:2131-2151.
- Al-Horani FA. 2005. Effects of changing seawater temperature on photosynthesis and calcification in the scleractinian coral *Galaxea fascicularis*, measured with O₂, Ca²⁺ and pH microsensors. *Sci. Mar.* 69:347-354.
- Allemand D. 1993. The biology and skeletogenesis of the Mediterranean Red Coral: a review. *Precious Corals Octocoral Res.* 2:19-39.
- Allemand D, Cuif JP, Watabe N, Oishi M, Kawaguchi T. 1994. The organic matrix of skeletal structures of the Mediterranean red coral, *Corallium rubrum*. *Bull. Inst. Oceanogr.* :129-139.
- Allemand D, Ferrier-Pagés C, Furla P, Houlbrèque F, Puverel S, Reynaud S, Tambutté É, Tambutté S, Zoccola D. 2004. Biomineralisation in reef-building corals: from molecular mechanisms to environmental control. *C. R. Palevol* 3:453-467.

- Allemand D, Tambutté E, Girard JP, Jaubert J. 1998. Organic matrix synthesis in the scleractinian coral *Stylophora pistillata*: role in biomineralization and potential target of the organotin tributyltin. *J. Exp. Biol.* 201:2001-2009.
- Allemand D, Tambutté É, Zoccola D, Tambutté S. 2011. Coral Calcification, Cells to Reefs. In: *Coral Reefs: An Ecosystem in Transition*. Springer Netherlands:119-150.
- Altschul SF, Gish W, Miller W, Myers EW, Lipman DJ. 1990. Basic local alignment search tool. *J. Mol. Biol.* 215:403-410.
- Amos FF, Destine E, Ponce CB, Evans JS. 2010. The N- and C-Terminal Regions of the Pearl-Associated EF Hand Protein, PFMG1, Promote the Formation of the Aragonite Polymorph in Vitro. *Cryst. Growth Des.* 10:4211-4216.
- Aouacheria A, Geourjon C, Aghajari N, Navratil V, Delage G, Lethias C, Exposito J-Y. 2006. Insights into early extracellular matrix evolution: spongin short chain collagen-related proteins are homologous to basement membrane *type IV* collagens and form a novel family widely distributed in invertebrates. *Mol. Biol. Evol.* 23:2288-2302.
- Apprill A, McNally S, Parsons R, Weber L. 2015. Minor revision to V4 region SSU rRNA 806R gene primer greatly increases detection of SAR11 bacterioplankton. *Aquat. Microb. Ecol.* 75:129-137.
- Arivalagan J, Yarra T, Marie B, Sleight VA, Duvernois-Berthet E, Clark MS, Marie A, Berland S. 2017. Insights from the Shell Proteome: Biomineralization to Adaptation. *Mol. Biol. Evol.* 34:66-77.
- Ausich WI, Babcock LE, Others. 1998. The phylogenetic position of *Echmatocrinus brachiatus*, a probable octocoral from the Burgess Shale. *Palaeontology* 41:193-202.
- Balthasar U, Cusack M. 2015. Aragonite-calcite seas – Quantifying the gray area. *Geology* 43:99-102.
- Banfield JF, Hamers RJ. 1997. Processes at minerals and surfaces with relevance to microorganisms and prebiotic synthesis. *Rev. Mineral. Geochem.* 35:81-122.
- Barnes DJ. 1970. Coral skeletons: an explanation of their growth and structure. *Science* 170:1305-1308.
- Barott KL, Perez SO, Linsmayer LB, Tresguerres M. 2015. Differential localization of ion transporters suggests distinct cellular mechanisms for calcification and photosynthesis between two coral species. *Am. J. Physiol. Regul. Integr. Comp. Physiol.* 309:235-246.
- Barron ME, Thies AB, Espinoza JA, Barott KL, Hamdoun A, Tresguerres M. 2018. A vesicular Na⁺/Ca²⁺ exchanger in coral calcifying cells. *PLoS One* 13:e0205367.
- Barshis DJ, Ladner JT, Oliver TA, Seneca FO, Traylor-Knowles N, Palumbi SR. 2013. Genomic basis for coral resilience to climate change. *Proc. Natl. Acad. Sci. USA.* 110:1387-1392.
- Bartram AK, Lynch MDJ, Stearns JC, Moreno-Hagelsieb G, Neufeld JD. 2011. Generation of multimillion-sequence 16S rRNA gene libraries from complex microbial communities by assembling paired-end Illumina reads. *Appl. Environ. Microbiol.* 77:3846-3852.
- Barzansky B, Lenhoff HM. 1974. On the chemical composition and developmental role of the mesoglea of *Hydra*. *Integr. Comp. Biol.* 14:575-581.
- Bayer FM. 1981a. *Seminarios de Biologia Marinha, Sao Paulo: Bibliography of Octocorallia 1469-1977*. Rio de Janeiro, Brasileria de Ciencia:29-102.

- Bayer FM. 1981b. Key to the genera of Octocorallia exclusive of Pennatulacea (Coelenterata: Anthozoa), with diagnosis of new taxa. *Proceedings of the Biological Society of Washington* 94:902-947.
- Bayer FM, Muzik KM. 1976. A new solitary octocoral, *Taiaroa tauhou* gen. et sp. nov. (Coelenterata: Protoalcyonaria) from New Zealand. *J. R. Soc. N. Z.* 6:499-515.
- Bechtel M, Keller MV, Bloch W, Sasaki T, Boukamp P, Zaucke F, Paulsson M, Nischt R. 2012. Different domains in nidogen-1 and nidogen-2 drive basement membrane formation in skin organotypic cocultures. *FASEB J.* 26:3637-3648.
- Behbehani M, Uddin S, Dupont S, Sajid S, Al-Musalam L, Al-Ghadban A. 2019. Response of corals *Acropora pharaonis* and *Porites lutea* to changes in pH and temperature in the Gulf. *Sustain. Sci. Pract. Policy* 11:3156.
- Benítez-Páez A, Portune KJ, Sanz Y. 2016. Species-level resolution of 16S rRNA gene amplicons sequenced through the MinION™ portable nanopore sequencer. *Gigascience* 5:4.
- Berkelmans R, Jones AM, Schaffelke B. 2012. Salinity thresholds of *Acropora* spp. on the Great Barrier Reef. *Coral Reefs* 31:1103-1110.
- Berntson EA, Bayer FM, McArthur AG, France SC. 2001. Phylogenetic relationships within the Octocorallia (Cnidaria: Anthozoa) based on nuclear 18S rRNA sequences. *Mar. Biol.* 138:235-246.
- Bertucci A, Moya A, Tambutté S, Allemand D, Supuran CT, Zoccola D. 2013. Carbonic anhydrases in anthozoan corals. A review. *Bioorg. Med. Chem.* 21:1437-1450.
- Bertucci A, Tambutté S, Supuran CT, Allemand D, Zoccola D. 2011. A new coral carbonic anhydrase in *Stylophora pistillata*. *Mar. Biotechnol.* 13:992-1002.
- Bhattacharya D, Agrawal S, Aranda M, Baumgarten S, Belcaid M, Drake JL, Erwin D, Foret S, Gates RD, Gruber DF, et al. 2016. Comparative genomics explains the evolutionary success of reef-forming corals. *Elife* 5:8.
- Bhattacharya G, Kalluri R, Orten DJ, Kimberling WJ, Cosgrove D. 2004. A domain-specific usherin/collagen IV interaction may be required for stable integration into the basement membrane superstructure. *J. Cell Sci.* 117:233-242.
- Bischoff JL. 1968. Kinetics of calcite nucleation: Magnesium ion inhibition and ionic strength catalysis. *J. Geophys. Res.* 73:3315-3322.
- Bourne GC. 1899. *Memoirs: Studies on the Structure and Formation of the Calcareous Skeleton of the Anthozoa.* *J. Cell. Sci.* 2:499-546.
- Braissant O, Cailleau G, Aragno M, Verrecchia EP. 2004. Biologically induced mineralization in the tree *Milicia excelsa* (Moraceae): its causes and consequences to the environment. *Geobiology* 2:59-66.
- Bruce Railsback L, Anderson TF. 1987. Control of Triassic seawater chemistry and temperature on the evolution of post-Paleozoic aragonite-secreting faunas. *Geology* 15:1002-1005.
- Bryan WH, Hill D. 1941. Spherulitic crystallization as a mechanism of skeletal growth in the hexacorals. *Proc. R. Soc. Qld.* 52:78-91.

- Bryant DM, Johnson K, Di Tommaso T, Tickle T, Couger MB, Payzin Dogru D, Lee TJ, Leigh ND, Kuo T-H, Davis FG, et al. 2017. A Tissue-Mapped *Axolotl* De Novo Transcriptome Enables Identification of Limb Regeneration Factors. *Cell Rep.* 18:762-776.
- Budd AF, Stolarski J. 2009. Searching for new morphological characters in the systematics of scleractinian reef corals: comparison of septal teeth and granules between Atlantic and Pacific Mussidae. *Acta Zool.* 90:142-165.
- Bushmanova E, Antipov D, Lapidus A, Prjibelski AD. 2019. rnaSPAdes: a de novo transcriptome assembler and its application to RNA-Seq data. *Gigascience* 8: giz100.
- Callahan BJ, McMurdie PJ, Rosen MJ, Han AW, Johnson AJA, Holmes SP. 2016. DADA2: High-resolution sample inference from Illumina amplicon data. *Nature Methods* 13:581-583.
- Caporaso JG, Kuczynski J, Stombaugh J, Bittinger K, Bushman FD, Costello EK, Fierer N, Peña AG, Goodrich JK, Gordon JI, et al. 2010. QIIME allows analysis of high-throughput community sequencing data. *Nat. Methods* 7:335-336.
- Caporaso JG, Lauber CL, Walters WA, Berg-Lyons D, Huntley J, Fierer N, Owens SM, Betley J, Fraser L, Bauer M, et al. 2012. Ultra-high-throughput microbial community analysis on the Illumina HiSeq and MiSeq platforms. *ISME J.* 6:1621-1624.
- Caporaso JG, Lauber CL, Walters WA, Berg-Lyons D, Lozupone CA, Turnbaugh PJ, Fierer N, Knight R. 2011. Global patterns of 16S rRNA diversity at a depth of millions of sequences per sample. *Proc. Natl. Acad. Sci. USA.* 108:4516-4522.
- Carlstrom D. 1963. A crystallographic study of vertebrate otoliths. *Biol. Bull.* 125:441-463.
- Cartwright P, Collins A. 2007. Fossils and phylogenies: integrating multiple lines of evidence to investigate the origin of early major metazoan lineages. *Integr. Comp. Biol.* 47:744-751.
- Castillo KD, Ries JB, Bruno JF, Westfield IT. 2014. The reef-building coral *Siderastrea siderea* exhibits parabolic responses to ocean acidification and warming. *Proc. Biol. Sci.* 281:20141856.
- Castresana J. 2000. Selection of conserved blocks from multiple alignments for their use in phylogenetic analysis. *Mol. Biol. Evol.* 17:540-552.
- Chandramouli K, Qian P-Y. 2009. Proteomics: challenges, techniques and possibilities to overcome biological sample complexity. *Hum. Genomics Proteomics* 2009:239204.
- Chan NCS, Connolly SR. 2013. Sensitivity of coral calcification to ocean acidification: a meta-analysis. *Glob. Chang. Biol.* 19:282-290.
- Chave KE. 1954. Aspects of the Biogeochemistry of Magnesium 1. *Calcareous Marine Organisms.* *J. Geol.* 62:266-283.
- Chomczynski P, Mackey K. 1995. Short technical reports. Modification of the TRI reagent procedure for isolation of RNA from polysaccharide- and proteoglycan-rich sources. *Biotechniques* 19:942-945.
- Chuang Y, Kitahara M, Fukami H, Tracey D, Miller DJ, Chen CA. 2017. Loss and Gain of Group I Introns in the Mitochondrial Cox1 Gene of the Scleractinia (Cnidaria; Anthozoa). *Zool. Stud.* 56:e9.

- Clapham DE. 2007. Calcium signaling. *Cell* 131:1047-1058.
- Cleves PA, Strader ME, Bay LK, Pringle JR, Matz MV. 2018. CRISPR/Cas9-mediated genome editing in a reef-building coral. *Proc. Natl. Acad. Sci. USA.* 115:5235-5240.
- Clode PL, Marshall AT. 2003. Calcium associated with a fibrillar organic matrix in the scleractinian coral *Galaxea fascicularis*. *Protoplasma* 220:153-161.
- Cogné JP, Humler E. 2004. Temporal variation of oceanic spreading and crustal production rates during the last 180 My. *Earth Planet. Sci. Lett.* 227:427-439.
- Cohen AL, McConnaughey TA. 2003. Geochemical Perspectives on Coral Mineralization. *Rev. Mineral. Geochem.* 54:151-187.
- Cole C, Finch A, Hintz C, Hintz K, Allison N. 2016. Understanding cold bias: Variable response of skeletal Sr/Ca to seawater pCO₂ in acclimated massive *Porites* corals. *Sci. Rep.* 6:26888.
- Cölfen H, Mann S. 2003. Higher-order organization by mesoscale self-assembly and transformation of hybrid nanostructures. *Angew. Chem. Int. Ed.* 42:2350-2365.
- Colgan MW. 1984. The Cretaceous Coral *Heliopora* (Octocorallia, Coenothecalia)- a Common Indo-Pacific Reef Builder. In: *Living Fossils*. Springer, New York:266-271.
- Comeau S, Carpenter RC, Edmunds PJ. 2013. Coral reef calcifiers buffer their response to ocean acidification using both bicarbonate and carbonate. *Proc. Biol. Sci.* 280:20122374.
- Conci N, Lehmann M, Vargas S, Wörheide G. 2019. Comparative proteomics of octocoral and scleractinian skeletomes and the evolution of coral calcification. *bioRxiv* 2019.12.30.891028.
- Conci N, Wörheide G, Vargas S. 2019. New non-bilaterian transcriptomes provide novel insights into the evolution of coral skeletomes. *Genome Biol. Evol.* 11:3068-3081.
- Constantz BR. 1986. Coral Skeleton Construction: a physiochemically dominated process. *Palaios* 1:152.
- Constantz B, Weiner S. 1988. Acidic macromolecules associated with the mineral phase of scleractinian coral skeletons. *J. Exp. Zool.* 248:253-258.
- Cooper TF, De'ath G, Fabricius KE, Lough JM. 2008. Declining coral calcification in massive *Porites* in two nearshore regions of the northern Great Barrier Reef. *Glob. Chang. Biol.* 14:529-538.
- Cope JCW. 2005. Octocorallia and hydroid fossils from the lower Ordovician of Wales. *Palaeontology* 48:433-445.
- Cox J, Hein MY, Lubner CA, Paron I, Nagaraj N, Mann M. 2014. Accurate proteome-wide label-free quantification by delayed normalization and maximal peptide ratio extraction, termed MaxLFQ. *Mol. Cell. Proteomics* 13:2513-2526.
- Cox J, Mann M. 2008. MaxQuant enables high peptide identification rates, individualized ppb-range mass accuracies and proteome-wide protein quantification. *Nat. Biotechnol.* 26:1367-1372.
- Cuif JP. 2016. Calcification in the Cnidaria through time: an overview of their skeletal patterns from individual to evolutionary viewpoints. In: *The Cnidaria, Past, Present and Future: The world of Medusa and her sisters*. Springer, Cham, Switzerland: 163-179.

- Cuif JP, Dauphin Y. 1998. Microstructural and physico-chemical characterization of 'centers of calcification' in septa of some recent scleractinian corals. *Paläontol. Z.* 72:257-269.
- Cuif JP, Dauphin Y. 2005. The Environment Recording Unit in coral skeletons - a synthesis of structural and chemical evidences for a biochemically driven, stepping-growth process in fibres. *Biogeosciences* 2:61-73.
- Cuif JP, Dauphin Y, Berthet P, Jegoudez J. 2004. Associated water and organic compounds in coral skeletons: Quantitative thermogravimetry coupled to infrared absorption spectrometry. *Geochem. Geophys. Geosyst.* 5:Q11011.
- Cuif JP, Dauphin Y, Sorauf JE. 2010. *Biominerals and Fossils Through Time*. Cambridge University Press, Cambridge UK.
- Cvejic J, Tambutté S, Lotto S, Mikov M, Slacanin I, Allemand D. 2007. Determination of canthaxanthin in the red coral (*Corallium rubrum*) from Marseille by HPLC combined with UV and MS detection. *Mar. Biol.* 152:855-862.
- Darriba D, Taboada GL, Doallo R, Posada D. 2011. ProtTest 3: fast selection of best-fit models of protein evolution. *Bioinformatics* 27:1164-1165.
- Davies SW, Marchetti A, Ries JB, Castillo KD. 2016. Thermal and pCO₂ stress elicit divergent transcriptomic responses in a resilient coral. *Front. Mar. Sci.* 3:112.
- De'ath G, Lough JM, Fabricius KE. 2009. Declining coral calcification on the Great Barrier Reef. *Science* 323:116-119.
- De Boer RB. 1977. Stability of Mg-Ca carbonates. *Geochim. Cosmochim. Acta* 41:265-270.
- Debreuil J, Tambutté E, Zoccola D, Deleury E, Guignon J-M, Samson M, Allemand D, Tambutté S. 2012. Molecular cloning and characterization of first organic matrix protein from sclerites of red coral, *Corallium rubrum*. *J. Biol. Chem.* 287:19367-19376.
- De Carlo TM, Comeau S, Cornwall CE, McCulloch MT. 2018. Coral resistance to ocean acidification linked to increased calcium at the site of calcification. *Proc. Biol. Sci.* 285:20180564.
- De Carlo TM. 2018. Characterizing coral skeleton mineralogy with Raman spectroscopy. *Nat. Commun.* 9:5325.
- De Choudens-Sanchez V, Gonzalez LA. 2009. Calcite and aragonite precipitation under controlled instantaneous supersaturation: elucidating the role of CaCO₃ saturation state and Mg/Ca ratio on calcium carbonate polymorphism. *J. Sediment. Res.* 79:363-376.
- Del Prete S, Vullo D, Zoccola D, Tambutté S, Capasso C, Supuran CT. 2017. Kinetic properties and affinities for sulfonamide inhibitors of an α -carbonic anhydrase (CruCA4) involved in coral biomineralization in the Mediterranean red coral *Corallium rubrum*. *Bioorg. Med. Chem.* 25:3525-3530.
- Demico RV, Lowenstein TK, Hardie LA, Spencer RJ. 2005. Model of seawater composition for the Phanerozoic. *Geology* 33:877-880.
- Dickson AG. 1990. Standard potential of the reaction - AgCl(S)+12H₂(G)=Ag(S)+HCl(Aq) and the standard acidity constant of the ion HSO₄⁻ in synthetic sea-water from 273.15 K to 318.15 K. *J. Chem. Thermodyn.* 22:113-127.

- Dickson AG, Millero FJ. 1987. A comparison of the equilibrium constants for the dissociation of carbonic acid in seawater media. *Deep Sea Res.* 34:1733-1743.
- Drake JL, Massa T, Haramaty L, Zelzion E, Bhattacharya D, Falkowski PG. 2013. Reply to Ramos-Silva et al.: Regarding coral skeletal proteome. *Proc. Natl. Acad. Sci. USA.* 110:E2147-E2148.
- Drake JL, Mass T, Haramaty L, Zelzion E, Bhattacharya D, Falkowski PG. 2013. Proteomic analysis of skeletal organic matrix from the stony coral *Stylophora pistillata*. *Proc. Natl. Acad. Sci. USA.* 110:3788-3793.
- Dunn CW, Howison M, Zapata F. 2013. Agalma: an automated phylogenomics workflow. *BMC Bioinformatics* 14:330.
- Dunn SR, Phillips WS, Green DR, Weis VM. 2007. Knockdown of actin and caspase gene expression by RNA interference in the symbiotic anemone *Aiptasia pallida*. *Biol. Bull.* 212:250-258.
- Edgar RC. 2004. MUSCLE: multiple sequence alignment with high accuracy and high throughput. *Nucleic Acids Res.* 32:1792-1797.
- Edgar RC. 2010. Search and clustering orders of magnitude faster than BLAST. *Bioinformatics* 26:2460-2461.
- Edgar RC. 2013. UPARSE: highly accurate OTU sequences from microbial amplicon reads. *Nat. Methods* 10:996-998.
- Edgar RC. 2016. UNCROSS: Filtering of high-frequency cross-talk in 16S amplicon reads. *bioRxiv*: 088666.
- Eguchi M. 1948. Fossil Helioporidae from Japan and the South Sea Islands. *J. Paleontol.* 22:362-364.
- Einbinder S, Mass T, Brokovich E, Dubinsky Z, Erez J, Tchernov D. 2009. Changes in morphology and diet of the coral *Stylophora pistillata* along a depth gradient. *Mar. Ecol. Prog. Ser.* 381:167-174.
- Eitel M, Francis WR, Varoqueaux F, Daraspe J, Osigus H-J, Krebs S, Vargas S, Blum H, Williams GA, Schierwater B, et al. 2018. Comparative genomics and the nature of placozoan species. *PLoS Biol.* 16:e2005359.
- Engel J. 1991. Common structural motifs in proteins of the extracellular matrix. *Curr. Opin. Cell Biol.* 3:779V785.
- Erickson AC, Couchman JR. 2000. Still more complexity in mammalian basement membranes. *J. Histochem. Cytochem.* 48:1291-1306.
- Erwin DH, Laflamme M, Tweedt SM, Sperling EA, Pisani D, Peterson KJ. 2011. The Cambrian conundrum: early divergence and later ecological success in the early history of animals. *Science* 334:1091-1097.
- Ettensohn CA. 1992. Cell interactions and mesodermal cell fates in the sea urchin embryo. *Dev.* 116:43-51.
- Fabricius K, Alderslade P. 2001. Soft corals and sea fans: a comprehensive guide to the tropical shallow water genera of the central-west Pacific, the Indian Ocean and the Red Sea. Australian Institute of Marine Science.

- Fabricius KE, Langdon C, Uthicke S, Humphrey C, Noonan S, De'ath G, Okazaki R, Muehllehner N, Glas MS, Lough JM. 2011. Losers and winners in coral reefs acclimatized to elevated carbon dioxide concentrations. *Nat. Clim. Chang.* 1:165-169.
- Falini G, Albeck S, Weiner S, Addadi L. 1996. Control of aragonite or calcite polymorphism by mollusk shell macromolecules. *Science* 271:67.
- Fallon SJ, McCulloch MT, Alibert C. 2003. Examining water temperature proxies in *Porites* corals from the Great Barrier Reef: a cross-shelf comparison. *Coral Reefs* 22:389-404.
- Farre B, Cuif JP, Dauphin Y. 2010. Occurrence and diversity of lipids in modern coral skeletons. *Zoology* 113:250-257.
- Farre B, Dauphin Y. 2009. Lipids from the nacreous and prismatic layers of two Pteriomorpha mollusc shells. *Comp. Biochem. Physiol. B Biochem. Mol. Biol.* 152:103-109.
- Feist P, Hummon AB. 2015. Proteomic challenges: sample preparation techniques for microgram-quantity protein analysis from biological samples. *Int. J. Mol. Sci.* 16:3537-3563.
- Felis T, Lohmann G, Kuhnert H, Lorenz SJ, Scholz D, Pätzold J, Al-Rousan SA, Al-Moghrabi SM. 2004. Increased seasonality in Middle East temperatures during the last interglacial period. *Nature* 429:164-168.
- Feng D, Li Q, Yu H, Kong L, Du S. 2017. Identification of conserved proteins from diverse shell matrix proteome in *Crassostrea gigas*: characterization of genetic bases regulating shell formation. *Sci. Rep.* 7:45754.
- Fernández-Martínez E, Coronado I, Rodríguez S, Tourneur F, Badpa M. 2019. Alcyonacea awakens: Palaeobiology and palaeoecology of Palaeozoic octocorals known from their sclerites. Wang X, editor. *Geol. J.* 54:3593-3618.
- Floquet N, Vielzeuf D. 2012. Ordered misorientations and preferential directions of growth in mesocrystalline red coral sclerites. *Cryst. Growth Des.* 12:4805-4820.
- Flores RL, Gonzales K, Seaver RW, Livingston BT. 2016. The skeletal proteome of the brittle star *Ophiothrix spiculata* identifies C-type lectins and other proteins conserved in echinoderm skeleton formation. *AIMS Mol. Sci.* 3:357-367.
- Flores RL, Livingston BT. 2017. The skeletal proteome of the sea star *Patiria miniata* and evolution of biomineralization in echinoderms. *BMC Evol. Biol.* 17:125.
- Flynn JM, Brown EA, Chain FJJ, MacIsaac HJ, Cristescu ME. 2015. Toward accurate molecular identification of species in complex environmental samples: testing the performance of sequence filtering and clustering methods. *Ecol. Evol.* 5:2252-2266.
- Forêt S, Knack B, Houliston E, Momose T, Manuel M, Quéinnec E, Hayward DC, Ball EE, Miller DJ. 2010. New tricks with old genes: the genetic bases of novel cnidarian traits. *Trends Genet.* 26:154-158.
- France SC, Rosel PE, Ewann J. 1996. DNA sequence variation of mitochondrial large-subunit rRNA. *Mol. Mar. Biol. Biotechnol.* 5:15-28.

- Francis WR, Eitel M, Vargas S, Adamski M, Haddock SHD, Krebs S, Blum H, Wörheide G. 2017. The genome of the contractile demosponge *Tethya wilhelma* and the evolution of metazoan neural signalling pathways. BioRxiv:120998.
- Frankel RB, Bazylinski DA. 2003. Biologically Induced Mineralization by Bacteria. Rev. Mineral. Geochem. 54:95-114.
- Frankel RB, Bazylinski DA, Johnson MS, Taylor BL. 1997. Magneto-aerotaxis in marine coccoid bacteria. Biophys. J. 73:994-1000.
- Fukami H, Chen CA, Budd AF, Collins A, Wallace C, Chuang Y-Y, Chen C, Dai C-F, Iwao K, Sheppard C, et al. 2008. Mitochondrial and nuclear genes suggest that stony corals are monophyletic but most families of stony corals are not (Order Scleractinia, Class Anthozoa, Phylum Cnidaria). PLoS One 3:e3222.
- Fukuda I, Ooki S, Fujita T, Murayama E, Nagasawa H, Isa Y, Watanabe T. 2003. Molecular cloning of a cDNA encoding a soluble protein in the coral exoskeleton. Biochem. Biophys. Res. Commun. 304:11-17.
- Furla P, Galgani I, Durand I, Allemand D. 2000. Sources and mechanisms of inorganic carbon transport for coral calcification and photosynthesis. J. Exp. Biol. 203:3445-3457.
- Fyfe WS, Bischoff JL. 1965. The Calcite-Aragonite problem. Dolomitization and Limestone Diagenesis: 3-13.
- Gabay Y, Benayahu Y, Fine M. 2013. Does elevated pCO₂ affect reef octocorals? Ecol. Evol. 3: 465-473.
- Gabay Y, Fine M, Barkay Z, Benayahu Y. 2014. Octocoral tissue provides protection from declining oceanic pH. PLoS One 9:e91553.
- Gagan MK, Ayliffe LK, Beck JW, Cole JE, Druffel ERM, Dunbar RB, Schrag DP. 2000. New views of tropical paleoclimates from corals. Quat. Sci. Rev. 19:45-64.
- Gagnon AC, Adkins JF, Erez J. 2012. Seawater transport during coral biomineralization. Earth Planet. Sci. Lett. 329-330:150-161.
- Gasteiger E, Hoogland C, Gattiker A, Duvaud S, Wilkins MR, Appel RD, Bairoch A. 2005. Protein identification and analysis tools on the ExpASY Server. In: The Proteomics Protocols Handbook. Totowa, NJ, Humana Press:571-607.
- Gauldie RW. 1986. Vaterite otoliths from chinook salmon (*Oncorhynchus tshawytscha*). N. Z. J. Mar. Freshwater Res. 20:209-217.
- Germer J, Mann K, Wörheide G, Jackson DJ. 2015. The skeleton forming proteome of an early branching metazoan: a molecular survey of the biomineralization components employed by the coralline sponge *Vaceletia* sp. PLoS One 10:e0140100.
- Gilbert DG. 2019. Genes of the pig, *Sus scrofa*, reconstructed with EvidentialGene. PeerJ 7:e6374.
- Goff CL, Le Goff C, Tambutté E, Venn AA, Techer N, Allemand D, Tambutté S. 2017. In vivo pH measurement at the site of calcification in an octocoral. Sci. Rep. 7:1-14.

- Goffredo S, Caroselli E, Mezzo F, Laiolo L, Vergni P, Pasquini L, Levy O, Zaccanti F, Tribollet A, Dubinsky Z, et al. 2012. The puzzling presence of calcite in skeletons of modern solitary corals from the Mediterranean Sea. *Geochim. Cosmochim. Acta* 85:187-199.
- Goffredo S, Vergni P, Reggi M, Caroselli E, Sparla F, Levy O, Dubinsky Z, Falini G. 2011. The skeletal organic matrix from Mediterranean coral *Balanophyllia europaea* influences calcium carbonate precipitation. *PLoS One* 6:e22338.
- Goldberg WM. 2001. Acid polysaccharides in the skeletal matrix and calicoblastic epithelium of the stony coral *Mycetophyllia reesi*. *Tissue Cell* 33:376-387.
- Goldberg WM, Benayahu Y. 1987a. Spicule formation in the gorgonian coral *Pseudoplexaura flagellosa*. 1: Demonstration of intracellular and extracellular growth and the effect of ruthenium red during decalcification. *Bull. Mar. Sci.* 40:287-303.
- Gómez CE, Paul VJ, Ritson-Williams R, Muehllhner N, Langdon C, Sánchez JA. 2015. Responses of the tropical gorgonian coral *Eunicea fusca* to ocean acidification conditions. *Coral Reefs* 34:451-460.
- González-Pech RA, Vargas S, Francis WR, Wörheide G. 2017. Transcriptomic resilience of the *Montipora digitata* holobiont to Low pH. *Front. Mar. Sci.* 4:403.
- Gouy M, Guindon S, Gascuel O. 2010. SeaView version 4: A multiplatform graphical user interface for sequence alignment and phylogenetic tree building. *Mol. Biol. Evol.* 27:221-224.
- Grabherr MG, Haas BJ, Yassour M, Levin JZ, Thompson DA, Amit I, Adiconis X, Fan L, Raychowdhury R, Zeng Q, et al. 2011. Full-length transcriptome assembly from RNA-Seq data without a reference genome. *Nat. Biotechnol.* 29:644-652.
- Grasshoff MV, Others. 1981. Die Gorgonaria, Pennatularia und Antipatharia des Tiefwasser der Biskaya (Cnidaria, Anthozoa). Ergebnisse der Franzosischen Expeditionen Biogas, Polygas, Geomanche, Incal, Noratlante und Fahrten der Thalassa. II: Taxonomischer Teil.
- Grillo MC, Goldberg WM, Allemand D. 1993. Skeleton and sclerite formation in the precious red coral *Corallium rubrum*. *Mar. Biol.* 117:119-128.
- Groffen AJ, Ruegg MA, Dijkman H, van de Velden TJ, Buskens CA, van den Born J, Assmann KJ, Monnens LA, Veerkamp JH, van den Heuvel LP. 1998. Agrin is a major heparan sulfate proteoglycan in the human glomerular basement membrane. *J. Histochem. Cytochem.* 46:19-27.
- Guindon S, Dufayard J-F, Lefort V, Anisimova M, Hordijk W, Gascuel O. 2010. New algorithms and methods to estimate maximum-likelihood phylogenies: assessing the performance of PhyML 3.0. *Syst. Biol.* 59:307-321.
- Guindon S, Gascuel O. 2003. A simple, fast, and accurate algorithm to estimate large phylogenies by maximum likelihood. *Syst. Biol.* 52:696-704.
- Haas BJ, Papanicolaou A, Yassour M, Grabherr M, Blood PD, Bowden J, Couger MB, Eccles D, Li B, Lieber M, et al. 2013. De novo transcript sequence reconstruction from RNA-seq using the Trinity platform for reference generation and analysis. *Nat. Protoc.* 8:1494-1512.
- Hardie LA. 1990. The roles of rifting and hydrothermal CaCl₂ brines in the origin of potash evaporites; an hypothesis. *Am. J. Sci.* 290:43-106.

- Hardie LA. 1996. Secular variation in seawater chemistry: An explanation for the coupled secular variation in the mineralogies of marine limestones and potash evaporites over the past 600 m.y. *Geology* 24:279-283.
- Hays JD, Pitman WC. 1973. Lithospheric Plate Motion, Sea Level Changes and Climatic and Ecological Consequences. *Nature* 246:18-22.
- Heath-Heckman EAC, Gillette AA, Augustin R, Gillette MX, Goldman WE, McFall-Ngai MJ. 2014. Shaping the microenvironment: evidence for the influence of a host galaxin on symbiont acquisition and maintenance in the squid-*Vibrio* symbiosis. *Environ. Microbiol.* 16:3669-3682.
- He H, Veneklaas EJ, Kuo J, Lambers H. 2014. Physiological and ecological significance of biomineralization in plants. *Trends Plant Sci.* 19:166-174.
- Higuchi T, Fujimura H, Yuyama I, Harii S, Agostini S, Oomori T. 2014. Biotic control of skeletal growth by scleractinian corals in Aragonite-Calcite Seas. *PLoS One* 9:e91021.
- Hoegh-Guldberg O, Mumby PJ, Hooten AJ, Steneck RS, Greenfield P, Gomez E, Harvell CD, Sale PF, Edwards AJ, Caldeira K, et al. 2007. Coral reefs under rapid climate change and ocean acidification. *Science* 318:1737-1742.
- Hohn S, Merico A. 2012. Modelling coral polyp calcification in relation to ocean acidification. *Biogeosciences* 9:4441-4454.
- Hohn S, Raymond CE. 2019. Coral calcification, mucus, and the origin of skeletal organic molecules. *Coral Reefs* 38:973-984.
- Holcomb M, Cohen AL, McCorkle DC. 2013/2. An evaluation of staining techniques for marking daily growth in scleractinian corals. *J. Exp. Mar. Bio. Ecol.* 440:126-131.
- Holstein T. 1981. The morphogenesis of nematocytes in *Hydra* and *Forskliia*: An ultrastructural study. *J. Ultrastruct. Res.* 75:276-290.
- Horita J, Zimmermann H, Holland HD. 2002. Chemical evolution of seawater during the Phanerozoic: Implications from the record of marine evaporites. *Geochim. Cosmochim. Acta* 66:3733-3756.
- Horvath EA. 2019. A review of gorgonian coral species (Cnidaria, Octocorallia, Alcyonacea) held in the Santa Barbara Museum of Natural History research collection: focus on species from Scleraxonia, Holaxonia, Calcaxonia - Part III: Suborder Holaxonia continued, and suborder Calcaxonia. *Zookeys* 860:183-306.
- Houck JE, Buddemeier RW, Chave KE. 1975. Skeletal low-magnesium calcite in living scleractinian corals. *Science* 189:997-999. Huber JA, Mark Welch DB, Morrison HG, Huse SM, Neal PR, Butterfield DA, Sogin ML. 2007. Microbial population structures in the deep marine biosphere. *Science* 318:97-100.
- Huelsenbeck JP, Ronquist F. 2001. MRBAYES: Bayesian inference of phylogenetic trees. *Bioinformatics* 17:754-755.
- Hughes TP. 1994. Catastrophes, phase shifts, and large-scale degradation of a Caribbean coral reef. *Science* 265:1547-1551.
- Hughes TP, Kerry JT, Baird AH, Connolly SR, Dietzel A, Eakin CM, Heron SF, Hoey AS, Hoogenboom MO, Liu G, et al. 2018. Global warming transforms coral reef assemblages. *Nature* 556:492-496.

- Hughes TP, Kerry JT, Connolly SR, Baird AH, Eakin CM, Heron SF, Hoey AS, Hoogenboom MO, Jacobson M, Liu G, et al. 2019. Ecological memory modifies the cumulative impact of recurrent climate extremes. *Nat. Clim. Chang.* 9:40-43.
- Illumina, 2016a. MiniSeq system specification sheet: sequencing. Available at: Support.illumina.com (accessed 08.05.2020)
- Illumina, 2016b. Optimizing cluster density on illumina sequencing systems. Available at: Support.illumina.com (accessed 08.05.2020)
- Illumina, 2016c. Illumina two-channel SBS sequencing technology. Available at: Support.illumina.com (accessed 08.05.2020)
- Illumina, 2016d. MiniSeq system denature and dilute libraries guide. Available at: Support.illumina.com (accessed 08.05.2020)
- Inoue M, Suzuki A, Nohara M, Hibino K, Kawahata H. 2007. Empirical assessment of coral Sr/Ca and Mg/Ca ratios as climate proxies using colonies grown at different temperatures. *Geophys. Res. Lett.* 34:419.
- Inoue S, Kayanne H, Yamamoto S, Kurihara H. 2013. Spatial community shift from hard to soft corals in acidified water. *Nat. Clim. Chang.* 3:683-687.
- Ip YK, Lim ALL, Lim RWL. 1991. Some properties of calcium-activated adenosine triphosphatase from the hermatypic coral *Galaxea fascicularis*. *Mar. Biol.* 111:191-197.
- Jackson DJ, Macis L, Reitner J, Degnan BM, Wörheide G. 2007a. Sponge paleogenomics reveals an ancient role for carbonic anhydrase in skeletogenesis. *Science* 316:1893-1895.
- Jackson DJ, Mann K, Häussermann V, Schilhabel MB, Lüter C, Griesshaber E, Schmahl W, Wörheide G. 2015. The *Magellania venosa* biomineralizing proteome: a window into brachiopod shell evolution. *Genome Biol. Evol.* 7:1349-1362.
- Jackson JB, Kirby MX, Berger WH, Bjorndal KA, Botsford LW, Bourque BJ, Bradbury RH, Cooke R, Erlandson J, Estes JA, et al. 2001. Historical overfishing and the recent collapse of coastal ecosystems. *Science* 293:629-637.
- Janiszewska K, Mazur M, Escrig S, Meibom A, Stolarski J. 2017. Aragonitic scleractinian corals in the Cretaceous calcitic sea. *Geology* 45:319-322.
- Jeng M-S, Huang HD, Dai CF, Hsiao YC, Benayahu Y. 2011. Sclerite calcification and reef-building in the fleshy octocoral genus *Sinularia* (Octocorallia: Alcyonacea). *Coral Reefs* 30:925-933.
- Jeon Y, Park SG, Lee N, Weber JA, Kim H-S, Hwang S-J, Woo S, Kim H-M, Bhak Y, Jeon S, et al (2019). The draft genome of an octocoral, *Dendronephthya gigantea*. *Genome Biol. Evol.* 11:949-953.
- Jones P, Binns D, Chang H-Y, Fraser M, Li W, McAnulla C, McWilliam H, Maslen J, Mitchell A, Nuka G, et al. 2014. InterProScan 5: genome-scale protein function classification. *Bioinformatics* 30:1236-1240.
- Junqua S, Robert L, Garrone R, Pavans de Ceccatty M, Vacelet J. 1974. Biochemical and morphological studies on collagens of horny sponges. *Ircinia* filaments compared to spongines. *Connect. Tissue Res.* 2:193-203.

- Kabalah-Amitai L, Mayzel B, Kauffmann Y, Fitch AN, Bloch L, Gilbert PUPA, Pokroy B. 2013. Vaterite crystals contain two interspersed crystal structures. *Science* 340:454-457.
- Kass-Simon G, Scappaticci, Jr., A A. 2002. The behavioral and developmental physiology of nematocysts. *Can. J. Zool.* 80:1772-1794.
- Katoh K, Standley DM. 2013. MAFFT multiple sequence alignment software version 7: improvements in performance and usability. *Mol. Biol. Evol.* 30:772-780.
- Kato T, Sugawara A, Hosoda N. 2002. Calcium carbonate–organic hybrid materials. *Adv. Mater.* 14:869-877.
- Kerswell AP, Jones RJ. 2003. Effects of hypo-osmosis on the coral *Stylophora pistillata*: nature and cause of low-salinity bleaching. *Mar. Ecol. Prog. Ser.* 253:145-154.
- Kiessling W, Baron-Szabo RC. 2004. Extinction and recovery patterns of scleractinian corals at the Cretaceous-Tertiary boundary. *Palaeogeogr. Palaeoclimatol. Palaeoecol.* 214:195-223.
- Kingsley RJ. 1984. Spicule Formation in the Invertebrates with Special Reference to the Gorgonian *Leptogorgia virgulata*. *Integr. Comp. Biol.* 24:883-891.
- Kitahara MV, Cairns SD, Stolarski J, Blair D, Miller DJ. 2010. A comprehensive phylogenetic analysis of the Scleractinia (Cnidaria, Anthozoa) based on mitochondrial CO1 sequence data. *PLoS One* 5:e11490.
- Kitahara MV, Lin M-F, Forêt S, Huttley G, Miller DJ, Chen CA. 2014. The 'naked coral' hypothesis revisited—evidence for and against scleractinian monophyly. *PLoS One* 9:e94774.
- Klaus JS, Budd AF, Heikoop JM, Fouke BW. 2007. Environmental controls on corallite morphology in the reef coral *Montastraea annularis*. *Bull. Mar. Sci.* 80:233-260.
- Kniprath E. 1981. Ontogeny of the Molluscan Shell Field: a Review. *Zool. Scr.* 10:61-79.
- Knoll AH. 2003. Biomineralization and evolutionary history. *Rev. Mineral. Geochem.* 54:329-356.
- Knowlton N, Brainard RE, Fisher R, Moews M, Plaisance L, Caley MJ. 2010. Coral Reef Biodiversity. In: *Life in the Worlds Oceans*. Wiley-Blackwell:65-78.
- Kocot KM, Aguilera F, McDougall C, Jackson DJ, Degnan BM. 2016. Sea shell diversity and rapidly evolving secretomes: insights into the evolution of biomineralization. *Front. Zool.* 13:23.
- Kocurko MJ, Kocurko DJ. 1992. Fossil Octocorallia of the Red Bluff Formation, Lower Oligocene, Mississippi. *J. Paleontol.* 66:594-602.
- Kozich JJ, Westcott SL, Baxter NT, Highlander SK, Schloss PD. 2013. Development of a dual-index sequencing strategy and curation pipeline for analyzing amplicon sequence data on the MiSeq Illumina sequencing platform. *Appl. Environ. Microbiol.* 79:5112-5120.
- Kralj D, Brečević L, Nielsen AE. 1990. Vaterite growth and dissolution in aqueous solution I. Kinetics of crystal growth. *J. Cryst. Growth* 104:793-800.
- Krampitz G, Drolshagen H, Häusle J, Hof-Irmscher K. 1983. Organic matrices of mollusc shells. In: Westbroek P, de Jong EW, editors. *Biomineralization and Biological Metal Accumulation: Biological and Geological Perspectives Papers*. Springer Netherlands:231-247.

- Krieger KJ, Wing BL. 2002. Megafauna associations with deepwater corals (*Primnoa* spp.) in the Gulf of Alaska. *Hydrobiologia* 471:83-90.
- Krogh A, Larsson B, von Heijne G, Sonnhammer EL. 2001. Predicting transmembrane protein topology with a hidden Markov model: application to complete genomes. *J. Mol. Biol.* 305:567-580.
- Laipnik R, Bissi V, Sun C-Y, Falini G, Gilbert PUPA, Mass T. 2019. Coral acid rich protein selects vaterite polymorph in vitro. *J. Struct. Biol.*:107431.
- Lang CJ. 1984. Whatever works : the variable importance of skeletal and non-skeletal characters in scleractinian taxonomy. *Palaeontogr. Am.* 54:18-44.
- Langmead B, Salzberg SL. 2012. Fast gapped-read alignment with Bowtie 2. *Nat. Methods* 9:357-359.
- Lau YW, Stokvis FR, Imahara Y, Reimer JD. 2019. The stoloniferous octocoral, *Hanabira yukibana*, gen. nov., sp. nov., of the southern Ryukyus has morphological and symbiont variation. *Contrib. Zool.* 88:54-77.
- Le Goff C, Ganot P, Zoccola D, Caminiti-Segonds N, Allemand D, Tambutté S. 2016. Carbonic Anhydrases in Cnidarians: Novel Perspectives from the Octocorallian *Corallium rubrum*. *PLoS One* 11:e0160368.
- Leek JT, Scharpf RB, Bravo HC, Simcha D, Langmead B, Johnson WE, Geman D, Baggerly K, Irizarry RA. 2010. Tackling the widespread and critical impact of batch effects in high-throughput data. *Nat. Rev. Genet.* 11:733-739.
- Lewis JB. 1976. Experimental tests of suspension feeding in Atlantic reef corals. *Mar. Biol.* 36:147-150.
- Lewis JC, Vonwallis E. 1991. The function of surface sclerites in gorgonians (Coelenterata, Octocorallia). *Biol. Bull.* 181:275-288.
- Li R, Li Y, Kristiansen K, Wang J. 2008. SOAP: short oligonucleotide alignment program. *Bioinformatics* 24:713V714.
- Liew YJ, Aranda M, Voolstra CR. 2016. Reefgenomics.Org - a repository for marine genomics data. *Database* 2016:baw152.
- Lin M-F, Moya A, Ying H, Chen CA, Cooke I, Ball EE, Forêt S, Miller DJ. 2017. Analyses of corallimorpharian transcriptomes provide new perspectives on the evolution of calcification in the Scleractinia (Corals). *Genome Biol. Evol.* 9:150-160.
- Littler K, Robinson SA, Bown PR, Nederbragt AJ, Pancost RD. 2011. High sea-surface temperatures during the Early Cretaceous Epoch. *Nat. Geosci.* 4:169-172.
- Liu X, Li J, Xiang L, Sun J, Zheng G, Zhang G, Wang H, Xie L, Zhang R. 2012. The role of matrix proteins in the control of nacreous layer deposition during pearl formation. *Proc. Biol. Sci.* 279:1000-1007.
- Lohmann JU, Endl I, Bosch TC. 1999. Silencing of developmental genes in *Hydra*. *Dev. Biol.* 214: 211-214.
- Lopes AR, Faleiro F, Rosa IC, Pimentel MS, Trubenbach K, Repolho T, Diniz M, Rosa R. 2018. Physiological resilience of a temperate soft coral to ocean warming and acidification. *Cell Stress Chaperones* 23:1093-1100.

- Love MI, Huber W, Anders S. 2014. Moderated estimation of fold change and dispersion for RNA-seq data with DESeq2. *Genome Biol.* 15:550.
- Lowenstam HA. 1981. Minerals formed by organisms. *Science* 211:1126-1131.
- Lowenstam HA. 1986. Mineralization processes in monerans and protoctists. In: *Biom mineralization in lower plants and animals* 30, Oxford University Press, Oxford UK:1-17.
- Lowenstein TK, Hardie LA, Timofeeff MN, Demicco RV. 2003. Secular variation in seawater chemistry and the origin of calcium chloride basinal brines. *Geology* 31:857-860.
- Mann K, Jackson DJ. 2014. Characterization of the pigmented shell-forming proteome of the common grove snail *Cepaea nemoralis*. *BMC Genomics* 15:249.
- Mann K, Poustka AJ, Mann M. 2008. The sea urchin (*Strongylocentrotus purpuratus*) test and spine proteomes. *Proteome Sci.* 6:22.
- Mann K, Siedler F. 2004. Ostrich (*Struthio camelus*) eggshell matrix contains two different C-type lectin-like proteins. Isolation, amino acid sequence, and post-translational modifications. *Biochim. Biophys. Acta* 1696:41-50.
- Mann K, Siedler F. 2006. Amino acid sequences and phosphorylation sites of emu and rhea eggshell C-type lectin-like proteins. *Comp. Biochem. Physiol. B Biochem. Mol. Biol.* 143:160-170.
- Mann K, Weiss IM, André S, Gabius H-J, Fritz M. 2000. The amino-acid sequence of the abalone (*Haliotis laevis*) nacre protein perlucin: Detection of a functional C-type lectin domain with galactose/mannose specificity. *Eur. J. Biochem.* 267:5257-5264.
- Mann S. 1983. Mineralization in biological systems. In: *Inorganic Elements in Biochemistry. Structure and Bonding*. Springer Berlin Heidelberg:125-174.
- Marie B, Jackson DJ, Ramos-Silva P. 2013. The shell-forming proteome of *Lottia gigantea* reveals both deep conservations and lineage-specific novelties. *FEBS J.* 280:214-232.
- Marie B, Joubert C, Tayalé A, Zanella-Cléon I, Belliard C, Piquemal D, Cochenec-Laureau N, Marin F, Gueguen Y, Montagnani C. 2012. Different secretory repertoires control the biomineralization processes of prism and nacre deposition of the pearl oyster shell. *Proc. Natl. Acad. Sci. USA.* 109: 20986-20991.
- Marie B, Marie A, Jackson DJ, Dubost L, Degnan BM, Milet C, Marin F. 2010. Proteomic analysis of the organic matrix of the abalone *Haliotis asinina* calcified shell. *Proteome Sci.* 8:54.
- Marin F, Bundeleva I, Takeuchi T, Immel F, Medakovic D. 2016. Organic matrices in metazoan calcium carbonate skeletons: Composition, functions, evolution. *J. Struct. Biol.* 196: 98-106.
- Marin F, Le Roy N, Marie B. 2012. The formation and mineralization of mollusk shell. *Front. Biosci.* 4: 1099-1125.
- Marques AC, Collins AG. 2005. Cladistic analysis of Medusozoa and cnidarian evolution. *Invertebr. Biol.* 123: 23-42.
- Mass T, Drake JL, Haramaty L, Kim JD, Zelzion E, Bhattacharya D, Falkowski PG. 2013. Cloning and characterization of four novel coral acid-rich proteins that precipitate carbonates *in vitro*. *Curr. Biol.* 23:1126-1131.

- Mass T, Drake JL, Heddleston JM, Falkowski PG. 2017. Nanoscale visualization of biomineral formation in coral proto-polyps. *Curr. Biol.* 27:3191-3196.
- Mass T, Giuffre AJ, Sun C-Y, Stifler CA, Frazier MJ, Neder M, Tamura N, Stan CV, Marcus MA, Gilbert PUPA. 2017. Amorphous calcium carbonate particles form coral skeletons. *Proc. Natl. Acad. Sci. USA.* 114:7670-7678.
- Mass T, Putnam HM, Drake JL, Zelzion E, Gates RD, Bhattacharya D, Falkowski PG. 2016. Temporal and spatial expression patterns of biomineralization proteins during early development in the stony coral *Pocillopora damicornis*. *Proc. Biol. Sci.* 283:20160322.
- Matsubara H, Hayashi T, Ogawa T, Muramoto K, Jimbo M, Kamiya H. 2008. Modulating effect of acorn barnacle C-type lectins on the crystallization of calcium carbonate. *Fish. Sci.* 74:418-424.
- McConnaughey T. 1991. Calcification in *Chara corallina*: CO₂ hydroxylation generates protons for bicarbonate assimilation. *Limnol. Oceanogr.* 36:619-628.
- McConnaughey TA, Whelan JF. 1997. Calcification generates protons for nutrient and bicarbonate uptake. *Earth-Sci. Rev.* 42:95-117.
- McCulloch MT, Gagan MK, Mortimer GE, Chivas AR, Isdale PJ. 1994. A high-resolution Sr/Ca and $\delta^{18}\text{O}$ coral record from the Great Barrier Reef, Australia, and the 1982–1983 El Niño. *Geochim. Cosmochim. Acta* 58:2747-2754.
- McFadden CS, France SC, Sanchez JA, Alderslade P. 2006. A molecular phylogenetic analysis of the Octocorallia (Cnidaria: Anthozoa) based on mitochondrial protein-coding sequences. *Mol. Phylogenet. Evol.* 41:513-527.
- McFadden CS, Sanchez JA, France SC. 2010. Molecular phylogenetic insights into the evolution of Octocorallia: a review. *Integr. Comp. Biol.* 50:389-410.
- McMenamin MA. 2000. The garden of Ediacara: discovering the first complex life. Columbia University Press.
- Mehrbach C, Culbertson CH, Hawley JE, Pytkowicz RM. 1973. Measurement of the apparent dissociation constants of carbonic acid in seawater at atmospheric pressure. *Limnol. Oceanogr.* 18:897-907.
- Meibom A, Cuif JP, Hillion F, Constantz BR, Juillet-Leclerc A, Dauphin Y, Watanabe T, Dunbar RB. 2004. Distribution of magnesium in coral skeleton. *Geophys. Res. Lett.* 31:L23306.
- Meibom A, Yurimoto H, Cuif JP, Domart-Coulon I, Houlbrèque F, Constantz B, Dauphin Y, Tambutté E, Tambutté S, Allemand D, et al. 2006. Vital effects in coral skeletal composition display strict three-dimensional control. *Geophys. Res. Lett.* 33: L11608.
- Michalski A, Cox J, Mann M. 2011. More than 100,000 detectable peptide species elute in single shotgun proteomics runs but the majority is inaccessible to data-dependent LC-MS/MS. *J. Proteome Res.* 10:1785-1793.
- Miglietta MP, McNally L, Cunningham CW. 2010. Evolution of calcium-carbonate skeletons in the Hydractiniidae. *Integr. Comp. Biol.* 50:428-435.
- Mitsuguchi T, Matsumoto E, Abe O, Uchida T, Isdale PJ. 1996. Mg/Ca Thermometry in Coral Skeletons. *Science* 274:961-963.

- Mitsuguchi T, Uchida T, Matsumoto E, Isdale PJ, Kawana T. 2001. Variations in Mg/Ca, Na/Ca, and Sr/Ca ratios of coral skeletons with chemical treatments: Implications for carbonate geochemistry. *Geochim. Cosmochim. Acta* 65:2865-2874.
- Mitterer RM. 1978. Amino acid composition and metal binding capability of the skeletal protein of corals. *Bull. Mar. Sci.* 28:173-180.
- Miyamoto H, Miyashita T, Okushima M, Nakano S, Morita T, Matsushiro A. 1996. A carbonic anhydrase from the nacreous layer in oyster pearls. *Proc. Natl. Acad. Sci. USA.* 93:9657-9660.
- Morgulis M, Gildor T, Roopin M, Sher N, Malik A, Lalzar M, Dines M, Ben-Tabou de-Leon S, Khalaily L, Ben-Tabou de-Leon S. 2019. Possible cooption of a VEGF-driven tubulogenesis program for biomineralization in echinoderms. *Proc. Natl. Acad. Sci. USA.* 116:12353-12362.
- Morrow C, Cárdenas P. 2015. Proposal for a revised classification of the Demospongiae (Porifera). *Front. Zool.* 12:7.
- Morse JW, Mackenzie FT. 1990. *Geochemistry of Sedimentary Carbonates*. In: *Developments in Sedimentology* 48. Elsevier Science.
- Morse JW, Wang Q, Tsio MY. 1997. Influences of temperature and Mg: Ca ratio on CaCO₃ precipitates from seawater. *Geology* 25:85-87.
- Mortensen PB, Buhl-Mortensen L. 2005. Morphology and growth of the deep-water gorgonians *Primnoa resedaeformis* and *Paragorgia arborea*. *Mar. Biol.* 147:775-788.
- Mosher DF, Adams JC. 2012. Adhesion-modulating/matricellular ECM protein families: a structural, functional and evolutionary appraisal. *Matrix Biol.* 31:155-161.
- Moya A, Tambutté S, Bertucci A, Tambutté E, Lotto S, Vullo D, Supuran CT, Allemand D, Zoccola D. 2008. Carbonic anhydrase in the scleractinian coral *Stylophora pistillata*: characterization, localization, and role in biomineralization. *J. Biol. Chem.* 283:25475-25484.
- Muko S, Kawasaki K, Sakai K, Takasu F, Shigesada N. 2000. Morphological plasticity in the coral *Porites sillimaniani* and its adaptive significance. *Bull. Mar. Sci.* 66:225-239.
- Murdock DJE, Donoghue PCJ. 2011. Evolutionary origins of animal skeletal biomineralization. *Cells Tissues Organs* 194:98-102.
- Muscatine L, Tambutté E, Allemand D. 1997. Morphology of coral desmocytes, cells that anchor the calciblastic epithelium to the skeleton. *Coral Reefs* 16:205-213.
- Naggi A, Torri G, Iacomini M, Colombo Castelli G, Reggi M, Fermani S, Dubinsky Z, Goffredo S, Falini G. 2018. Structure and Function of Stony Coral Intraskelatal Polysaccharides. *ACS Omega* 3:2895-2901.
- Nothdurft LD, Webb GE, Bostrom T, Rintoul L. 2007. Calcite-filled borings in the most recently deposited skeleton in live-collected *Porites* (Scleractinia): Implications for trace element archives. *Geochim. Cosmochim. Acta* 71:5423-5438.
- Obst M, Wehrli B, Dittrich M. 2009. CaCO₃ nucleation by cyanobacteria: laboratory evidence for a passive, surface-induced mechanism. *Geobiology* 7:324-347.

- Oksanen AJ, Blanchet FG, Kindt R, Legendre P, O'Hara RB, Simpson GL, Solymos P, Stevens MHH, Wagner H. 2012. Package 'vegan'. Community ecology package version 2:1-295.
- Oliver JK. 1984. Intra-colony variation in the growth of *Acropora formosa*: extension rates and skeletal structure of white (zooxanthellae-free) and brown-tipped branches. *Coral Reefs* 3:139-147.
- Oliver JK, Chalker BE, Dunlap WC. 1983. Bathymetric adaptations of reef-building corals at Davies reef, Great Barrier Reef, Australia. I. Long-term growth responses of *Acropora formosa* (Dana 1846). *J. Exp. Mar. Bio. Ecol.* 73:11-35.
- Orsi WD, Coolen MJL, Wuchter C, He L, More KD, Irigoien X, Chust G, Johnson C, Hemingway JD, Lee M, et al. 2017. Climate oscillations reflected within the microbiome of Arabian Sea sediments. *Sci. Rep.* 7:6040.
- Palumbi SR, Barshis DJ, Traylor-Knowles N, Bay RA. 2014. Mechanisms of reef coral resistance to future climate change. *Science* 344:895-898.
- Pandolfi JM, Bradbury RH, Sala E, Hughes TP, Bjorndal KA, Cooke RG, McArdle D, McClenahan L, Newman MJH, Paredes G, et al. 2003. Global trajectories of the long-term decline of coral reef ecosystems. *Science* 301:955-958.
- Parada AE, Needham DM, Fuhrman JA. 2016. Every base matters: assessing small subunit rRNA primers for marine microbiomes with mock communities, time series and global field samples. *Environ. Microbiol.* 18:1403-1414.
- Patro R, Duggal G, Love MI, Irizarry RA, Kingsford C. 2017. Salmon provides fast and bias-aware quantification of transcript expression. *Nat. Methods* 14:417-419.
- Pérez CD, de Moura Neves B, Cordeiro RT, Williams GC, Cairns SD. 2016. Diversity and Distribution of Octocorallia. In: *The Cnidaria, Past, Present and Future: The world of Medusa and her sisters*. Springer, Cham, Switzerland:109-123.
- Petersen TN, Brunak S, von Heijne G, Nielsen H. 2011. SignalP 4.0: discriminating signal peptides from transmembrane regions. *Nat. Methods* 8:785-786.
- Pierleoni A, Martelli P, Casadio R. 2008. PredGPI: a GPI-anchor predictor. *BMC Bioinformatics* 9:392.
- Pierrot D, Lewis E, Wallace D. 2006. MS Excel program developed for CO₂ system calculations. ORNL/CDIAC-105a. Carbon Dioxide Information Analysis Center, Oak Ridge National Laboratory, US Department of Energy, Oak Ridge, Tennessee.
- Power IM, Wilson SA, Thom JM, Dipple GM, Southam G. 2007. Biologically induced mineralization of dypingite by cyanobacteria from an alkaline wetland near Atlin, British Columbia, Canada. *Geochem. Trans.* 8:1-16.
- Pratchett MS, Anderson KD, Hoogenboom MO, Widman E, Baird AH, Pandolfi JM, Edmunds PJ, Lough JM. 2015. Spatial, temporal and taxonomic variation in coral growth – Implications for the structure and function of coral reef ecosystems. *Oceanogr. Mar. Biol. Annu. Rev.* 53:215-295.
- Pratlong M, Haguenauer A, Chabrol O, Klopp C, Pontarotti P, Aurelle D. 2015. The red coral (*Corallium rubrum*) transcriptome: a new resource for population genetics and local adaptation studies. *Mol. Ecol. Resour.* 15:1205-1215.

- Pratlong M, Rancurel C, Pontarotti P, Aurelle D. 2017. Monophyly of Anthozoa (Cnidaria): why do nuclear and mitochondrial phylogenies disagree? *Zool. Scr.* 46:363-371.
- Puverel S, Houlbrèque F, Tambutté E, Zoccola D, Payan P, Caminiti N, Tambutté S, Allemand D. 2007. Evidence of low molecular weight components in the organic matrix of the reef building coral, *Stylophora pistillata*. *Comp. Biochem. Physiol. A Mol. Integr. Physiol.* 147:850-856.
- Puverel S, Tambutté E, Pereira-Mouries L, Zoccola D, Allemand D, Tambutté S. 2005. Soluble organic matrix of two Scleractinian corals: partial and comparative analysis. *Comp. Biochem. Physiol. B Biochem. Mol. Biol.* 141:480-487.
- Puverel S, Tambutté E, Zoccola D, Domart-Coulon I, Bouchot A, Lotto S, Allemand D, Tambutté S. 2004. Antibodies against the organic matrix in scleractinians: a new tool to study coral biomineralization. *Coral Reefs* 24:149-156.
- Quast C, Pruesse E, Yilmaz P, Gerken J, Schweer T, Yarza P, Peplies J, Glöckner FO. 2012. The SILVA ribosomal RNA gene database project: improved data processing and web-based tools. *Nucleic Acids Research* 41:590-596.
- Quinn TM, Sampson DE. 2002. A multiproxy approach to reconstructing sea surface conditions using coral skeleton geochemistry. *Paleoceanography* 17:14-11.
- Radha AV, Forbes TZ, Killian CE, Gilbert PUPA, Navrotsky A. 2010. Transformation and crystallization energetics of synthetic and biogenic amorphous calcium carbonate. *Proc. Natl. Acad. Sci. USA.* 107:16438-16443.
- Rahman MA, Isa Y, Uehara T. 2006. Studies on two closely related species of octocorallians: biochemical and molecular characteristics of the organic matrices of endoskeletal sclerites. *Mar. Biotechnol.* 8:415-424.
- Rahman MA, Oomori T. 2009. In Vitro Regulation of CaCO₃ Crystal Growth by the Highly Acidic Proteins of Calcitic Sclerites in Soft Coral, *Sinularia polydactyla*. *Connect. Tissue Res.* 50: 285-293.
- Rahman MA, Oomori T, Wörheide G. 2011. Calcite formation in soft coral sclerites is determined by a single reactive extracellular protein. *J. Biol. Chem.* 286:31638-31649.
- Ramesh K, Yarra T, Clark MS, John U, Melzner F. 2019. Expression of calcification-related ion transporters during blue mussel larval development. *Ecol. Evol.* 9:7157-7172.
- Ramos-Silva P, Kaandorp J, Huisman L, Marie B, Zanella-Cléon I, Guichard N, Miller DJ, Marin F. 2013. The skeletal proteome of the coral *Acropora millepora*: the evolution of calcification by co-option and domain shuffling. *Mol. Biol. Evol.* 30:2099-2112.
- Ramos-Silva P, Marin F, Kaandorp J, Marie B. 2013. Biomineralization toolkit: the importance of sample cleaning prior to the characterization of biomineral proteomes. *Proc. Natl. Acad. Sci. USA.* 110:E2144-E2146.
- Randle V, Engler O. 2000. Introduction to Texture Analysis: Macrotecture. Microtexture and Orientation mapping:125-151.

- Reef R, Kaniewska P, Hoegh-Guldberg O. 2009. Coral skeletons defend against ultraviolet radiation. *PLoS One* 4:e7995.
- Reggi M, Fermani S, Samorì C, Gizzi F, Prada F, Dubinsky Z, Goffredo S, Falini G. 2016. Influence of intra-skeletal coral lipids on calcium carbonate precipitation. *Cryst. Eng. Comm.* 18:8829-8833.
- Reyes-Bermudez A, Lin Z, Hayward DC, Miller DJ, Ball EE. 2009. Differential expression of three galaxin-related genes during settlement and metamorphosis in the scleractinian coral *Acropora millepora*. *BMC Evol. Biol.* 9:178.
- Reynaud S, Leclercq N, Romaine-Lioud S, Ferrier-Pages C, Jaubert J, Gattuso JP. 2003. Interacting effects of CO₂ partial pressure and temperature on photosynthesis and calcification in a scleractinian coral. *Glob. Chang. Biol.* 9:1660-1668.
- Richards MA, Engebretson DC. 1992. Large-scale mantle convection and the history of subduction. *Nature* 355:437-440.
- Riesgo A, Farrar N, Windsor PJ, Giribet G, Leys SP. 2014. The analysis of eight transcriptomes from all poriferan classes reveals surprising genetic complexity in sponges. *Mol. Biol. Evol.* 31:1102-1120.
- Ries JB. 2010. Review: geological and experimental evidence for secular variation in seawater Mg/Ca (calcite-aragonite seas) and its effects on marine biological calcification. *Biogeosciences* 7:2795-2849.
- Ries JB, Anderson MA, Hill RT. 2008. Seawater Mg/Ca controls polymorph mineralogy of microbial CaCO₃: A potential proxy for calcite-aragonite seas in Precambrian time. *Geobiology* 6:106-119.
- Ries JB, Stanley SM, Hardie LA. 2006. Scleractinian corals produce calcite, and grow more slowly, in artificial Cretaceous seawater. *Geology* 34:525-528.
- Robertson G, Schein J, Chiu R, Corbett R, Field M, Jackman SD, Mungall K, Lee S, Okada HM, Qian JQ, et al. 2010. De novo assembly and analysis of RNA-seq data. *Nat. Methods* 7:909-912.
- Rodolfo-Metalpa R, Houlbrèque F, Tambutté E, Boisson F, Baggini C, Patti FP, Jeffree R, Fine M, Foggo A, Gattuso JP, et al. 2011. Coral and mollusc resistance to ocean acidification adversely affected by warming. *Nat. Clim. Chang.* 1:308-312.
- Romano SL, Cairns SD. 2000. Molecular phylogenetic hypotheses for the evolution of scleractinian corals. *Bull. Mar. Sci.* 67:1043-1068.
- Romano SL, Palumbi SR. 1996. Evolution of Scleractinian Corals Inferred from Molecular Systematics. *Science* 271:640-642.
- Ronquist F, Teslenko M, van der Mark P, Ayres DL, Darling A, Höhna S, Larget B, Liu L, Suchard MA, Huelsenbeck JP. 2012. MrBayes 3.2: efficient Bayesian phylogenetic inference and model choice across a large model space. *Syst. Biol.* 61:539-542.
- Ruppert EE, Barnes RD, Fox RS. 2004. *Invertebrate zoology: a functional evolutionary approach*. Thomson Brooks Cole, Belmont, USA.
- Ruzicka RR, Colella MA, Porter JW, Morrison JM, Kidney JA, Brinkhuis V, Lunz KS, Macaulay KA, Bartlett LA, Meyers MK, et al. 2013. Temporal changes in benthic assemblages on Florida Keys reefs 11 years after the 1997/1998 El Niño. *Mar. Ecol. Prog. Ser.* 489:125-141.

- Sanchez S, Hourdez S, Lallier FH. 2007. Identification of proteins involved in the functioning of *Riftia pachyptila* symbiosis by Subtractive Suppression Hybridization. *BMC Genomics* 8:337.
- Sandberg PA. 1983. An oscillating trend in Phanerozoic non-skeletal carbonate mineralogy. *Nature* 305:19-22.
- Sarashina I, Endo K. 2006. Skeletal matrix proteins of invertebrate animals: Comparative analysis of their amino acid sequences. *Paleontol. Res.* 10:311-336.
- Schmidt N-H, Olesen NO. 1989. Computer-aided determination of crystal-lattice orientation from electron channeling patterns in the SEM. *Can. Mineral.* 27:15-22.
- Schrag DP. 1999. Rapid analysis of high-precision Sr/Ca ratios in corals and other marine carbonates. *Paleoceanography* 14:97-102.
- Schwanhäusser B, Busse D, Li N, Dittmar G, Schuchhardt J, Wolf J, Chen W, Selbach M. 2011. Global quantification of mammalian gene expression control. *Nature* 473:337-342.
- Sevilgen DS, Venn AA, Hu MY, Tambutté E, de Beer D, Planas-Bielsa V, Tambutté S. 2019. Full in vivo characterization of carbonate chemistry at the site of calcification in corals. *Sci. Adv.* 5:e7447.
- Shimizu K, Luo Y-J, Satoh N, Endo K. 2017. Possible co-option of engrailed during brachiopod and mollusc shell development. *Biol. Lett.* 13.8:20170254
- Shinzato C, Shoguchi E, Kawashima T, Hamada M, Hisata K, Tanaka M, Fujie M, Fujiwara M, Koyanagi R, Ikuta T, et al. 2011. Using the *Acropora digitifera* genome to understand coral responses to environmental change. *Nature* 476:320-323.
- Sikes CS, Wheeler AP. 1983. A Systematic Approach to Some Fundamental Questions of Carbonate Calcification. In: Westbroek P, de Jong EW, editors. *Biomineralization and Biological Metal Accumulation: Biological and Geological Perspectives Papers*. Springer Netherlands:285-289.
- Simão FA, Waterhouse RM, Ioannidis P, Kriventseva EV, Zdobnov EM. 2015. BUSCO: assessing genome assembly and annotation completeness with single-copy orthologs. *Bioinformatics* 31:3210-3212.
- Simion P, Philippe H, Baurain D, Jager M, Richter DJ, Di Franco A, Roure B, Satoh N, Quéinnec [É], Ereskovsky A, et al. 2017. A Large and Consistent Phylogenomic Dataset Supports Sponges as the Sister Group to All Other Animals. *Curr. Biol.* 27:958-967.
- Simpson A, Watling L. 2011. Precious corals (Coralliidae) from north-western Atlantic Seamounts. *J. Mar. Biol. Assoc. UK.* 91:369-382.
- Smith KM, Gee L, Bode HR. 2000. HyAlx, an aristaless-related gene, is involved in tentacle formation in *Hydra*. *Development* 127:4743-4752.
- Sodergren E, Weinstock GM, Davidson EH. 2006. The genome of the sea urchin *Strongylocentrotus purpuratus*. *Science* 314:941-952.
- Sogin ML, Morrison HG, Huber JA, Welch DM, Huse SM, Neal PR, Arrieta JM, Herndl GJ. 2006. Microbial diversity in the deep sea and the underexplored 'rare biosphere'. *Proc. Natl. Acad. Sci. USA.* 103:12115-12120.
- Sonnhammer EL, von Heijne G, Krogh A. 1998. A hidden Markov model for predicting transmembrane helices in protein sequences. *Proc. Int. Conf. Intell. Syst. Mol. Biol.* 6:175-182.

- Sprung J. 1999. Corals: a quick reference guide. Ricordea Publishing, Miami, USA.
- Srivastava M, Simakov O, Chapman J, Fahey B, Gauthier MEA, Therese Mitros, Richards GS, Conaco C, Dacre M, Hellsten U, et al. 2010. The *Amphimedon queenslandica* genome and the evolution of animal complexity. *Nature* 466:720.
- Stanley GD. 2003. The evolution of modern corals and their early history. *Earth-Sci. Rev.* 60:195-225.
- Stanley SM, Hardie LA. 1998. Secular oscillations in the carbonate mineralogy of reef-building and sediment-producing organisms driven by tectonically forced shifts in seawater chemistry. *Palaeogeogr. Palaeoclimatol. Palaeoecol.* 144:3-19.
- Stanley SM, Hardie LA. 1999. Hypercalcification: paleontology links plate tectonics and geochemistry to sedimentology. *GSA Today* 9:1-7.
- Stanley SM, Ries JB, Hardie LA. 2002. Low-magnesium calcite produced by coralline algae in seawater of Late Cretaceous composition. *Proc. Natl. Acad. Sci. USA.* 99:15323-15326.
- Stanley SM, Ries JB, Hardie LA. 2010. Increased production of calcite and slower growth for the major sediment-producing alga *Halimeda* as the Mg/Ca ratio of seawater is lowered to a 'Calcite Sea' level. *J. Sediment. Res.* 80:6-16.
- Stolarski J, Kitahara MV, Miller DJ, Cairns SD, Mazur M, Meibom A. 2011. The ancient evolutionary origins of Scleractinia revealed by azooxanthellate corals. *BMC Evol. Biol.* 11:316.
- Stolarski J, Meibom A, Przenioslo R, Mazur M. 2007. A Cretaceous scleractinian coral with a calcitic skeleton. *Science* 318:92-94.
- Sunagawa S, DeSalvo MK, Voolstra CR, Reyes-Bermudez A, Medina M. 2009. Identification and gene expression analysis of a taxonomically restricted cysteine-rich protein family in reef-building corals. *PLoS One* 4:e4865.
- Swulius MT, Waxham MN. 2008. Ca^{2+} /calmodulin-dependent protein kinases. *Cell. Mol. Life Sci.* 65:2637-2657.
- Szent-Györgyi AG. 1975. Calcium regulation of muscle contraction. *Biophys. J.* 15:707-723.
- Sultemeyer D, Rinast K-A. 1996. The CO_2 permeability of the plasma membrane of *Chlamydomonas reinhardtii*: mass-spectrometric ^{18}O -exchange measurements from $^{13}\text{C}^{18}\text{O}_2$ in suspensions of carbonic anhydrase-loaded plasma-membrane vesicles. *Planta* 200:358-368.
- Tai CY, Chen F-B. 1998. Polymorphism of CaCO_3 , precipitated in a constant-composition environment. *AIChE J.* 44:1790-1798.
- Takeuchi T, Plasseraud L, Ziegler-Devin I, Brosse N, Shinzato C, Satoh N, Marin F. 2018. Biochemical characterization of the skeletal matrix of the massive coral, *Porites australiensis*—The saccharide moieties and their localization. *J. Struct. Biol.* 203:219-229.
- Takeuchi T, Yamada L, Shinzato C, Sawada H, Satoh N. 2016. Stepwise Evolution of Coral Biomineralization Revealed with Genome-Wide Proteomics and Transcriptomics. *PLoS One* 11:e0156424.

- Tambutté E, Tambutté S, Segonds N, Zoccola D, Venn A, Erez J, Allemand D. 2012. Calcein labelling and electrophysiology: insights on coral tissue permeability and calcification. *Proc. Biol. Sci.* 279:19-27.
- Tambutté S, Holcomb M, Ferrier-Pagés C, Reynaud S, Tambutté é, Zoccola D, Allemand D. 2011. Coral biomineralization: From the gene to the environment. *J. Exp. Mar. Bio. Ecol.* 408:58-78.
- Tambutté S, Tambutté E, Zoccola D, Caminiti N, Lotto S, Moya A, Allemand D, Adkins J. 2006. Characterization and role of carbonic anhydrase in the calcification process of the azooxanthellate coral *Tubastrea aurea*. *Mar. Biol.* 151:71-83.
- Taylor PD, Berning B, Wilson MA. 2013. Reinterpretation of the Cambrian 'bryozoan' *Pywackia* as an octocoral. *J. Paleontol.* 87:984-990.
- Tentori E, van Ofwegen LP. 2011. Patterns of distribution of calcite crystals in soft corals sclerites. *J. Morphol.* 272:614-628.
- Todd PA, Ladle RJ, Lewin-Koh NJI, Chou LM. 2004. Genotype x environment interactions in transplanted clones of the massive corals *Favia speciosa* and *Diploastrea heliopora*. *Mar. Ecol. Prog. Ser.* 271:167-182.
- Tringe SG, Hugenholtz P. 2008. A renaissance for the pioneering 16S rRNA gene. *Curr. Opin. Microbiol.* 11:442-446.
- True JR, Carroll SB. 2002. Gene co-option in physiological and morphological evolution. *Annu. Rev. Cell Dev. Biol.* 18:53-80.
- Vaccaro AM, Motta M, Tatti M, Scarpa S, Masuelli L, Bhat M, Vanier MT, Tylki-Szymanska A, Salvioli R. 2010. Saposin C mutations in Gaucher disease patients resulting in lysosomal lipid accumulation, saposin C deficiency, but normal prosaposin processing and sorting. *Hum. Mol. Genet.* 19:2987-2997.
- Van Iten H, Leme JM, Mírian L A, Simões MG, Fairchild TR, Rodrigues F, Galante D, Boggiani PC, Marques AC. 2016. Origin and Early Diversification of Phylum Cnidaria: Key Macrofossils from the Ediacaran System of North and South America. In: *The Cnidaria, Past, Present and Future*. Springer, Cham, Switzerland:31-40.
- Veis A. 2005. A Window on Biomineralization. *Science* 307:1419-1420.
- Velimirov B. 1980. Growth Aspects and Magnesium Carbonate Concentrations of the Reef Building Octocoral *Heliopora coerulea* (Pallas) after Transplantation. *Mar. Ecol.* 1:155-168.
- Velimirov B, Böhm EL. 1976. Calcium and magnesium carbonate concentrations in different growth regions of gorgonians. *Mar. Biol.* 35:269-275.
- Veron J. 2013. Overview of the taxonomy of zooxanthellate Scleractinia. *Zool. J. Linn. Soc.* 169: 485-508.
- Veron J. 1995. *Corals in space and time: the biogeography and evolution of the Scleractinia*. Cornell University Press.
- Veron J, Stafford-Smith M. 2000. *Corals of the World*. Volumes 1-3. AIMS, Townsville, Australia.

- Veron J. 1986. Corals of Australia and the Indo-pacific. Sydney: Angus & Robertson:26-43.
- Vielzeuf D, Garrabou J, Baronnet A, Grauby O, Marschal C. 2008. Nano to macroscale biomineral architecture of red coral (*Corallium rubrum*). Am. Mineral. 93:1799-1815.
- Voigt O, Adamski M, Sluzek K, Adamska M. 2014. Calcareous sponge genomes reveal complex evolution of α -carbonic anhydrases and two key biomineralization enzymes. BMC Evol. Biol. 14:230.
- Von Euw S, Zhang Q, Manichev V, Murali N, Gross J, Feldman LC, Gustafsson T, Flach C, Mendelsohn R, Falkowski PG. 2017. Biological control of aragonite formation in stony corals. Science 356: 933-938.
- Voolstra C, Miller D, Ragan M, Hoffmann A, Hoegh-Guldberg O, Bourne D, Ball E, Ying H, Foret S, Takahashi S, et al. 2015. The ReFuGe 2020 Consortium - using 'omics' approaches to explore the adaptability and resilience of coral holobionts to environmental change. Front. Mar. Sci. 2:68.
- Voolstra CR, Li Y, Liew YJ, Baumgarten S, Zoccola D, Flot J-F, Tambutté S, Allemand D, Aranda M. 2017. Comparative analysis of the genomes of *Stylophora pistillata* and *Acropora digitifera* provides evidence for extensive differences between species of corals. Sci. Rep. 7:17583.
- Vullo D, Nishimori I, Scozzafava A, Supuran CT. 2008. Carbonic anhydrase activators: Activation of the human cytosolic isozyme III and membrane-associated isoform IV with amino acids and amines. Bioorg. Med. Chem. Lett. 18:4303-4307.
- Weinbauer MG, Brandstätter F, Velimirov B. 2000. On the potential use of magnesium and strontium concentrations as ecological indicators in the calcite skeleton of the red coral (*Corallium rubrum*). Mar. Biol. 137:801-809.
- Weinbauer MG, Vellmirov B. 1995. Calcium, magnesium and strontium concentrations in the calcite sclerites of Mediterranean gorgonians (Coelenterata: Octocorallia). Estuar. Coast. Shelf Sci. 40:87-104.
- Weiner S. 1984. Organization of organic matrix components in mineralized tissues. Integr. Comp. Biol. 24: 945-951. Weiner S, Dove PM. 2003. An Overview of Biomineralization Processes and the Problem of the Vital Effect. Rev. Mineral. Geochem. 54:1-29.
- Weiner S, Hood L. 1975. Soluble protein of the organic matrix of mollusk shells: a potential template for shell formation. Science 190:987-989.
- Weiss IM, Kaufmann S, Mann K, Fritz M. 2000. Purification and characterization of perlucin and perlustrin, two new proteins from the shell of the mollusc *Haliotis laevigata*. Biochem. Biophys. Res. Commun. 267:17-21.
- Wells JW. 1956. Scleractinia. In: Treatise on invertebrate paleontology Part F, Coelenterata. University of Kansas Press:328-444.
- Wen-Tang Z, Babcock E, Others. 2001. New Extraordinarily Preserved Enigmatic Fossils, Possibly with Ediacaran Affinities, from the Lower Cambrian of Yunnan. China. Acta Palaeontol. Sin. 40:201-213.
- Wessel D, Flügge UI. 1984. A method for the quantitative recovery of protein in dilute solution in the presence of detergents and lipids. Anal. Biochem. 138:141-143.

- Wheeler AP, George JW, Evans CA. 1981. Control of calcium carbonate nucleation and crystal growth by soluble matrix of oyster shell. *Science* 212:1397-1398.
- Wijsman-Best M. 1974. Habitat-induced modification of reef corals (Faviidae) and its consequences for taxonomy. In: *Proc 2nd int coral Reef Symp* 2:217-228.
- Wild C, Hoegh-Guldberg O, Naumann MS, Florencia Colombo-Pallotta M, Ateweberhan M, Fitt WK, Iglesias-Prieto R, Palmer C, Bythell JC, Ortiz JC, et al. 2011. Climate change impedes scleractinian corals as primary reef ecosystem engineers. *Mar. Freshwater Res.* 62:205-215.
- Williams GC. 1986. Morphology, systematics, and variability of the southern African soft coral *Alcyonium variable* (J. Stuart Thomson, 1921)(Octocorallia, Alcyoniidae). *Ann. S. Afr. Mus.* 96:241-270
- Williams GC. 1992. The alcyonacea of Southern Africa: stoloniferous octocorals and soft corals (coelenterata, Anthozoa). *Ann. S. Afr. Mus.* 100:249-358
- Willis BL. 1985. Phenotypic plasticity versus phenotypic stability in the reef corals *Turbinaria mesenterina* and *Pavona cactus*. In: *Proceedings of the Fifth International Coral Reef Symposium* 4:107-112.
- Wilt FH. 2002. Biomineralization of the spicules of sea urchin embryos. *Zoolog. Sci.* 19:253-261.
- Wilt, H F. 1988. Development of the endoskeletal spicule of the sea urchin embryo. In: *Self-Assembling Architecture*. Alan R. Liss, New York:203-228.
- Wood R. 1999. *Reef Evolution*. Oxford University Press on Demand.
- Wray JL, Daniels F. 1957. Precipitation of Calcite and Aragonite. *J. Am. Chem. Soc.* 79:2031-2034.
- Yagi H, Iwazawa A, Sonobe R, Matsubara T, Hikita H. 1984. Crystallization of calcium carbonate accompanying chemical absorption. *Ind. Eng. Chem. Fundam.* 23:153-158.
- Yuyama I, Higuchi T. 2019. Differential gene expression in skeletal organic matrix proteins of scleractinian corals associated with mixed aragonite/calcite skeletons under low mMg/Ca conditions. *PeerJ* 7:e7241.
- Zeebe RE. 2001. Seawater pH and isotopic paleotemperatures of Cretaceous oceans. *Palaeogeogr. Palaeoclimatol. Palaeoecol.* 170:49-57.
- Zhuravlev AY, Wood RA. 2008. Eve of biomineralization: Controls on skeletal mineralogy. *Geology* 36:923-926.
- Zilberberg C, Edmunds PJ. 1999. Patterns of Skeletal Structure Variability in Clones of the Reef Coral *Montastraea franksi*. *Bull. Mar. Sci.* 64:373-381.
- Zoccola D, Ganot P, Bertucci A, Caminiti-Segonds N, Techer N, Voolstra CR, Aranda M, Tambutté E, Allemand D, Casey JR, et al. 2015. Bicarbonate transporters in corals point towards a key step in the evolution of cnidarian calcification. *Sci. Rep.* 5:9983.
- Zoccola D, Tambutté E, Kulhanek E, Puverel S, Scimeca JC, Allemand D, Tambutté S. 2004. Molecular cloning and localization of a PMCA P-type calcium ATPase from the coral *Stylophora pistillata*. *Biochim. Biophys. Acta* 1663:117-126.

- Zoccola D, Tambutté E, Sénégas-Balas F, Michiels JF, Failla JP, Jaubert J, Allemand D. 1999. Cloning of a calcium channel alpha-1 subunit from the reef-building coral, *Stylophora pistillata*. *Gene* 227:157-167.
- Zou X, Shen J, Chen F, Ting K, Zheng Z, Pang S, Zara JN, Adams JS, Soo C, Zhang X. 2011. NELL-1 binds to APR3 affecting human osteoblast proliferation and differentiation. *FEBS Lett.* 585:2410-2418.

Supplementary Figures of Chapter 2

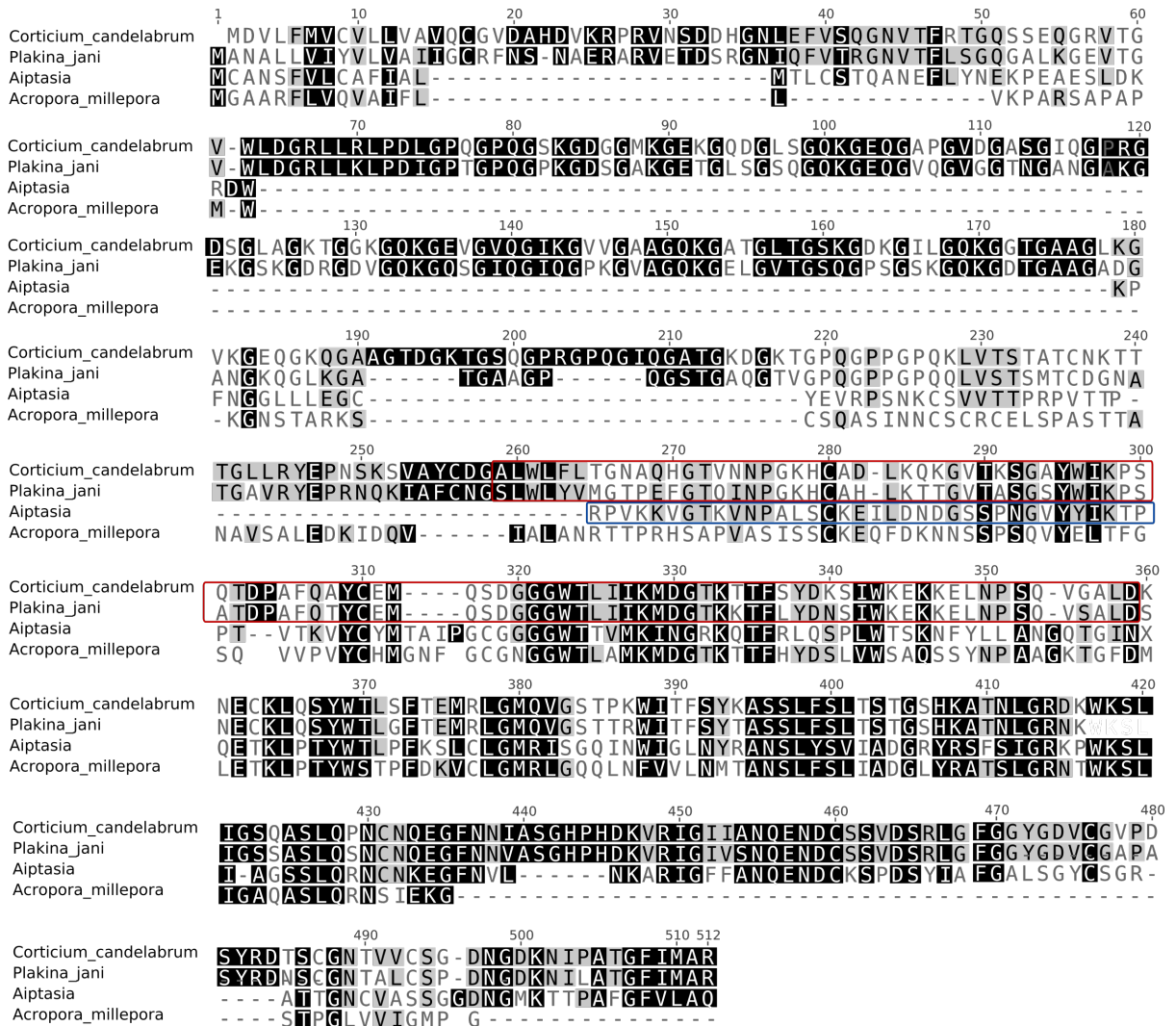


Figure S2.1: Alignment of USOMP5-like sequences showing the position of the homologous superfamily Fibrinogen, alpha/beta/gamma-chain, C-terminal globular, subdomain 1 (IPR014716) in homoscleromorph sponges (red boxes) and *Aiptasia* (blue boxes). No domain was detected in *A. millepora*.

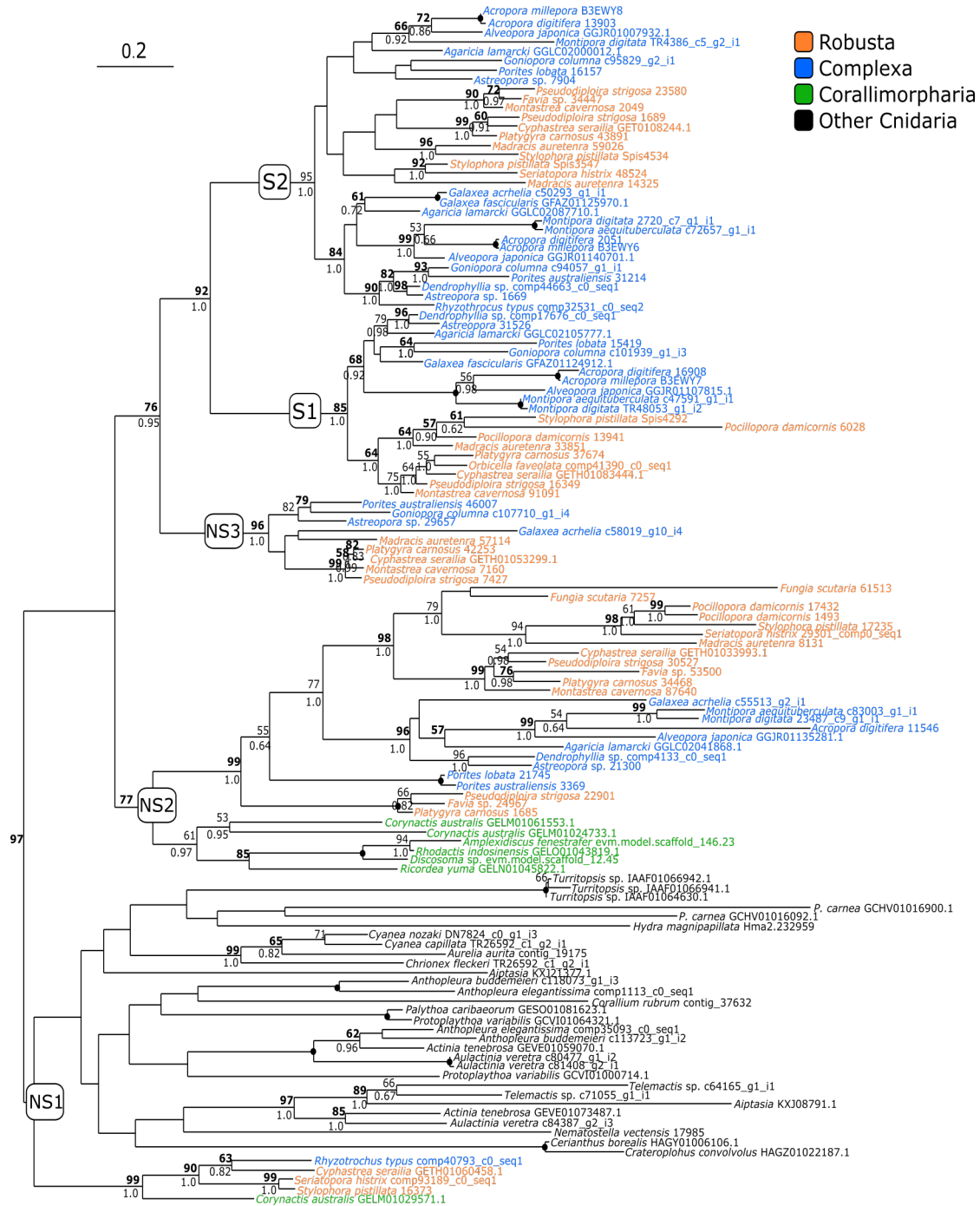


Figure S2.2: Maximum Likelihood tree (500 bootstrap replicates) of cnidarian acidic proteins. Protein sequences aligned with MUSCLE. Best-fit model: WAG + Γ + I. Black dot on node indicates full support (100 bootstrap - 1.0 Posterior Probability). Bootstrap values in bold: support is > 50 also in phylogeny based on MAFFT alignment.

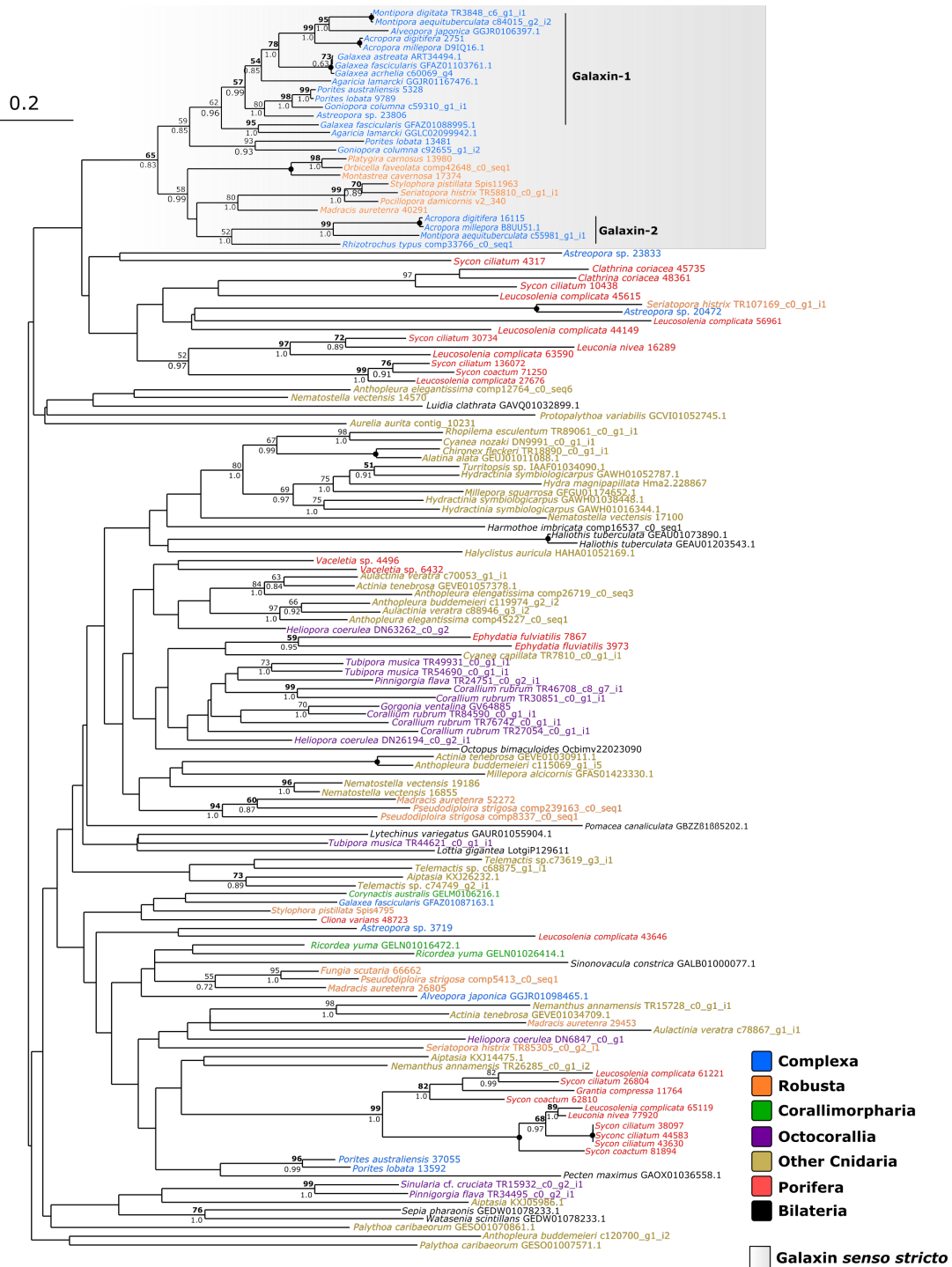


Figure S2.3: Phylogenetic analysis (500 bootstraps) of metazoan galaxin-related proteins. Tree displayed in figure based on protein sequences aligned with MUSCLE alignment. Bold number: node supported (>50) also in MAFFT phylogeny. Dot on node indicates full support (100 bootstrap - 1.0 Posterior Probability) in both phylogenies. Support for nodes >50 not shown regardless of posterior probability value.

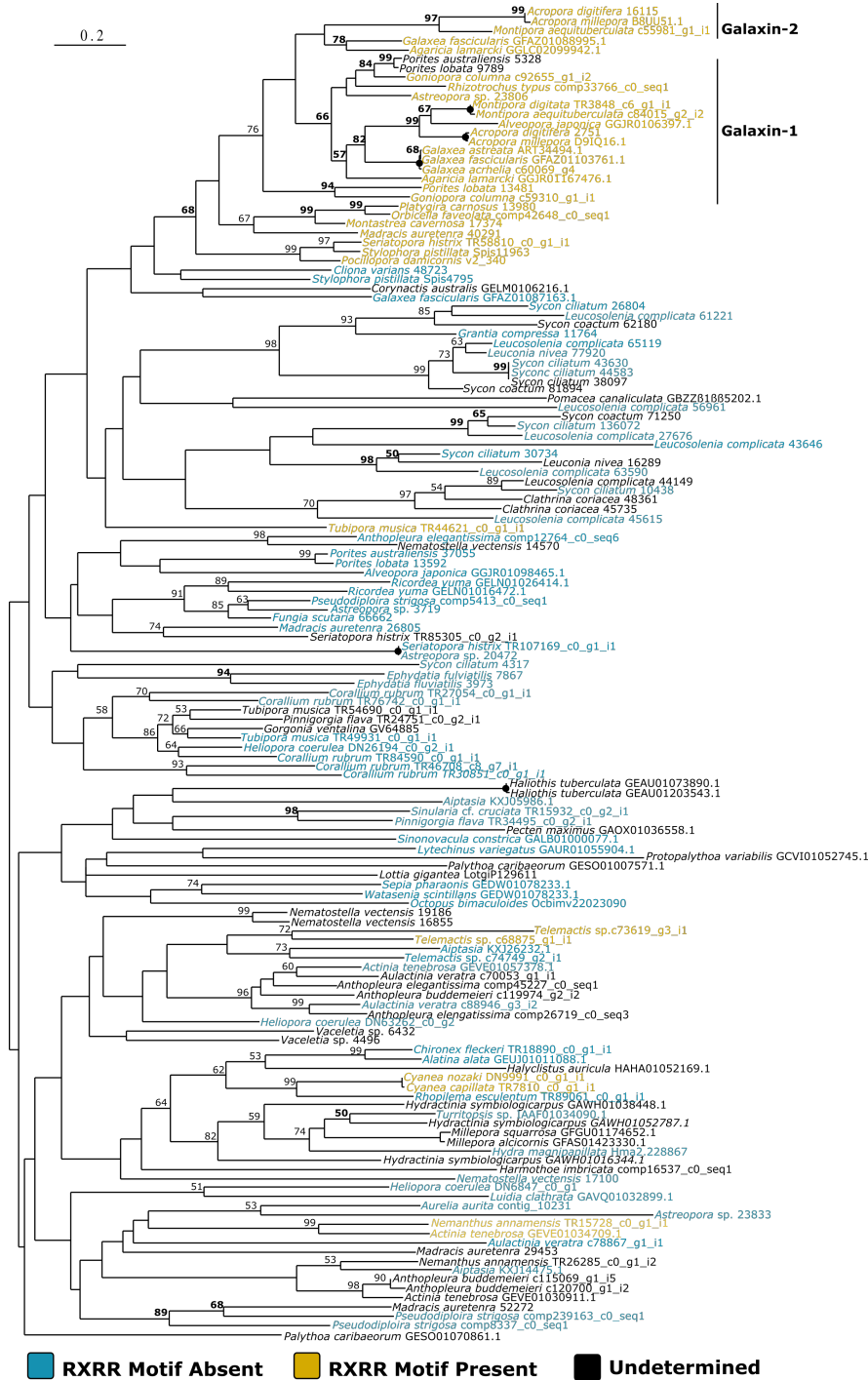


Figure S2.4: MAFFT-based phylogenetic analysis of galaxin-related proteins highlighting the presence of the RXRR motif described in Fukuda et al. (2003).

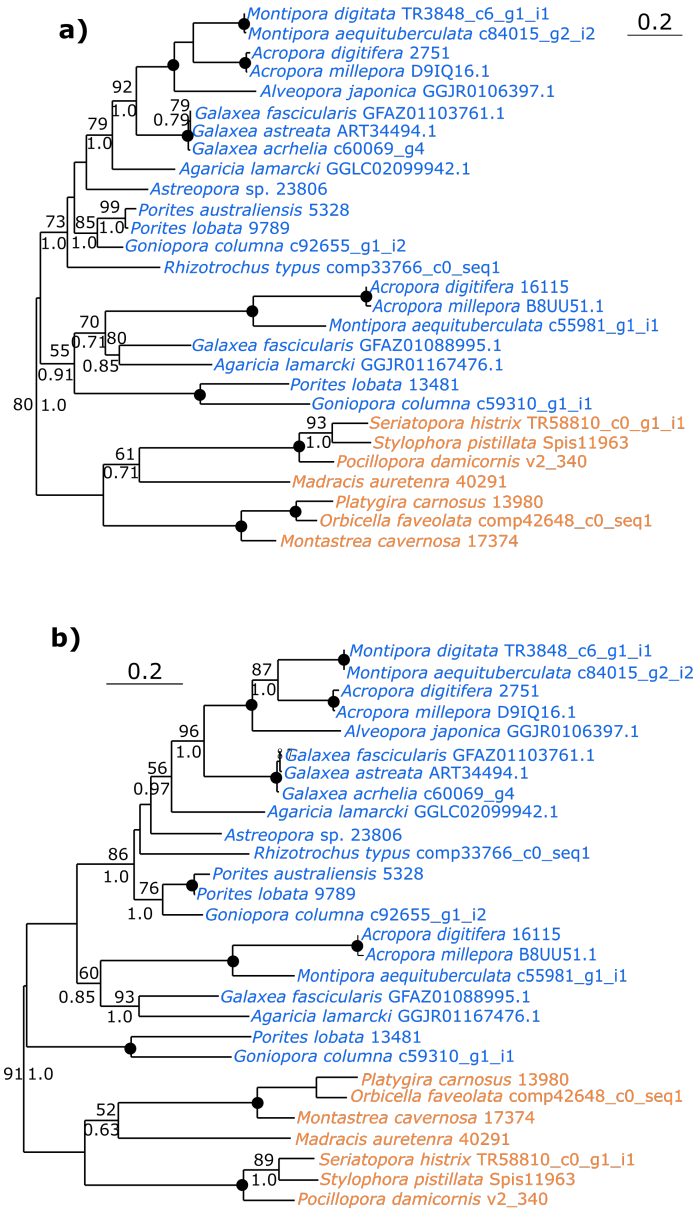


Figure S2.5: Phylogenetic analysis (500 bootstrap replicates) of galaxin sensu stricto based on MUSCLE (a) and MAFFT (b) aligned sequences. Best-fit model for both alignments: JTT+ Γ +I. Black dots on node indicates full support (100 bootstrap - 1.0 Posterior Probability). Maximum-likelihood and bayesian analyses were performed with PhyML 3.1 (in Seaview 4) and MrBayes 3.2.6, respectively. For the latter, a burn-in fraction of 20% was applied.

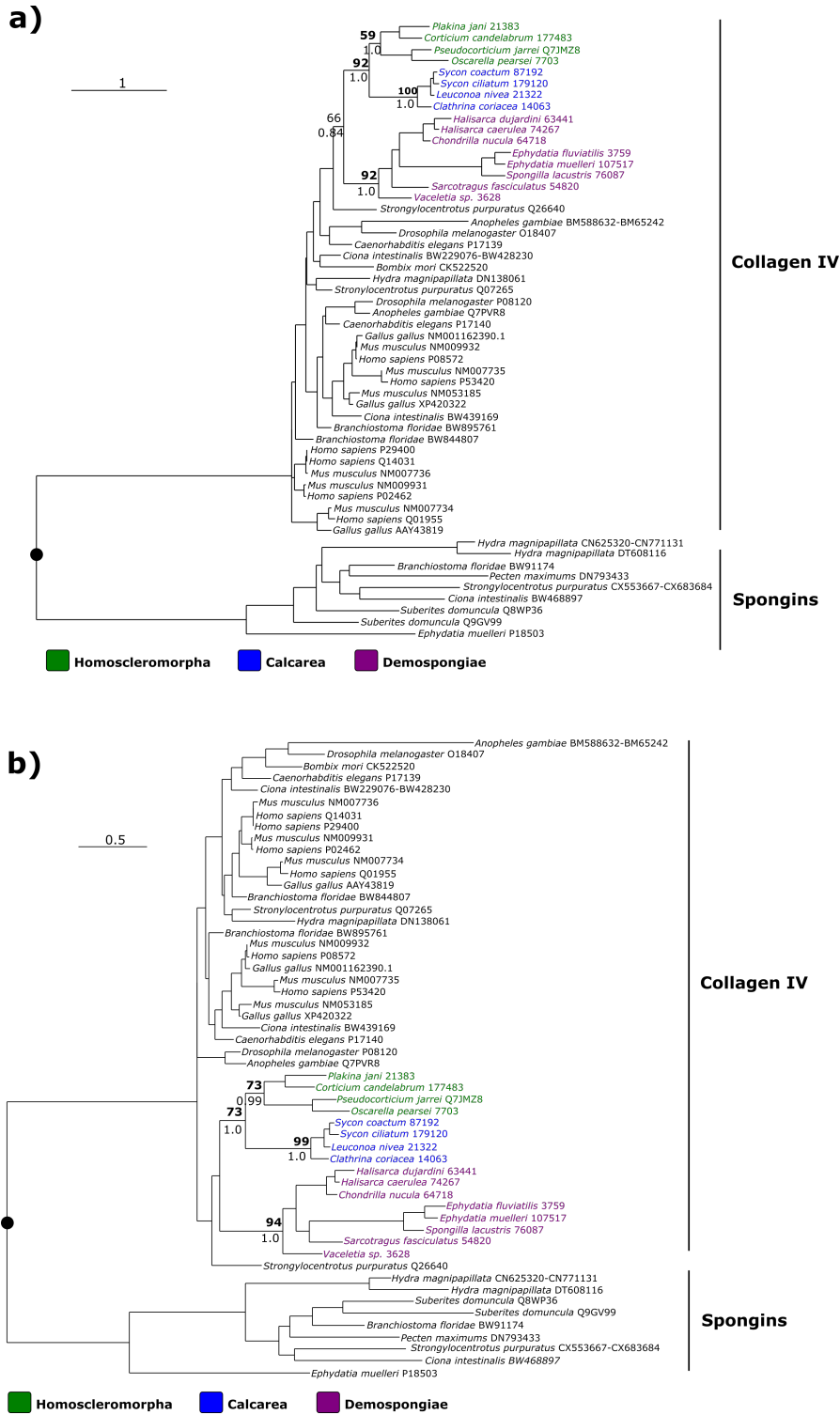


Figure S2.6: Phylogenetic analysis (500 bootstrap replicates) of Collagen IV NC1 domain and putative homolog in spongins. Colored sequences (with exception of Q7JMZ8) were identified with BLASTp as part of this study. Other sequences from Auouacheria et al. (2006). Sequences were aligned in a) MAFFT and b) MUSCLE. Best-fit model: LG + Γ + I and WAG + Γ + I respectively. Numbers in bold: node support >50 also in both phylogenies. Support showed for nodes of interest only

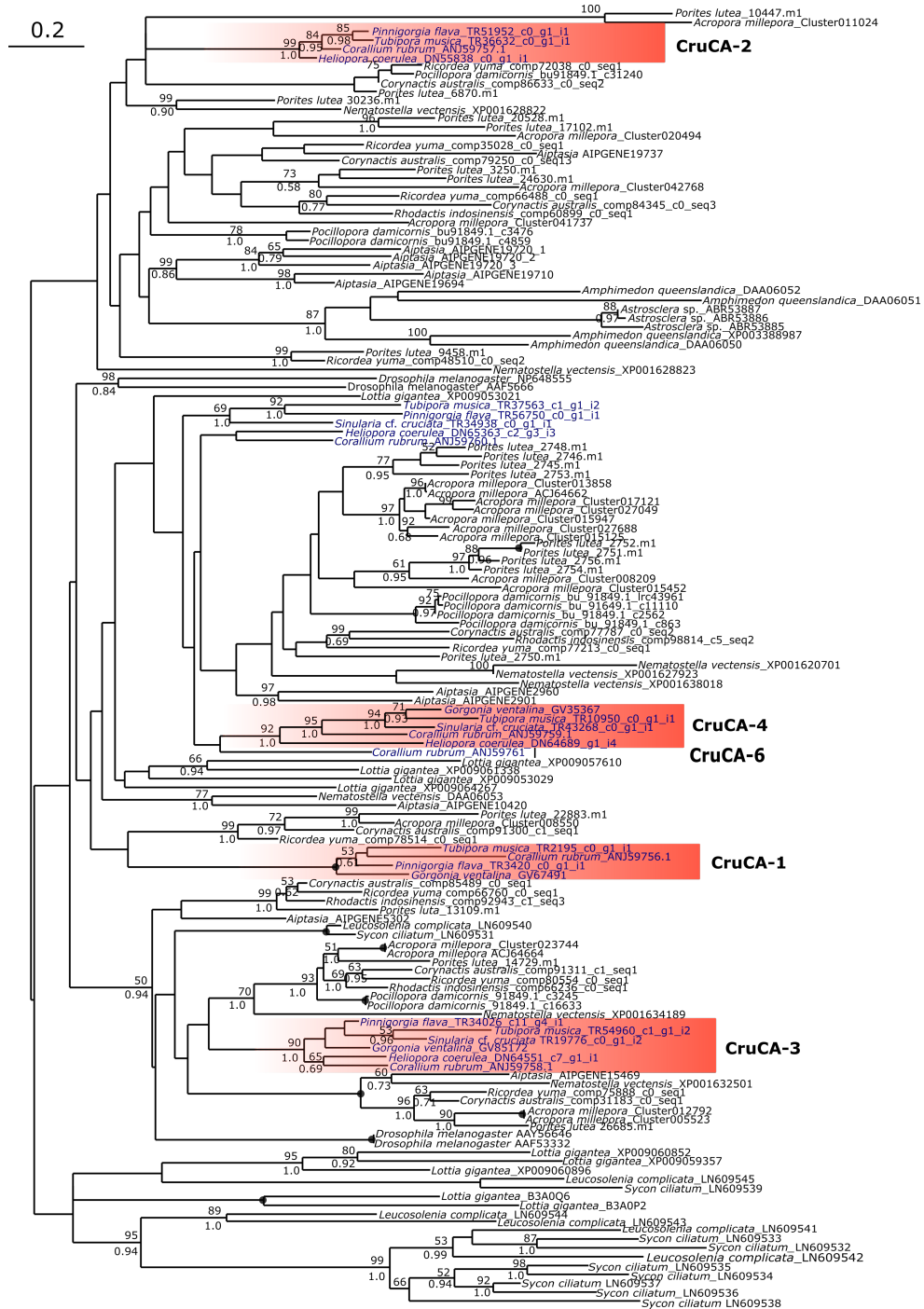


Figure S2.7: Phylogenetic analysis (500 bootstrap replicates) of octocoral carbonic anhydrases (CA) (MAFFT). Octocoral CAs are in blue. Sequences added to the dataset used in Lin et al. (2017). Best-fit model: LG + Γ . Black dots on node indicates full support (100 bootstrap - 1.0 Posterior Probability).

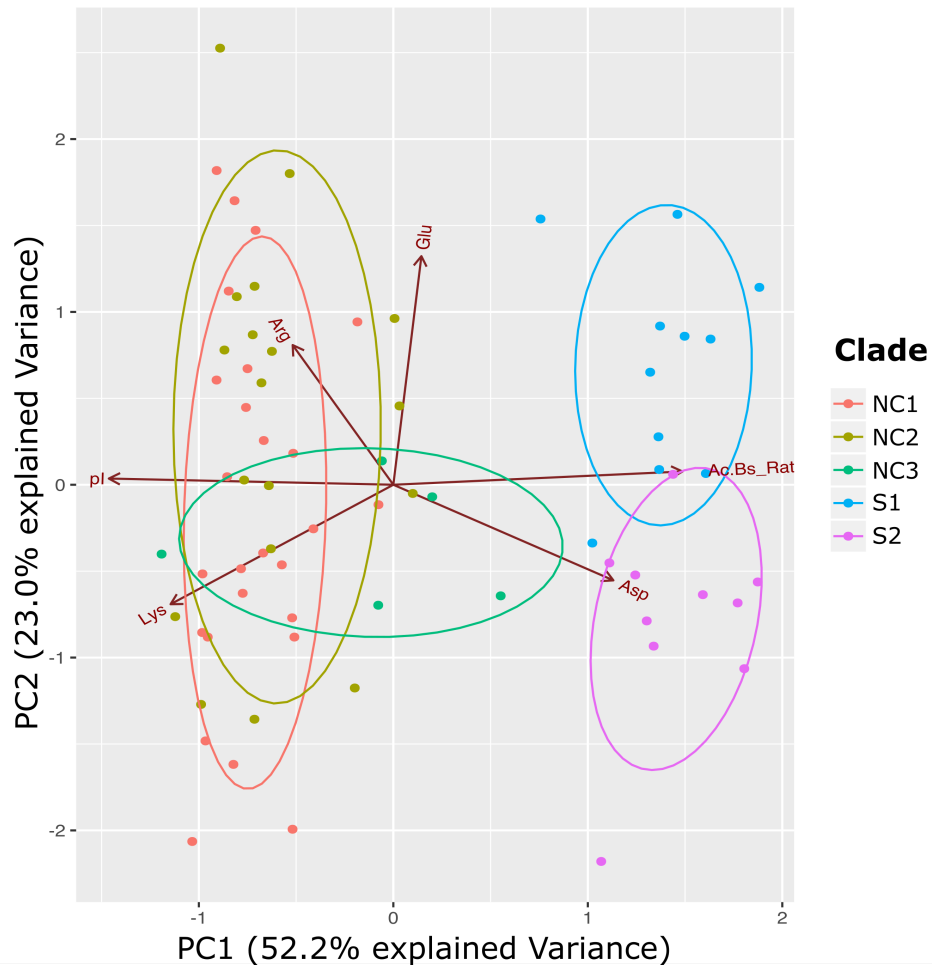


Figure S2.9: Principal Component Analysis of acidic proteins. Amino acid percentages within sequences and isoelectric point determined with ProtParam. Parameters calculated for complete sequences only. pI = isoelectric point, Lys = Lysine, Arg = Arginine, Glu = Gultammic Acid, Asp = Aspartic Acid. Ac.Bs.Ratio = Acidic-Basic Ratio $[(\text{Asp}+\text{Glu}) / (\text{Arg}+\text{Lys})]$.

Supplementary Figures of Chapter 3

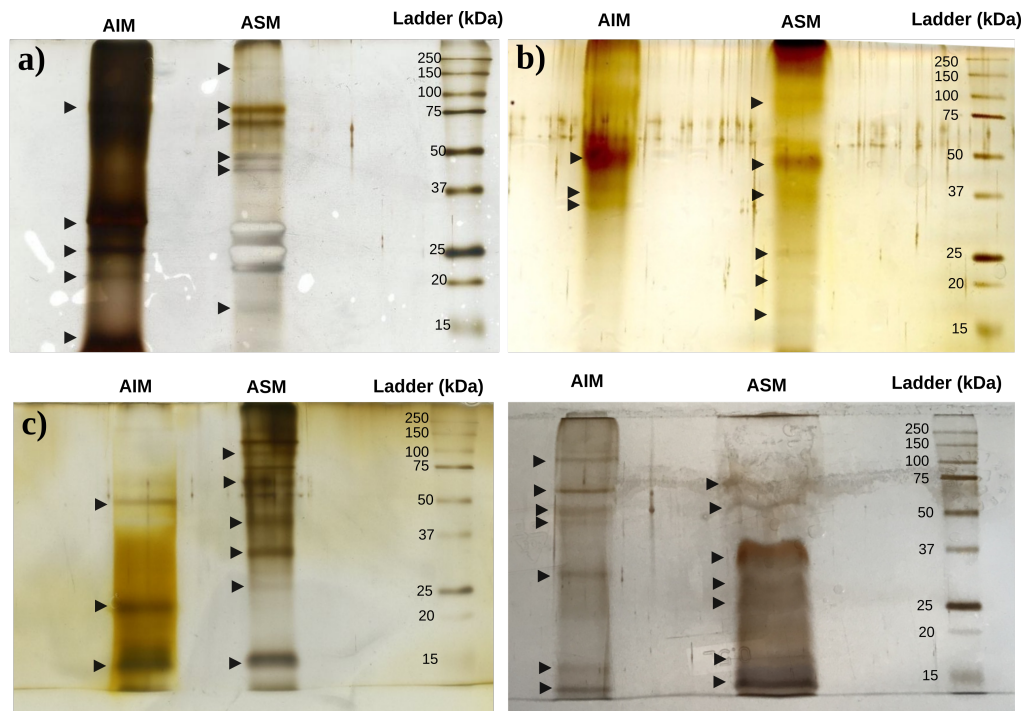


Figure S3.1: Silver-stained 1D SDS gels of a) *H. coerulea*, b) *M. digitata*, c) *T. musica* and d) *S. cf. cruciata*.

	1				
Heliopora_coerulea_DN64689_c5_g1_i4	MKSLILSSLL	FVSFQLFYSI	DFVEPSQEW	YK-GPLGPK	
Heliopora_coerulea_DN62651_c6_g1	MKLLTPSSLV	LVVQLFYLYLH	GPVVVAVKYT	YE-GKLGPAH	
Heliopora_coerulea_DN64224_c6_g1_i1	MNLLIRSSLV	LVILQLIYLN	GLIASEPKFA	YY-GPKGPCN	
Corallium_rubrum_ANJ59759.1	MKLVILSFLF	VSLQAFYFAE	A---AQIKWS	FT-GVNGPSQ	
CNID_Antho_Xenia_sp_18393	-MVFSILAFL	VAVF-VSWS	S---SYVGS	FQ-GENGPMF	
CNID_Antho_Clavularia_sp_60972	MYTLLINCLL	ASIYFISYTE	S---SAIEWS	FHDGKNGPSQ	
Sinularia_cf_cruciata_TR43268 c0_g1_i1	MKVLVISAFF	ILITLAFSE	S---TKIDWS	FH-GANGPPY	
Tubipora_musica_TR10950 c0_g1_i1	MNALRLSSFL	VAISLATPCE	S---ASNEWS	FH-GKNGPEN	
CNID_Antho_Dendronephthya_gigantea_23303	MRSPLLSYF	LAVSLTFPTE	S---AKIDWS	FH-GKNGPSH	
CNID_Antho_Eunicella_verrucosa_9997	MKTLLLISFF	VVISATTFSE	S---FKIDWS	FH-GRNGPSH	
CNID_Antho_Gorgonia_ventalina_8411	MKTLVL--IF	VIIIGITVSE	S---SKVEWS	FH-GRNGPSH	
CNID_Antho_Eunicea_calyculata_22715	MKTLVLVSIF	IVIGVTFPSE	G---AKVDWS	FH-GRNGPSH	
	41				
Heliopora_coerulea_DN64689_c5_g1_i4	WKKRFPK-CG	RKKQSPINIP	LSKTKYSPLL	RDSIEFNYS	
Heliopora_coerulea_DN62651_c6_g1	WPKLWKHQCA	GRKQSPINIP	ITTTKYVASL	KKSLHFPGYS	
Heliopora_coerulea_DN64224_c6_g1_i1	WPRLPDFPCA	GRRQSPINIP	VSRTWYSSSL	KNSLRFHDYS	
Corallium_rubrum_ANJ59759.1	WKEHYPA-CK	SKQQSPINIP	VFKKEYNSSL	KGSLKFTHYS	
CNID_Antho_Xenia_sp_18393	WSKLYPR-CS	NRRQSPINLP	LFKKDFHPSL	RSSTKLIQYS	
CNID_Antho_Clavularia_sp_60972	WSTFFPK-CK	SKRQSPIDIP	LQKKEYLPSL	RHSIVLSHYT	
Sinularia_cf_cruciata_TR43268 c0_g1_i1	WSKSFPI-CS	NKRQSPINIP	VSKKVEPKL	KRALELSHYT	
Tubipora_musica_TR10950 c0_g1_i1	WAKLFPK-CS	NARQSPINIP	LFKQYEPAL	RESLEFAHYT	
CNID_Antho_Dendronephthya_gigantea_23303	WSRSFPL-CS	NKRQSPINIP	LYKKDFRPSL	RSSLKFSHYT	
CNID_Antho_Eunicella_verrucosa_9997	WSKSFPI-CS	NKRQSPINIP	VFKKDFQPSL	KASLEFSHYT	
CNID_Antho_Gorgonia_ventalina_8411	WSKSFPI-CS	NARQSPINIP	LFKKVFKPSL	KASLEFAHYT	
CNID_Antho_Eunicea_calyculata_22715	WSELFPI-CS	HKRQSPINIP	VLKKYFKPSL	KTSLKFSHYT	
	81				
Heliopora_coerulea_DN64689_c5_g1_i4	C--PCDEFL	LENKCTTLEV	NVATAGASIK	LKDLREYNL	
Heliopora_coerulea_DN62651_c6_g1	C-HACKGKFE	LENKCTTLEV	FVESAGASIR	LNG-IGNFTL	
Heliopora_coerulea_DN64224_c6_g1_i1	CSHPDGEFE	LENKCTTLEV	IVTSADASIT	LKDLGRKYIL	
Corallium_rubrum_ANJ59759.1	C--PCGGDFK	MRNTGCTLKL	YVTTAFATLT	LQR-KERYWL	
CNID_Antho_Xenia_sp_18393	C--PCQGDPL	LKNNGKVLMI	DVKTANASLI	LKN-EHHPKL	
CNID_Antho_Clavularia_sp_60972	C--PCRQKQV	MQNNGKTLII	NLQNTFATIT	MNG-EKRFML	
Sinularia_cf_cruciata_TR43268 c0_g1_i1	R--PYRGDFT	MLNNGKTLVI	DLRNALASLT	ISR-EKRYML	
Tubipora_musica_TR10950 c0_g1_i1	C--PCRQDFV	MQNNGKTLVI	DARNTLASLT	LNR-ERRFML	
CNID_Antho_Dendronephthya_gigantea_23303	C--PCRQDFT	MQNNGKTFKI	DLRNALASLT	LNR-ARRYLL	
CNID_Antho_Eunicella_verrucosa_9997	C--PCRGEFA	MQNNGKTLRI	DVRNATFATLT	LNR-KRRFML	
CNID_Antho_Gorgonia_ventalina_8411	C--PCRGNFV	MRNNGKTLII	DARNALASLT	LNG-KRRFL	
CNID_Antho_Eunicea_calyculata_22715	C--PCRGNFT	IQNSCTTLKI	DVRNALASIS	LSR-SRRYLL	
	121				
Heliopora_coerulea_DN64689_c5_g1_i4	EQFHFWGKK	NSRGSEHRY	GKVFSAEMHL	VHYNVYSSSL	
Heliopora_coerulea_DN62651_c6_g1	REFHFWGKV	NSRGSEHRY	GKAYSAMHV	VHYNTKYSSV	
Heliopora_coerulea_DN64224_c6_g1_i1	EQFHFWGKV	NSRGSEHRY	GRIFSAEMHL	VHHSKDYSSV	
Corallium_rubrum_ANJ59759.1	DQIHFWGSD	NTQGSERFD	KERFPAEIHF	VHYNIKYKQL	
CNID_Antho_Xenia_sp_18393	DHLHFWGSS	DEYGSERQPD	GRSFPALHF	VHYNLNFEDI	
CNID_Antho_Clavularia_sp_60972	DHLHFWGSK	NEFGSEHLFD	GRHFAELHF	VHYNIMFPNL	
Sinularia_cf_cruciata_TR43268 c0_g1_i1	DHVHFWGSN	NQVGSERQPD	GRSFPALHL	VHYNIKFANL	
Tubipora_musica_TR10950 c0_g1_i1	DHFHFWGSN	NEQGSERLFD	GRSFPALHF	VHYNIKFANL	
CNID_Antho_Dendronephthya_gigantea_23303	DHLHFWGSS	NEIGSEHQFE	GRSFPALHF	VHYNIKFQNL	
CNID_Antho_Eunicella_verrucosa_9997	DHLHFWGSN	NQVGSERHFD	GRSFPALHF	VHYNIEFDSL	
CNID_Antho_Gorgonia_ventalina_8411	DHLHFWGSN	NQIGSERQPD	GRSFPALHF	VHYNIKFTSL	
CNID_Antho_Eunicea_calyculata_22715	DHLHFWGSN	NQIGSERHFN	GRSFPALHF	VHYNIEFGYL	
	161				
Heliopora_coerulea_DN64689_c5_g1_i4	VEALD--KPD	GLAVLAVMIK	IGKHNPAPDN	FLKYIDEVIE	
Heliopora_coerulea_DN62651_c6_g1	DVAQK--KHD	GIAALAVMIK	IGKHNSAFDK	FLKHTKVIK	
Heliopora_coerulea_DN64224_c6_g1_i1	SEAVEENEPD	STAVLAVMIK	VGRHNPAFEK	FLFKIDKVE	
Corallium_rubrum_ANJ59759.1	LEAFN--KPS	GLAVLGVMVK	IGKANPAFNN	FLRHINEVRM	
CNID_Antho_Xenia_sp_18393	SVAMD--KPN	GLAVLGVIK	IGKLNAAFNK	FLKYIHTVKS	
CNID_Antho_Clavularia_sp_60972	VAAID--KPD	ALAVLGVMIK	VGKRNPAPDK	FLKYIHRVCR	
Sinularia_cf_cruciata_TR43268 c0_g1_i1	TVAVD--QPH	ALAVLGVMIK	IGQRNKAQDK	FLKYMHRVHF	
Tubipora_musica_TR10950 c0_g1_i1	SVAID--QEN	ALAVLGVMIK	LGRPNAAFNN	FLKYAHRVKD	
CNID_Antho_Dendronephthya_gigantea_23303	SVAID--QPK	ALAVLGVMIE	VGRNPNVFDN	FLKYIHRVKN	
CNID_Antho_Eunicella_verrucosa_9997	SVAID--QPH	ALAVLGVMIK	LGRNNSAFDG	FLKYLHRVKE	
CNID_Antho_Gorgonia_ventalina_8411	SAAID--QPD	ALAVLGVMIK	VGRNPNAPDN	FLKYPHRVQE	
CNID_Antho_Eunicea_calyculata_22715	PQAID--KPD	ALAVLGVMIK	VGKRNIAPDN	FLKYIHRVSD	

 Zinc-binding histidines

 Proton shuttle residue

Figure S3.2: Alignment (MUSCLE) of octocoral CruCA4 homologs. Position of zinc binding and proton shuttle residues based on Del Prete et al. (2017).

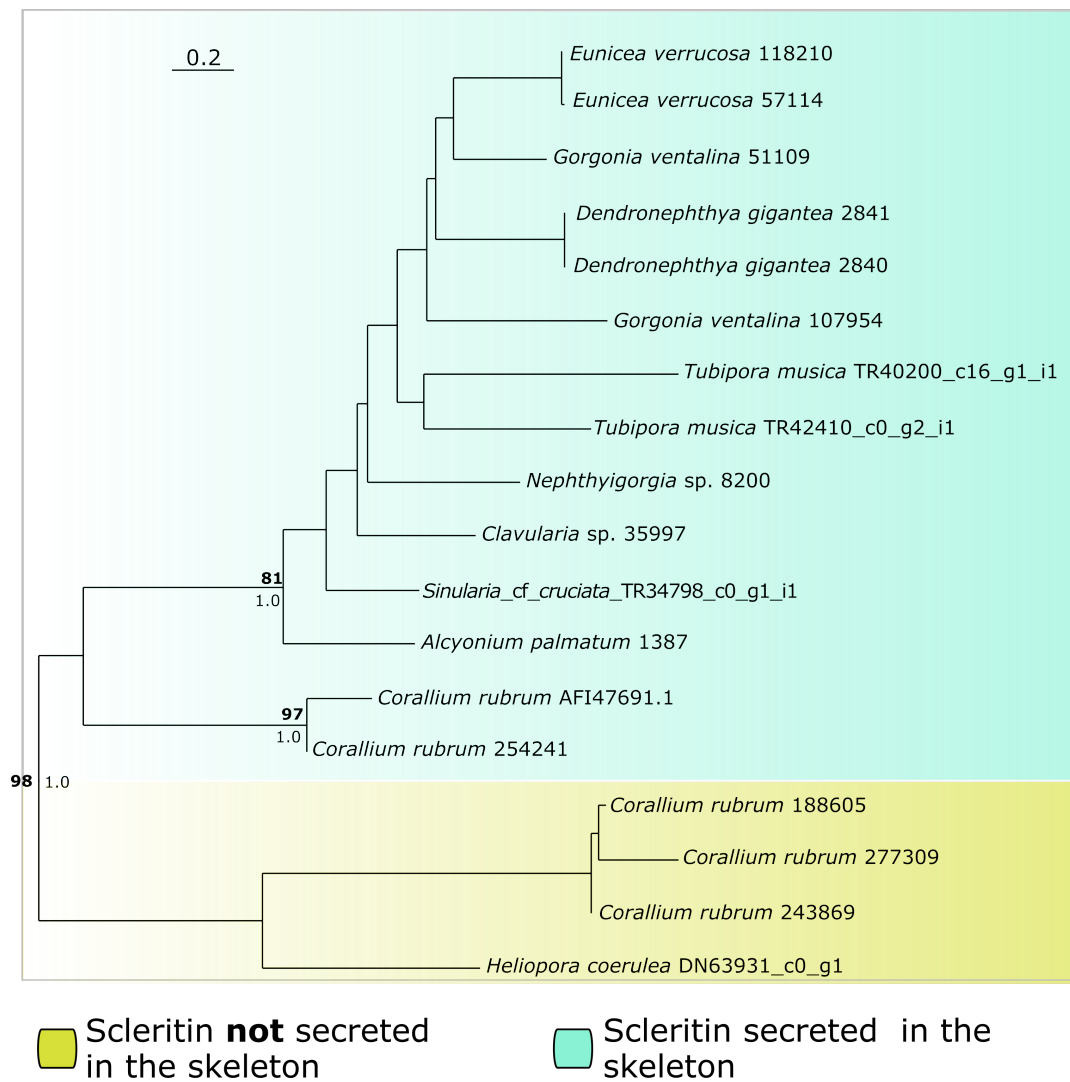


Figure S3.3: Phylogenetic analysis (400 bootstrap replicates) of octocoral scleritin homologs. Aligning algorithm: MAFFT. Best-fit model: LG + Γ + I. Number on nodes: bootstrap support and posterior probability values. Support values in bold represents nodes supported in the MAFFT-based phylogeny. Support showed for nodes of interes only.

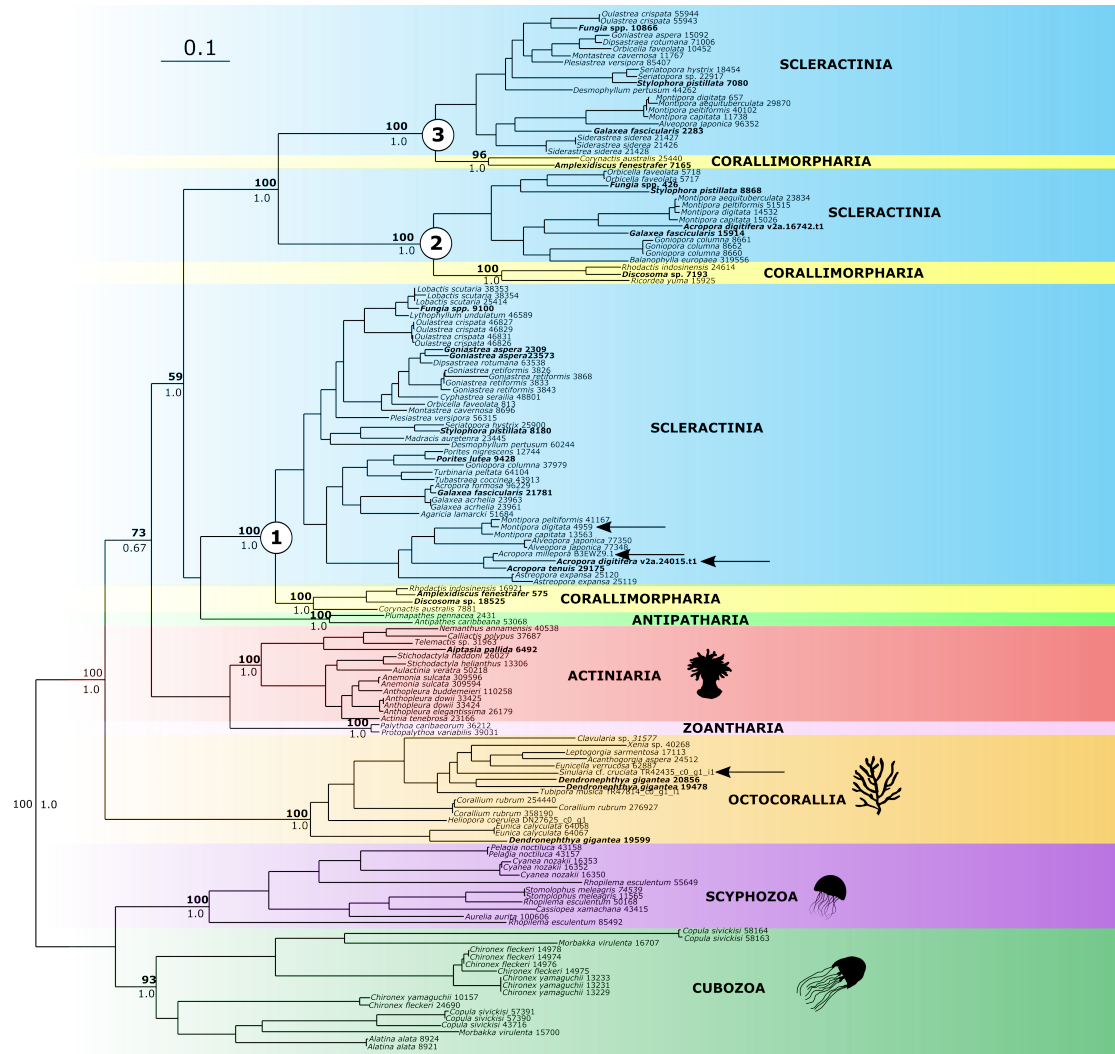


Figure S3.4: Phylogenetic analysis (400 bootstrap replicates) of cnidarian multicopper oxidases (MCOs). Aligning algorithm: MUSCLE. Best-fit model: WAG + Γ + I. Number on nodes: bootstrap support and posterior probability values. Support values in bold represents nodes supported in the MAFFT-based phylogeny.

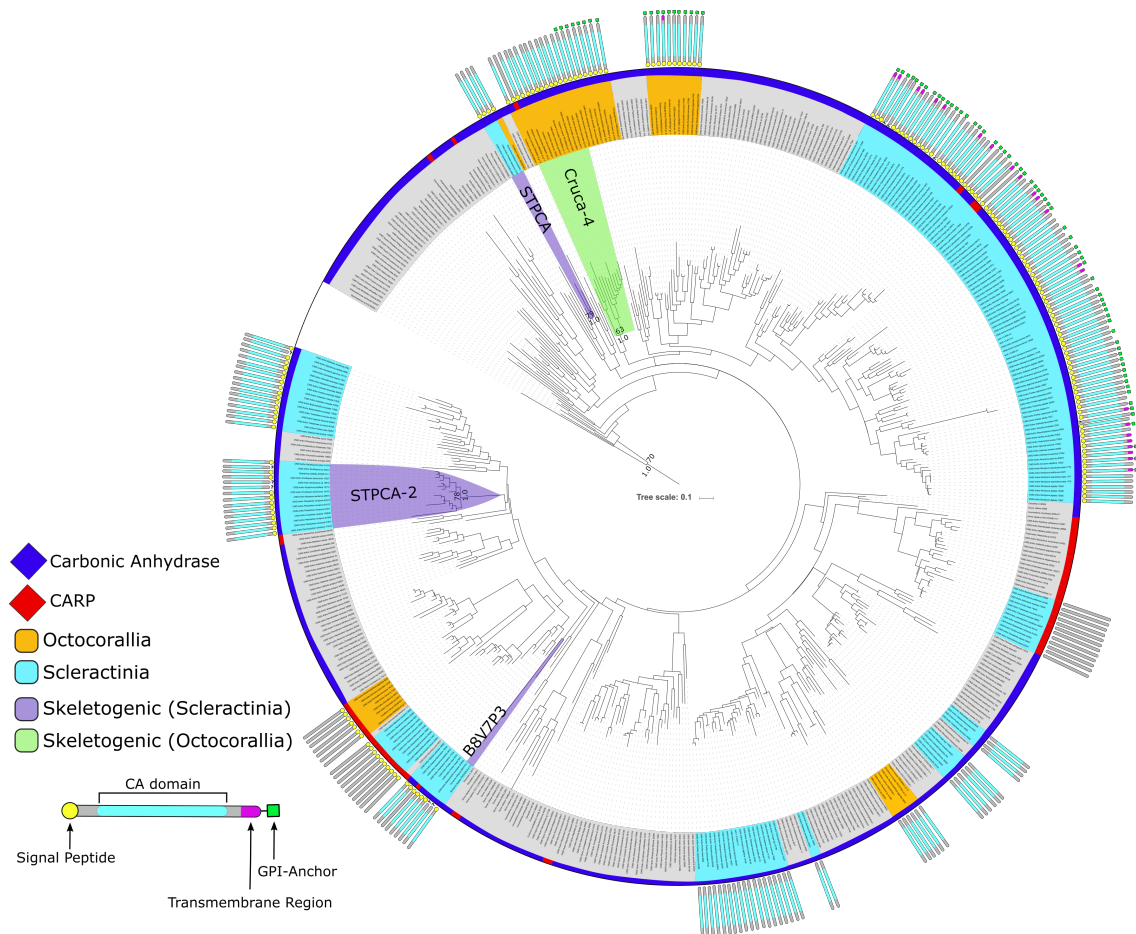
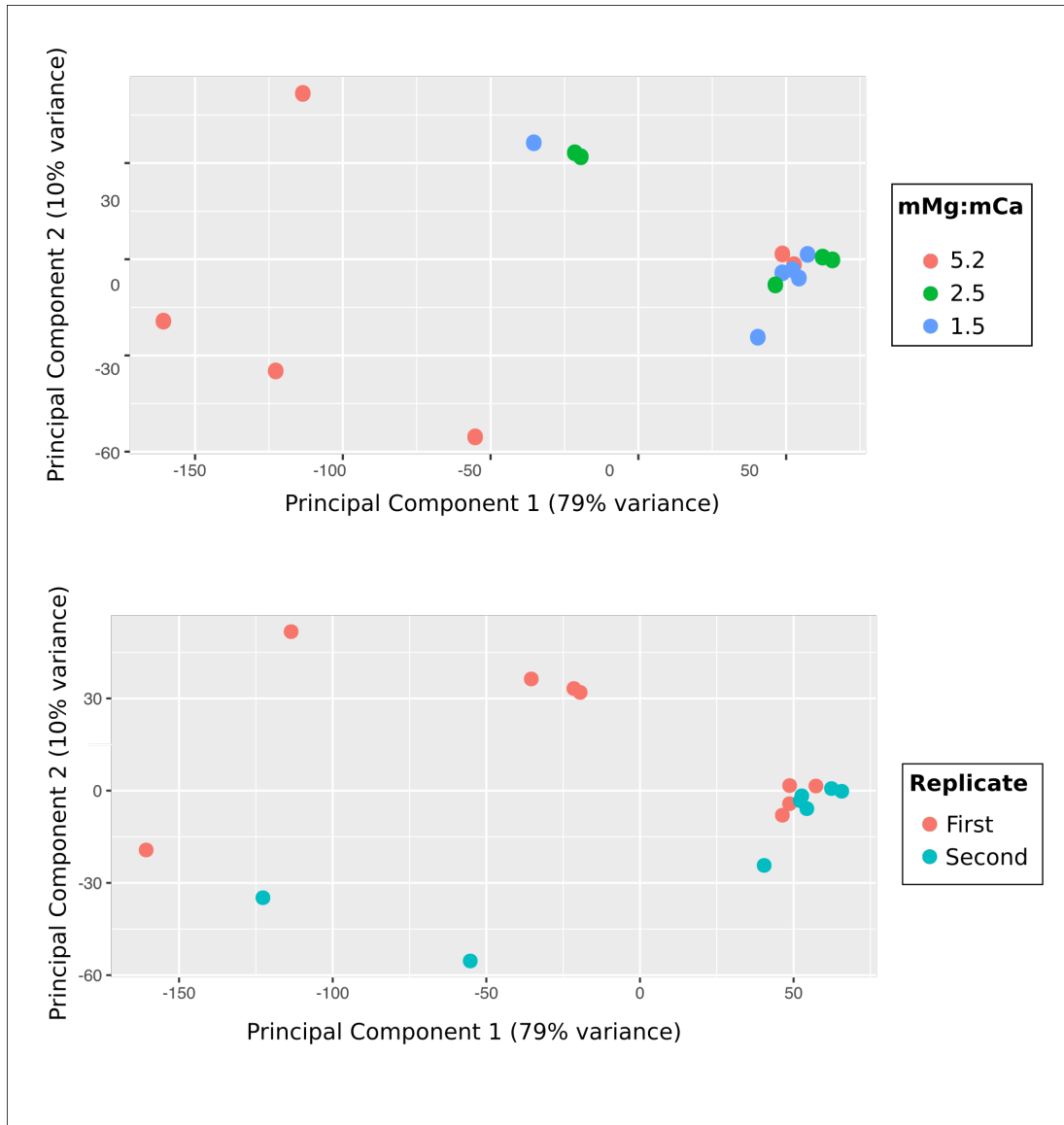
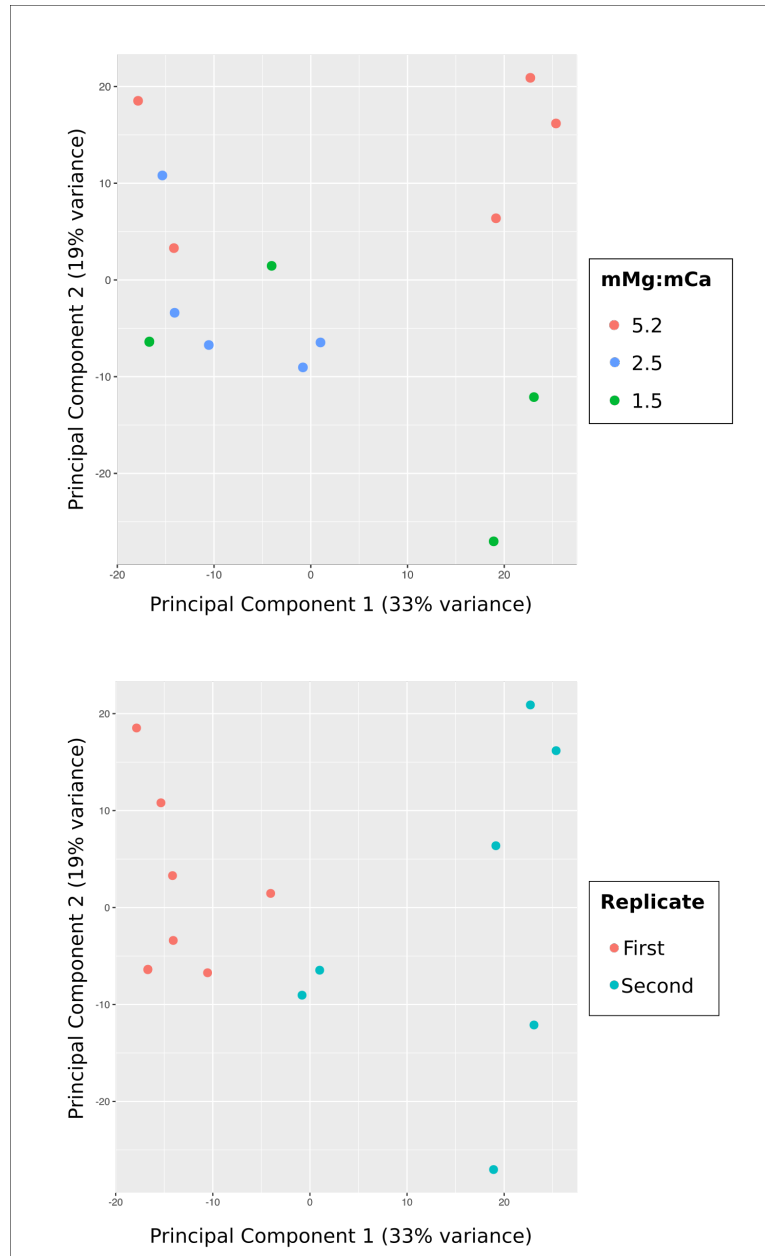


Figure S3.5: Maximum-likelihood analysis (400 bootstrap replicates) of cnidarian carbonic anhydrases and carbonic anhydrases related proteins (CARPs). Sequences aligned with MUSCLE. Best-fit model: WAG+ Γ + I. Involvement of CruCA4, STPCA, STPCA-2 and B8V7P3 based on Le Goff et al. (2016), Moya et al. (2008), Bertucci et al. (2011) and Ramos-Silva et al. (2013) respectively. Other taxa include: *Homo sapiens*, Porifera, Cubozoa, Hydrozoa, Staurozoa, Scyphozoa, Ceriantharia, Actiniaria, Corallimorpharia. Outgroup: *Chlamydomonas reinhardtii* (P20507) and *Desmodesmus* sp. (AOL92959.1).

Supplementary Figures of Chapter 4

Figure S4.1: PCA plots for the differentially expression analysis of *H. coerulea*

Figure S4.2: PCA plots for the differentially expression analysis of *M. digitata*

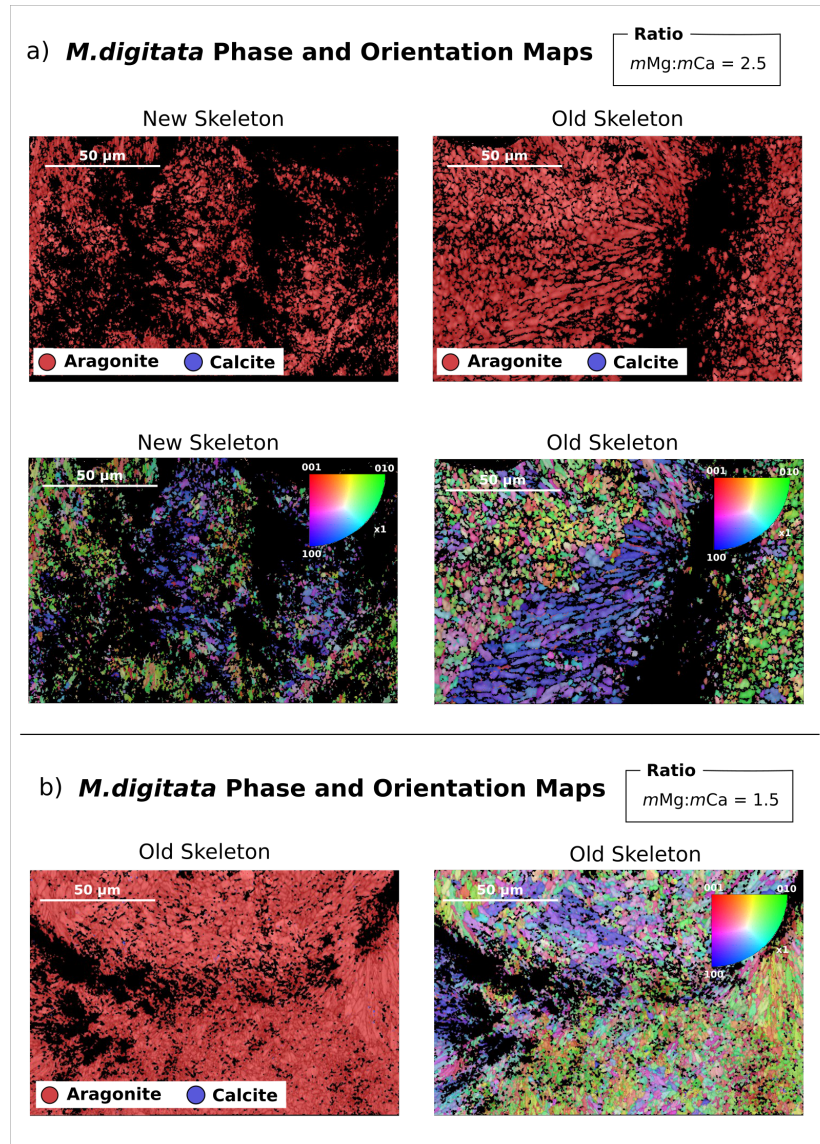


Figure S4.3: Phase map and inverse pole figures (IPF) of *M. digitata* skeletons exposed to a) $m\text{Mg}:m\text{Ca} = 2.5$ and b) $m\text{Mg}:m\text{Ca} = 1.5$. 'Old skeleton' and 'new skeleton' refer to mineral deposited before and after the experiment.

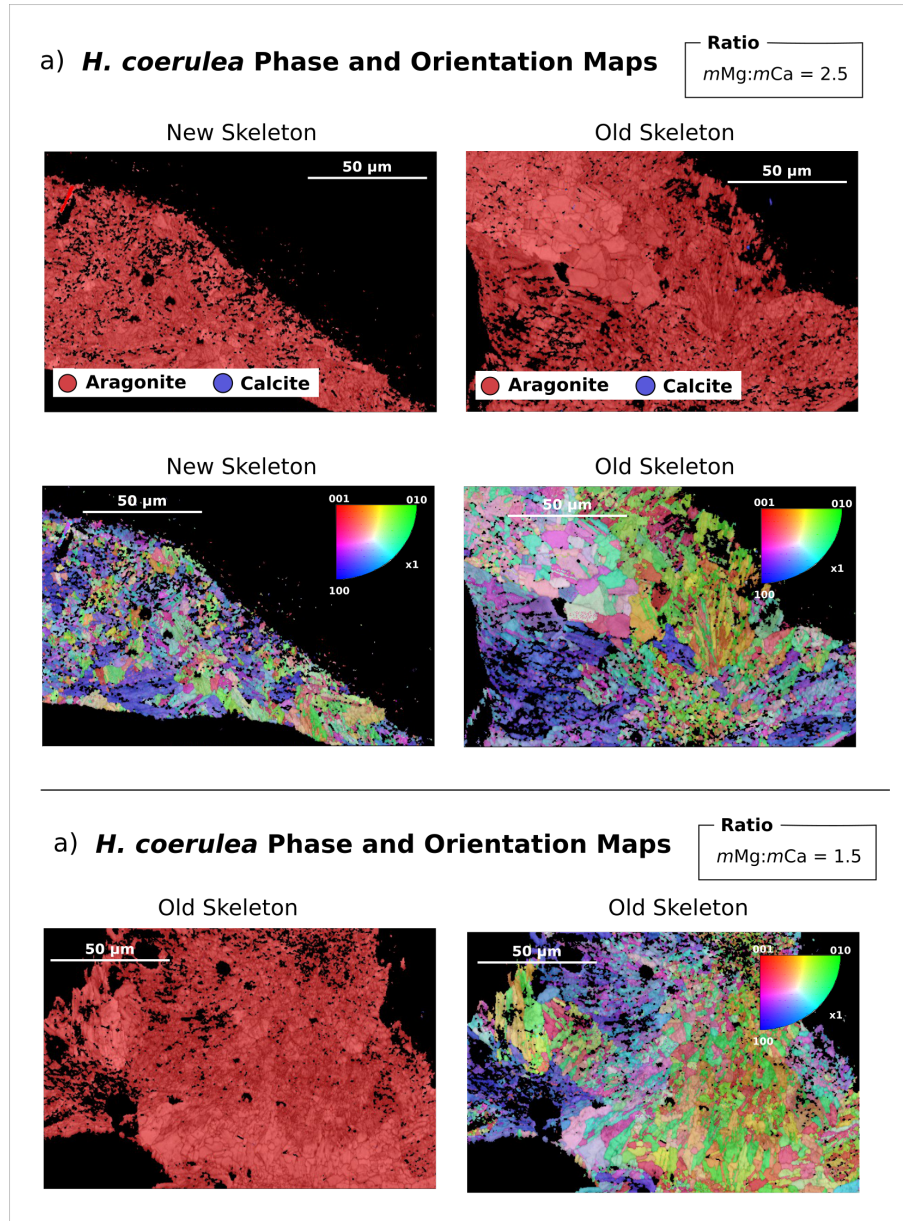


Figure S4.4: Phase map and inverse pole figures (IPF) of *H. coerulea* skeletons exposed to **a)** $m\text{Mg}:m\text{Ca} = 2.5$ and **b)** $m\text{Mg}:m\text{Ca} = 1.5$. 'Old skeleton' and 'new skeleton' refer to mineral deposited before and after the experiment.

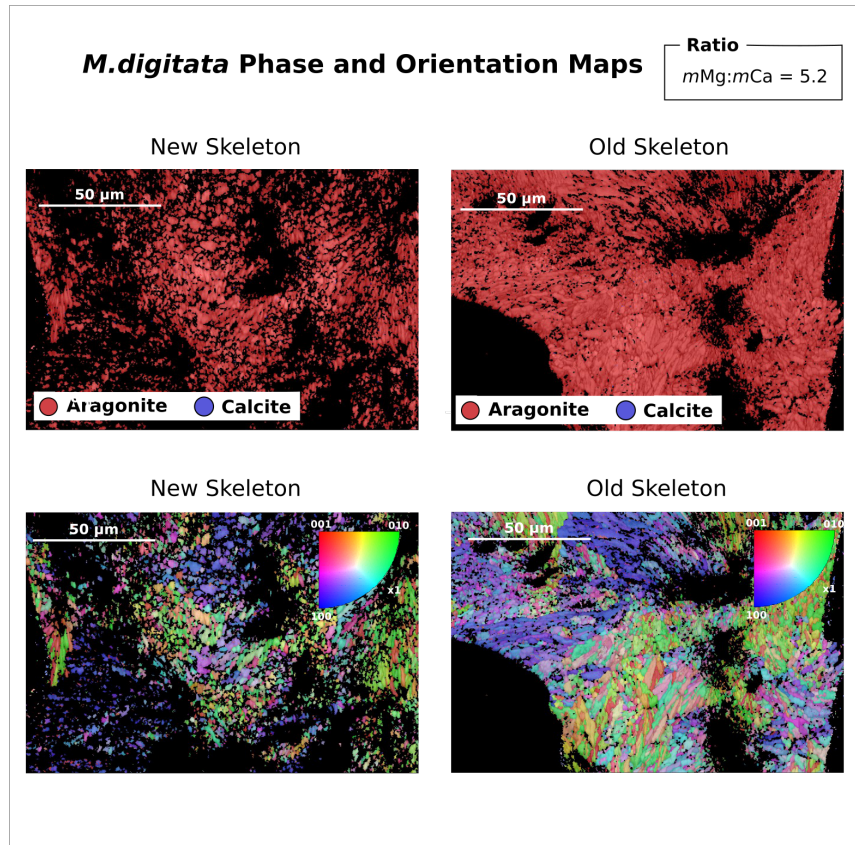


Figure S4.5: Phase map and inverse pole figures (IPF) of *M. digitata* skeletons exposed to $m\text{Mg}:m\text{Ca} = 5.2$. 'Old skeleton' and 'new skeleton' refer to mineral deposited before and after the experiment.

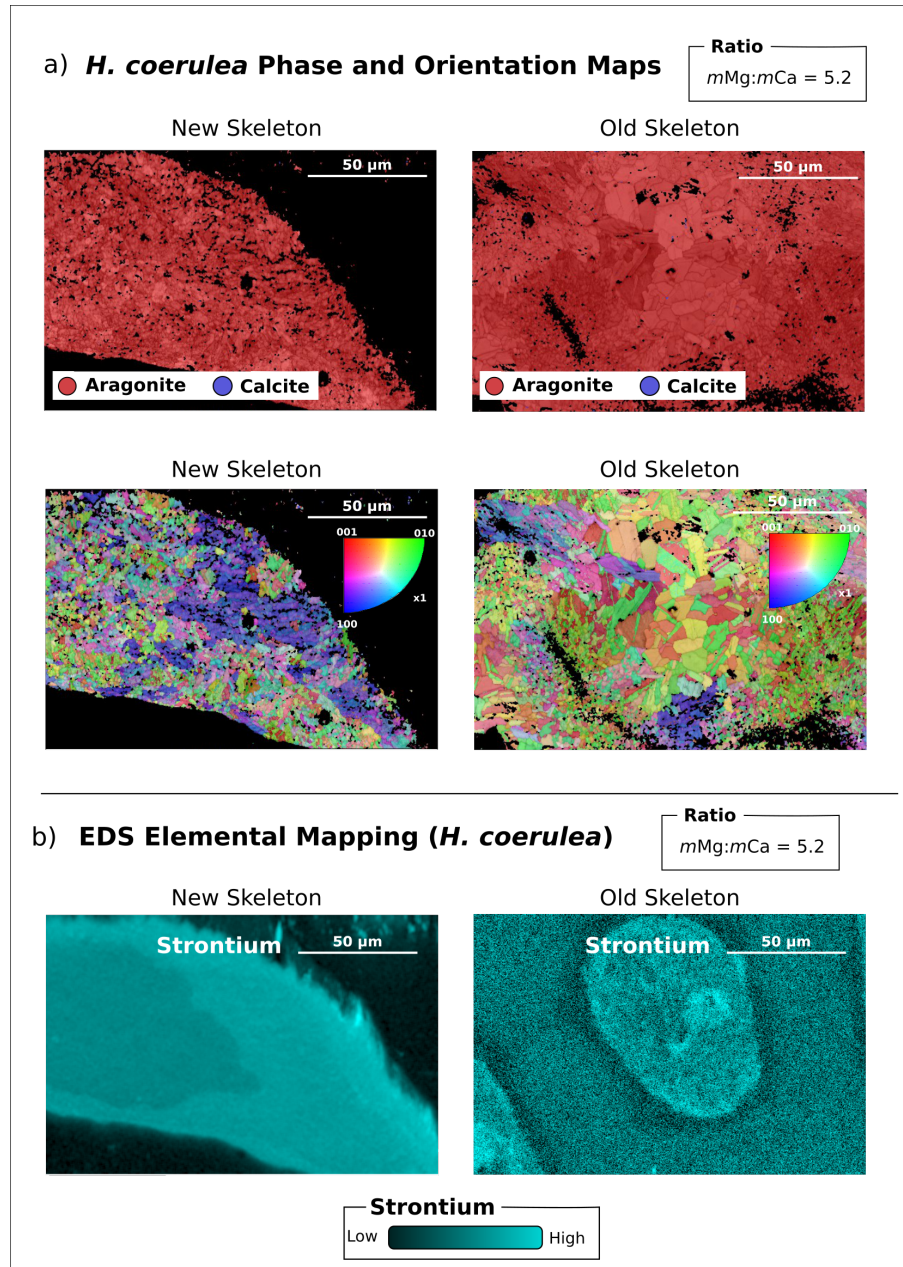


Figure S4.6: **a)** Phase map and inverse pole figures (IPF) and **b)** strontium distribution in *H. coerulea* skeletons exposed to $m\text{Mg}:m\text{Ca} = 5.2$. 'Old skeleton' and 'new skeleton' refer to mineral deposited before and after the experiment.

Supplementary Figures of Chapter 5

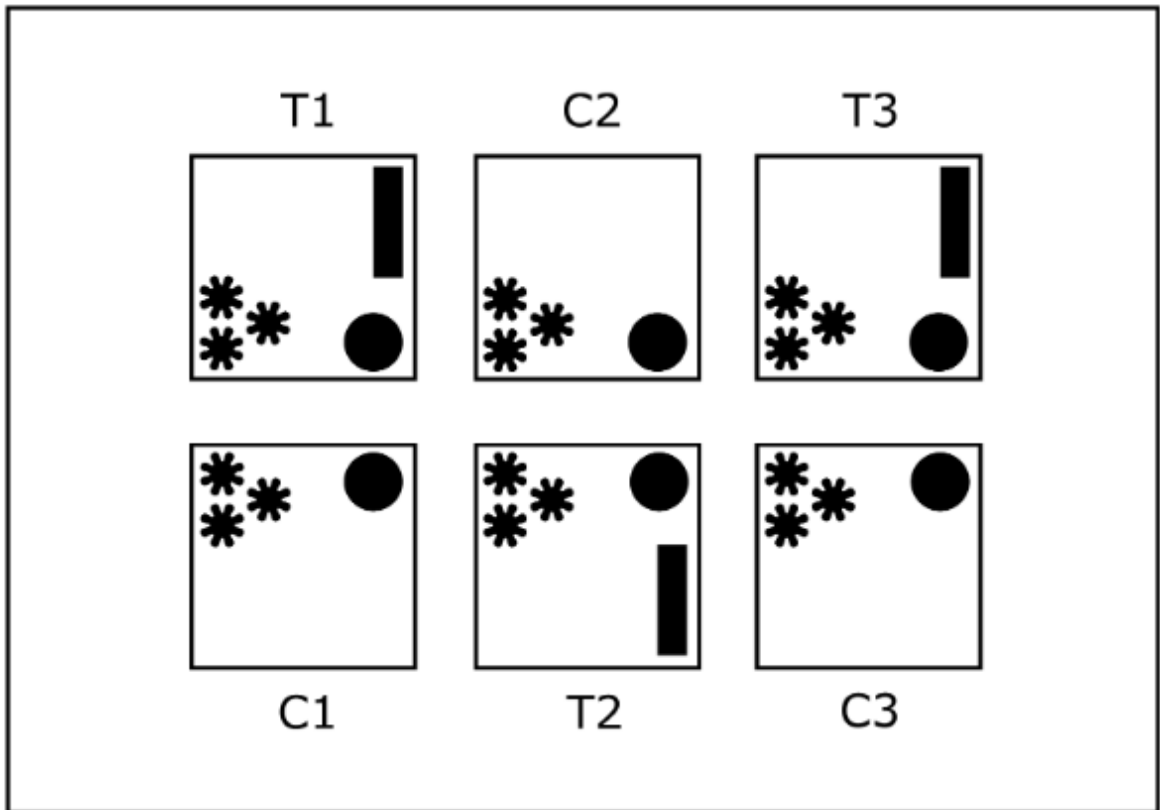


Figure S5.1: Top view of the heat shock experimental setup. Each aquarium contained 3 nubbins (black stars) and one submersible pump (black circle). Treatment aquaria (T1-T3) were additionally equipped with one heater (black rectangle).

Supplementary Figures of Chapter 6

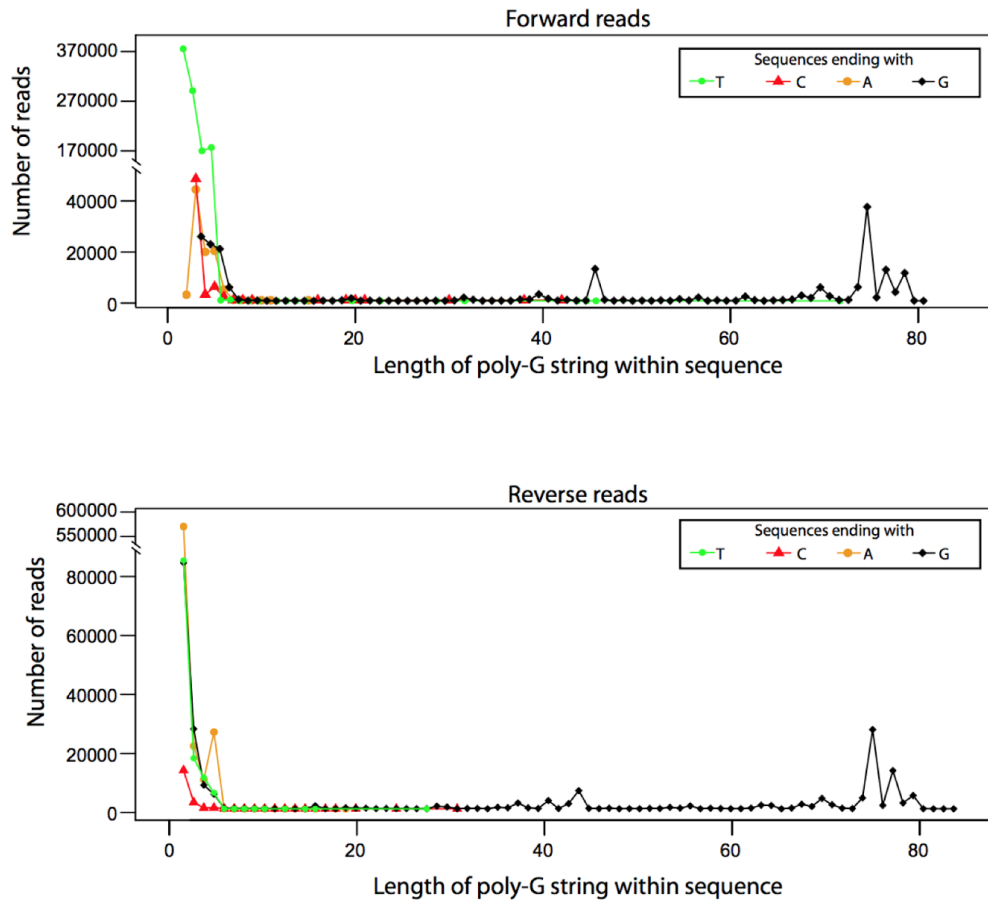


Figure S6.1

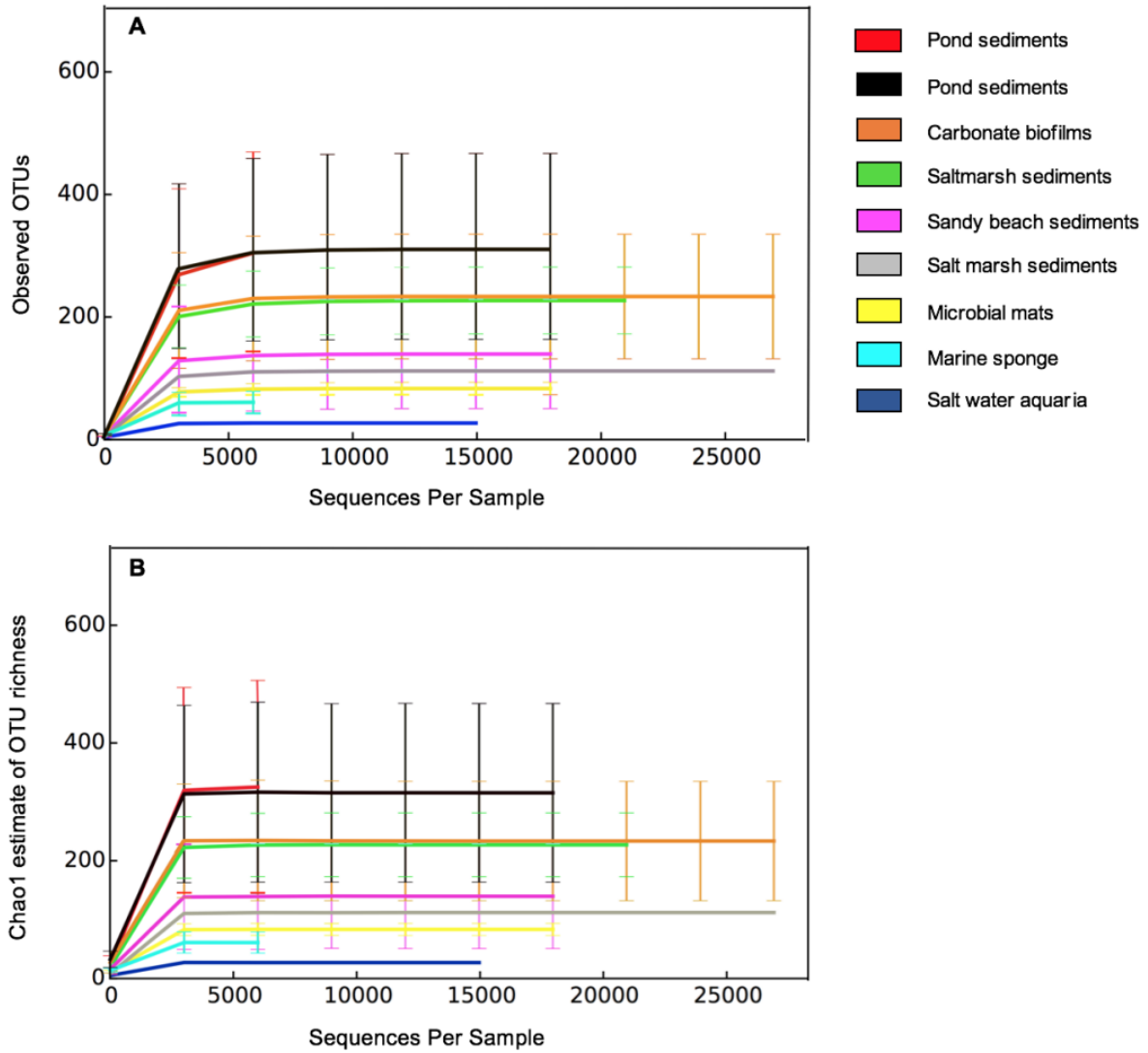


Figure S6.2

Bacterial isolate in mock community	Closest hit to GenBank entry	Accession Number	Isolated from	Author	Read numbers		
					Run A	Run C	Run D
<i>Staphylococcus sp.</i>	<i>Staphylococcus pasteurii</i>	KX453962.1	no information	Smith et al. 2017	2,077	2,309	6,151
<i>Bacillus sp.</i>	<i>Bacillus simplex</i>	KX866679.1	metal contaminated soil	Alaniz-Andrade et al. 2017	4,278	1,425	2,377
<i>Bacillus sp.</i>	<i>Bacillus sp.</i>	KX785129.1	no information	Alnaimat 2016	4,673	450	523
<i>Micrococcus sp.</i>	<i>Micrococcus luteus</i>	KX866674.1	metal contaminated soil	Alaniz-Andrade et al. 2017	3,204	633	581
<i>Acinetobacter sp.</i>	<i>Acinetobacter lwoffii</i>	KX953868.1	sediment	Xiong et al. 2016	6,868	3,221	4,168
<i>Enterobacter sp.</i>	<i>Enterobacter sp.</i>	KX364035.1	Quebrada del Zoquete	Cornejo et al. 2016	9,357	5,282	12,360
<i>Aeromonas sp.</i>	<i>Aeromonas veronii</i>	KX946876.1	no information	Kang et al. 2016	10,169	5,964	17,779
<i>Carnobacterium sp.</i>	<i>Carnobacterium maltaromaticum</i>	KU244600.1	exfoliated sandstone	Zanardini et al. 2016	2,514	1,882	3,834
<i>Exiguobacterium sp.</i>	<i>Exiguobacterium sibiricum</i>	KR857420.1	Siberian permafrost	Schuerger et al. 2016	3,187	1,702	4,020
<i>Janthinobacterium sp.</i>	<i>Janthinobacterium sp.</i>	LC189077.1	farm soil	Arif et al. 2017	-	-	-
<i>Pseudomonas sp.</i>	<i>Pseudomonas fluorescens</i>	KT695823.1	Wyoming Soil	Tao 2015	2,735	3,548	4,084
<i>Photobacterium sp.</i>	<i>Photobacterium rosenbergii</i>	KP843685.1	coral mucus	Embarcadero-Jimenez et al. 2015	5,938	2,082	4,916
<i>Pseudoalteromonas sp.</i>	<i>Pseudoalteromonas flavipulchra</i>	LC189370.1	coral	Wijayanti et al. 2016	697	126	267
<i>Vibrio sp.</i>	<i>Vibrio natriegens</i>	KT986142.1	ocean water	Jiang et al. 2015	1,019	500	1,059
<i>Rhodococcus sp.</i>	<i>Rhodococcus sp.</i>	KY970076.1	soil	Chitranshi et al. 2017	558	171	110
<i>Sphingobium sp.</i>	<i>Sphingobium sp.</i>	KY927392.1	soil	Cai 2017	38	-	118
<i>Arthrobacter sp.</i>	<i>Arthrobacter sp.</i>	KY970072.1	soil	Chitranshi et al. 2017	48	-	-
<i>Mycobacterium sp.</i>	<i>Mycobacterium sp.</i>	KX509812.1	activated sludge	Zhang and Yuan 2016	353	151	85

Figure S6.3

PCR Primer	Barcode	Sequence (5' to 3')
515F-Y.A501	ATCGTACG	AATGATACGGCGACCACCGAGATCTACACATCGTACGTATGGTAATTGTGTGYCAGCMGCCGCGGTAA
515F-Y.A502	ACTATCTG	AATGATACGGCGACCACCGAGATCTACACTATCTGTATGGTAATTGTGTGYCAGCMGCCGCGGTAA
515F-Y.A503	TAGCGAGT	AATGATACGGCGACCACCGAGATCTACACTAGCGAGTTATGGTAATTGTGTGYCAGCMGCCGCGGTAA
515F-Y.A504	CTGCGTGT	AATGATACGGCGACCACCGAGATCTACACCTGCGTGTATGGTAATTGTGTGYCAGCMGCCGCGGTAA
515F-Y.A505	TCATCGAG	AATGATACGGCGACCACCGAGATCTACACTCATCGAGTATGGTAATTGTGTGYCAGCMGCCGCGGTAA
515F-Y.A506	CGTGAGTG	AATGATACGGCGACCACCGAGATCTACACCGTGAGTGTATGGTAATTGTGTGYCAGCMGCCGCGGTAA
515F-Y.A507	GGATATCT	AATGATACGGCGACCACCGAGATCTACACGGATATCTTATGGTAATTGTGTGYCAGCMGCCGCGGTAA
515F-Y.A508	GACACCGT	AATGATACGGCGACCACCGAGATCTACACGACCCGTTATGGTAATTGTGTGYCAGCMGCCGCGGTAA
806RB.A701	AACTCTCG	CAAGCAGAAGACGGCATAACGAGATAACTCTCGAGTCAGTCAGCCGGACTACNVGGGTWTCTAAT
806RB.A702	ACTATGTC	CAAGCAGAAGACGGCATAACGAGATACGATGTCAGTCAGTCAGCCGGACTACNVGGGTWTCTAAT
806RB.A703	AGTAGCGT	CAAGCAGAAGACGGCATAACGAGATAGTAGCGTAGTCAGTCAGCCGGACTACNVGGGTWTCTAAT
806RB.A704	CAGTGAGT	CAAGCAGAAGACGGCATAACGAGATCAGTGAGTAGTCAGTCAGCCGGACTACNVGGGTWTCTAAT
806RB.A705	CGTACTCA	CAAGCAGAAGACGGCATAACGAGATCGTACTCAAGTCAGTCAGCCGGACTACNVGGGTWTCTAAT
806RB.A706	CTACGCAG	CAAGCAGAAGACGGCATAACGAGATCTACGCAGAGTCAGTCAGCCGGACTACNVGGGTWTCTAAT
806RB.A707	GGAGACTA	CAAGCAGAAGACGGCATAACGAGATGGAGACTAAGTCAGTCAGCCGGACTACNVGGGTWTCTAAT
806RB.A708	GTCGCTCG	CAAGCAGAAGACGGCATAACGAGATGTCGCTCGAGTCAGTCAGCCGGACTACNVGGGTWTCTAAT
806RB.A709	GTCGTAGT	CAAGCAGAAGACGGCATAACGAGATGTCGTAGTAGTCAGTCAGCCGGACTACNVGGGTWTCTAAT
806RB.A710	TAGCAGAC	CAAGCAGAAGACGGCATAACGAGATTAGCAGACAGTCAGTCAGCCGGACTACNVGGGTWTCTAAT
806RB.A711	TCATAGAC	CAAGCAGAAGACGGCATAACGAGATTCATAGACAGTCAGTCAGCCGGACTACNVGGGTWTCTAAT
806RB.A712	TCGCTATA	CAAGCAGAAGACGGCATAACGAGATTCGCTATAAGTCAGTCAGCCGGACTACNVGGGTWTCTAAT

Figure S6.4

Declaration

I hereby confirm that my thesis entitled **Molecular Biomineralization of Octocoral Skeletons: Calcite versus Aragonite**, is the result of my own original work. Furthermore, I certify that this work contains no material which has been accepted for the award of any other degree or diploma in my name, in any university and, to the best of my knowledge and belief, contains no material previously published or written by another person, except where due reference has been made in the text. In addition, I certify that no part of this work will, in the future, be used in a submission in my name, for any other degree or diploma in any university or other tertiary institution without the prior approval of the LudwigMaximilians-University Munich.

Place and Date

Signature

Munich, 03.03.2020 Nicola Conci

Acknowledgements

First I would like to thank Prof. Dr. Gert Wörheide and Dr. Sergio Vargas for believing in me by giving me the opportunity to work on this project, and for their constant supervision and insight. Special thanks go to Dr. Erika Griesshaber for her invaluable help with the mineralogical analysis, and to Prof. Dr. Wolfgang Schmahl. My thanks are extended to Moritz Zenkert for preparing the samples for EBSD. I would also like to thank Dr. Martin Lehmann and the whole team at the Biozentrum der LMU München, for their help and assistance with the mass spectrometry analysis. Special thanks go also to Jaroslava Obel at the Fakultät für Chemie und Pharmazie for performing the ICP-OES analysis, and to Dr. Peter Naumann for his help in the aquarium and providing for the wellbeing of the animals.

Special thanks to Gabriele Büttner, Simone Schätzle and Dr. Dirk Erpenbeck for their daily assistance in the lab and for all their support. Thank you to Rene Neumeier and Dominik Bastl for their assistance with all PC-related issues and for answering all my (sometimes naive) questions. I owe a big thank you to all past and present lab members Benedetta, Ramon, Ksenia, Fabian, Catalina, Luis, Martin Michi, Warren, Astrid, Angelo, Gaurav. Thanks for the nice memories, the laughs and the support during hard times.

Finally, his project could have never happened without the financial support of the Deutsche Forschung Gemeinschaft (DFG).